UNIVERSITY OF CALIFORNIA,
IRVINE

A Novel Non-Destructive Test (NDT) Methodology for Evaluating the Integrity of Adhesively-Bonded Joints

THESIS

submitted in partial satisfaction of the requirements
for the degree of

MASTER OF SCIENCE

in Engineering with concentration in
Material and Manufacturing Technology (MMT)

by

Sean Naraghi (Shaham Naraghijalili)

Thesis Committee:
Professor James Earthman, Co-Chair
Professor Ayman Mosallam, Co-Chair
Professor Lorenzo Valdevit

2020

DEDICATION

To my parents for their love and support

TABLE OF CONTENTS

LIST OF FIGURES

LIST OF TABLES

ACKNOWLEDGMENTS

I would like to thank both of my advisors, Prof. Earthman and Prof. Mosallam for their mentorship. This journey wasn't possible without their dedication and compassion.

I would like to thank Prof. Valdevit for serving on my committee. His dedication and cooperation is much appreciated.

I would like to thank Mr. Tucker Parris for machining some of my parts and mentoring me throughout my time at UCI. His dedication and patience is much appreciated.

I would like to thank Mr. Mark Steinborn for giving me machining training. His help with machining is much appreciated.

I would like to thank Mr. Steve Weinstock for his dedication. He always did his best to make it possible for me to do my project.

I would like to thank Mr. Zach McKee from KEYENCE™ for his demo and taking pictures from some my sample with KEYENCE™ optical microscope.

I would like to thank Mr. Antonios Tontisakis and Dr. Johnny Lincoln from Axiom Materials for providing the adhesive film and giving me technical help throughout my project.

I would like to thank Mr. Edward R. Fyfe from DYMAT for providing carbon fiber and epoxy resin used in fabricating the carbon/epoxy (CFRP) composite specimens.

I would like to thank Mr. Sergio Carnalla for his help throughout my project.

I would like to thank my lab mate, Mr. Louai Wafa. His help throughout the project is much appreciated.

ABSTRACT OF THE THESIS

A Novel Non-Destructive Test (NDT) Methodology for Evaluating the Integrity of Adhesively-Bonded Joints

By

Sean Naraghi (Shaham Naraghijalili)

MASTER OF SCIENCE

in Engineering with concentration in
Material and Manufacturing Technology (MMT)

University of California, Irvine, 2020

Professor James Earthman, Co-Chair
Professor Ayman Mosallam, Co-Chair

The Climate Crisis is pushing engineers to use lighter materials in their designs to lower CO_2 emission. This is the primary reason behind the shift from steel to lighter metallic alloys such as Aluminum Alloys, and recently to Fiber Reinforced Polymer (FRP) composites. Adhesive bonding introduces a smooth stress transfer and therefore is the most appropriate joining method when it comes to FRPs compared to mechanical fasteners such as rivets, bolts, etc. Besides, adhesive bonding has other advantages over mechanical fasteners, including reducing the final weight of the assembly, protecting the assembly against galvanic corrosion, absorbing shock and vibration, and introducing the ability to repair damaged assemblies.

The biggest hurdle against mainstream usage of adhesive bonding as the primary method of joining is the lack of reliable quality control tests to ensure a reliable bonding. This has led many

engineers to avoid adhesive bonding in their designs or to take a harsh conservative approach when it comes to designing with adhesive bonding.

In this project, the possibility of using the Quantitative Percussion Diagnostics (QPD) to detect a weak bond (kiss bond) is investigated. Intentional flaws were introduced to adhesively bonded joints through multiple procedures. Samples with the ideal well bond were also fabricated. The QPD was performed on these two sets of samples, and the results were compared to see if there is a significant difference that can be used to distinguish between a well bond and a kiss bond. QPD shows some promising signs that it is capable of detecting a kiss bond.

Finite Element Analysis (FEA) is used to calculate the stress distribution in different joint conditions and configurations. The results are used to investigate the effect of joint configuration, substrate's modulus, and bondline length. The general conclusion is that joint configurations with lower eccentricity experience lower bending, and that leads to the development of lower peel stresses. Joints that include substrates with higher modulus experience less bending and therefore develop lower peel stresses. Also, longer bondline generally enhance the performance of the joint.

A literature review was conducted in regards to surface science, surface treatment, joint design, environmental durability of joints, Non-Destructive Tests (NDTs), Fiber Reinforced polymers (FRPs), etc.

1) Introduction and Literature Review

1.1) Introduction to Adhesion and Adhesives

Why, when two pieces of broken china are pushed against each other, they do not instantaneously attach? Questions like this have been on the mind of scientists for centuries. Isaac Newton explored this topic by pressing highly polished microscope slides and studying the attractive force between the two slides [1, pp. 3-22]. Although there was some attractive force between the two slides, it was nothing near the strength of a solid glass. So what prevents two pieces from coming together and attaching instantaneously?

The answer is that forces between atoms are applicable in a very short range. When two pieces of broken china or two pieces of microscope slides are pressed against each other, there are still small gaps between two surfaces that prevent them to bond instantaneously. Plus, surfaces are always covered with layers of contamination, dirt, oil, absorbed gas, and moisture. These contaminants would prevent the surfaces from getting close enough to form a strong bond [1, pp. 3-22]. In a typical adhesively bonded joint, the atomistic thickness that determines the bond's quality and strength is roughly 6 molecules thick. On comparison, a fingerprint is about 1000 molecules thick, and the residues from human breath could be around 40-100 molecules thick [2].

From a thermodynamic point of view, the 2nd law of thermodynamics states that any change is accompanied by doing work or dissipating some energy (heat). In other words, it is impossible to have 100% efficiency, unless we get to 0 K. The 3rd law states that it is impossible to reach 0 K. Combining these two laws and we end up with the fact that it is impossible to get to an initial

state unless we do some work. Let us assume that two pieces of broken china would instantaneously bond upon pushing together. That would fundamentally violate the laws of thermodynamics. In reality, we have to clean the surfaces to remove contaminants (doing work) and then use glue to bond two pieces together.

So far, it is impossible to get two surfaces close enough on atomic levels for instantaneous bonding. Therefore the gaps between two surfaces have to be filled with a third material that bonds with both surfaces and acts as a bridge between two surfaces. We need a viscous pasty material to flow and infuse into all the nooks and crannies and gaps between two surfaces and then solidifies. Let us look at two of the typical methods of joining material together, namely welding and gluing.

In welding, both surfaces come to close contact, and then upon applying heat and pressure, two surfaces melt and diffuse into each other and create a solid body. In some cases, a third substance (wire) is necessary to melt and create an interphase between two surfaces consist of all the three substances. In gluing, a viscous pasty polymeric substance comes between two surfaces and infuse into gaps between two surfaces and bond with both of them and finally solidify.

Most polymers have T_g[1] around room temperature or higher than room temperature up to 200°C. So by applying heat, they pass their T_g and enter a viscous pasty state. In this state, they can flow

[1] T_g refers to the Glass Transition Temperature. Polymer chains only have short-range motions of several contiguous chain segments and motions of substituent groups at temperatures lower than Tg. Upon increasing temperature, the internal energy of polymer chains increase and at some point, the internal energy is high enough for long-range

and infuse into gaps between two surfaces. The solidification process could happen in two distinguished way: physically (thermoplastic polymers), or chemically (thermoset polymers).

Thermoplastic polymers solidify upon cooling from high temperatures, and it is a reversible process. So it is possible to dismantle a bond, and that gives us more flexibility and reduction in the production waste. In some cases, the polymer is dissolved in a solvent, with polymer content varies between 5-95%, with 20-50% being the most common [3, pp. 261-291]. Here solidification happens upon the evaporation of the solvent. Some examples of thermoplastic adhesives are mentioned below [3, pp. 261-291]:

- High-Performance Thermoplastics
    - Polyamides (nylon)
    - Polyamide-imide
    - Polyarylates
    - Polyaryletherketones
    - Polyarylsulfones
    - Polybenzimidazoles
    - Polyetherimides
    - Polysulfones

segmental motions. The temperature that mark this transition is called Glass Transition Temperature or T_g. Polymers soften extensively after the temperature surpassing their T_g, and their modulus drop roughly by three orders of magnitude (from approximately 1GPa to 1MPa) [23, p. 154].

- Other Thermoplastics
    - Acetals
    - Acrylics
    - Acrylonitrile-butadiene-styrene
    - Polycarbonates
    - Polyethylene
    - Polyethylene terephthalates
    - Polystyrene
    - Polyvinylchloride

Thermoset polymers solidify by an irreversible chemical crosslinking process. In this process, polymer chains chemically bond with each other and end up with a 3D network. The thermoset adhesive system consists of a resin and a curing agent. Curing agent acts as a bridge and bonds polymer chains together and creates a 3D network. A typical example of a thermoset adhesive system is epoxy resin and amine-based curing agents. In this case, the viscosity of the curing agent is much lower than the resin, so the curing agent works as a diluent as well [4]. Some of the thermoset adhesives are mentioned below [3, pp. 261-291]:

- General-purpose thermosets
    - Amino
    - Phenolics
    - Polyesters
    - Acrylics
    - Engineering Thermosets

    - Epoxy
    - Polyurethane
- Specialty Thermosets
    - Silicone
    - Polyimide

Elastomeric adhesives are a subcategory of thermoset adhesives. Elastomers are very flexible polymers with very low T_g that need to be chemically crosslinked to achieve good properties. The crosslinking process in elastomers is called vulcanization. A typical example is the vulcanization of natural rubber using sulfur as a crosslinking agent. Elastomeric adhesives have low modulus and rarely are used for structural applications. They are more suitable for applications that require more damping and energy dissipation. Some of the elastomeric adhesives are mentioned below [3, pp. 261-291]:

- EPDM (Ethylene-Propylene)
- Fluorocarbons
- Natural
- Nitrile (Acrylonitrile butadiene)
- Polybutadiene
- Silicon
- Styrene-butadiene rubber (SBR)

1.2) Factors Affecting Adhesion

The presence of contamination on the surface has an enormous effect on the strength of the bond between the adhesive and the substrate. Contaminants come between the adhesive and the substrate and prevent the formation of a strong bond. Therefore, the first step in achieving strong adhesion should be removing the contamination from the surface of the substrate. This could be achieved through mechanical procedures such as hand abrasion, grit blasting, or through solvent wiping, chemical etching, or usually a combination of these methods [5].

The nature of the bond between the adhesive and the substrate depends on the chemical characteristics of both the adhesive and the substrate's surface. To create a strong and durable bond, it is beneficial to establish a strong covalent bond between the adhesive and the substrate. This can be achieved by introducing reactive chemical groups that can covalently bond with the adhesive into the surface of substrates such as plastics, polymer-based composites, etc. through surface treatments like flame treatment, corona treatment, plasma treatment, etc [3, pp. 119-147].

In some cases, it is beneficial to use a coupling agent to improve the adhesion. Coupling agents are molecules with the capability to bond with both adhesive and substrate and therefore enhance the adhesion [3, pp. 237-260].

The texture and roughness of the surface also deeply affect the performance of an adhesively bonded joint. Surface roughness increases the bonding surface and also provides "lock and key sites" for mechanical interlocking. The viscosity of the adhesive is the factor that should be carefully monitored to make sure adhesive can flow and infuse into all the nooks and crannies in

the surface of the substrate; otherwise, it will result in the creation of voids in the bond surface. Another contribution of surface roughness is that it is harder for cracks to propagate alongside a rough interface. In rough interfaces, cracks have to maneuver and take a longer path, and that gives the adhesive and the substrate the chance to plastically deform and arrest the crack [6]. Even though the general consensus is that surface roughness improves adhesion, this topic is still controversial. Kevin Kendal makes the argument that the mechanical interlocking is a macroscopic approach that does not represent the reality in the atomistic level. He argues that on the atomistic level, a different set of forces comes into play, making the mechanical interlocking approach irrelevant. He believes that in the atomistic level, atoms instantaneously bond when gets close enough and stick together, and that prevents them from infusing into holes and gaps between two surfaces [1].

Surface energy plays a crucial rule in the adhesion process. In bulk, atoms are surrounded by a particular number of like atoms (coordination number). However, on the interface between two distinct phases, contrary to the bulk, atoms are surrounded by both like and dislike atoms. So some of the bonds between like atoms are replaced by bonds between dislike atoms. Because any bond has its own strength, force balance in the interface is no longer valid, and that is the source of surface tension. Let us look at it from the energy perspective. Any bond has its own potential energy, and on the surface, some of the bonds between like atoms are replaced by bonds between dislike atoms. So some bonds have to be broken, and some new bonds have to be made. The difference between the potential energy of broken and made bonds is the excess energy of the surface, aka surface energy. So surface energy and surface tension are two terms that describe the same phenomena. The work that has to be done to create a new surface

(surface tension) is equal to the excess energy of that newly created surface (surface energy). The more disparity between the chemical bonding of atoms on the two sides of the interface will mean more difference between their bond strength which leads to the development of a higher surface tension. There are two major tests to measure the surface tension of liquids [6]:

- Drop Weight/Volume Method: In this method, a particular volume of liquid is inserted into a syringe with a micro-meter driven plunger. The micro-meter plunger is slowly driven until a droplet falls from the tip of the needle. By counting the number of droplets and measuring the volume of the liquid, the average volume necessary to cause the droplet to fall can be calculated and used to calculate surface tension.
- Du Nuoy Tensiometer: In this method, the surface tension is measured by measuring the force necessary to pass a platinum ring from a liquid surface.

There are numbers of methods to measure the surface tension of solids, but probably the easiest and most applicable one is the "Contact Angle" measurement. In this typical experiment, as shown in Figure 1-1, the angle between a liquid droplet (usually Deionized (DI) water) and the solid surface is measured. This angle is called contact angle, and it related to surface tension following the Young's Equation (Equation (1-1)) [6]:

$$\gamma^{sv} = \gamma^{sl} + \gamma^{lv}\cos\theta \;\Rightarrow \cos\theta = \frac{\gamma^{sl} - \gamma^{sv}}{\gamma^{lv}} \qquad (1\text{-}1)$$

γ^{sv}: Solid/Vapor surface energy, γ^{sl}: Solid/Liquid surface energy, γ^{lv}:Liquid/Vapor surface energy, θ: Contact Angle

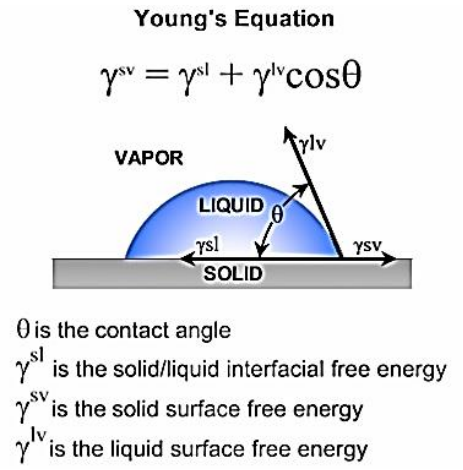

Figure 1-1: Contact Angle fundamental and the Young's Equation- γ^{sv}: Solid/Vapor surface energy, γ^{sl}: Solid/Liquid surface energy, γ^{lv}: Liquid/Vapor surface energy, ϑ: Contact Angle [7]

There are two ways to measure the contact angle: Static and Dynamic. In the static test, a droplet of DI water is placed on the surface, and the angle between the droplet and the surface is measured. In the dynamic test, the size of the droplet changes between two states, and the contact angle is measured in both cases, or the droplet is placed on a slanting surface, and both angles that the droplet makes with the surface are measured [8].

For an adhesive to adequately wet the substrate's surface, the surface energy of the substrate should be higher than the adhesive to enforce the adhesive to spread and cover the substrate's surface.

1.3) Adhesively Bonded Joint Design, Configuration, Durability

Adhesively bonded joints have some advantages and disadvantages over other joining methods. In this case, the stress transfer is much smoother, and there is much less stress concentration than mechanical fasteners such as bolts, rivets, etc. Mechanical fasteners require drilling a hole

to attach two materials. Introducing a hole in a material leads to the development of a huge stress concentration around the hole. Stress concentration could be catastrophic, especially in the case of FRP substrates that are inherently anisotropic[2], inhomogeneous[3], and have low transverse mechanical strength and local bearing strength [9] & [3, p. 1050] & [10]. In FRP substrates, stress concentration can cause a crack in the matrix, and crack can easily propagate in the matrix domain. This could result in the premature failure of the FRP laminate. By removing the need to introduce a hole into a material to be attached to another material, adhesive bonding prevents stress concentration and also removes all the fabrication steps required to introducing a hole into the material. Adhesive bonding reduces the overall weight of an assembly compared to mechanical fasteners.

Adhesively bonded joints give us the ability to join dissimilar substrates with appropriate surface treatment. It is also possible to attach thin substrates effectively with adhesive bonding. Most adhesives are polymer-based, so they have higher damping capability, and that will improve the fatigue performance of the joint, and gives the joint the ability to absorb shocks and vibration without failure. Most adhesives are electrical insulators, so they will protect metallic substrates against galvanic corrosion. The adhesive layer also creates a layer of protection that seals the joint and limits the joint exposure to environmental elements that cause or promote corrosion.

[2] Anisotropic means that thermo-mechanical properties are direction-dependent.
[3] Inhomogeneous means that physical properties are location-dependent.

In applications that need electrical conductivity in the joint, it is possible to make the adhesive conductive by incorporating appropriate fillers such as carbon black, CNT, metal powders, etc.

Adhesives need high temperature and pressure for the curing process. Specialized equipment such as a furnace, autoclave, hot press, etc. is required to provide the required temperature and pressure for curing the adhesive, and that could be costly. The temperature, pressure, and humidity should be closely monitored during the curing process to achieve a strong bond. Plus, the curing can take a couple of hours, which will add to the cost of fabrication as well, especially considering that the appropriate fabrication time is in the order of minutes and seconds in many industries. That is why, in many industries, such as the automotive industry, there is a big push toward fast curing adhesive systems (Flash cure). The joint needs to be fixed during the curing, and that will add to the fabrication challenge. Adhesives are polymer, and polymers creep at high temperatures, so it is not possible to expect good creep performances from adhesively bonded joints, especially at high temperatures. Relatively high temperatures would initially chemically degrade the adhesive, and at high temperatures, the adhesive would burn. So especial fire, smoke, and toxicity (FST) measures are necessary when dealing with adhesively bonded joints. Adhesives show extensive brittleness at low temperatures, and that would jeopardize their performance.

To achieve a strong and durable bond, substrates must have high surface energy. That is why it is usually necessary to perform surface treatment on the surface of a substrate to increase its surface energy. Some polymers such as Polyethylene inherently have low surface energy and therefore are not suitable for adhesive bonding. In many cases, it is hard to control and quantify

these surface treatment processes, and that leads to a variation in a joint performance. A reliable QC method to inspect the surface before bonding is crucial in the bonding process [10].

There are three main modes of failure in an adhesively bonded joint. Figure 1-2 schematically depicts these modes. In (a) cohesive failure, the crack propagates entirely in the bulk of the adhesive. This indicates a very well bond between the adhesive and the substrates. In this case, after the failure, the adhesive is present on the surface of both substrates. Cohesive failure is the preferred mode of failure. Cohesive failure could also be the result of inadequate curing of the adhesive. Several factors such as incorrect mixing ratio, improper mixing, improper curing condition (such as temperature, pressure, and humidity), non-uniformity of temperature and pressure during curing, etc. could result in inadequate curing of the adhesive. In (b) interfacial (adhesive) failure, the crack propagates in the interface between the adhesive and a substrate. This indicates poor bonding between the adhesive and the substrates as the result of poor surface preparation/treatment. Here, the adhesive is only present on the surface of one substrate after failure. This mode of failure should be avoided at all costs. (c) mixed-mode failure is somewhere between these two extreme cases. Crack propagates erratically in this case. The crack can initiate in the interface and then deviate toward the bulk of the adhesive layer or vice versa. In this case, when looking at the fracture surface, both adhesive and substrate are apparent for both substrates. In practice, most joints experience a mixed-mode failure.

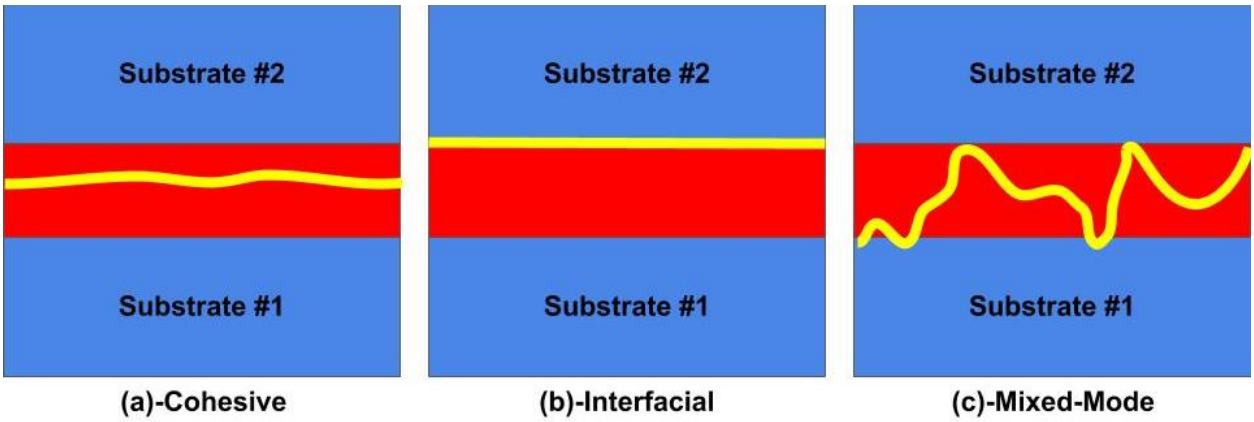

Figure 1-2: Schematic representation of the modes of failure in adhesively bonded joints: (a)-Cohesive, (b)-Interfacial, (c)-Mixed-mode (Blue illustrates substrates, red illustrates the adhesive, yellow illustrates the crack propagation path)

Many factors affect the short term and long term performance of adhesively bonded joints:

1.3.1) Joint configuration

In almost all joint configurations other than the butt joint, loads are not inline, and that causes bending in the joint, and the bending will introduce peel stress in the joint. So even though it seems that the adhesive layer should only experience shear stress, but in fact, there is a considerable amount of peel stress as the result of bending as well.

Adhesives naturally perform well under shear, but they are susceptible to tensile stress. That is why butt joints are not suitable for any structural application, even though they are the easiest to be fabricated. The rule of thumb is that the more symmetrical the joint is, there would be less eccentricity and, therefore, less peel stress in the joint. Figure 1-3 schematically depicts some of the prominent joint configurations. For the detailed description of joint configurations, refer to the page 160-161 of [10].

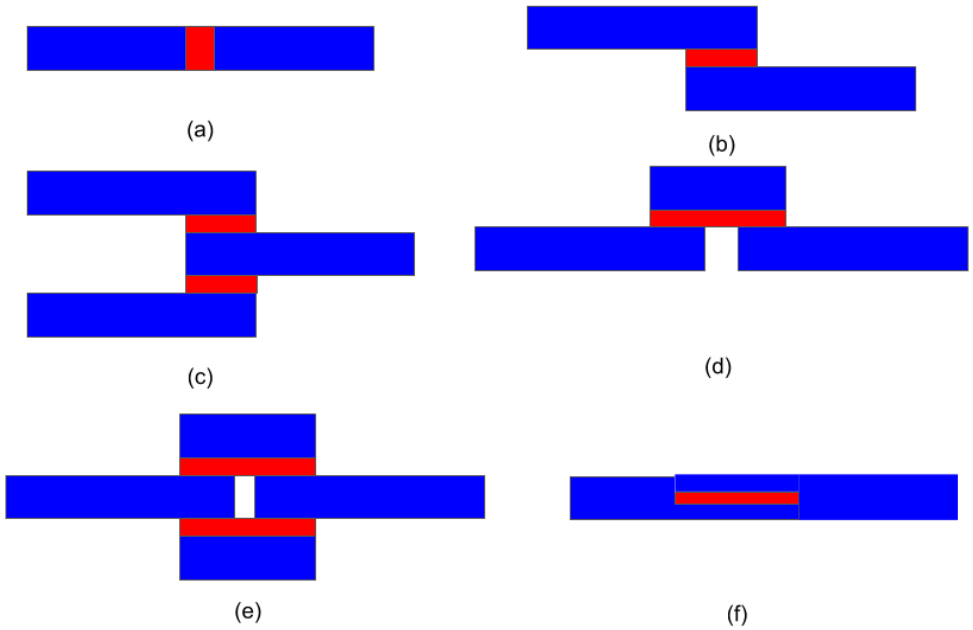

Figure 1-3: Schematic representation of some of the prominent joint configurations. (a): butt joint, (b): single lap joint, (c) double lap joint, (d): single strap joint, (e): double strap joint, (f): stepped joint (Blue illustrates substrates, red illustrates the adhesive)

The stress distribution in an adhesively bonded joint is very complex and varies through the bondline. Both peel and shear stresses are maximum at both edges of the bondline and are lowest at the middle of the bond. So the failure would most likely initiate from the edges of the bond and progress toward the middle of the bond. Figure 1-4 depicts the shear and peel stress distribution in the Single-Lap joint [11].

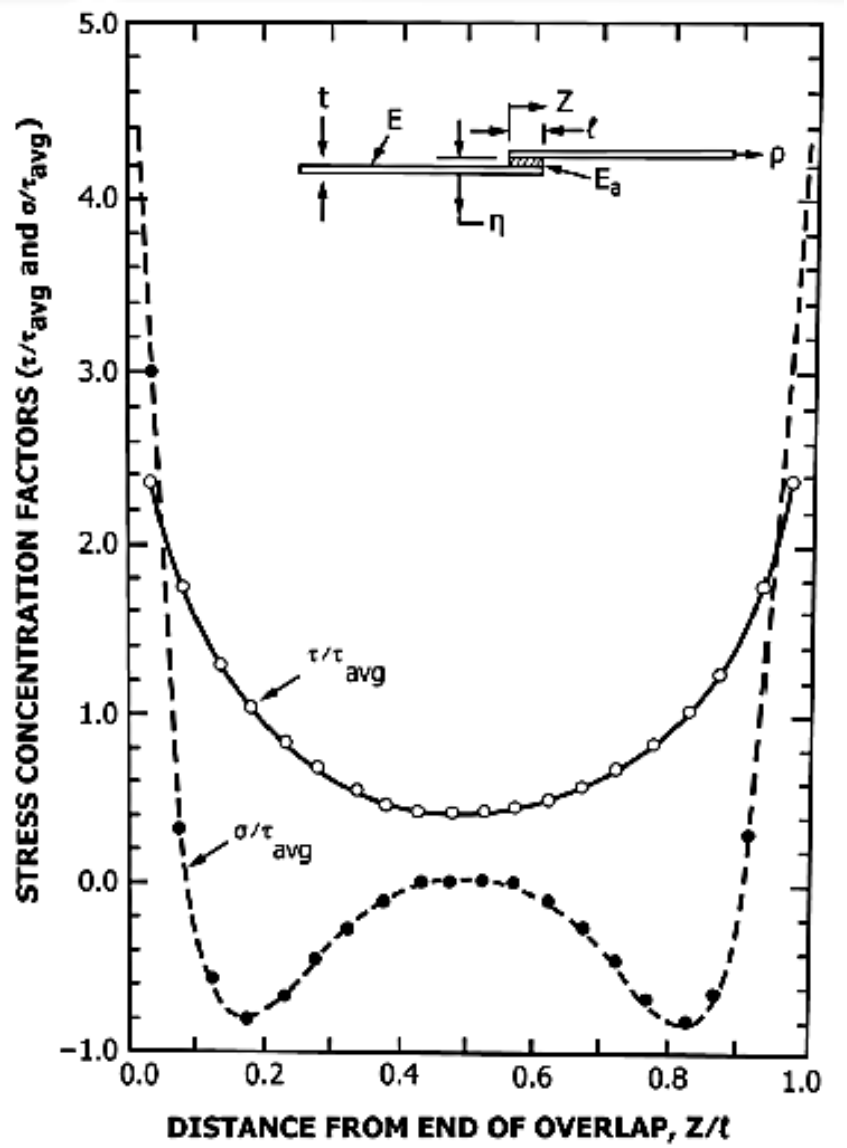

τ	=	actual adhesive shear stress at a point
τ_{avg}	=	average (nominal) adhesive shear stress in the joint
σ	=	actual adhesive normal stress at a point
E_a	=	adhesive modulus
E	=	adherend modulus
η	=	adhesive layer thickness
t	=	adherend thickness
υ	=	adhesive Poisson's ratio
ℓ	=	overlap length
Z	=	location of a point along the overlap length
p	=	tensile stress in the adherends away from the joint

Figure 1-4: Peel and Shear stresses over the bondline for a Single Lap Joint (SLJ). τ, σ represent the shear and peel stresses, respectively. Both shear and peel stresses are maximum at both edges of the bond. The magnitude of the stress in both cases is minimum at the middle of the bond (copy of the FIG 1 in [11] with permission)

There are two famous analytical models that calculate the stress distribution in the Single Lap Joint (SLJ): 1) Volkersen, which only predicts the shear stress in the bondline 2) Goland and Reissner, which predicts both shear and peel stresses in the bondline. For the detailed description of these two models, check out chapter 24 of the handbook of adhesion Technology [3, pp. 597-629]. The online program called "JointDesigner" developed by Prof. L.F.M da Silva and his team [12] and the program by Prof. Steve Abbott [13] are good sources to calculate stress distribution in the bondline using these aforementioned models. With the advances in computing, the Finite Element Modelling (FEM) or Finite Element Analysis (FEA) approach is a more realistic approach to calculate the stress distribution in the bondline for different joint configurations and conditions.

There is a significant difference between the stress distribution in the flexible adhesives and stiff, brittle adhesives. Flexible adhesives share the stress over the entire bondline, and that causes less stress concentration in the edges. Plus, plasticity also helps to dull the stress concentration in the edges. On the other hand, in the brittle adhesives, the stress is concentrated in the edges, and the middle part of the bondline basically experience no stress [3, p. 694].

1.3.2) Bondline Thickness

It is hard to make a definite conclusion about the effect of bondline thickness and joint strength. Many factors come into play, such as adhesive mechanical behavior (ductile vs. brittle), adherend mechanical behavior, joint configuration, etc. For example, Liao et al. found out that for ductile adhesives, the fracture energy of the joint increase as the bondline thickness increase, but the effect is opposite for brittle adhesives [14]. For the Single-Lap Joint (SLJ), the general consensus

is that joint strength increase as the bondline thickness decrease, and the optimum strength is achieved when the bondline thickness is between 0.1-0.2 mm [3, p. 696]. One way to explain this is that the amount of void and flaws in the bond increase as the bondline thickness increase, and that leads to premature failure of the bond.

1.3.3) Bondline overlap

The effect of bondline overlap drastically depend on the mechanical nature of the adhesive. As mentioned before, ductile adhesives share the stress throughout the bondline, so an increase in the bondline overlap would result in less stress concentration in the edges. On the other hand, for brittle adhesives, the stress is concentrated in the edges, and an increase in the overlap length has some effect up to a certain point, and there is a plateau after that [15].

1.3.4) Environmental durability

1.3.4.1) Moisture:

Moisture has a profound effect on the initial and ultimate performance of the joint. The existence of pre-bond moisture on the adherend surface can act as contamination and prevent strong bonding. Plus, surface moisture plasticizes the matrix on the surface in FRP substrates and decrease its mechanical performance. Plus, this entrapped moisture leaves voids and porosity behind if it finds a way to escape during the curing step.

Exposure to moisture during the lifetime of a joint can reduce its strength in multiple ways. 1) Moisture can diffuse into the bulk of adhesive and reduce its mechanical properties by plasticizing it 2) moisture can cause hydrolysis in the adhesive and that is a form of chemical aging that leads to premature failure 3) moisture can get to bond surface either by capillary motion

from bond edges or by diffusion through the adhesive bulk. There are multiple possible scenarios in this case: I) water can replace the adhesive in the bond and cause debonding II) water can plasticize the adhesive and adherend (in the case of FRP substrates) in the vicinity of the bond and therefore reduce the mechanical performance of the joint III) water can cause or accelerate the formation of an oxide layer on the metallic substrates. Some metallic oxide layers are brittle and easily detach from the substrate, and that will lead to premature failure of the bond. 4) Moisture can cause swelling in the adhesive layer, and that can cause stress and lead to cracking and crazing. 5) In the case of FRP substrates, moisture can degrade the mechanical properties of the matrix and also damage or totally destroy the fiber/matrix adhesion [16] & [10] & [17].

The high temperature would exacerbate the effect of moisture by increasing the rate of diffusion and hydrolysis reaction. Also, in the case of metallic adherends or CFRP composites, salty water can increase the rate of electrochemical corrosion.

1.3.4.2) Temperature:

Adhesives are polymer and susceptible to creep at high temperatures. The mechanical performance of all polymers degrades as the temperature goes up, especially after temperature surpasses their T_g. The residual stress caused by the difference in Coefficient of Thermal Expansion (CTE) of the adhesive and the substrate during the curing and cooling cycle can cause premature failure in the bond. One way to further study this effect is to investigate the cyclic freeze/thaw behavior of the joint. It is, in fact, a form of thermal fatigue (aging) test. Plus examining the behavior of joints with structural adhesives such as epoxy reveals that the strength decrease at very high and very low temperatures. At high temperatures, low mechanical

performance is the root of the problem, and at low temperatures, excessive brittleness of the adhesive is problematic [3] & [15].

1.4) Surface Cleanness Measurement

As mentioned before, the presence of contamination on the substrate's surface inhibits the formation of a strong bond. It is crucial to remove the contamination prior to adhesive bonding. That makes it necessary to be able to detect and measure the contamination on the substrate's surface. There are many tests to investigate the cleanness of a surface. Not all inspection methods can detect all types of contamination and are not effective for all types of substrates. Chawla [18] gives an extensive summary of multiple tests to study and measure the surface cleanness. The water break test, contact angle measurement, Optically Stimulated Electron Emission (OSEE), XPS, and FTIR are explained more extensively due to their practical importance.

1.4.1) Water Break Test

This method takes advantage of the fact that most contaminants are hydrophobic and cause the water to bead up. In this method, a flow of DI water moves over the surface. If the water channels and beads, it means that there is contamination present on the surface. It is a pass/fail test that can only detect organic contaminants that are not soluble in water and cannot detect inorganic contaminants such as oxide layers. It is not very effective to detect a small amount of contamination.

1.4.2) Contact Angle

Contact angle measurement is a more elaborate version of the water break test. The fundamentals of this test are mentioned on pages 8 & 9. Contaminants have low surface energy

and therefore reduce the surface energy of the substrates. Low contact angle means the surface has high surface energy and free from any contaminant, which forces water to spread and cover a large area. It is possible to establish a threshold for an acceptable contact angle to achieve a particular goal. For example, as a rule of thumb, in the case of applying coating or adhesives, samples with contact angle lower than 25° are acceptable, and the rest go back to the surface preparation step [2]. Plastics naturally have a high contact angle, so this technique is not very suitable for them and is more suitable for metallic substances.

1.4.3) Optically stimulated electron emission (OSEE)

In this technique, the surface emits electron upon being bombarded with UV light. These emitted electrons would be collected by a detector and measured as current. So the substrate should be able to emit electron upon being bombarded with UV light (i.e., it should be photo-emissive). The contamination could increase or decrease the current based on its photo-emissive characteristics, but in most cases, the contaminants are not photo-emissive and therefore reduce the current [19].

The contamination affects the current value in two ways: 1) it reduce the UV light that reaches the substrate, and 2) it attenuate the emitted electrons from the surface. As the thickness of the contamination layer increase, the measured current decrease exponentially [19].

This technique is very sensitive towards the presence of a thin layer of contamination and can measure the thickness of a very thin film (typically less than 15 nm), but it is not suitable for detecting particulate contamination [19]. This technique is quantitative, noncontact, and nondestructive. It can detect both organic and inorganic contamination, such as oxides. The

spatial resolution for this technique is about 10% of the field of view of the sensor [19]. The surface roughness of the substrate can introduce noise into the data, but for the typical roughness that is encountered in the industry, the change in the signal due to the presence of contamination is much more severe than the effect of surface roughness. This technique is very fast and can be mounted on the production line to inspect the cleanness online.

By measuring the current for an ideally clean surface and preparing samples with a known level of contamination (samples with different thicknesses of contamination layer), it is possible to calibrate this technique and measure the cleanness quantitatively.

NASA founded this technique to inspect the cleanness of the outer surface of the space shuttle prior to the bonding of tiles to protect it against high temperature upon reentry. Prior to using OSEE to inspect the cleanness, the lowest level of contamination that was detectable was 100 mg/ 0.1 m^2. That level of cleanness would result in joints with average strength in the range of 1054 Kg/m (59 pounds per linear inch (PLI)). Using OSEE leads to optimizing cleaning processes and gave NASA the capability to monitor cleanness up to 0.25 mg/ 0.1 m^2. The average strength of the joints with this level of cleanness reached 3500 Kg/m (196 PLI), more than a threefold increase [19].

It is possible to detect any moisture, thermal degradation, or thin layers of contamination, such as release agent or hydraulic oil on the surface of CFRP substrates using OSEE [19].

Brune et al. [20] prepare CFRP samples with unfavorable surface states. Samples undergo moisture uptake, thermal degradation, coated with a layer of release agent, and coated with a layer of Skydrol hydraulic oil. A CFRP sample is sanded up to the point of fiber exposure. This

sample shows a very high OSEE signal and is taken as the reference sample with the highest level of cleanness. Their observation states that all the samples with an unfavorable surface state have a lower OSEE signal, so OSEE is effective to distinguish between a compromised surface and an ideal surface. Also, the OSEE signal decreases as the concentration of the release agent on the surface increases.

Parker et al. [21] use OSEE to distinguish between CFRP laminates prepared using different methods. They use as molded substrates containing release agent and then prepare three groups of samples 1) untreated 2) hand abraded 3) grit blasted. They discover that grit blasting is the most successful procedure in removing surface contamination, and the OSEE signal and mechanical strength are highest for these samples. The mode of failure is mainly cohesive in this case as well. The hand abrading show inferior performance compared to grit blasting, and the mode of failure, in this case, is mainly interfacial. The mode of failure for untreated samples is completely interfacial. They deduce that OSEE is an effective test in order to distinguish between a clean surface and a contaminated one, and in order to reach a joint with adequate mechanical performance, the OSEE signal must be higher than %60 of a clean reference substrate.

1.4.4) Electron spectroscopy for chemical analysis (ESCA) or X-ray Photoelectron Spectroscopy (XPS)

In this technique, the surface of the substrate is bombarded with x-ray light. X-ray light excites the atom on the surface and knocks out electrons from the atoms at the top layers of the substrate [18]. Only excited electrons from the top 10 nm of the substrate can escape and be analyzed by XPS, and therefore XPS gives information about the sample's surface, not its bulk

[22]. The number of released electrons and their energy indicate the chemical characterization and the environment that the atom is present in. XPS not only tells us what elements are present on the surface, but it also helps us to determine what chemical functional groups are present on the surface. For example, it tells us that there are C, O elements on the surface and also tells us they are bonded together to create ether, ester, or carboxylic functional group.

1.4.5) Fourier Transform Infrared Spectroscopy (FTIR)

In this technique, the sample is bombarded with IR light, and the reflected light is analyzed. Each chemical bond has an inherent frequency in the range of IR frequency. The IR light excites the bond, and that particular frequency gets absorbed from the reflected light. This technique helps us to determine what chemical functional groups are present on the surface.

1.5) Non-Destructive Tests (NDTs) to investigate the integrity of the joint

One of the biggest challenges facing the widespread use of adhesively bonded joints is the lack of reliable Quality Control (QC) tests to ensure the integrity of the joint. This is the main reason that many engineers are reluctant to incorporate adhesively bonded joints in their structural designs and also leads to a more conservative design when it comes to adhesively bonded joints. There is a crucial need to optimize the current NDTs or come up with new, more reliable NDTs. Some of the main NDTs that are in use today is followed:

1.5.1) NDTs for evaluating the degree of cure

1.5.1.1) Differential Scanning Calorimetry (DSC)

In this technique, a sample (usually 10-30 mg) and a reference material (usually an empty holder) undergo the same temperature ramp, and the difference between the heat-flow is measured [23].

Any physical or chemical change is accompanied by release or absorption of heat and therefore appears as a peak in the DSC curve. The curing reaction is an exothermic reaction, and DSC helps us to determine at what temperature the curing reaction of the adhesive occurs and how much energy is released during the curing process. So the position of the peak gives us the curing temperature, and by comparing the area of the peak with a reference case that underwent full cure, it is possible to determine the level of cure. When a sample is fully cured, no curing peak should appear in the curing temperature range for that adhesive system. In order to determine the level of cure in an adhesive joint, it is possible to remove a small piece of adhesive and perform DSC. If a peak in the curing temperature range of that adhesive system appears, it means that the adhesive is not fully cured. The larger the area of the peak, the lower is the degree of cure [24].

1.5.1.2) Dielectric analysis (DEA)

In this technique, the sample is placed between two electrodes with an opposite electrical charge. In this situation, ions start to migrate toward the electrode with the opposite electrical charge, and the dipoles start to rotate and align to the electrical field. This phenomenon causes an electrical current. Upon applying a voltage, it takes time for ions and dipoles to react to the

applied voltage, which result in a delay in the development of a current. Applying a sinusoidal voltage causes a sinusoidal current with a phase shift (delay). The amplitude of the current wave and its phase shift against the voltage determine the resistance of the system [23, pp. 232-239] & [25].

In the curing reaction, the viscosity of the system increases dramatically, and that restricts the mobility of ions and dipoles, and therefore the resistance of the system also increases. So DEA gives us the opportunity to measure the viscosity indirectly and monitor the curing process by monitoring the change in the viscosity of the system. Initially, upon Applying temperature, viscosity drops due the fact that polymers soften when temperature increases. When temperature reaches the curing temperature, the crosslinking reaction begins and the viscosity increase dramatically. In the end, viscosity reaches a plateau that indicates the complete curing is achieved.

DEA is the best method for in situ monitoring of the adhesive system curing process. It is also a powerful tool for establishing the optimum curing condition in terms of curing temperature, temperature ramp, pressure, etc. For example, monitoring the cure with DEA determined that increasing the pressure from 3 bar to 50 bar in the production line of a Sheet Molding Compound (SMC) increased the final degree of cure and accelerated the curing process [25].

1.5.2) NDTs to detect the presence of flaws in a joint after fabrication

Many types of flaws and defects could be present in an adhesively bonded joint. Volatiles, by-products from the curing reaction, entrapped moisture, etc. could leave the adhesive during the curing process or in the field and leave behind pores. The mismatch between the Coefficient of

Thermal Expansion (CTE) of the adhesive and the substrate could result in the development of residual stress during any thermal cycle. The residual stress can lead to the development of cracks in the adhesive. This would be of more concern in the case of brittle adhesives. When the amount of adhesive or the pressure during the curing is not sufficient, the adhesive will not be able to fully wet the surface of the substrates and leaves voids on the surface. The incorrect mixing ratio between the resin and the curing agent, improper mixing, low temperature and/or pressure during the curing process, non-uniform temperature and/or pressure distribution throughout the bond during the fabrication process can lead to local areas of poor cure in the adhesive. There could be areas that adhesive and substrate are in touch, but there is no bond or a very weak bond between them. This defect is called a “Kiss Bond” (also a kissing bond, or a zero volume debond) [3, pp. 1053-1054]. The nature of a kiss bond is very complex, and much research is underway to study the properties of a kiss bond and factors that contribute to the creation of a kiss bond. A kiss bond could be the result of poor surface treatment, presence of contaminants or inclusions, residual stress from the thermal and/or mechanical mismatch between the adhesive and the substrate, moisture ingress, insufficient curing, chemistry of the adhesive or combination of these factors [26] & [27]. A kiss bond could be a result of a phenomenon called “Amin Blush,” as well. This phenomenon happens in the epoxy resin system with a low molecular weight amine as the curing agent. Amines tend to react with the moisture and CO_2 in the air and create a milky, waxy compound on the surface. This compound hinders the adhesion of the adhesive to the substrate. This phenomenon also consumes some of the amine molecules required for the curing of the epoxy, so it will interfere in the curing process and leads to a lower degree of cure or distribution in the curing degree throughout the bond. Cold temperature favors the creation of

an amine blush because it slows down the rate of the crosslinking reaction, and the rate of the reaction that produces amine blush becomes comparable with the rate of the crosslinking reaction [28].

In order for a bond to be qualified to be referred to as a kiss bond, its mechanical strength should be less than 20% of a flawless reference bond. Plus, the mode of failure should be completely interfacial (adhesive). Finally, it should not be detectable by classical amplitude ultrasonic C-scans [26].

Existence of void in the middle of the bond can have minimal effect on the strength of the joint because most of the load is carried by the edges of the bond and the middle of the bond experience basically no load [29].

Jeenjitkaew et al. investigate the kiss bond extensively on chromic acid etched substrates. They examine the capability of Silicone-based Frekote 700NC, artificial sweat, and cutting oil lubricant in creating a kiss bond. They use SEM/EDS to study the elemental distribution through the bond thickness. They find out that artificial sweat and cutting oil diffuse into the bulk of the adhesive, especially at high curing temperatures and compromise the mechanical performance of the adhesive bulk; however, Frekote 700NC remains on the surface. The mode of failure is entirely interfacial in the case of Frekote 700NC, but it is mixed-mode for the other two cases. Observations from the mode of failure and the failure load determine that only Frekote 700NC can effectively create a kiss bond [27].

Detection of a kiss bond is one of the most challenging problems facing the adhesion industry. Many NDTs are capable of detecting defects that cause a discontinuity in the sample, such as

cracks, voids, etc. In the case of a kiss bond, there is no apparent discontinuity, and that makes it really hard to reliably and efficiently detect a kiss bond. Mainstream NDTs are not capable to detect a kiss bond reliably at the moment [27]. Some of the prominent NDTs to detect defects in adhesively bonded joints are mentioned below:

1.5.2.1) Ultrasonic Test (UT):

This is a routine test to detect debonds, voids, and porosity in the joint. In this technique, the interaction between an ultrasonic wave and the sample is analyzed. "A general rule of thumb is that a discontinuity must be larger than one-half the wavelength to stand a reasonable chance of being detected" [30]. The difference in the acoustic impedance (Z) in an interface between two dissimilar materials determines the ratio of the reflected vs. transmitted sound. The acoustic impedance follows Equation (1-2):

$$Z = \rho v \qquad (1\text{-}2)$$

In this equation, ρ represents the material's density, and v represents the velocity of sound in that material. The ratio of the sound that is reflected from any interface that experience impedance mismatch follows Equation (1-3):

$$R = \left(\frac{z_2 - z_1}{z_2 + z_1}\right)^2 \qquad (1\text{-}3)$$

Therefore, a higher difference in acoustic impedance causes a higher reflection ratio. This is beneficial when it comes to detecting discontinuities embedded inside a solid homogeneous

material. On the other hand, the air has a low density and, therefore, low acoustic impedance, which leads to a significant impedance mismatch between air and most solid samples. That is the primary reason that a coupling medium such as water or a gel is necessary between the ultrasonic transducer and the sample to ensure a higher ratio of the ultrasonic wave penetrates the sample. For example, when a steel sample is submerged in a water tank for a pulse-echo ultrasonic test, 88% of the ultrasonic wave gets reflected from the interface between the sample and the water, and only 12% penetrate the sample. Following the same pattern, in the end, only 1.3% of the initial energy return to the transducer.

Higher frequency means lower wavelength, and as mentioned before, ultrasonic waves with lower wavelength can detect smaller flaws and discontinuity and therefore higher frequency increase the sensitivity of the UT. Higher frequency also improves the resolution of the UT. The drawback of the higher frequency is that the rate of wave attenuation, which is the combination of wave scattering and absorption, is related to the square of the wave frequency. In other words, waves with high frequency cannot penetrate to the bulk of thick samples. The scattering incidences become more frequent and prominent at higher frequencies, and that increases the level of noise in the data as well [30].

The ultrasonic test is categorized under two main subcategories: 1) transmission 2) pulsed-echo.

In transmission UT, a sender and a receiver are placed on both sides of the sample. The existence of flaws that act as discontinuity causes the ultrasonic wave to scatter, attenuating the amplitude of the wave that reaches the receiver. Transmission ultrasonic is easier and more straightforward to interpret, but access to both sides of the sample is not always practically possible.

In the pulse-echo ultrasonic test, a single probe is placed on one side of the sample and works both as a sender and a receiver. Any discontinuity reflects the wave and will show as a pick in the ultrasonic curve. The location of the pick can tell us how deep the flaw is. This technique also commonly is used to precisely measure the thickness of a sample or a film. For a solid sample, the wave reflects from the top and bottom surface, but the presence of a flaw causes a third reflection pick. Knowing the thickness of the sample makes it possible to measure how deep the flaw is located.

Traditional ultrasonic probes need a substance to come between the probe and the substrate to transfer the ultrasonic wave. An improvement to this is to use an elastomeric wheel and slide the ultrasonic probe on the surface of the sample to scan the part [31]. Another advancement in this area is Electromagnetic acoustic transducer (EMAT) probes that use magnetic resonance to create ultrasonic waves and are completely non-contact [30]. This eliminates the need to use a gel or submerge the sample in a medium (mainly water) to perform the ultrasonic test. Submerging the sample in the water tank is not possible for large samples, and the exposure to water has a detrimental effect on some samples such as plastics and FRPs.

1.5.2.2) Sonic and Ultrasonic Vibrations:

In these techniques, the vibrational response of a sample is measured. A flawless sample has higher stiffness, which leads to higher natural frequencies. Also, the existence of a flaw in a sample increases the damping capacity of the sample. Therefore, by comparing the natural frequencies and/or damping of a sample with a reference flawless sample, it is possible to detect the presence of defects such as debond, void, delamination, etc. [32] & [3]

Yang et al. studied the vibrational response of double lap joints with the different sanded bonded areas. They concluded that as the percentage of unsanded areas increases, the system's natural frequency diminishes, and the damping increases [32]. Overall, the damping results showed more sensitivity, and therefore damping could be the characteristic to look at to detect the presence of any flaw.

1.5.2.3) Tapping (coin test):

In this test, the sample is taped with a coin or a hammer, and the sound is analyzed. It is a qualitative and subjective test that relies on the experience and expertise of the operator. For a good bond, the sound is crisp and with high pitch, but for a bond with flaws, the sound is dull [3]. Also, if the hammer is equipped to measure the returned force, the force is higher and sharper for a good bond. Cawley and Adams extensively explain the mechanics of the coin-tap method [33].

1.5.2.4) Thermal methods:

Thermography: Any discontinuity would decrease the rate of thermal diffusion, so by heating a surface of the joint and monitoring the temperature profile on both surfaces, it is possible to detect discontinuities [3]. The heating source could be a heat lamp, optical flash lamp, ultrasonic excitation, etc. The temperature mapping could be done with a highly sensitive IR camera [28]. If we look at the surface that is heated, the points with discontinuity appear hotter. On the other hand, if we look at the other surface, points with flaws appear cooler. It is better to monitor the temperature of the surface over a period of time (for example, 500ms) to increase the accuracy and resolution [3]. This technique is best suitable for flaws that are close to the surface (a few

mm deep [28]). As the flaw gets further away from the surface that is heated, the sensitivity of this technique goes down. This technique can be performed by pulsed or continuous heating. Schroeder et al. [34]used pulsed thermography to detect an area of debond in the sidewalls of a composite pick-up truck.

Vibrothermography: This technique is closely similar to thermography. In this technique, the sample undergoes cyclic loading. The internal friction and energy dissipation is higher in the vicinity of defects, and therefore, upon applying cyclic loading, the temperature would rise around the defects. It is possible to capture these hotspots by using a high-resolution IR camera [32].

1.5.2.5) Visual inspection:

Visual inspection of the adhesive fillet can give us valuable information. If the fillet is porous, it could mean that the rate of temperature increase during curing was too high or moisture was present in the joint. Lack of any fillet could be related to inadequate pressure during the curing process. The angle between the fillet and the substrate is formed when the adhesive could flow. So it is a good representative of the contact angle of the substrate, which could determine if there was any contamination on the surface [35] & [3].

1.5.2.6) Novel Technique by Bossi and coworkers at Boeing

In this technique, a laser beam is focused on the joint to break any weak (kiss) bond between the adhesive and the substrates. Subsequently, these areas of debonding are detected using conventional methods such as ultrasonic [36]. This technique is still at the R&D level, and it is not possible to state with full confidence that this technique is truly nondestructive yet [28].

1.5.2.7) Shearography:

In this technique, a shearography camera takes two interferometric photos from a surface, first in the unloaded stage as the reference point and 2nd after applying stress that causes out-of-plane displacement. The stress could be as a result of applying heat, pressure, vibration, and vacuum [28] & [37]. Upon heating, the sample wants to expand, and the existence of flaws would enable the sample to expand even more. It is possible to interpret this technique as determining a relative topography between unloaded vs. loaded cases. By comparing and subtracting the two photo, the flaws would appear as hills, and the size of the hills are related to the size of flaws [37].

Hung [38] was able to detect multiple delaminations in a composite honeycomb panel using shearography by applying a partial vacuum.

1.5.2.8) Quantitative Percussion Diagnostics (QPD):

In this technique, a probe is accelerated by an electromagnetic coil to a specific speed and then tap the sample, creating a propagating stress wave. A force sensor is placed on the top of the probe to measure the amount of the returned force over time. In this test, the probe always has constant kinetic energy before hitting the sample, and by measuring the amount of returned force, it is possible to determine the damping (energy dissipation) characteristics of the sample [39]. The QPD instrument perform 16 impacts in 4s and transfer the force vs. time data to a computer. The computer analyzes 10 of these impacts. Each percussion takes around 0.6 ms, which corresponds to the vibrational loading frequency of 1700 Hz, and the amount of force that it applies to the material is around 5N [40] & [41].

The fundamental equations related to the QPD that are mentioned below are adapted from [40]. The damping characteristics of any material could be characterized by loss coefficient (η), which is given by Equation (1-4):

$$\eta = \left(\frac{1}{2\pi}\right)\frac{D}{U} \qquad (1\text{-}4)$$

Here, U is the total strain energy, and D is the amount of dissipated energy. The loss coefficient is usually measured through cyclic loading, and therefore the 2π denominator is to normalize the result per radian. In the QPD test, the total strain energy is assumed to be equal to the kinetic energy (E_k) of the probe prior to the collision. Upon collision, the elastic strain energy is returned to the probe (E_s). Assuming no other source of energy dissipation other than the sample, the dissipated energy (D) would follow Equation (1-5):

$$D = E_k - E_s \qquad (1\text{-}5)$$

Substituting D into the pervious equation will lead to Equation (1-6):

$$\eta = \frac{1}{2\pi}\left(1 - \frac{E_s}{E_k}\right) \qquad (1\text{-}6)$$

Where

$$E_k = \frac{1}{2}mv^2 \qquad (1\text{-}7)$$

And

$$E_s = \frac{1}{2}\left(\frac{\sigma^2}{E}\right) = \frac{1}{2}\left(\frac{m^2a^2}{A^2E}\right) \quad (1\text{-}8)$$

Here, m is equal to the mass of the probe, A is the cross-sectional area of the probe, E is the elastic modulus of the probe, a is the maximum acceleration of the probe as a result of the stress wave, and v is the velocity of probe prior to the collision. The accuracy of this test would further improve by incorporating a factor to account for other sources of energy dissipation other than the sample (D_p). In this case, the amount of dissipated energy by the sample (D) would be as Equation (1-9):

$$D = E_k - E_s - D_p \quad (1\text{-}9)$$

It is possible to determine the D_p by comparing the damping values from QPD and the literature [40]. Brenner and Earthman successfully used the QPD to measure the damping capacity of multiple materials [40]. Lincoln et al. used QPD to investigate the damping response of composite sandwich structures [41]. Figure 1-5 shows the QPD instrument [28].

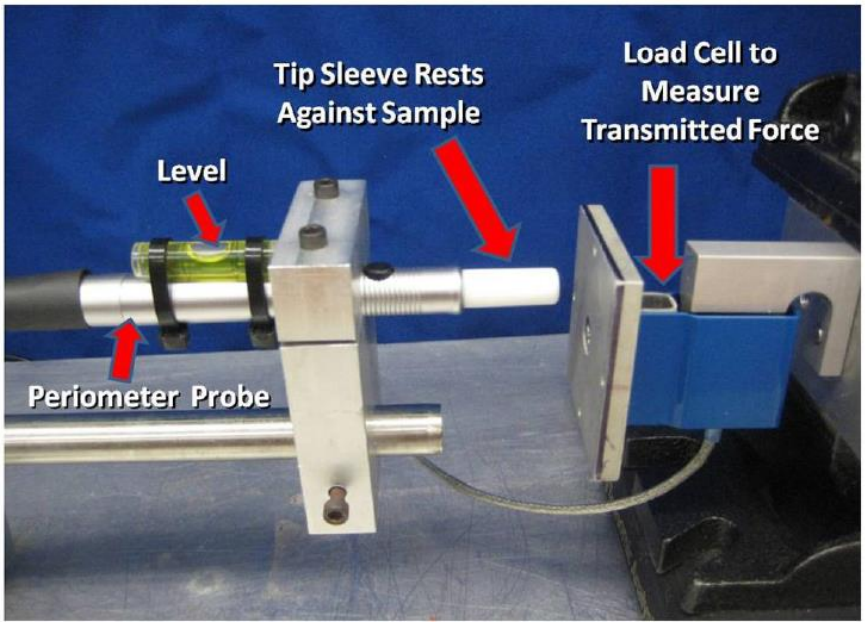

Figure 1-5: QPD Instrument [42] & [28] (reprinted with permission)

The existence of the flaws in the sample increases the energy dissipation in the sample due to the increase in internal friction and scattering and attenuation of stress waves. So, for a sample with internal flaws, the amount of damping or loss coefficient increases, and consequently, the amount of returned force (energy) decreases. The internal friction increase as the result of the movement of crack and delamination surface. Also, in the FRP samples, flaws like the breaking of fibers transfer more load to the polymeric matrix that inherently has more damping characteristics. Fiber sliding can also dissipate energy and contribute to the increase in the loss coefficient of the sample [28].

For a perfect solid sample without any crack, the response curve is symmetrical, and it has only one pick. The existence of any discontinuity like a crack changes the shape of the response curve. In this case, more than one pick is present, or in some cases, the shape of the response curve is

not symmetrical. Figure 1-6 illustrates the difference between the QPD result of a flawless sample (left) and a sample with discontinuity (right).

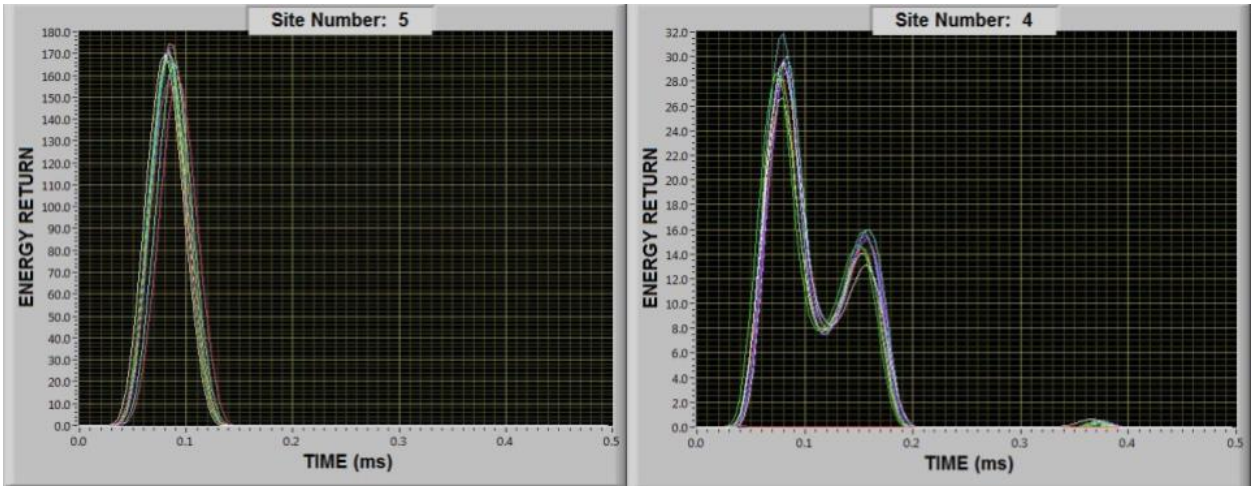

Figure 1-6: Left) QPD result for a flawless sample, Right) QPD result for a sample with a discontinuity (crack, debond, etc.)

When there is a discontinuity in the material such as a crack, debond, or delamination, the closure of the crack causes a 2nd pick, as in the right figure above. In the case of a kiss bond, there is no discontinuity in the material, so it is almost impossible to get a result with more than one pick. In this case, the value of the maximum energy return and energy dissipation could determine the presence of a kiss bond. By statistically comparing the maximum return energy and energy dissipation between a sample and a flawless reference sample and calculating the p-value through t-test, it is possible to distinguish between a sample with a kiss bond and a sample with a well bond. If the p-value is less than 0.05, it means that there is a significant difference between the two sets of data (the p-value limit could be taken as 0.02 to be more sensitive).

Two useful data from the QPD test are Stability Index and Defect Severity Quotient (DSQ). The stability index is proportional to the maximum energy return. Higher stability index indicates that the sample has a lower damping. The DSQ is proportional to the area between the QPD result data and the ideal symmetric bell shaped response. Lower DSQ means that the result deviates less form the ideal symmetric response.

Poveromo et al. [42] study the capability of QPD to distinguish between samples with a kiss bond and samples with a well bond. They manufacture a kiss bond between CFRP laminates by using a release agent. They also manufacture well-bonded samples following the ideal preparation guidelines. They use QPD to measure the loss coefficient and the amount of transferred force to the other side of the bond. They discover that for samples with a kiss bond, the loss coefficient is generally higher. On the other hand, the amount of the transferred force to the other side of the bond is generally higher for well-bonded samples. They concluded that QPD shows some promising sign that it can distinguish between samples with a kiss bond and well-bonded samples.

Stanly et al. [43] use QPD to investigate the evolution of damage in carbon fiber/epoxy laminates with the increase in impact energy. They find out that the loss coefficient and, therefore, the damping of the sample increase as the level of damage increases.

2) Design

A Single Lap Joint (SLJ) is one of the most popular choices for investigation, among other joint configurations. In many cases, SLJ represents real applications more than other joint configurations. Also, the peel stress in SLJ is higher than other joint configurations due to higher eccentricity, so it can represent a worst-case scenario. The typical procedure to fabricate single lap joints (SLJs) with metallic substrates is to use different shims to control the thickness of the bondline and fix the sample in place during the curing process [44]. Another approach to control the thickness of the bondline is to mix the adhesive system with glass beads with known diameter. Another approach is to use an adhesive film instead of an adhesive paste. This approach has been taken as the desired approach in this project. The sample could then be placed in a hot press for curing. It is also possible to place the sample in a typical furnace/oven and place some weight on top of the sample. This technique only works when the adhesive system needs low pressure for curing. In practice, most structural adhesive systems need high temperatures and pressure to achieve a high level of cure and low void content; therefore, hot press and ideally autoclave is the most suitable option. The drawback of using an autoclave is its high acquisition and operation cost, and that is why autoclave is not always readily available.

In this study, adhesive film AX-2116N-0.085 (0.085 pounds per square foot (psf)) with a Nylon knit carrier by AXIOM Materials has been used. The optimum curing condition for this adhesive system is 2 hours at 121°C [250°F] or 1 hour at 177°C [350°F]. The appropriate pressure range for curing is between 0.21-0.34 MPa [30-50 psi]. Ideally, an autoclave is necessary to fabricate an SLJ with this adhesive system, but as mentioned before, an autoclave is not readily available. The samples were fabricated in a typical oven, and different methods were used to apply pressure.

In order to mount an SLJ sample in typical tensile grips, it is necessary to use tabs with appropriate thickness to make the whole assembly symmetrical.

2.1) First Grip Design

The project's initial goal was to investigate the presence of flaws in the SLJs among CFRP substrates. CFRP laminates have low compressive strength through the thickness and easily get crushed by clamping forces. The traditional grips use a compressive clamping force to prevent samples from sliding during the tensile test. The clamping force evolves as the test progress to make sure that the sample does not slide. CFRP laminates would be crushed under this clamping force, and that would introduce error in the integrity of the test result. That is why a new grip design that does not put any clamping force on the laminate was necessary. Figure 2-1-Figure 2-4 depict the initial design of the grip.

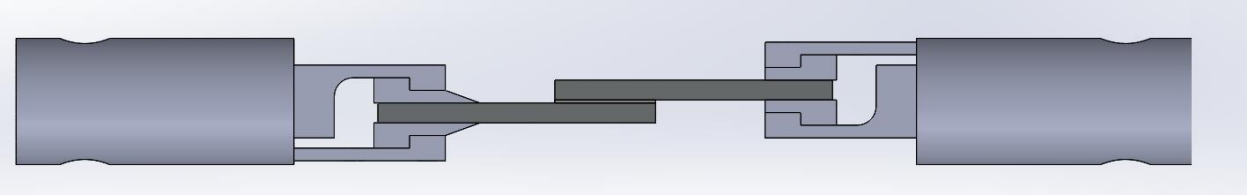

Figure 2-1: 1st Grip design, whole assembly

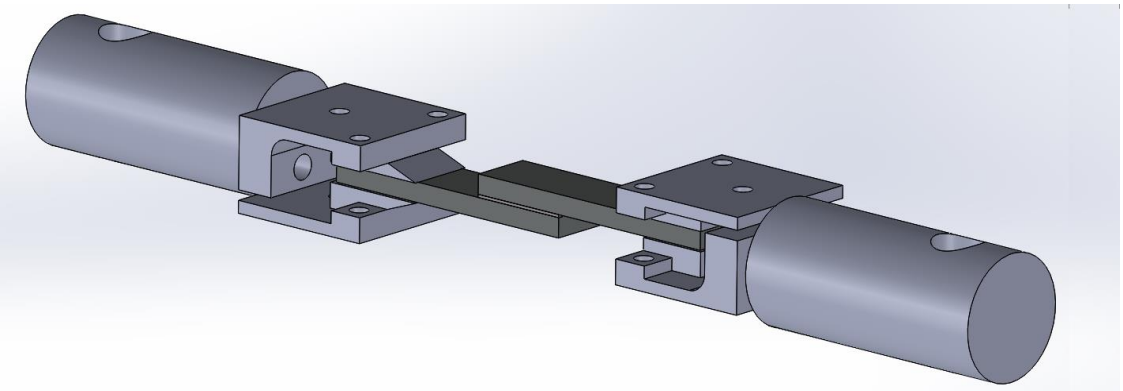

Figure 2-2: 1st Grip design, whole assembly

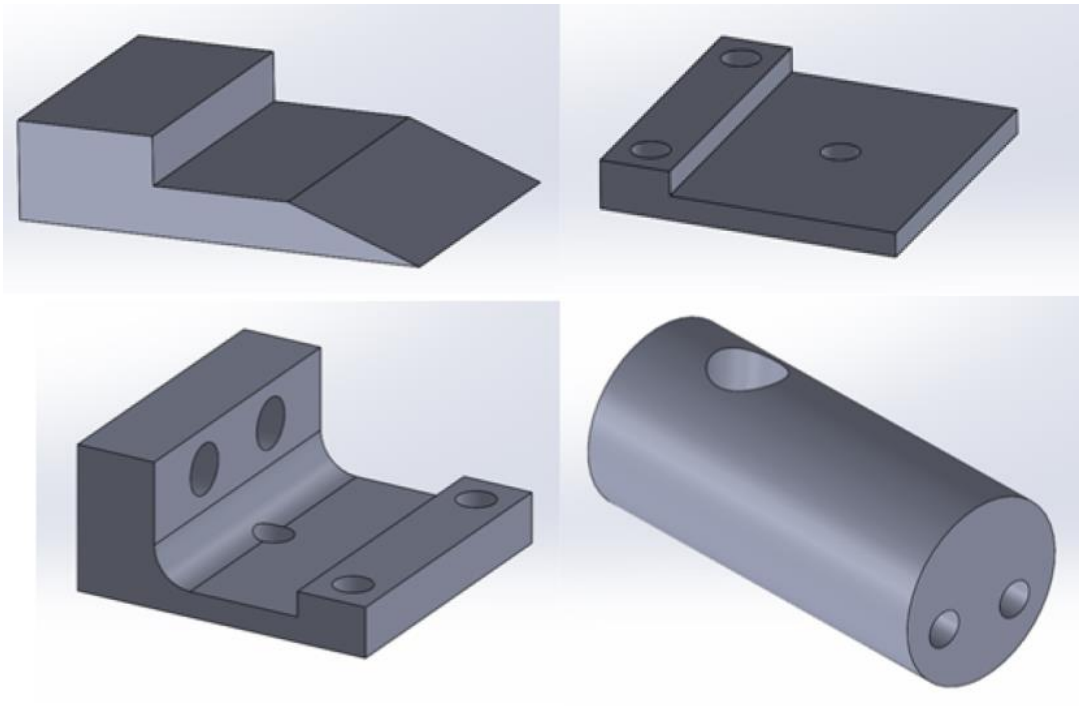

Figure 2-3: Top Left: Part 1, Top Right: Part 2, Bottom Left: Part 3, Bottom Right: Part 4

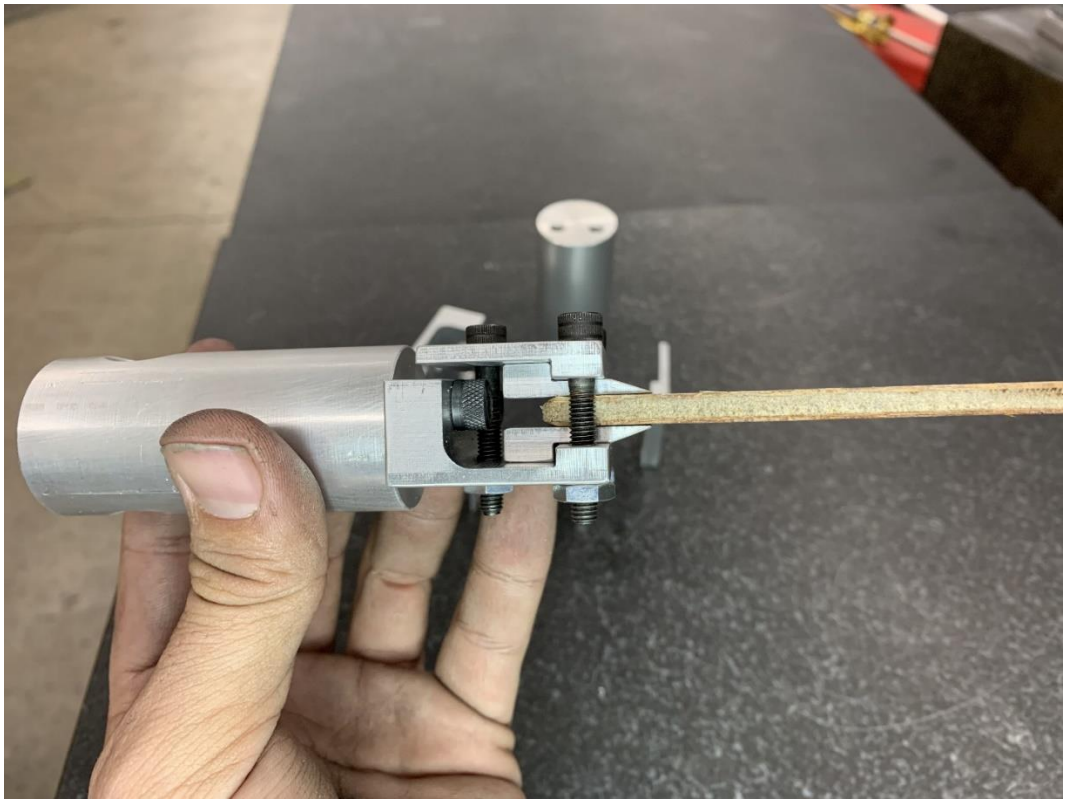

Figure 2-4: 1st grip design, actual machined assembly

The grip was machined using aluminum. The maximum load in the tested samples surpassed the estimated 5 KN derived from FEM and reached around 9 KN (the detail of the samples' results will be discussed later). In practice, the stress in the grip passed the yield strength of the aluminum and resulted in plastic deformation and excessive bending in the grip. Figure 2-5 depicts the condition of the grip after it went through a couple of tests.

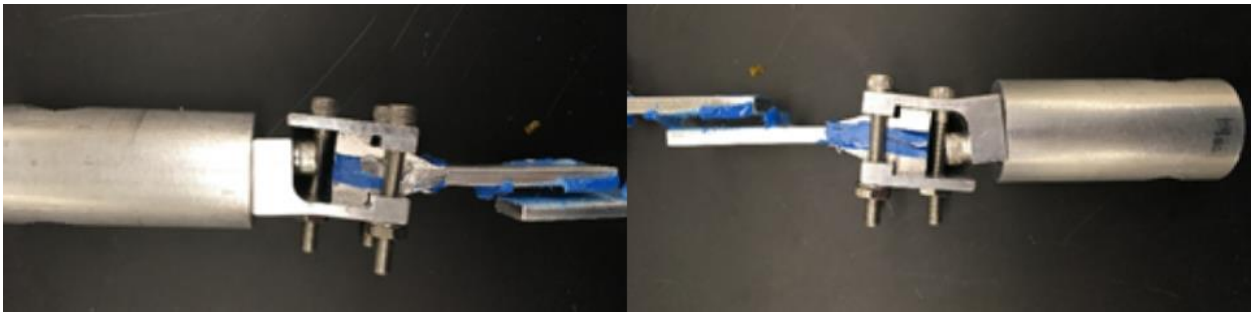

Figure 2-5: Deformed Grip after multiple test

2.2) Second Grip Design

It was necessary to optimize the design. In the 2nd iteration, the thickness of parts 2 and 3 increased. Also, a threaded hole was incorporated in part 3 to be used to connect parts 2 and 3. Additional nuts were also incorporated to work alongside the threading to ensure that the bolt does not strip and completely prevent the assembly from excessive bending. Figure 2-6- Figure 2-8 depict the second iteration.

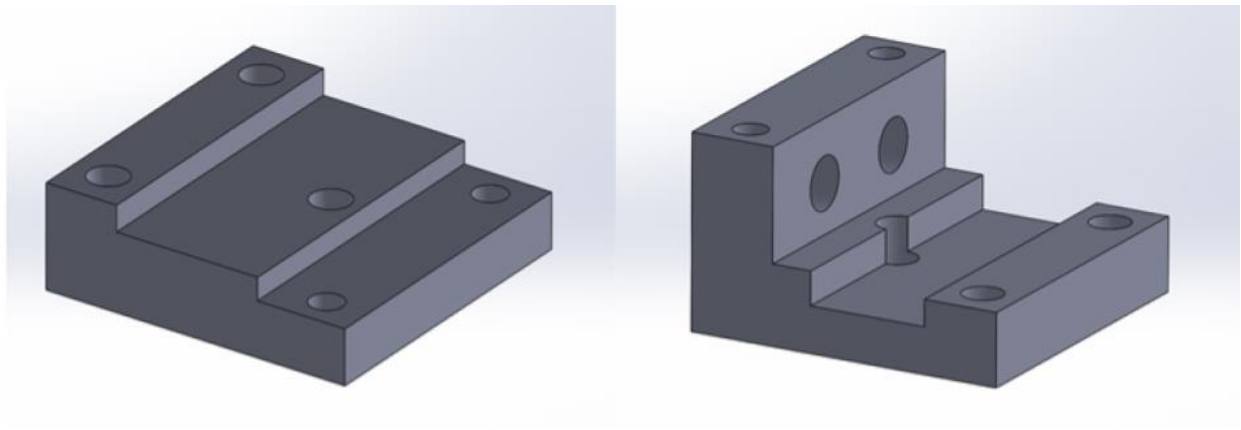

Figure 2-6: 2nd grip design: Left: Part 2, Right: Part 3

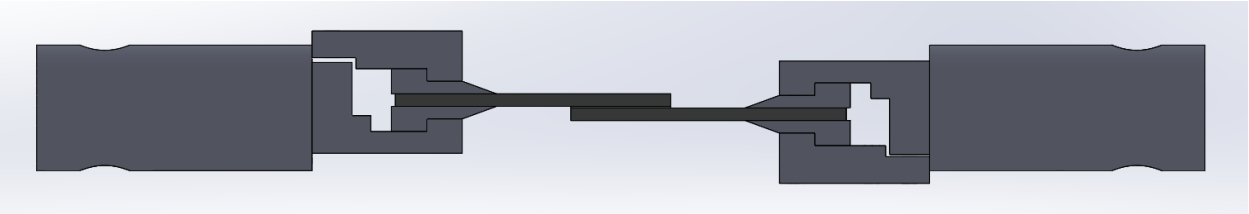

Figure 2-7: 2nd grip design, the whole assembly

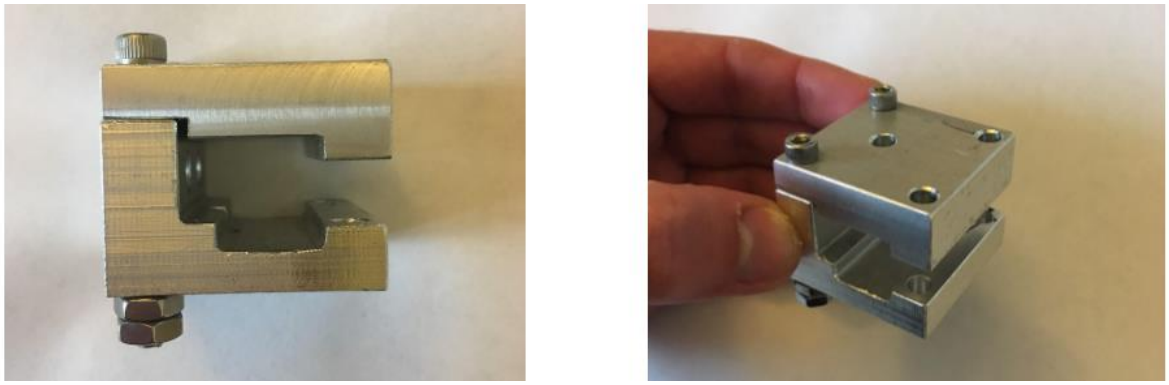

Figure 2-8: 2nd grip design, final machined part

2.3) Holder

It is crucial to fix the substrates during the curing process. It is also necessary to apply pressure to ensure adequate curing in the adhesive. All of these factors pushed me to design a holder to holds the sample during curing. Figure 2-9 & Figure 2-10 depict the design for a holder.

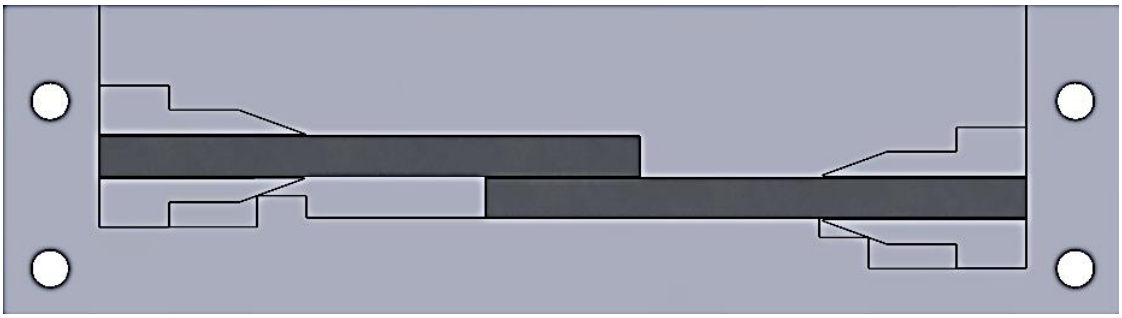

Figure 2-9: Holder assembly

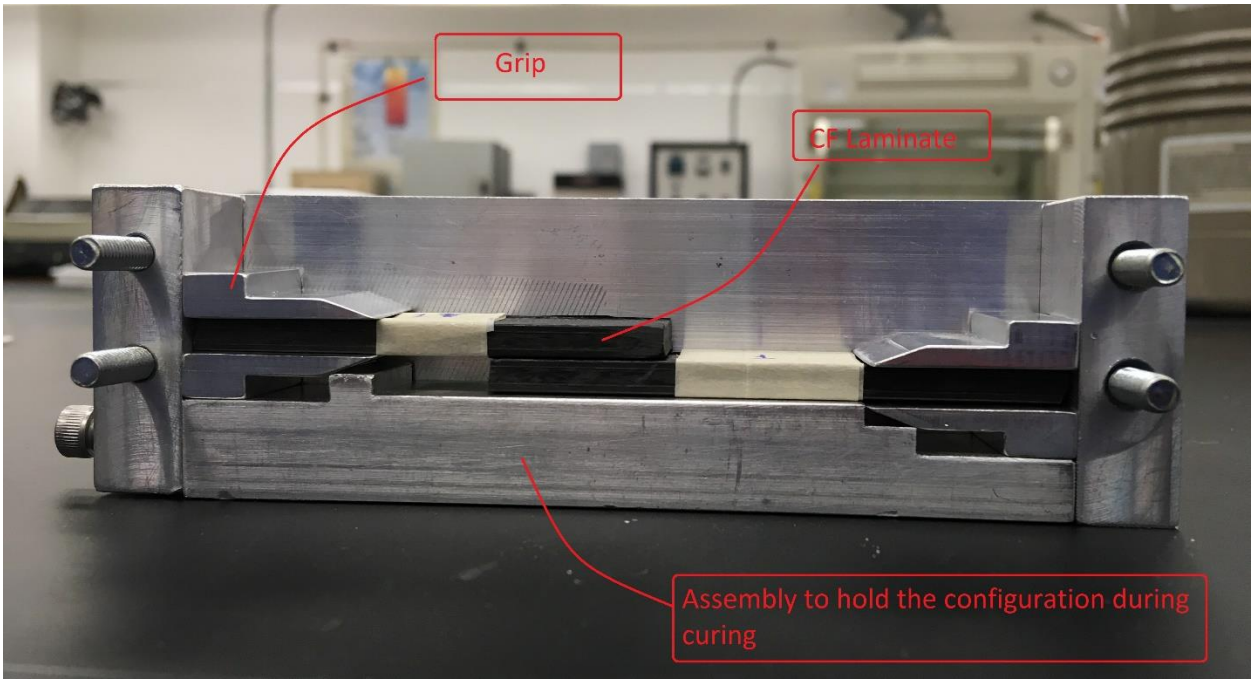

Figure 2-10: Holder assembly

C-clamps had been used to apply pressure on the bondline to satisfy the curing requirements of the adhesive system. Figure 2-11 depicts a sample with high-temperature cure.

Figure 2-11: C-clamps to apply pressure

This turned out not to be an effective method. Upon raising the temperature, the adhesive starts to flow under pressure from the C-clamp. As the adhesive flow, the adhesive layer's thickness goes down, causing the whole assembly to recede. Even a couple of micrometer descending means the surface that used to be in contact with the clamp is no longer in touch with it, and therefore, no clamping force is inserted on the bond.

2.4) Holder for multiple sample at the same time

A new holder was designed to solve this problem and also give the possibility to fabricate multiple samples at the same time. Figure 2-12-Figure 2-16 depict the improved holder design.

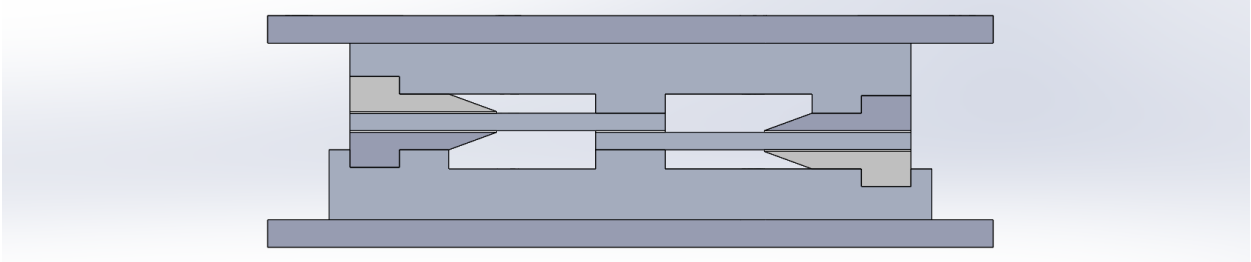

Figure 2-12: Holder for multiple samples, the whole assembly

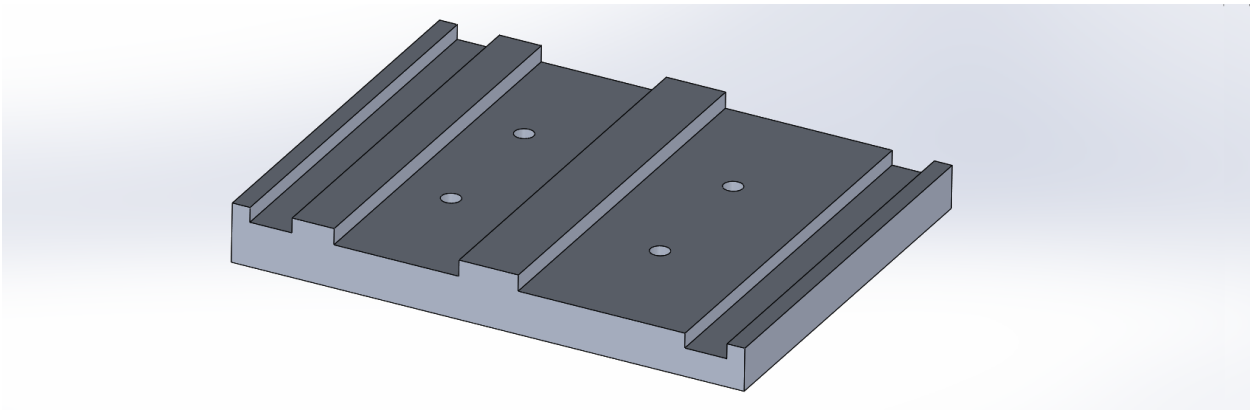

Figure 2-13: Main part of the holder

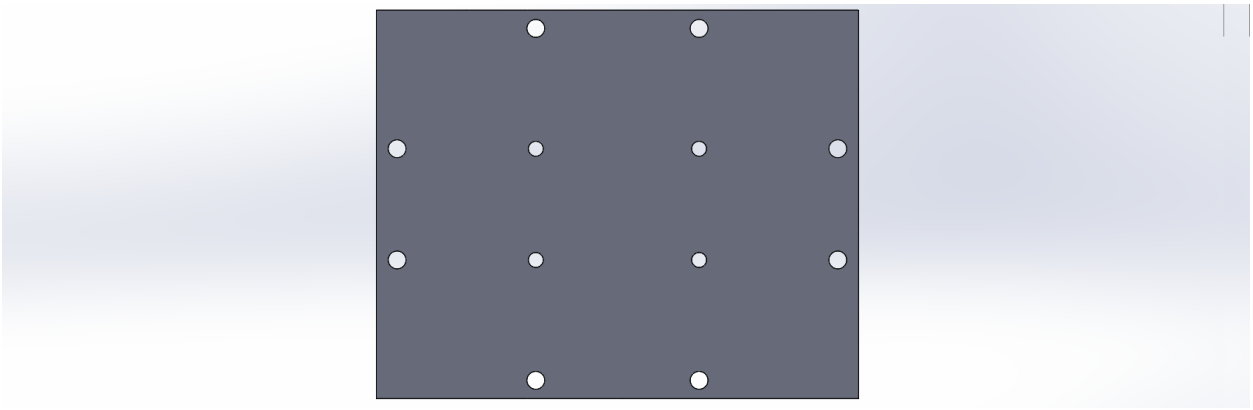

Figure 2-14: Bottom Plate

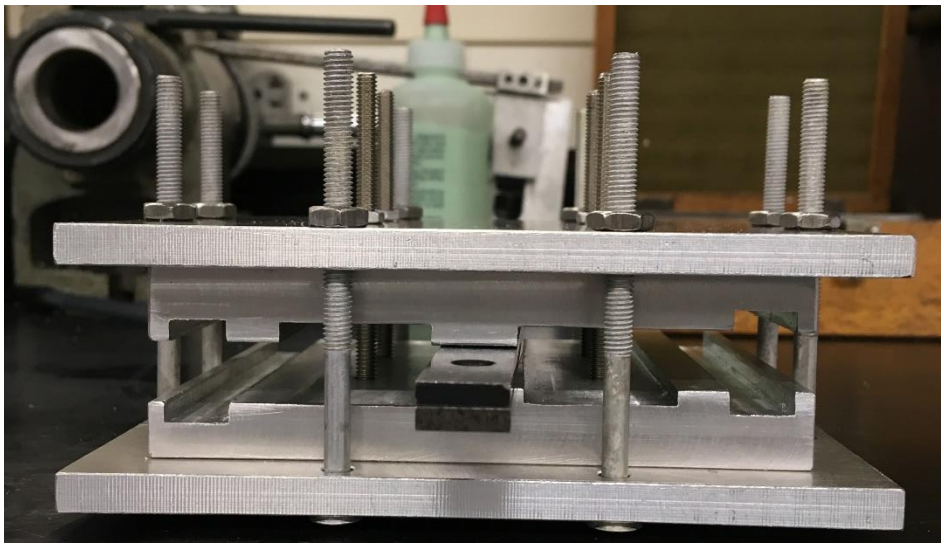

Figure 2-15: Holder for multiple samples, machined part

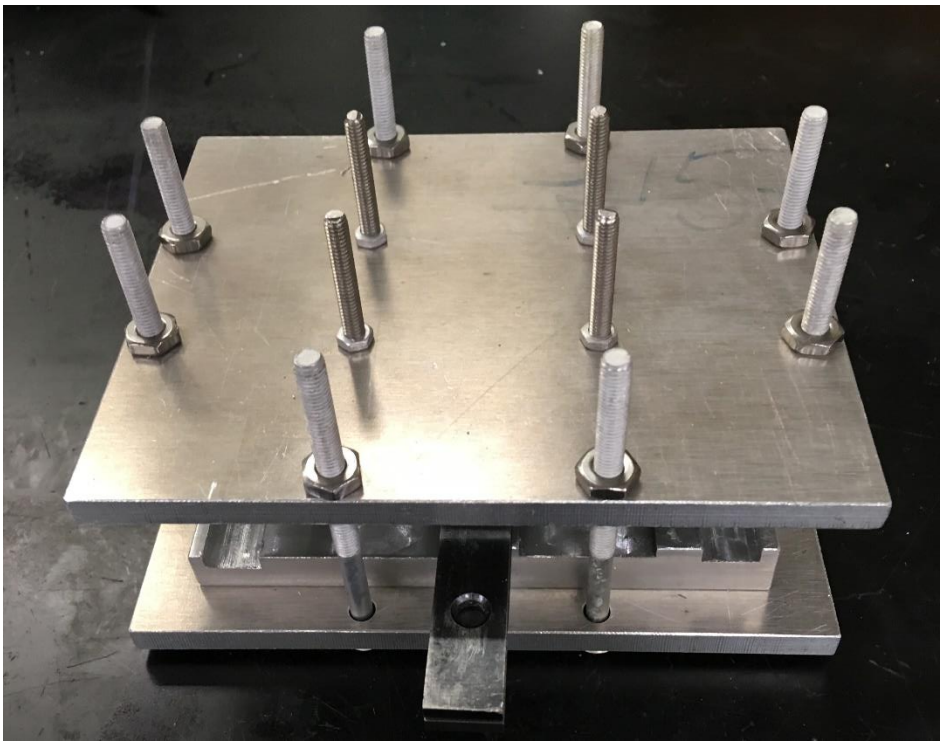

Figure 2-16: Holder for multiple samples, machined part

Using compression spring would ensure that the bond experience almost constant pressure throughout the curing process and also gives good repetitive reliability because the amount of force is equal to the maximum force capacity of the spring. This is the best that is possible to fabricate a bond in a typical furnace instead of using an autoclave.

2.5) Stepped Joint Design

Due to the lack of CFRP substrates and also lack of time, I decided to use only aluminum substrates, and therefore the aforementioned designs for grip and holder were not necessary. I also decided to fabricate stepped joints, which made it possible to use typical tensile grips without the need for any additional accessories due to the fact that in the stepped joint, two forces are in line. Figure 2-17-Figure 2-21 depict the stepped joint design.

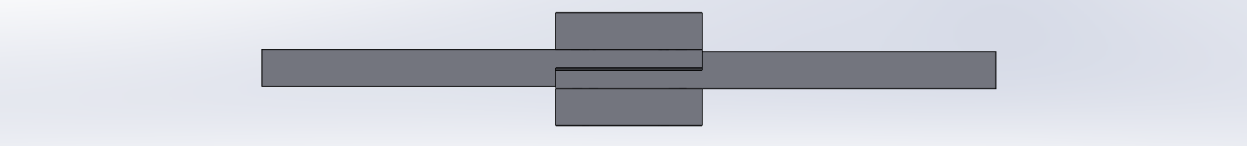

Figure 2-17: Stepped Joint Design

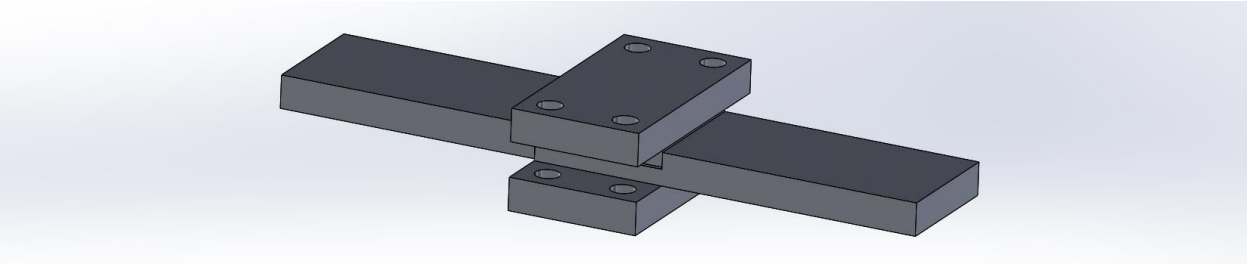

Figure 2-18: Stepped Joint Design

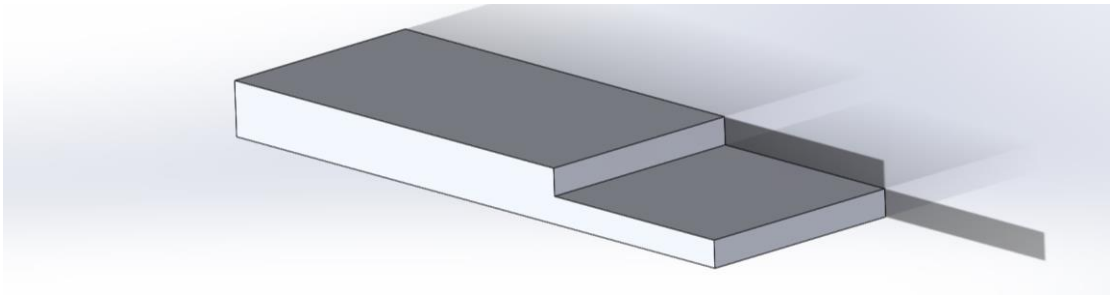

Figure 2-19: Coupon for the Stepped Joint Design

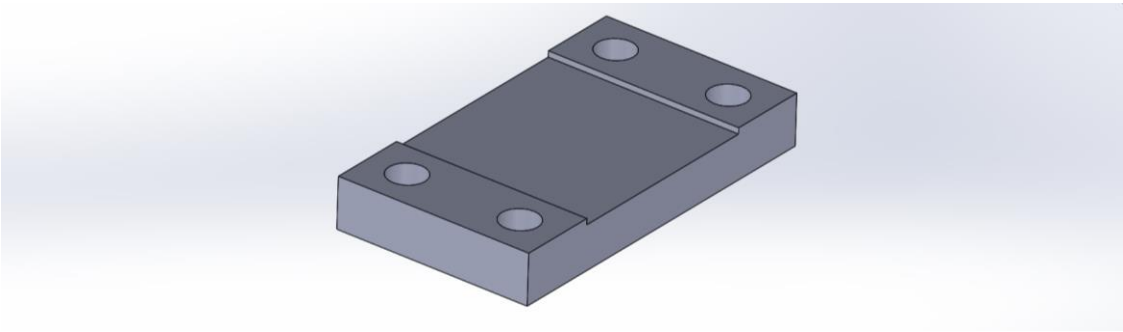

Figure 2-20: Holder for Stepped Joint Design

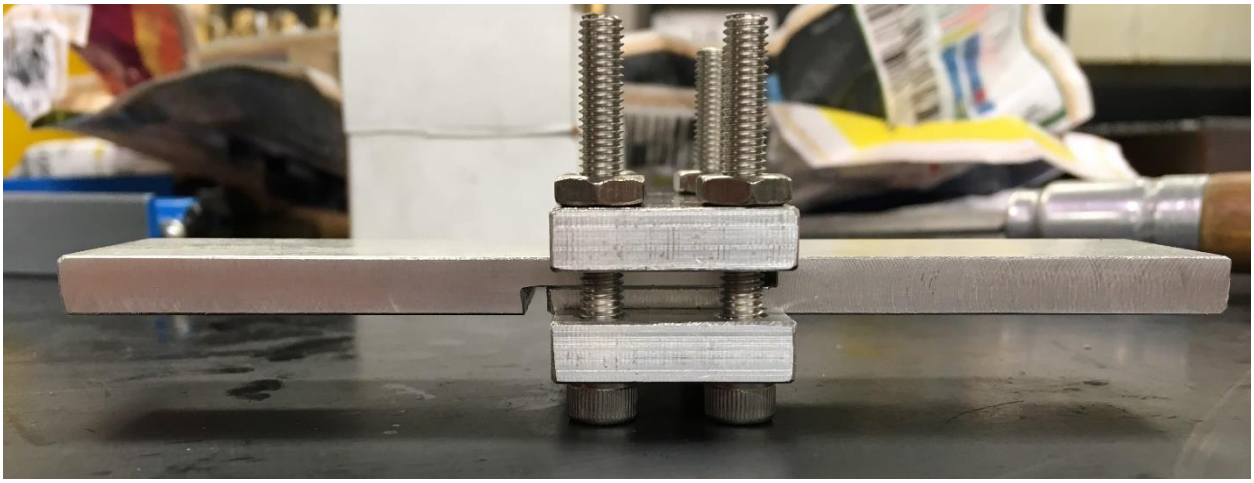

Figure 2-21: Stepped Joint Design, the whole assembly

To create a partial flaw in the bond, only a partial area of the bond needs to be covered with the release agent. In order to do that, multiple masks that cover different area percentages were designed (80, 53, 35% released area). Figure 2-22 depicts the designs for these masks.

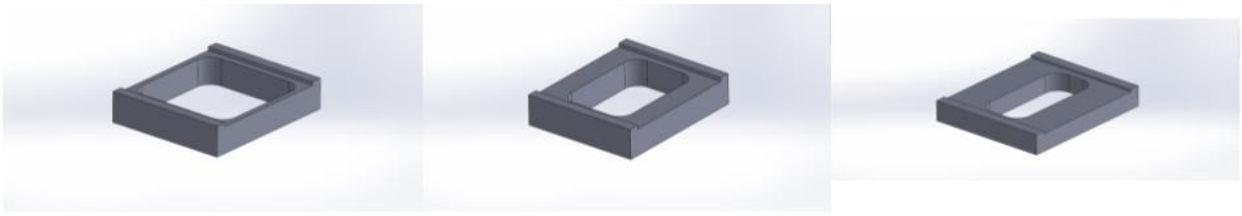

Figure 2-22: Left) 80% - Middle) - 53% - Right) 35%

Compression springs were used to apply a constant pressure over the bondline during the cure. Figure 2-23 depicts a sample. Aluminum foil is used as release film to facilitate the demolding.

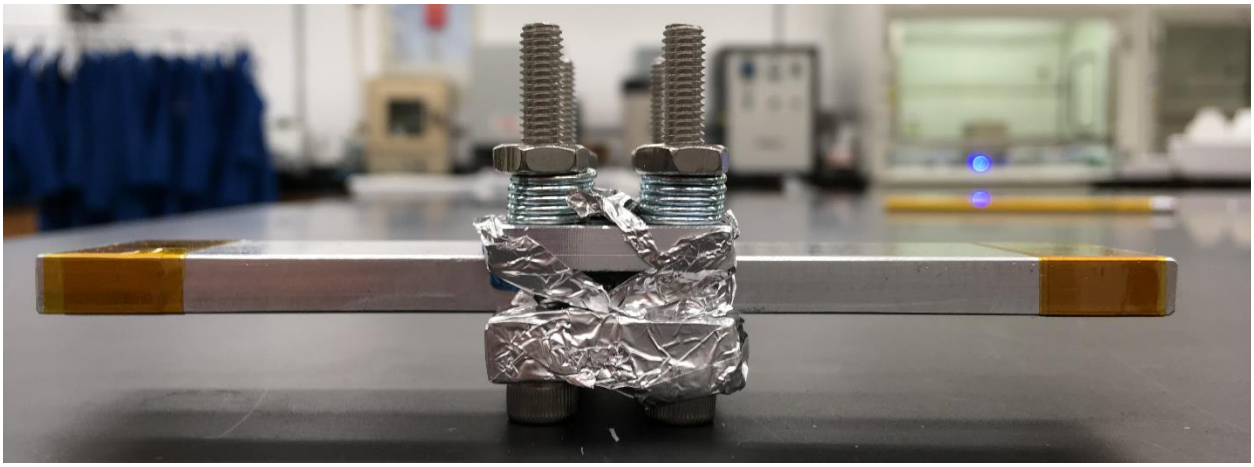

Figure 2-23: Stepped joint assembly for curing process

3) Single Lap Joint (SLJ) Samples

Surface preparation:

- Substrates were hand abraded using a 120 grit sand paper.
- Substrates were solvent wiped with acetone and KIMTECH wipe
- Substrates were solvent wiped with propanol and KIMTECH wipe
- Finally, Substrates were solvent wiped with acetone and KIMTECH wipe [5]

SLJs made with aluminum substrates and AX-2116N adhesive film by AXIOM Materials. Table 3-1 summarizes the dimensions for theses samples.

Table 3-1: Dimensions for SLJ samples

	Length, mm [in]	Width, mm [in]	Thickness, mm [in]
Substrate	58.42 [2.3]	16 [0.63]	5.08 [0.2]
Adhesive	28-30 [1.102-1.18]*	16 [0.63]	Case by case

*bondline overlap

Samples were cured at 177°C [350°F] for 1 and a half hours. After the mechanical test, in order to remove part 1 for the following samples, the sample was cut using a band saw to remove the bond surface for the archive, and then the substrate and part1 were put in a furnace at 450°c for 1 hour in order to degrade the epoxy and turn it to graphite. Following this step, it was dismantled and then put in a DI water container in an ultrasonic dissolver in order to get rid of the excess graphite. The solvent then labeled and discarded in a liquid waste container. Subsequently, the surface of part 1 was polished for future samples. Figure 3-1 shows part 1 before polishing.

Figure 3-1: Residue from adhesive on the Grip after thermal degradation

3.1) Sample 1 (Well Bonded)

Figure 3-2 depicts the Load vs. Displacement graph for this sample. The displacement rate for this test was 0.1 mm/min.

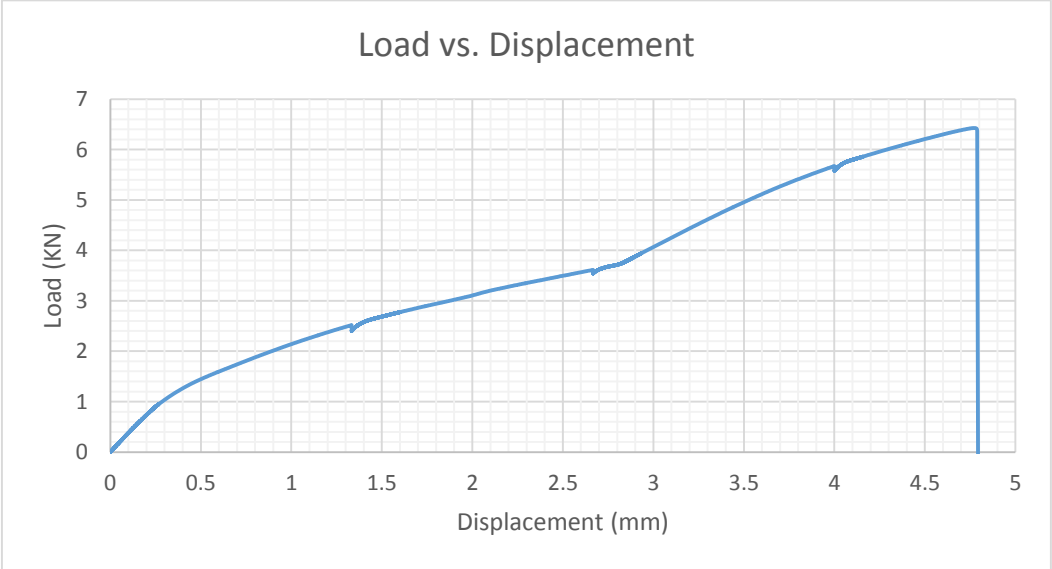

Figure 3-2: SLJ: Sample 1-Load vs. Displacement

Figure 3-3 depicts the fracture surface for this sample. As mentioned in Figure 1-2, the rough fracture surface and the appearance of both adhesive and the substrate at the same time, indicate a mixed-mode of fracture, which is representative of a well bond. Figure 3-4 depicts the fracture surface which is captured by an optical microscope.

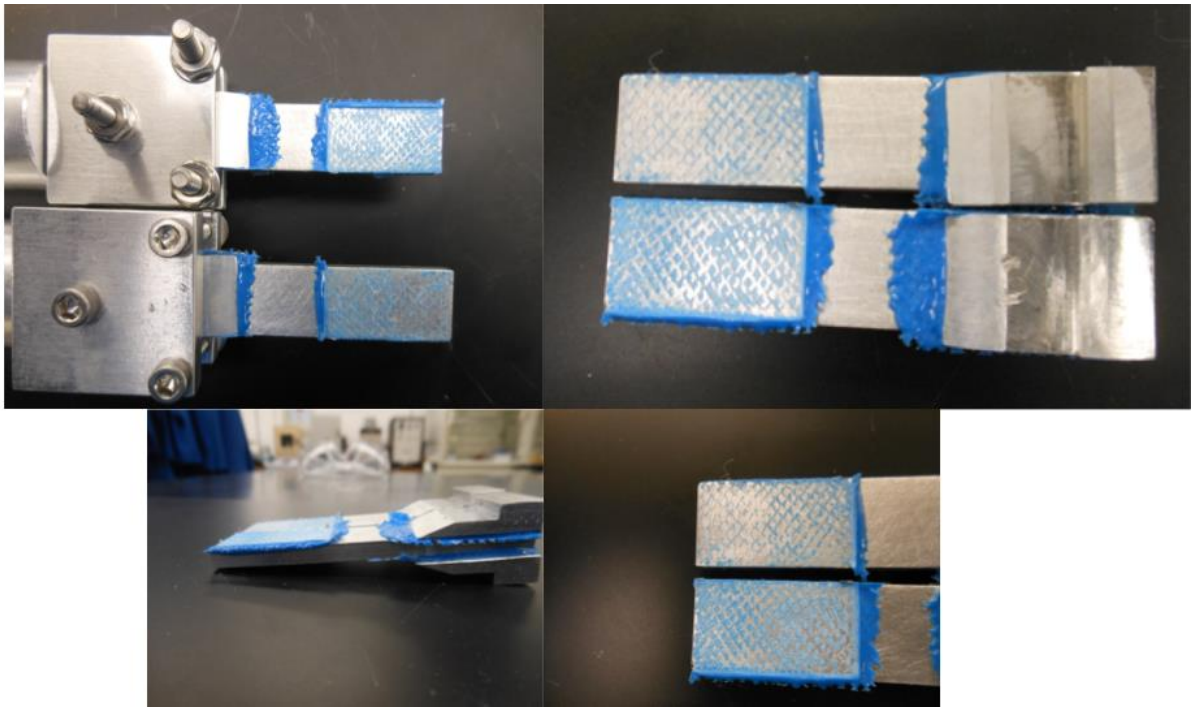

Figure 3-3:SLJ-Sample 1-Fracture Surface

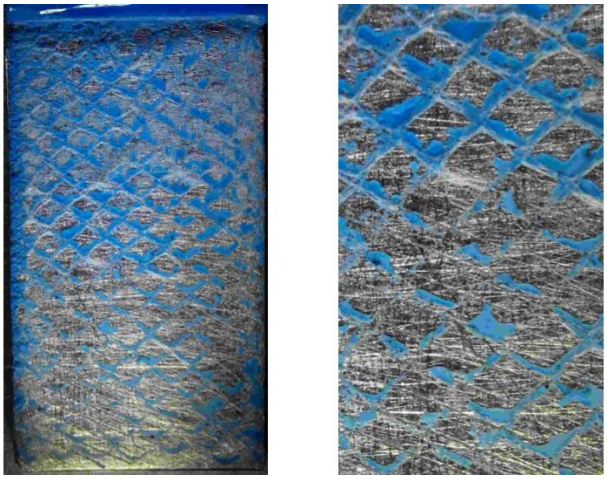

Figure 3-4: SLJ-Sample1-fracture surface which is captured by an optical microscope

3.2) Sample 2 (Well bond)

Figure 3-5 depicts the Load vs. Displacement graph for this sample. The displacement rate for this test was 0.1 mm/min.

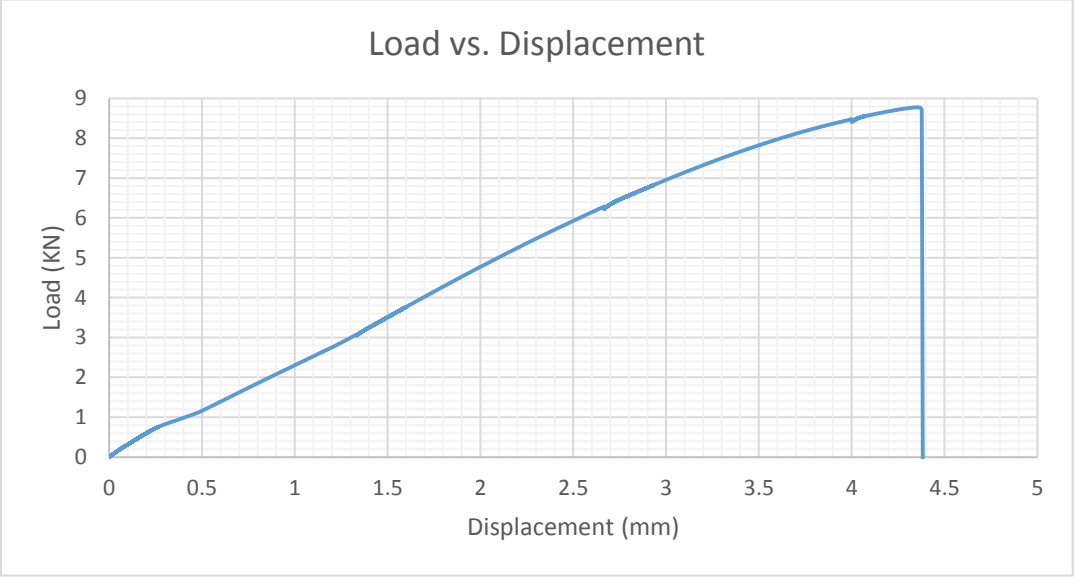

Figure 3-5: SLJ-Sample2-Load vs. Displacement

Figure 3-6 depicts the fracture surface for this sample. As mentioned in Figure 1-2, the rough fracture surface and the appearance of both adhesive and the substrate at the same time, indicate a mixed-mode of fracture, which is representative of a well bond.

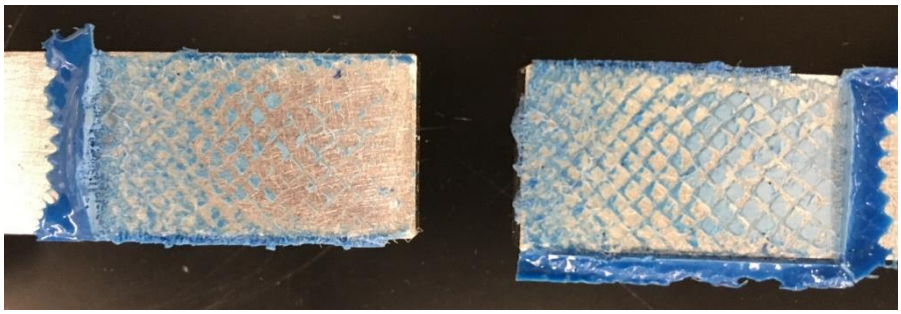

Figure 3-6: SLJ- Sample 2-Fracture Surface

3.3) Sample 3 (Well bond)

The surface of the substrates for this sample were roughened by machining the surface. QPD test was performed on this sample on three locations through the bondline, before the mechanical test and during the test in 10 min intervals. Figure 3-7 depicts the Load vs. Displacement curve for this sample. The displacement rate for this test was 0.1 mm/min.

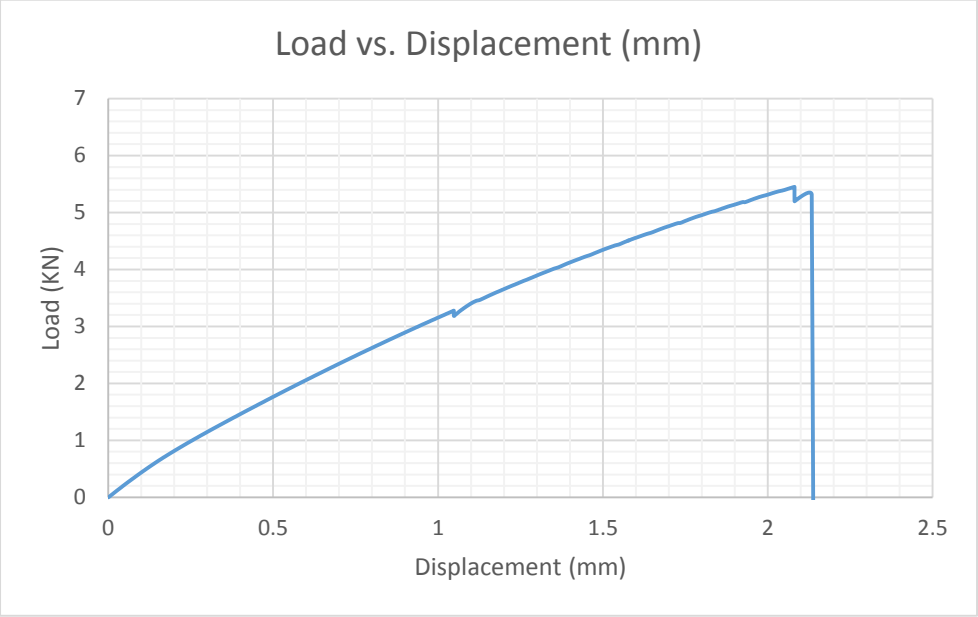

Figure 3-7: SLJ- Sample 3-Load vs. Displacement

Figure 3-8 depicts the fracture surface for this sample. As mentioned in Figure 1-2, the rough fracture surface and the appearance of both adhesive and the substrate at the same time, indicate a mixed-mode of fracture, which is representative of a well bond.

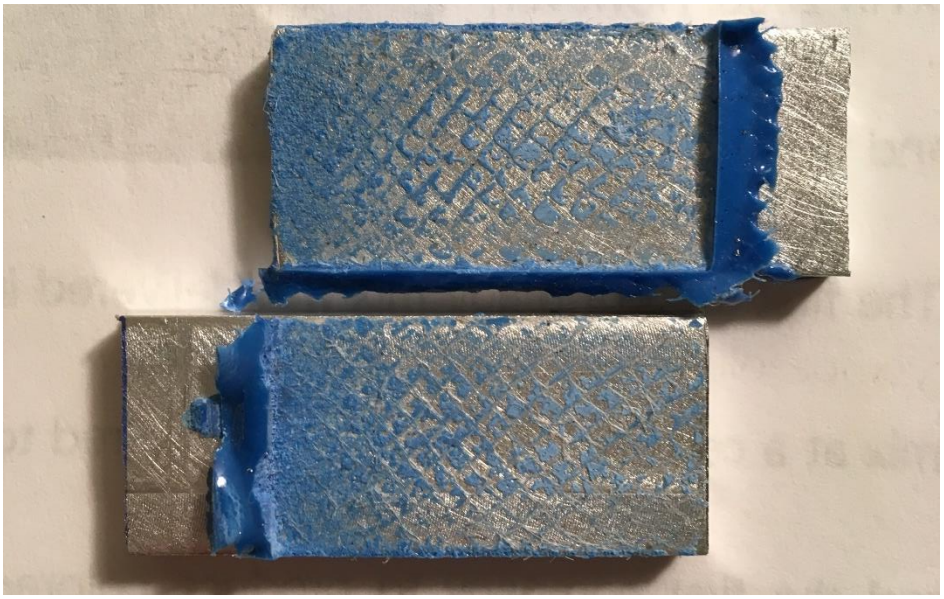

Figure 3-8: SLJ-Sample 3- Fracture Surface

Figure 3-9 depicts the QPD set up and locations.

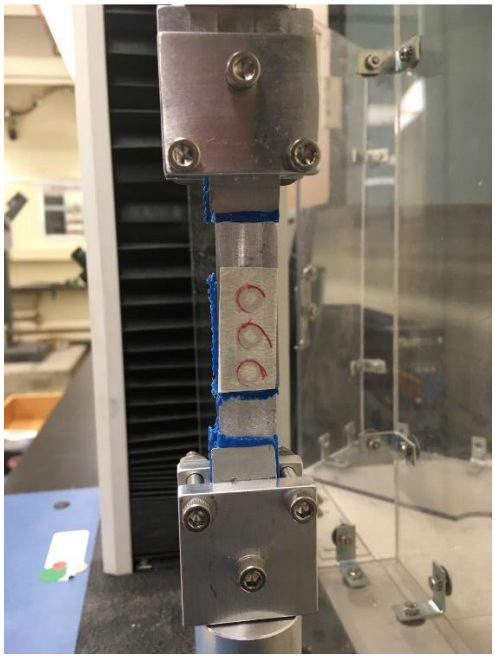

Figure 3-9: SLJ-Sample 3: QPD set up

QPD test was performed before the mechanical test and each 10 min. Figure 3-10-Figure 3-13 depict the QPD results for the middle point.

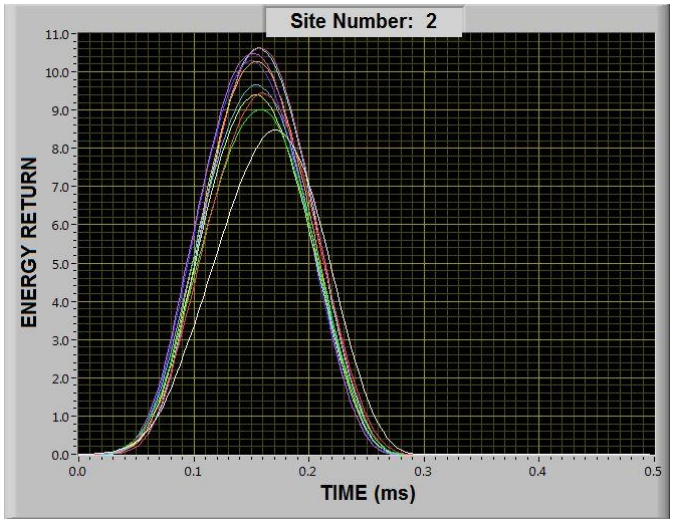

Figure 3-10: SLJ-Sample 3-QPD result before the mechanical test

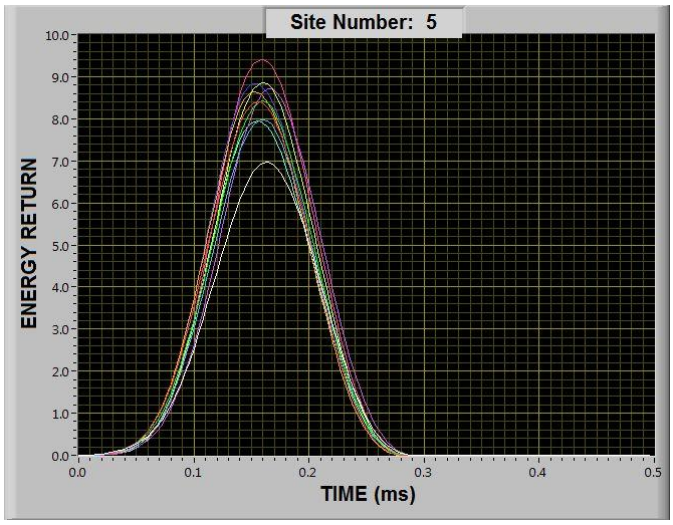

Figure 3-11: SLJ-Sample 3- QPD result after 10 min

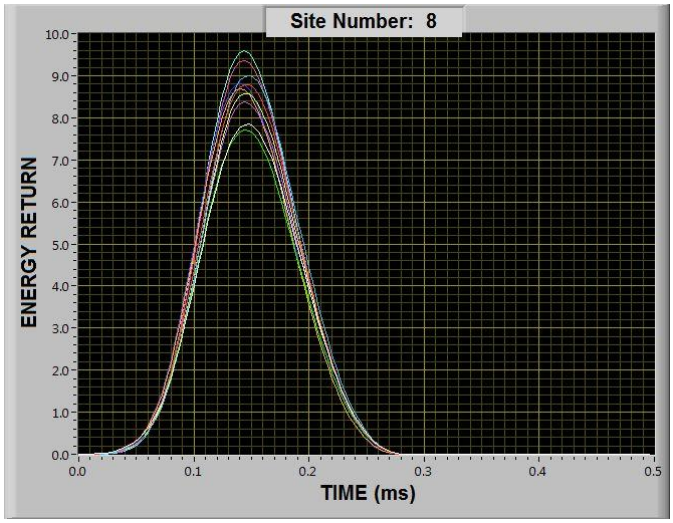

Figure 3-12: SLJ-Sample 3-QPD result after 20 min

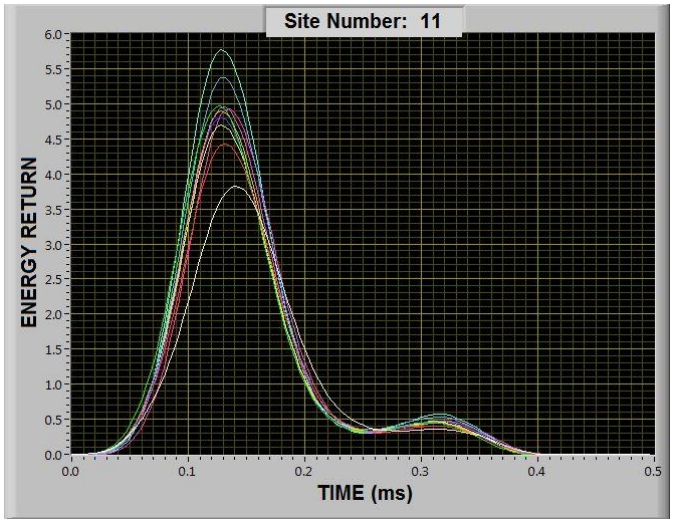

Figure 3-13: SLJ-Sample 3-QPD result after failure, two picks clearly states debonding

Figure 3-14 depicts the stability index data for the middle of the bond during the mechanical test. As it is apparent in Figure 3-9, masking tape was used to mark the sample. The masking tape introduced much damping, and therefore the stability index for this sample is generally very low.

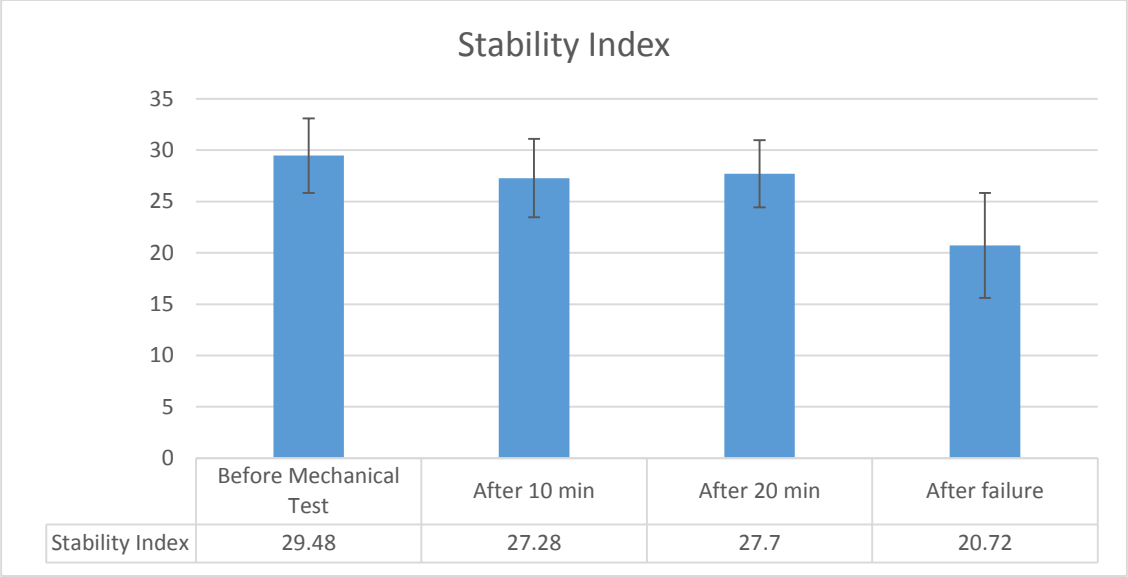

Figure 3-14: Stability Index for Sample 3

3.4) Sample 4 (Well-CFRP)

This was the only sample that was prepared using CFRP as substrates. The curing and surface preparation is the same as Al samples. The length of the CFRP substrates match the length of the previous aluminum substrates. In this case, the bond overlap is 24.5 mm. Due to the lack of enough CFRP material, lack of time, and also lack of appropriate equipment to cut CFRPs, I decided to make all the following samples with aluminum substrates.

Figure 3-15 depicts the Load vs. Displacement graph for this sample. The displacement rate for this test was 0.1 mm/min. Multiple dents in the Load vs. Displacement curve is due to stopping the test each 5 min in order to perform the QPD test.

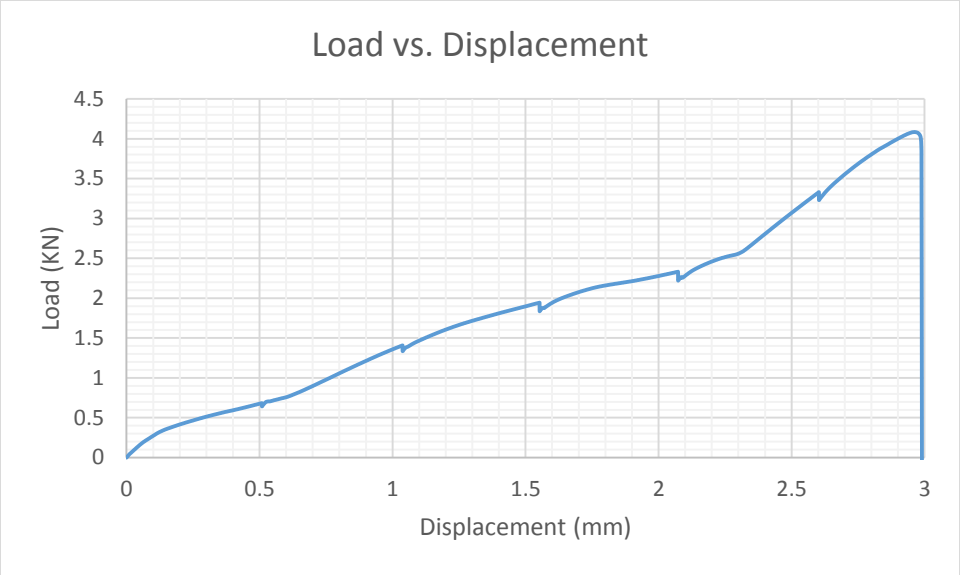

Figure 3-15: Sample 4-Load vs. Displacement

Figure 3-16 shows the fracture surface for this sample. This fracture surface can be classified as a "mixed-mode" according to the Figure 1-2 which is representative of a well bond.

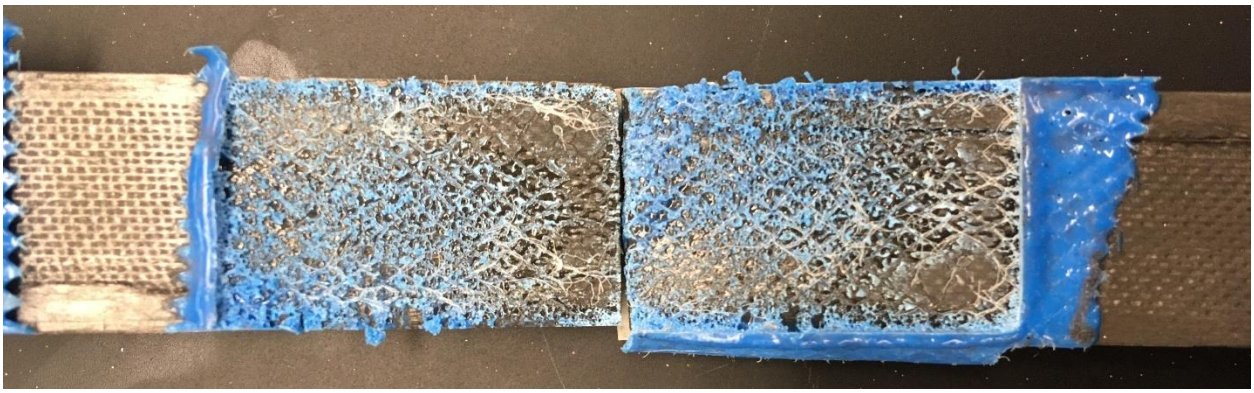

Figure 3-16: SLJ-Sample 4-Fracture Surface

As mentioned before, the QPD test was performed on this sample in the same manner as the previous sample. The only difference is that, this test was performed with 5 min intervals. Figure 3-17 through Figure 3-23 show the QPD results for the middle of the bond in each case.

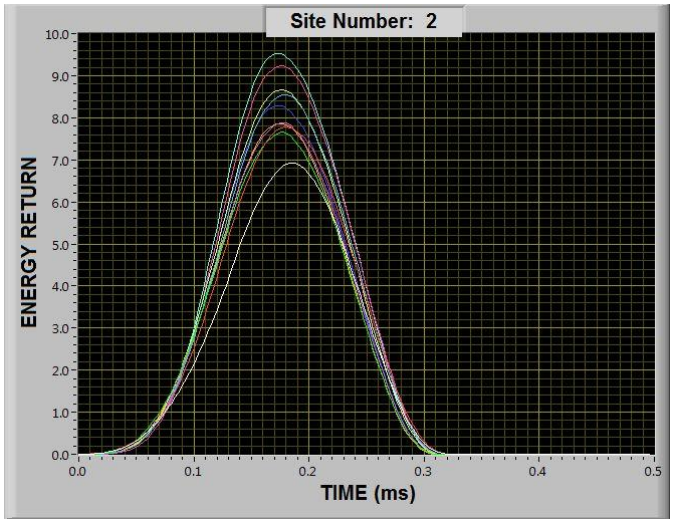

Figure 3-17: SLJ-Sample 4-QPD result-before mechanical test

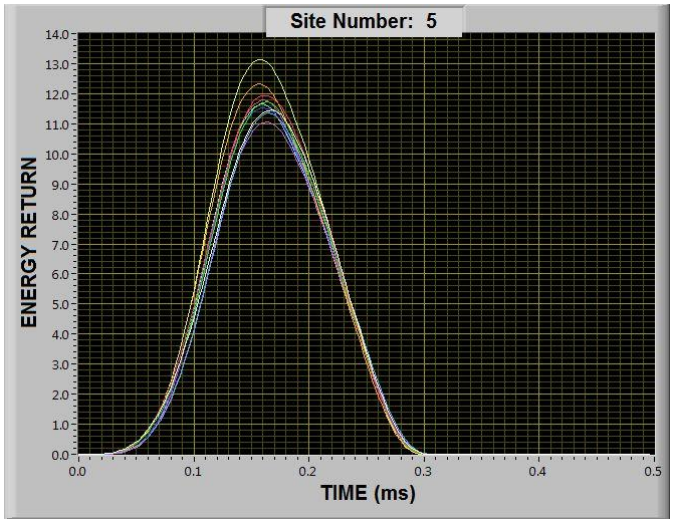

Figure 3-18: SLJ-Sample 4-QPD result after 5min

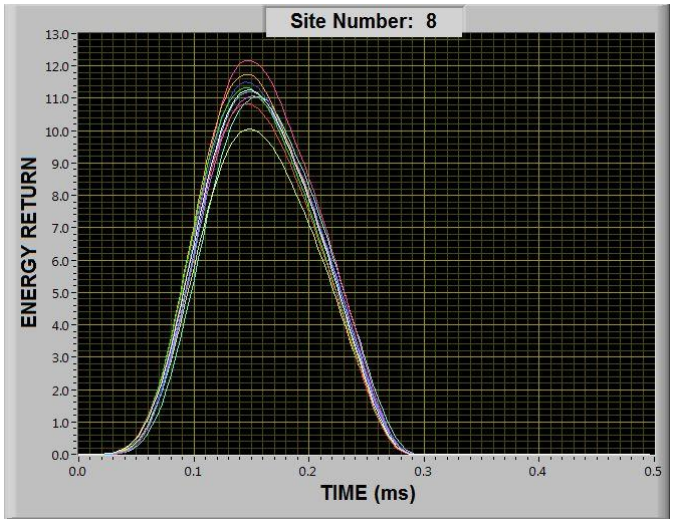

Figure 3-19: SLJ-Sample 4-QDP result after 10min

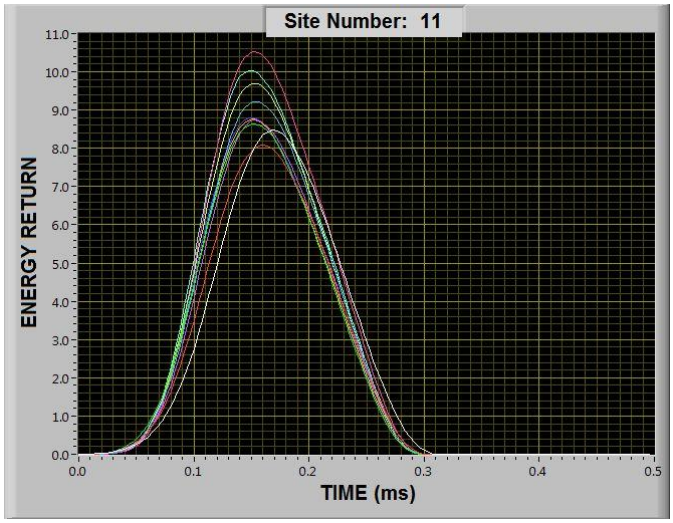

Figure 3-20: SLJ-Sample 4-QPD result after 15min

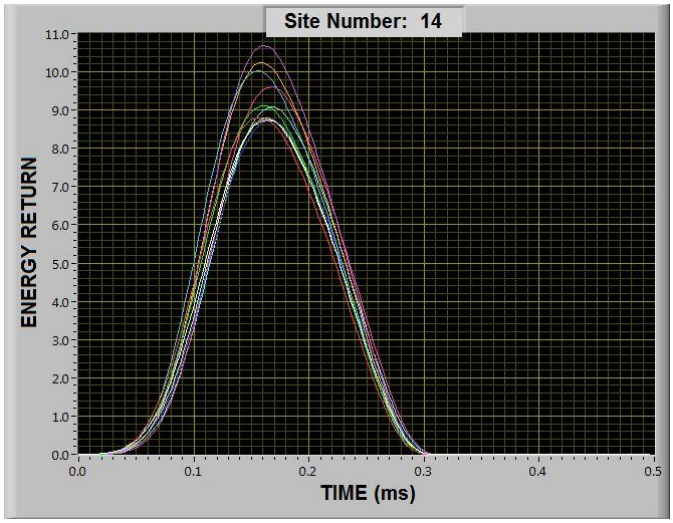

Figure 3-21: SLJ-Sample 4-QPD result after 20min

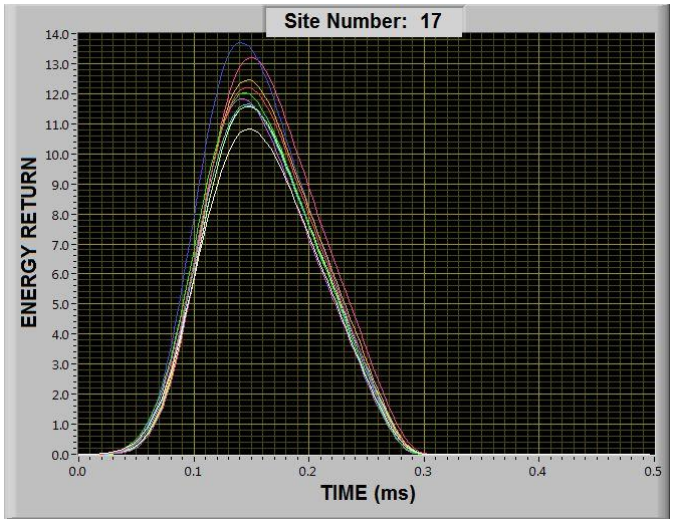

Figure 3-22: SLJ-Sample 4-QPD result after 25min

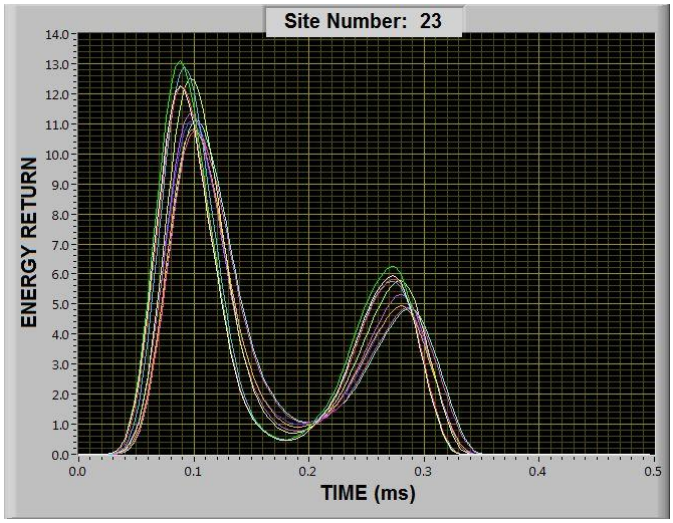

Figure 3-23: SLJ-Sample 4-QDP result after failure-two peaks clearly indicate debonding

Figure 3-24 depicts the stability index data for the middle of the bond during the mechanical test. The general low stability index is likely the result of the polymeric matrix's high damping capacity in CFRP compared to the metallic substrates.

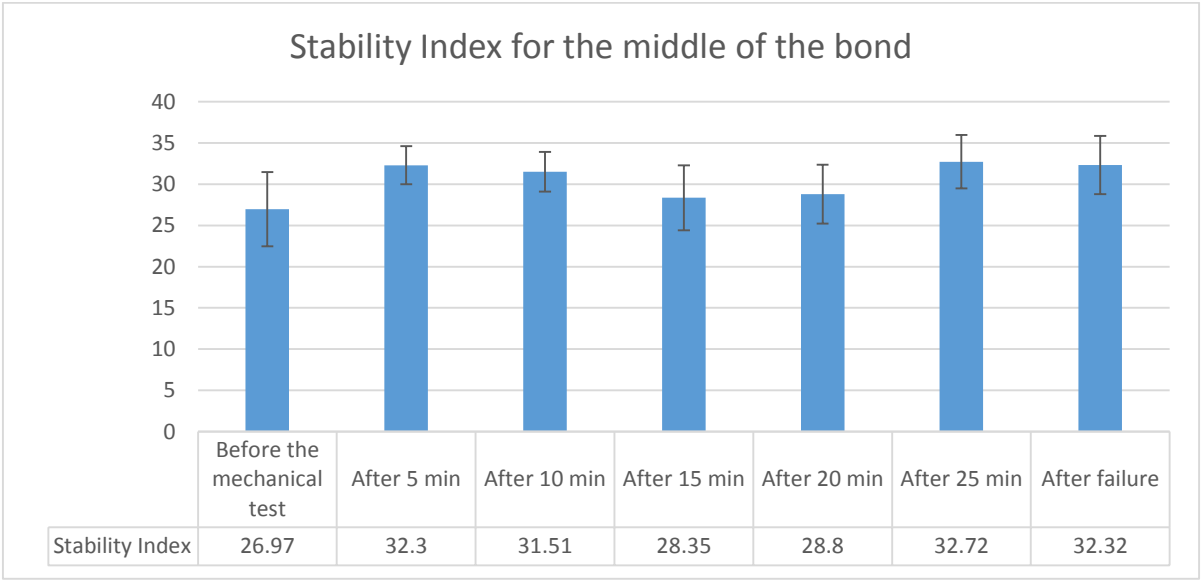

	Before the mechanical test	After 5 min	After 10 min	After 15 min	After 20 min	After 25 min	After failure
Stability Index	26.97	32.3	31.51	28.35	28.8	32.72	32.32

Figure 3-24: Stability Index for CFRP sample

3.5) Sample 5 (Released)

This sample was prepared by applying 5 coats of Silicone-based Frekote 770 Release Agent on one substrate in order to create a kiss bond. The substrate then heat-treated for 2 hours at 121°C [250°F] to increase the function of the release agent [28]. After heat treatment, a milky layer developed on the substrate. The bond failed immediately with a small load during the demolding step. This illustrates that the resultant bond is too weak and does not represent a practical kiss bond.

Figure 3-25 depicts the fracture surface for this sample. As mentioned in Figure 1-2, the smooth fracture surface and appearance of adhesive on only one substrate indicate an interfacial-mode of fracture, which represents a kiss bond.

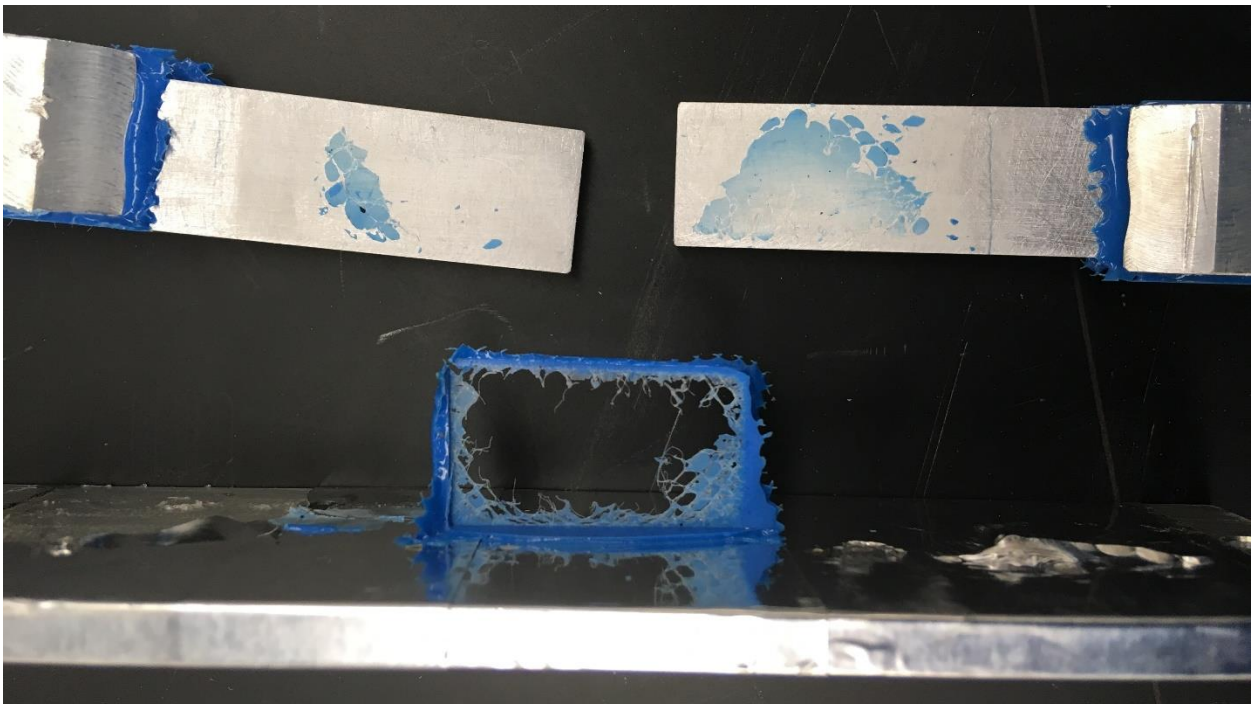

Figure 3-25: SLJ-Sample 5-Fracture Surface

3.6) Sample 6 (Released)

In this sample, two coats of release agent were used. Still, the sample failed upon demolding, and the failure was totally in the interface. This sample does not represent a practical kiss bond either.

Figure 3-26 depicts the fracture surface for this sample. As mentioned in Figure 1-2, the smooth fracture surface and appearance of adhesive on only one substrate indicate an interfacial-mode of fracture, which represents a kiss bond.

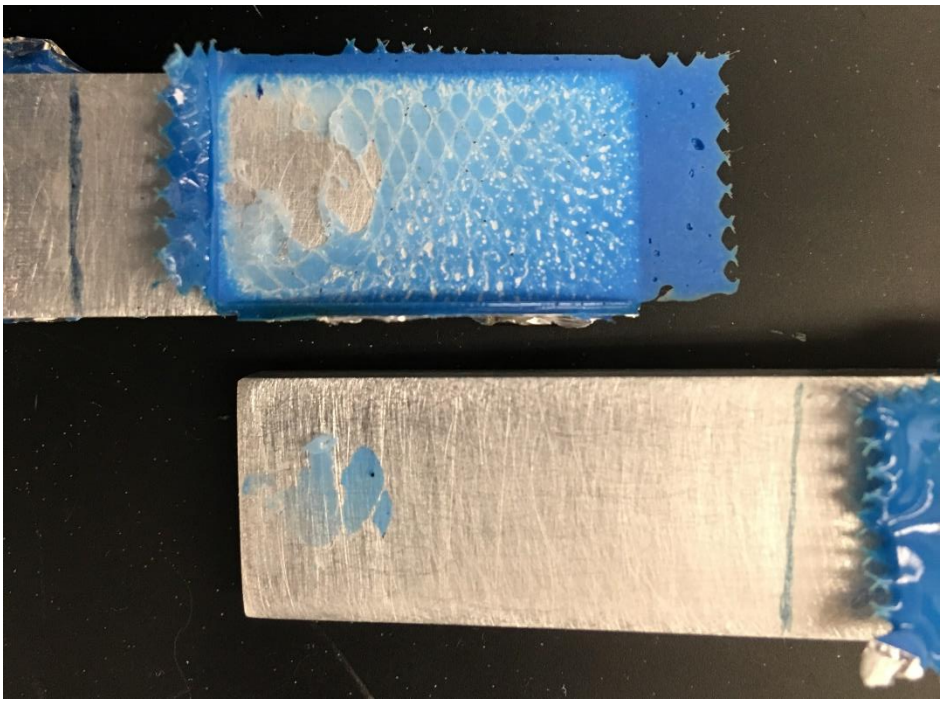

Figure 3-26: SLJ-Sample 6-Fracture Surface

3.7) Sample 7 (Released)

In this sample, 1 coats of release agent were used. Still, the sample failed upon demolding, and the failure was totally in the interface. This sample does not represent a practical kiss bond either.

Figure 3-27 presents the fracture surface for this sample. As mentioned in Figure 1-2, the smooth fracture surface and appearance of adhesive on only one substrate indicate an interfacial-mode of fracture, which represents a kiss bond.

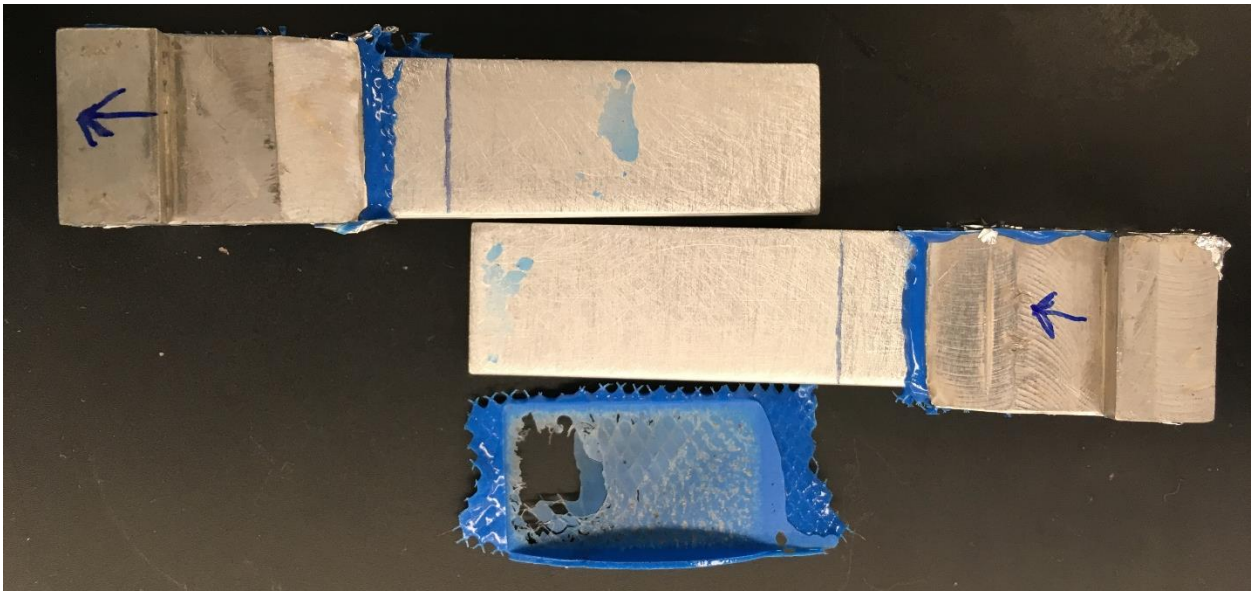

Figure 3-27: SLJ-Sample 7-Fracture Surface

3.8) Sample 8- Large Substrate (Released)

A different approach was taken in the fabrication of this sample. Two big Al plates were bonded together. Only 1 coat of released agent was used in the fabrication of this sample. QPD test was performed on this sample. The QPD instrument is designed to be used horizontally in order to cancel the effect of gravity on the movement of the QPD probe. The sample was horizontal (therefore, the QPD was vertical) during the QPD test. This can introduce some error into the results. Figure 3-28 through Figure 3-29 depict the sample, and the marked points are the QPD test locations.

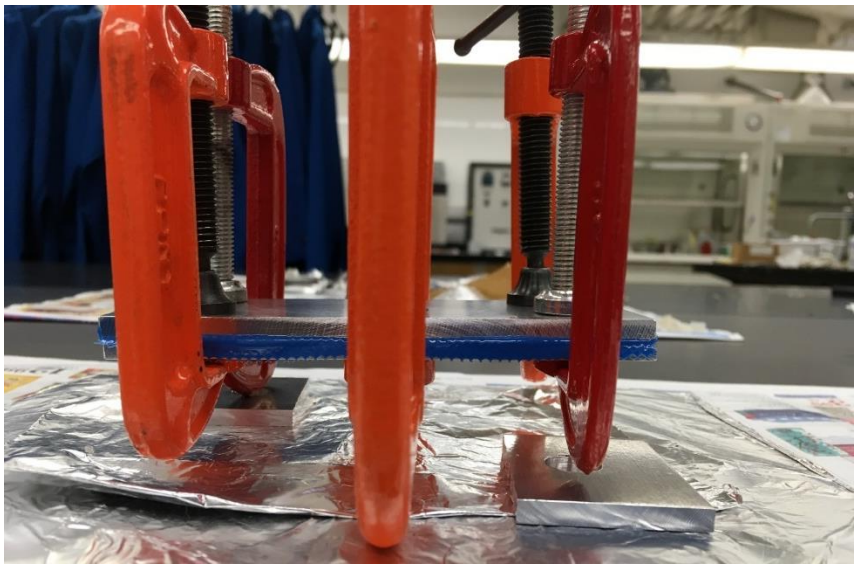

Figure 3-28: Sample 8

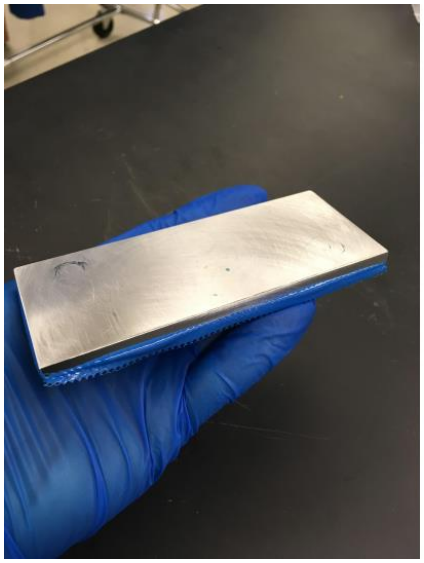

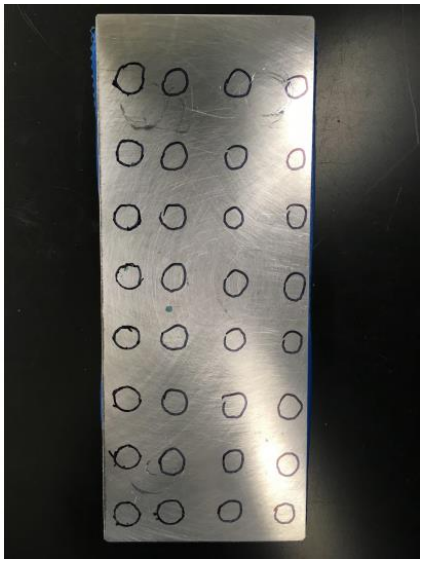

Figure 3-29: Sample 8

Figure 3-30 shows a QPD result for one of the locations. The stability index for this site is 127.6, and the average stability index over all the test sites is 127.63, which correlates well with the result for a well bond. Not the shape of the curve, nor its amplitude, shows any sign that QPD

was able to detect the kiss bond in this case (the maximum 180 energy return is typical for an Al sample with a well bond).

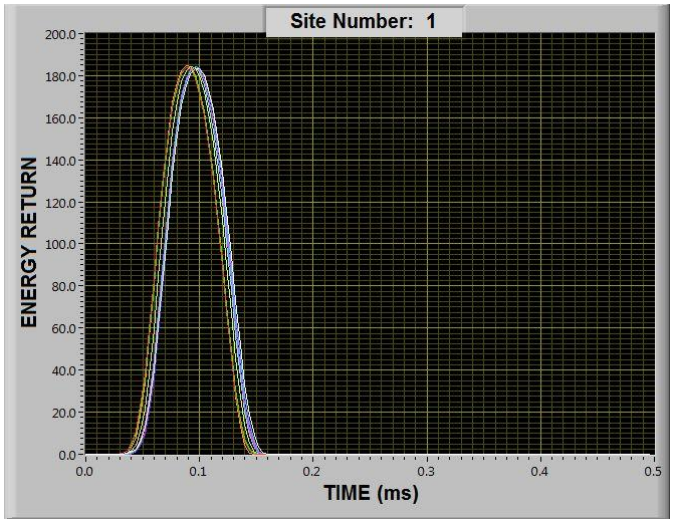

Figure 3-30: Sample 8-QPD result

3.9) Sample 9 (Released)

The surface of only one substrate was coated with 1 coat of release agent. The sample again failed upon demolding, and the failure was totally in the interface. This case does not represent a real kiss bond either.

Figure 3-31 depicts the fracture surface for this sample. As mentioned in Figure 1-2, the smooth fracture surface and appearance of adhesive on only one substrate indicate an interfacial-mode of fracture, which represents a kiss bond.

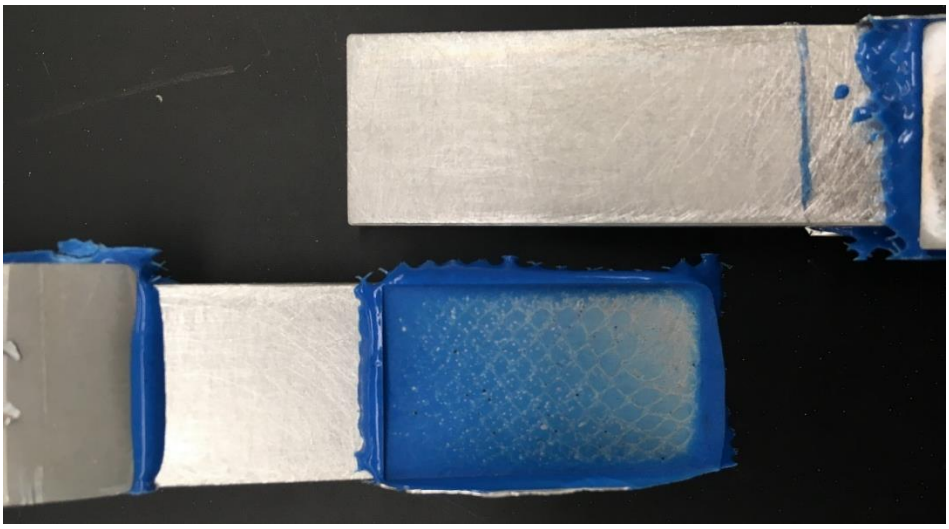

Figure 3-31: SLJ-Sample 9-Fracture Surface

3.10)Sample 10 (Well)

This sample was prepared without any release agent. Initially, the crosshead speed was taken as 0.1 mm/min for previous samples. The justification behind that was to observe any minor change in the mechanical behavior of the sample. After testing multiple samples, it turns out this crosshead speed is too low, and it is even possible for the adhesive to experience some level of creep in this condition. So after consulting with multiple standards [45] & [46] , the 1 mm/min was chosen as crosshead speed moving forward. The thickness of the bondline was measured using a Micrometer. The thickness of each substrate and the overall thickness of the bond were measured in three separate locations, and the average was used to calculate the bondline thickness [44].

Table 3-2 states the measurements for this sample. The bondline thickness for this sample turns out to be 9.599-4.764333-4.749=0.086 mm or 86 µm.

Table 3-2: Thickness measurements to calculate the thickness of the bond. The average thickness of each substrate subtracted from the average overall thickness of the bond to determine the bondline thickness.

Substrate 1 measurements (mm) [in]	Substrate 2 measurements (mm) [in]	Overall Thickness (mm) [in]
4.758 [0.1873]	4.75 [0.1870]	9.555 [0.3762]
4.749 [0.1870]	4.765 [.1876]	9.598 [0.3779]
4.74 [0.1866]	4.778 [1881]	9.644 [0.3797]
4.749 [0.1870]*	4.764333 [0.1876]*	9.599 [0.3779]*

*Average value

Figure 3-32 depicts the Load vs. Displacement graph for this sample. The displacement rate for this test was 1 mm/min.

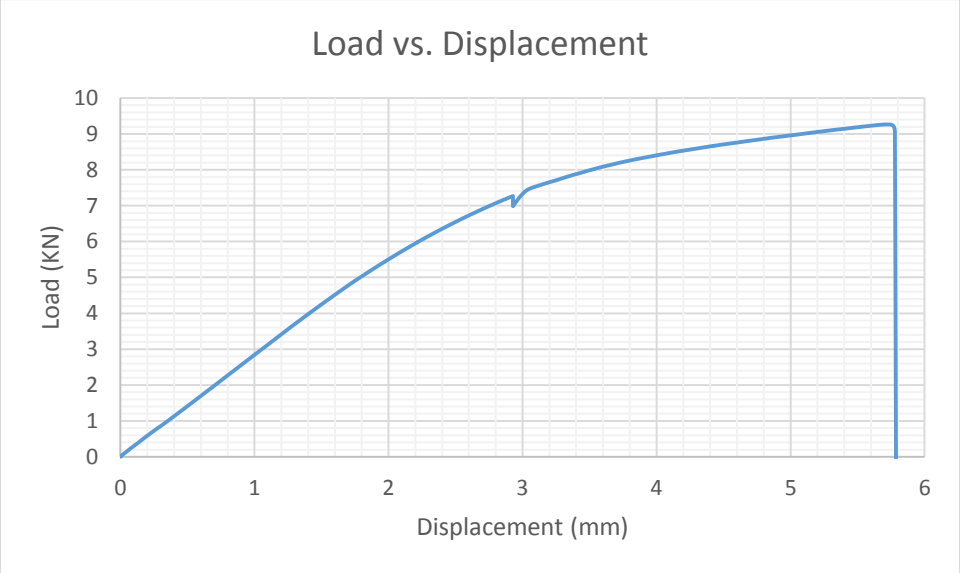

Figure 3-32: SLJ-Sample 10-Load vs. Displacement

Figure 3-33 depicts the fracture surface for this sample, which can be classified according to Figure 1-2 as a "mixed-mode of fracture", which is representative of a well bond.

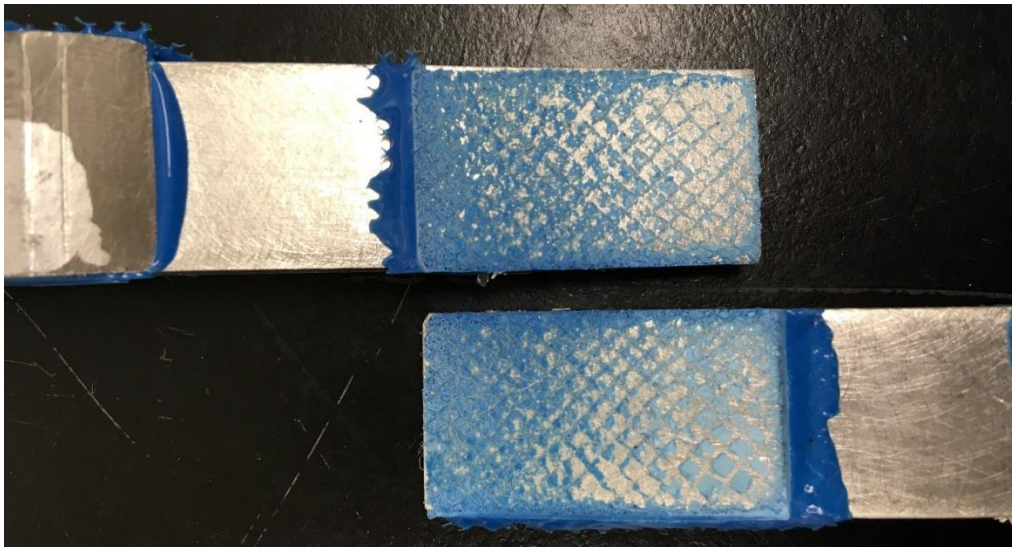

Figure 3-33: SLJ-Sample 10-Fracture Surface

The QPD test was performed on this sample before the mechanical test and during the mechanical test in 3 min intervals. QPD curve and amplitude did not change during the test and was only able to detect the total debonding after the failure. Figure 3-34-Figure 3-36 depict the QDP results for the middle of the bond.

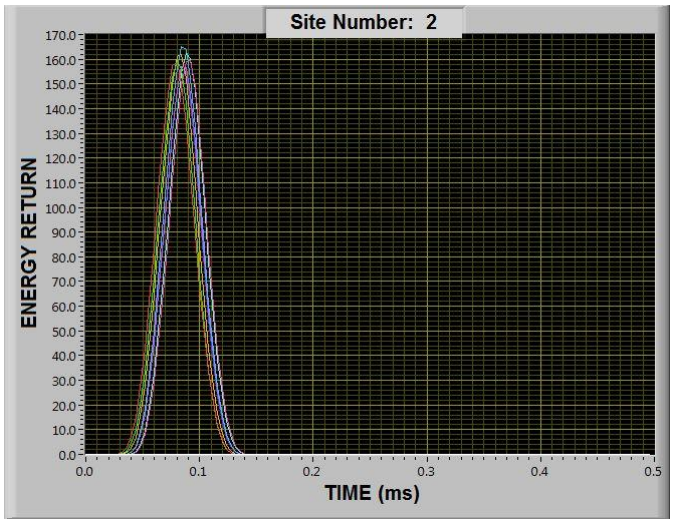

Figure 3-34: SLJ-Sample 10-QPD result before mechanical test

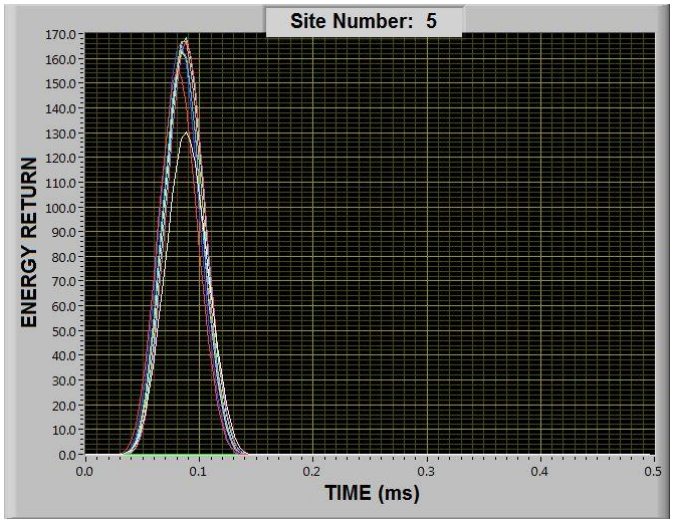

Figure 3-35: SLJ-Sample 10-QPD result after 3min

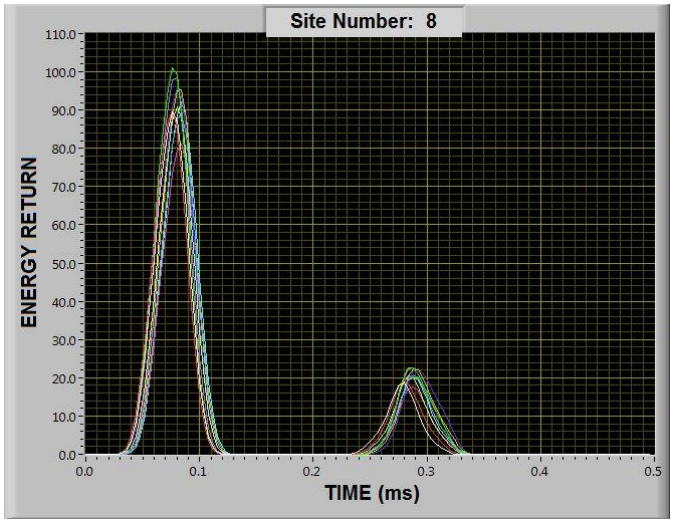

Figure 3-36: SLJ-Sample 10-QPD result after failure- two peaks clearly states total debonding

Figure 3-37 depicts the stability index during the test for the middle of the bond.

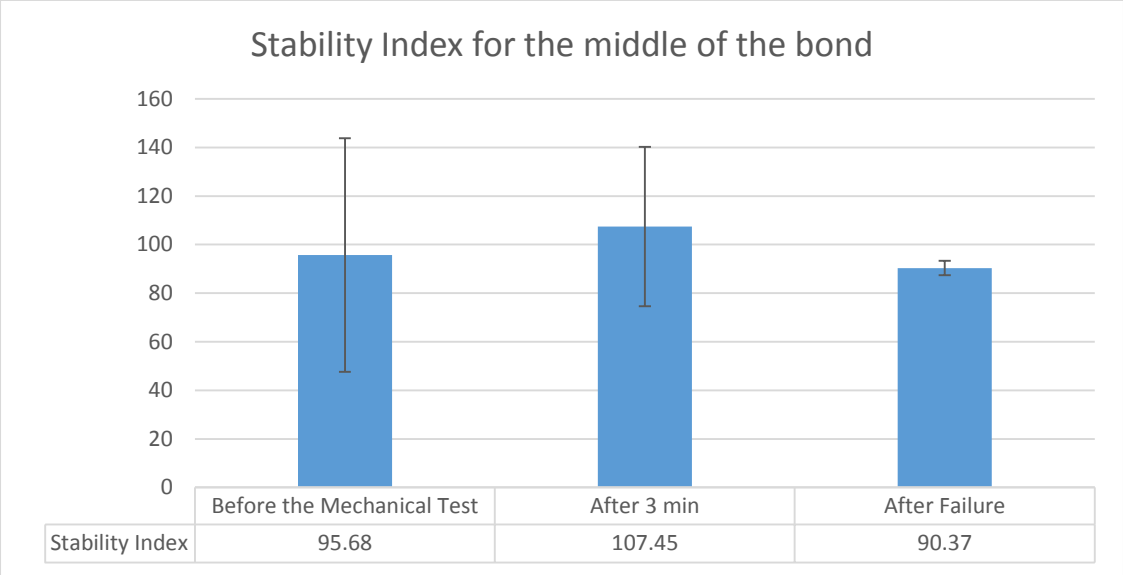

Figure 3-37: Sample 10- Stability Index for the middle of the bond

3.11)Sample 11 (Well)

In the fabrication of this sample, three layers of the adhesive film were used. The thickness of the bondline became 0.153 mm (153 µm). The thickness raises almost twofold instead of threefold, and the excessive amount of adhesive fillet apparent in Figure 3-39 indicates that the reason could be because of the excess amount of adhesive bleeds out and form the excessive amount of fillet.

Figure 3-38 depicts the Load vs. Displacement graph for this sample. The displacement rate for this test was 1 mm/min.

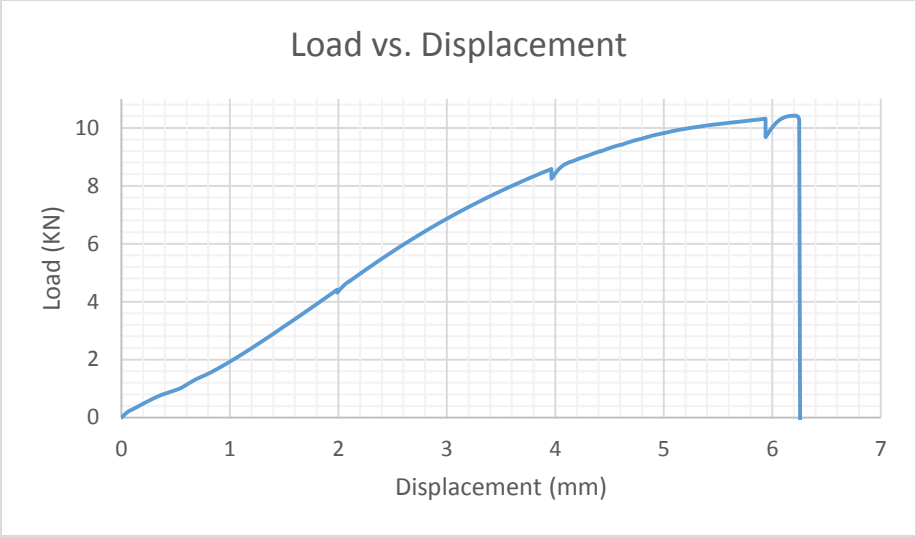

Figure 3-38: SLJ-Sample11-Load vs. Displacement

Figure 3-39 depicts the fracture surface for this sample. As mentioned in Figure 1-2, the rough fracture surface and the appearance of both adhesive and the substrate at the same time, indicate a mixed-mode of fracture, which is representative of a well bond. Figure 3-40 shows the extent of bending in an SLJ.

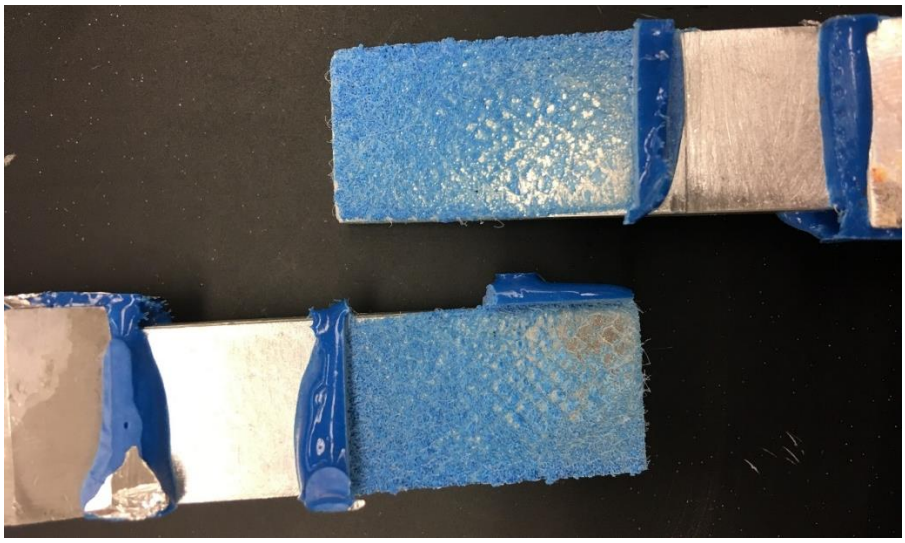

Figure 3-39: SLJ-Sample 11-Fracture Surface

Figure 3-40: The extent of bending in sample 11

QPD test was performed before the mechanical test and during the mechanical test in 2 min intervals. Figure 3-41 through Figure 3-45 depict the QPD results in the middle of the bond. QPD results changed dramatically after failure, and QPD was only able to detect the total debonding. Figure 3-46 depicts the stability index data during the mechanical test.

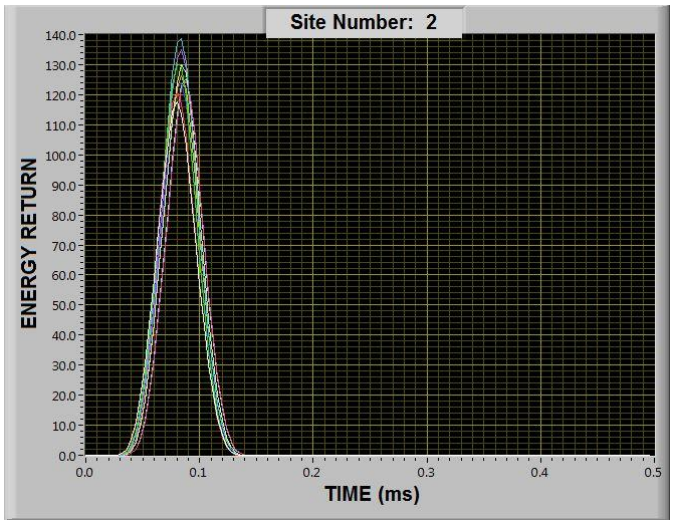

Figure 3-41: SLJ-Sample 11-QPD result before mechanical test

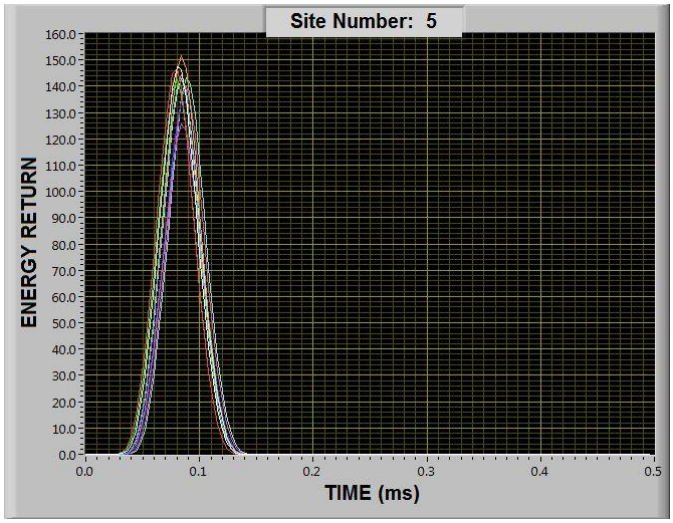

Figure 3-42: SLJ-Sample 11-QPD result after 2 minutes

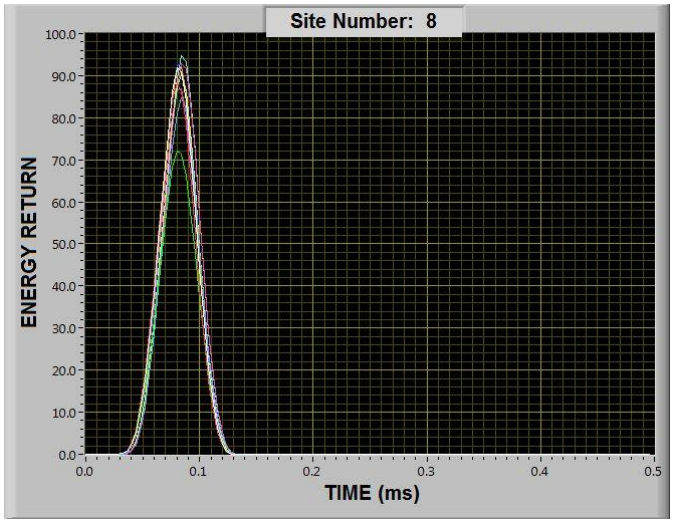

Figure 3-43: SLJ-Sample 11-QPD result after 4 minutes

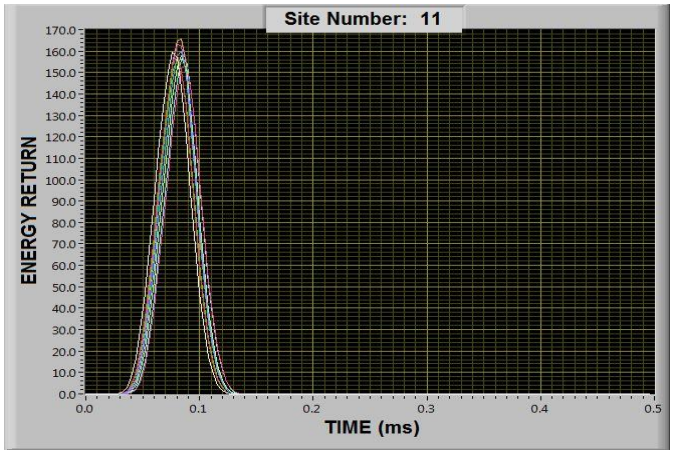

Figure 3-44: SLJ-Sample 11-QPD result after 6 minutes

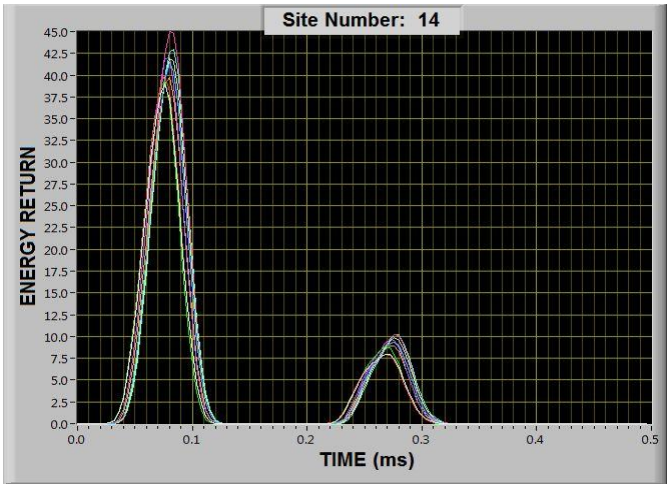

Figure 3-45: SLJ-Sample 11-QPD result after failure- two peaks clearly states total debonding

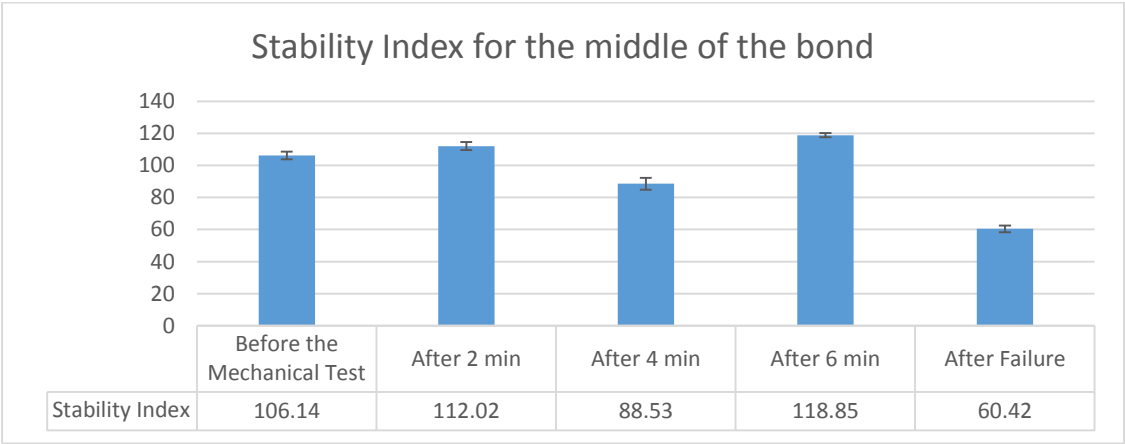

Figure 3-46: Sample 11- Stability Index for the middle of the bond

Table 3-3 summarizes all the mechanical properties of these samples.

Table 3-3: Summary of mechanical properties for SLJ samples

	Sample 1 (0.1 mm/min)	*Sample 2 (0.1 mm/min)*	*Sample 3 (0.1 mm/min)*	*Sample 4 CFRP(0.1 mm/min)*	*Sample 5 (1 mm/min)*	*Sample 6 (1 mm/min)*
Bond Area	*448*	*448*	*480*	*392*	*448*	*448*
Max Load (KN)	*6.427*	*8.777*	*5.451*	*4.085*	*9.266*	*10.421*
Max Load/ Bond area (Mpa)	*14.346*	*19.592*	*11.356*	*10.420*	*20.684*	*23.261*
Max Displacement (mm)	*4.776*	*4.357*	*2.081*	*2.962*	*5.716*	*6.189*
Bondline Thickness (µm)	*NA*	*NA*	*NA*	*NA*	*86*	*153*
Max Displacement/ bonline thickness	*NA*	*NA*	*NA*	*NA*	*66.720*	*40.386*
Max Load/ Max Displacement (KN/mm)	*1.346*	*2.014*	*2.619*	*1.379*	*1.621*	*1.684*
Initial Tangent (KN/mm)	*3.772*	*3.086*	*4.210*	*2.917*	*2.853*	*3.279*

4) Stepped Joints Samples

Figure 4-1 shows the substrate used for the stepped joint. The thicker section is roughly 6.35 mm [0.25in] and the thin part that is involved in creating the bond is roughly 3.175 mm [0.125in]. The length and width of the bond area is 25.4 mm [1 in] (so the bond area is 645.16 mm^2 [1 in^2]). However, it is necessary to measure the thickness with a micrometer in order to measure the bondline thickness accurately. So, the thickness of the stepped section (the thin section) is measured in 3 positions. Figure 4-2 illustrates the thickness measurement for all the substrates at 3 positions and the average thickness.

Figure 4-1: Stepped Joint Coupon

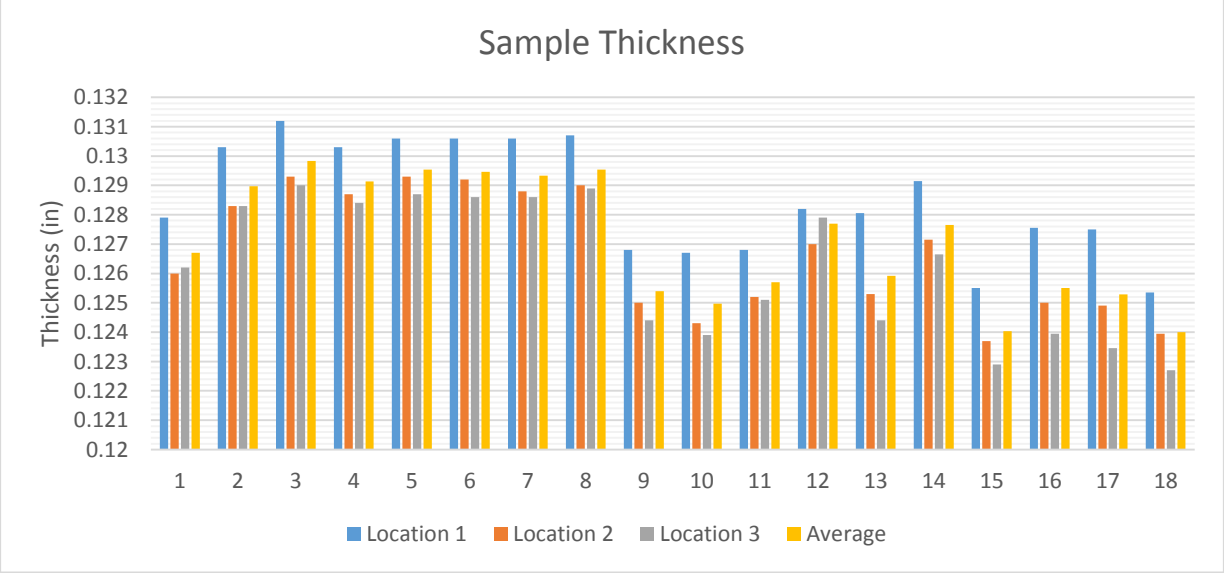

Figure 4-2: Thickness of Stepped Joint Coupons (1 inch==25.4 mm)

4.1) Kiss bond Samples using Silicon-based release agent

In this section, the Silicone-based Frekote 770 release agent is used to create a kiss bond. All substrates were numbered, and samples are named a simple way. For example, S1-1-4-R80 means: S1 means it is the first sample. The next two numbers determine which substrates were used to fabricate this sample. Subsequently, if the sample has W designation, it means that it is a well bond. If the sample has R designation, it means that the release agent was used to fabricate the sample, and the following number determines the percentage of the released area, also the released agent was applied to the first substrate. Three sets of masks depicted in Figure 2-22 were used to cover the bond surface of the substrate before spraying the surface with the release agent.

By using the measured thickness of each substrate, and measuring the overall thickness of the samples at three locations and deriving an average, the bondline thickness for each sample was calculated. Figure 4-3 illustrates the bondline thickness for all the samples in this section.

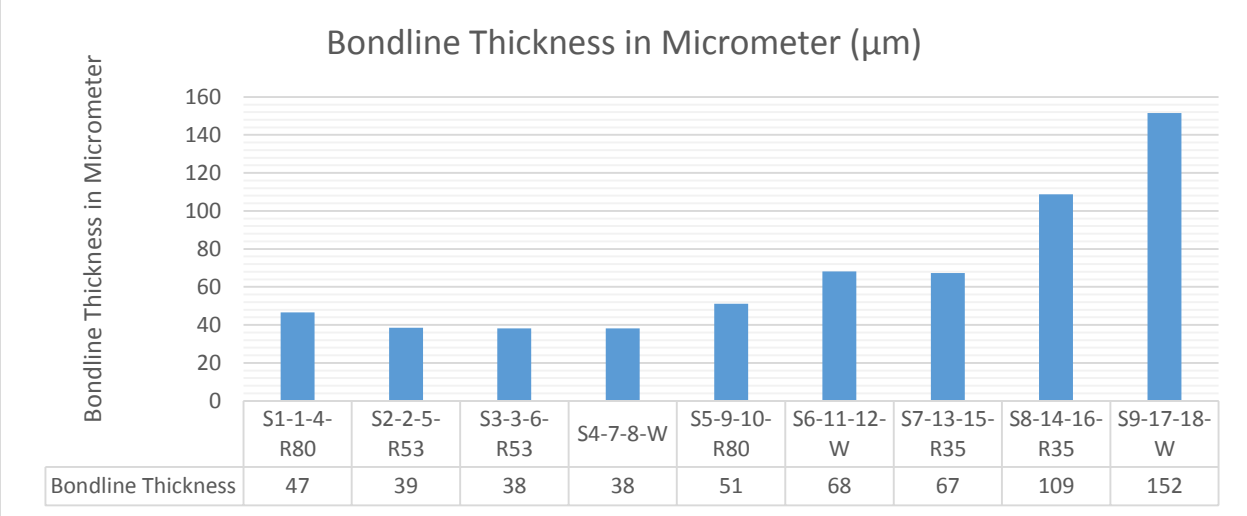

Figure 4-3: Stepped Joints Bondline Thickness in Micrometer (µm)

Figure 4-4 depicts the curing cycle for the samples. The temperature of the furnace was set to 178 °C [350°F]. It took almost 22 minutes for the furnace to reach this temperature. Then the sample stayed at that temperature for 1 hour and 15 min. Then, the furnace was turned off, and the lid was removed, and the sample stayed in the furnace for another 20min. at the end of this step, the temperature reached 158°C. Subsequently, the sample was removed and placed in the room temperature to cool down overnight.

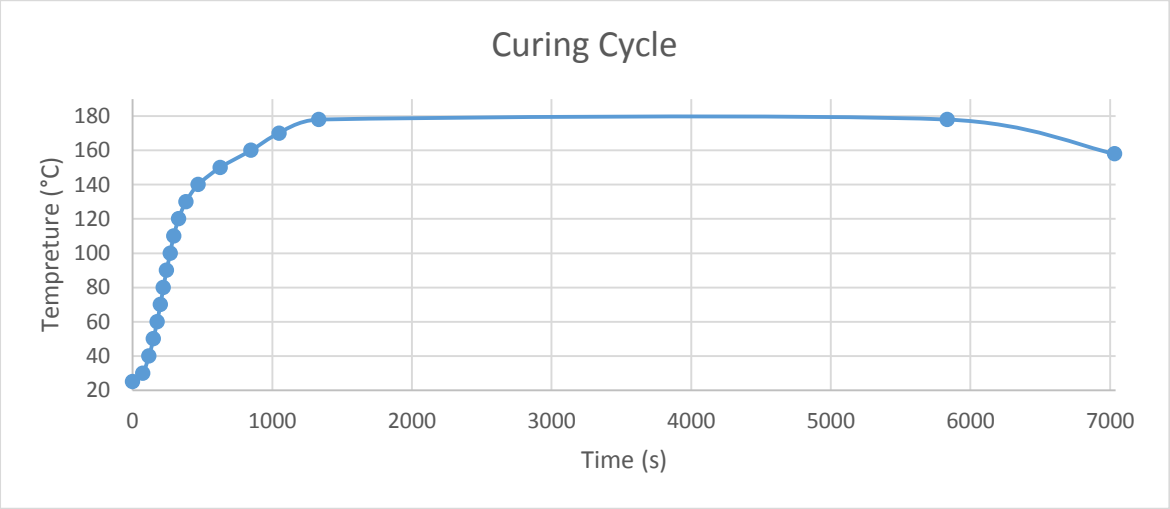

Figure 4-4: Stepped joint samples curing cycle

The mechanical test was performed while 27.94 mm [1.1 in] of the sample from each side was placed in the grips. The displacement rate for all the tests was 1mm/min. All the test was performed at room temperature.

Figure 4-5 schematically depicts a joint with a released substrate. All the QPD tests were performed on 6 locations (3 locations from edge to edge and on both sides of the bond) before

the mechanical test while the sample was mounted in the Instron machine. Tests were performed on the front side of the bond that the release agent was applied first.

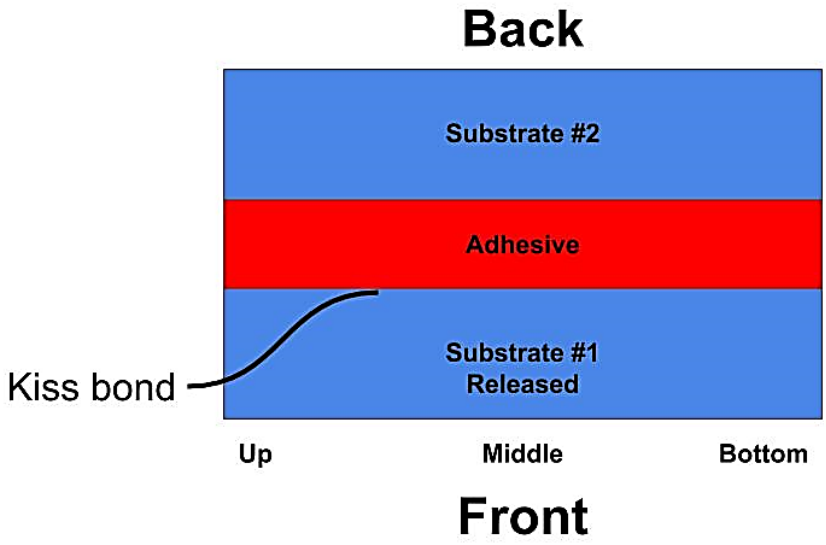

Figure 4-5: Schematic Depiction of the bond with a release agent

4.1.1) Sample S1-1-4-R80

This sample is made with substrate 1 and 4, and 80% of the bond area of the substrate 1 is covered with the release agent. The sample fails immediately in the instron machine, and the applied load does not even reach 0.5 KN. The failure is completely interfacial along the whole bond area, which means that the procedure to create partial flaw using masks was not successful. In fact, the release agent diffused from beneath the mask and covered the whole surface. The same result was achieved for all the released samples, regardless of the percentage of the bond area that was covered with the release agent.

Figure 4-6 depicts the fracture surface for this sample. As mentioned in Figure 1-2, the smooth fracture surface and appearance of adhesive on only one substrate indicate an interfacial-mode of fracture, which represents a kiss bond.

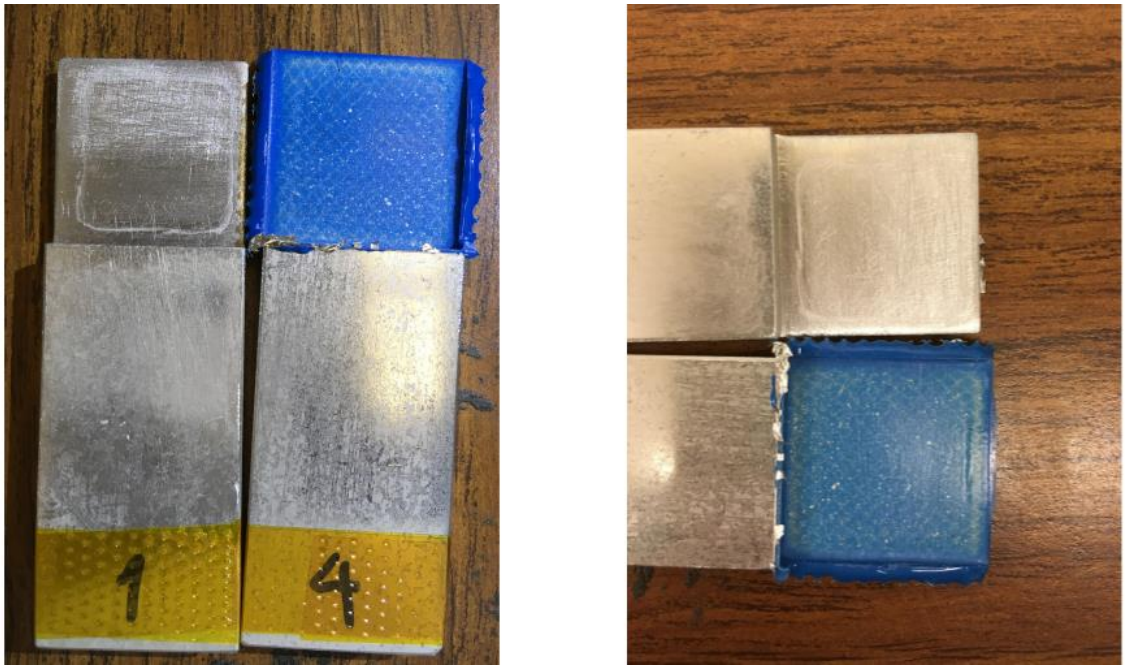

Figure 4-6: S1-1-4-R80- Fracture Surface

The QPD test was performed on 6 locations (3 locations from edge to edge and on both sides of the bond) before the mechanical test while the sample was mounted in the Instron machine. During the mounting, it is necessary to apply high force in order to prevent the sample from sliding. This can introduce peel force to the sample, and that can cause the sample to fail even before the mechanical test begin. From the QPD result, it is evident that the sample failed before the mechanical test begin. Figure 4-7 depicts the QPD result for the middle of the bond.

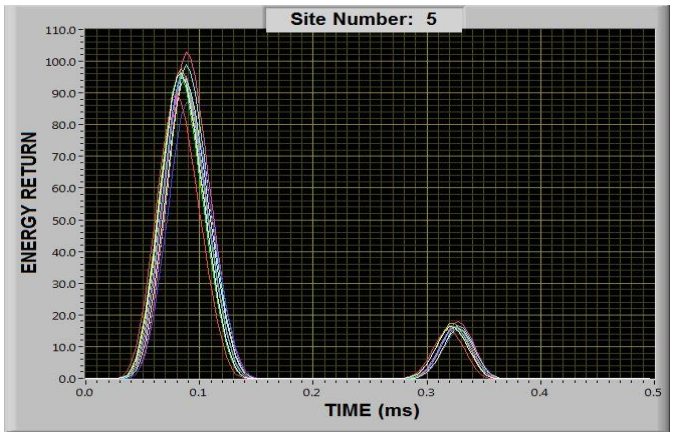

Figure 4-7: S1-1-4-R80-QPD result for the middle of the bond on the back side

Figure 4-8 summarizes the stability index, which is proportional to the maximum energy return for all the test locations. As mentioned in the introductory to QPD, data for 10 impact is analyzed in each case. The relative standard deviation[4] is used for error bars.

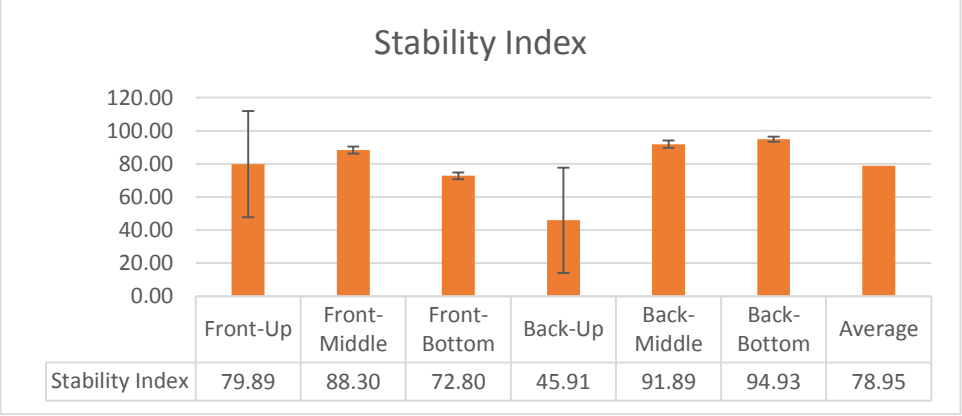

	Front-Up	Front-Middle	Front-Bottom	Back-Up	Back-Middle	Back-Bottom	Average
Stability Index	79.89	88.30	72.80	45.91	91.89	94.93	78.95

Figure 4-8: Stability Index for all the test locations for S1-1-4-R80. Relative Standard Deviation is used for error bars

[4] $Relative\ Standard\ Deviation = \frac{Standard\ Deviation}{Mean}\ X\ 100$

4.1.2) Sample S2-2-5-R50

The same result was achieved compared to the previous sample. Figure 4-9 depicts the fracture surface for this sample. As mentioned in Figure 1-2, the smooth fracture surface and appearance of adhesive on only one substrate indicate an interfacial-mode of fracture, which represents a kiss bond. The failure was totally in the interface across the bond area.

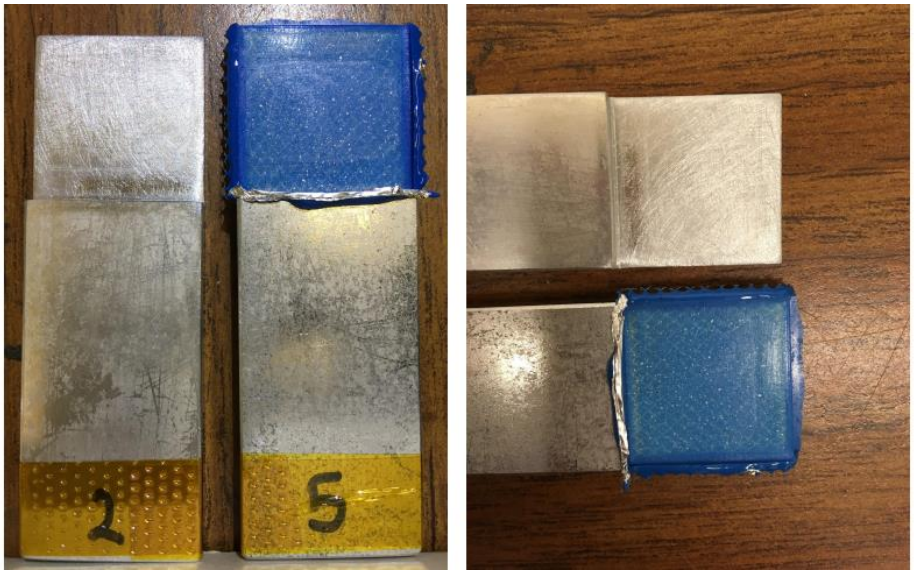

Figure 4-9: S2-2-5-R50-Fracture Surface

The QPD test was performed with extra caution to avoid introducing any peel stress to the joint. First, the sample became loosely mounted in the Instron machine, and the QPD test was performed, and subsequently, the grip was tightened to ensure no slippage happens during the mechanical test. Figure 4-10 depicts the QPD result for the middle of the bond.

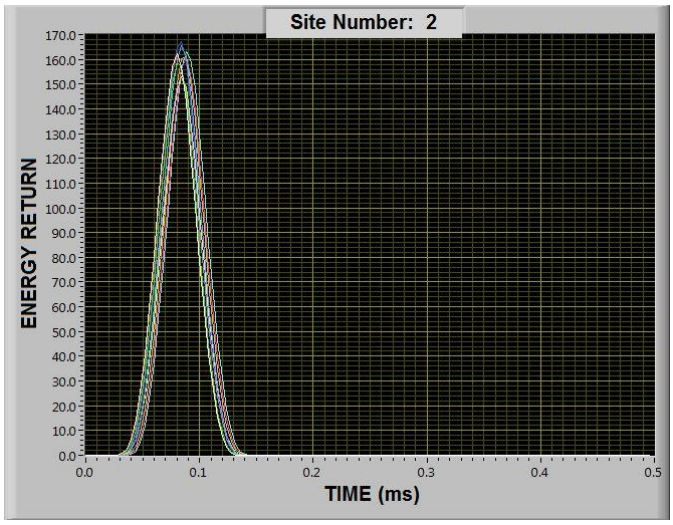

Figure 4-10: S2-2-5-R50-QPD result for the middle of the bond on the front

Figure 4-11 summarizes the stability index, which is proportional to the maximum energy return for all the test locations.

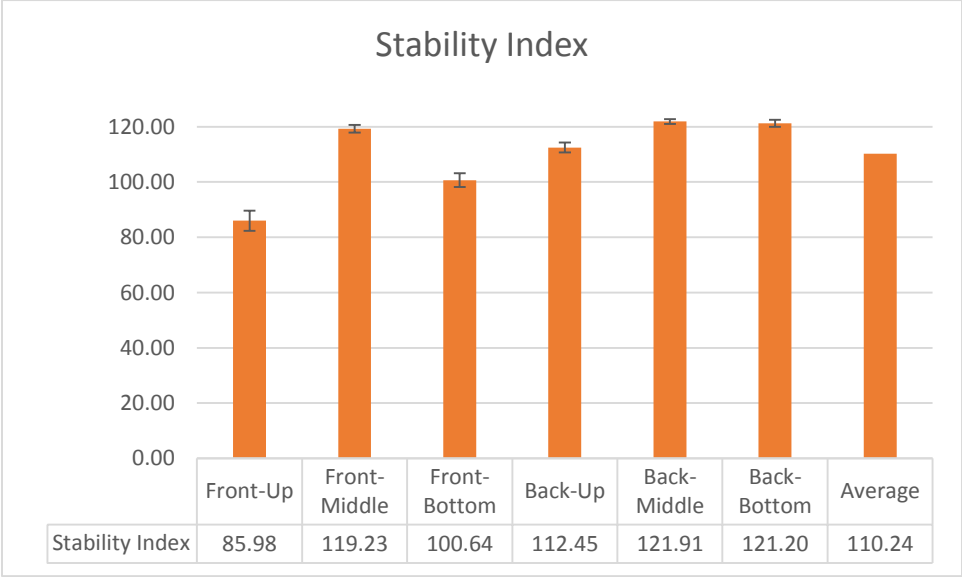

	Front-Up	Front-Middle	Front-Bottom	Back-Up	Back-Middle	Back-Bottom	Average
Stability Index	85.98	119.23	100.64	112.45	121.91	121.20	110.24

Figure 4-11: Stability Index for all the test locations for S2-2-5-R50. Relative Standard Deviation is used for error bars

4.1.3) Sample S3-3-6-R50

The result is the same as other released samples. Figure 4-12 depicts the fracture surface for this sample. As mentioned in Figure 1-2, the smooth fracture surface and appearance of adhesive on only one substrate indicate an interfacial-mode of fracture, which represents a kiss bond.

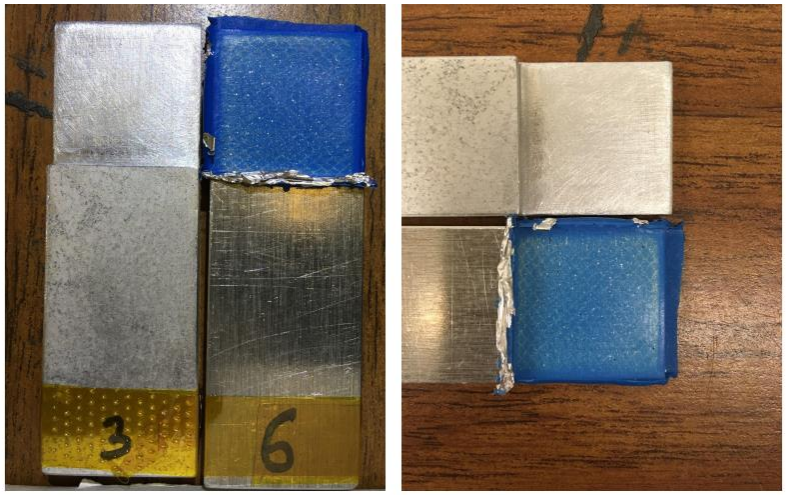

Figure 4-12: S3-3-6-R50-Fracture Surface

Figure 4-13 depicts the QPD result for the middle of the bond.

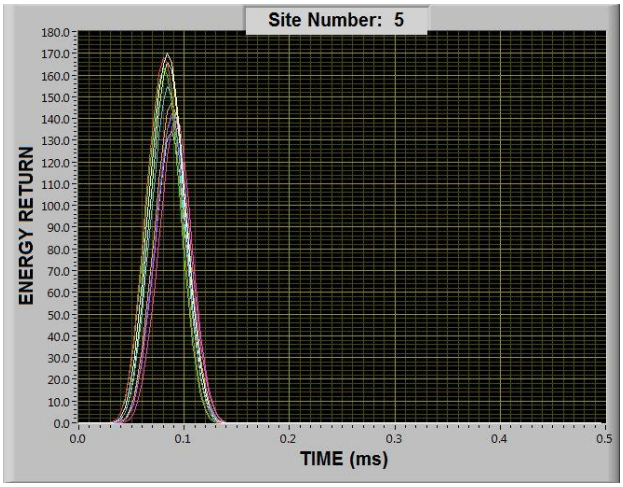

Figure 4-13: S3-3-6-R50-QPDfor the middle of the bond on the back

Figure 4-14 summarizes the stability index, which is proportional to the maximum energy return for all the test locations.

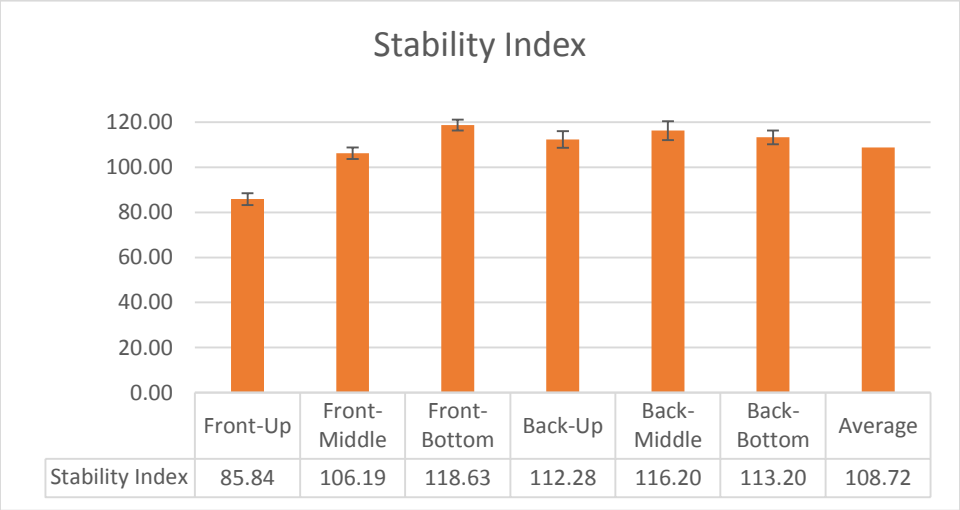

Figure 4-14: Stability Index for all the test locations for S3-3-6-R50. Relative Standard Deviation is used for error bars

4.1.4) Sample S4-7-8-W

No release agent was used to fabricate this sample, and it is completely apparent in the fracture surface and the mechanical performance.

Figure 4-15 depicts the Load vs. Displacement graph for this sample. The displacement rate for this test was 1 mm/min.

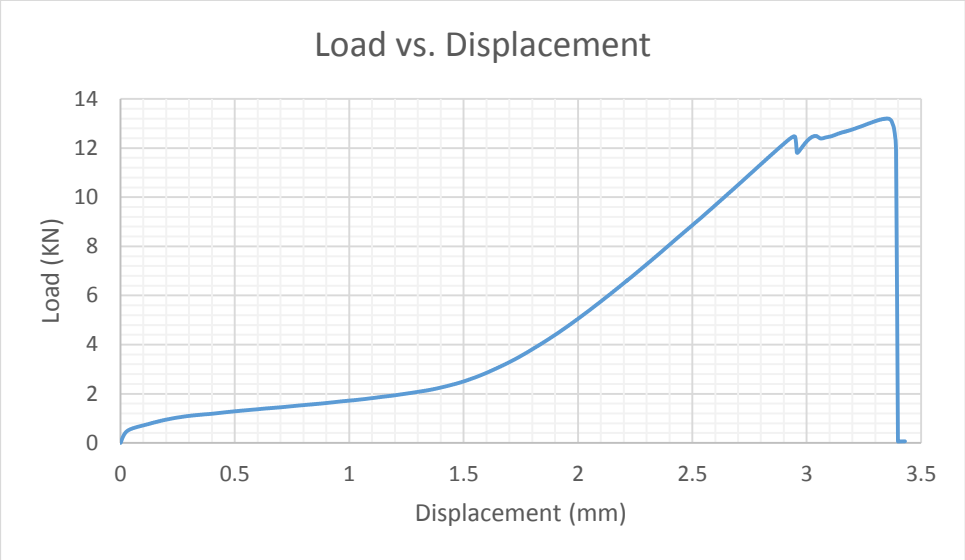

Figure 4-15: S4-7-8-W-Load vs. Displacement

Figure 4-16 depicts the fracture surface for this sample. As mentioned in Figure 1-2, the rough fracture surface and the appearance of both adhesive and the substrate at the same time, indicate a mixed-mode of fracture, which is representative of a well bond.

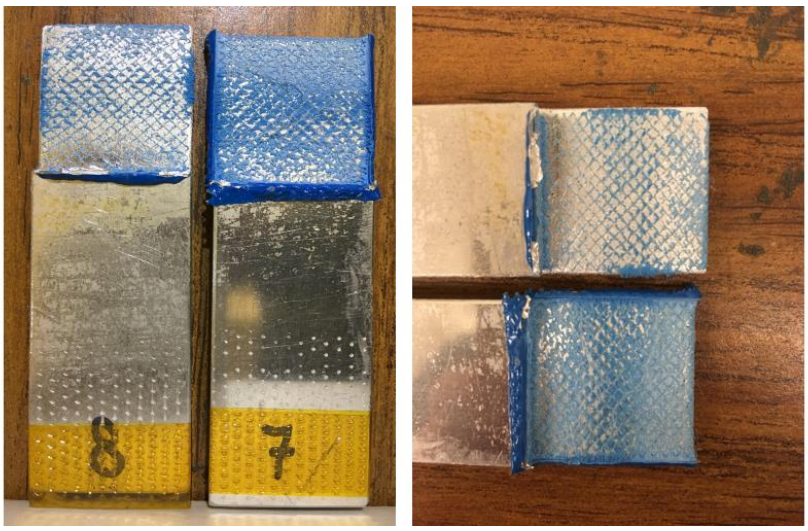

Figure 4-16: S4-7-8-W-Fracture Surface

Figure 4-17 depicts the QPD result for the middle of the bond. It totally represents a QPD result for a well bond.

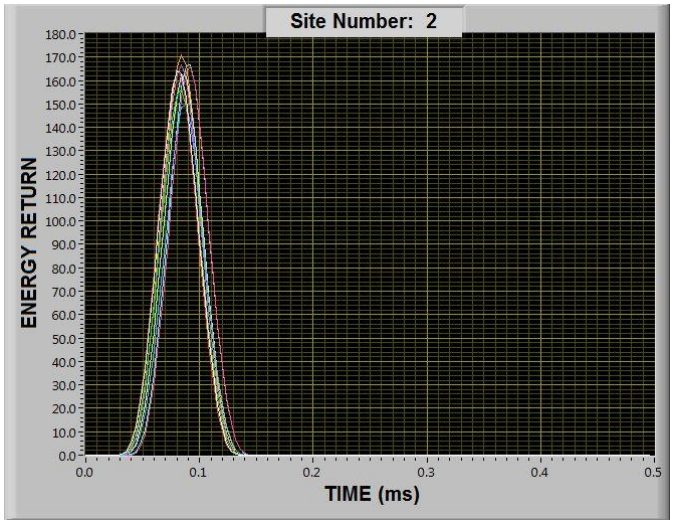

Figure 4-17: S4-7-8-W-QPD for the middle of bond on the front side

Figure 4-18 summarizes the stability index, which is proportional to the maximum energy return for all the test locations.

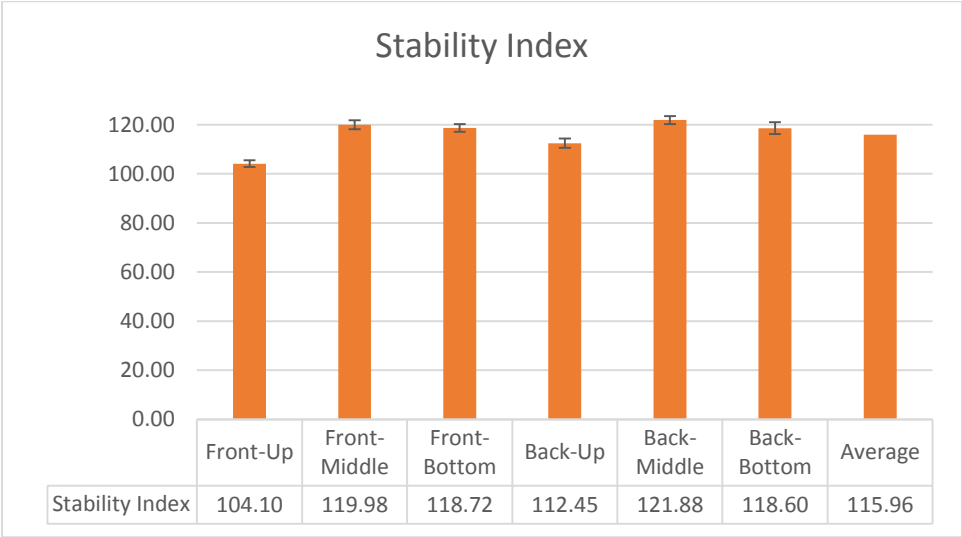

	Front-Up	Front-Middle	Front-Bottom	Back-Up	Back-Middle	Back-Bottom	Average
Stability Index	104.10	119.98	118.72	112.45	121.88	118.60	115.96

Figure 4-18: Stability Index for all the test locations for S4-7-8-W. Relative Standard Deviation is used for error bars

4.1.5) Sample S5-9-10-R80

Figure 4-19 depicts the fracture surface for this sample. As mentioned in Figure 1-2, the smooth fracture surface and appearance of adhesive on only one substrate indicate an interfacial-mode of fracture, which represents a kiss bond.

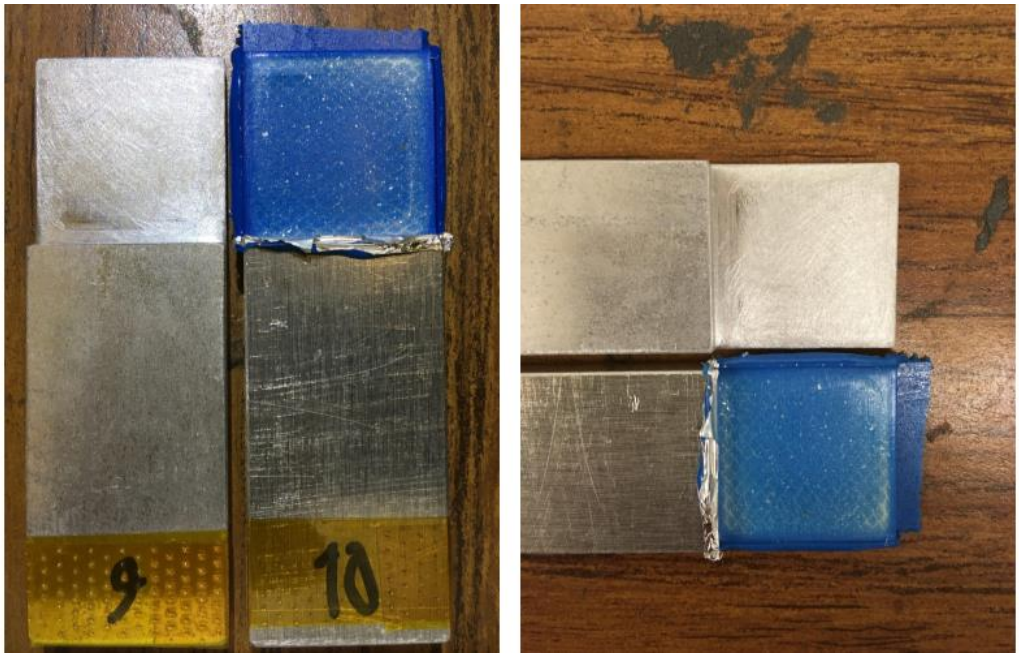

Figure 4-19: S5-9-10-R80-Fracture Surface

Figure 4-20 depicts the QPD result for the middle of the bond. The maximum energy return is much lower than the value for a well bond (around 180). This difference could be a factor to distinguish between a well bond and a kiss bond.

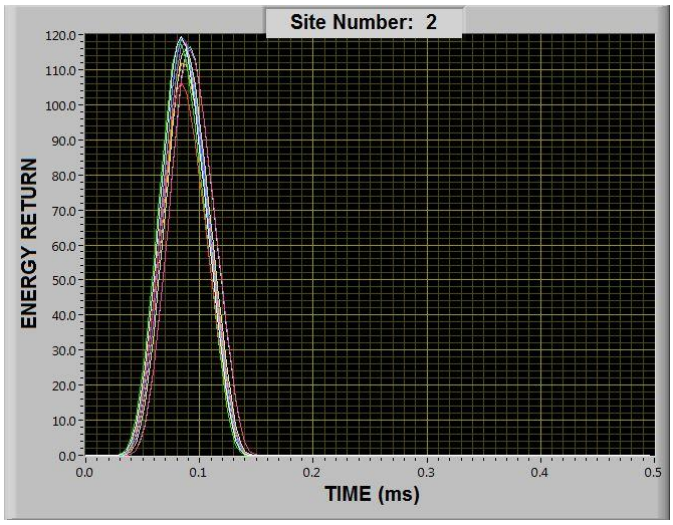

Figure 4-20: S5-9-10-R80-QPD for the middle of the bond on the front side

Figure 4-21 summarizes the stability index, which is proportional to the maximum energy return for all the test locations.

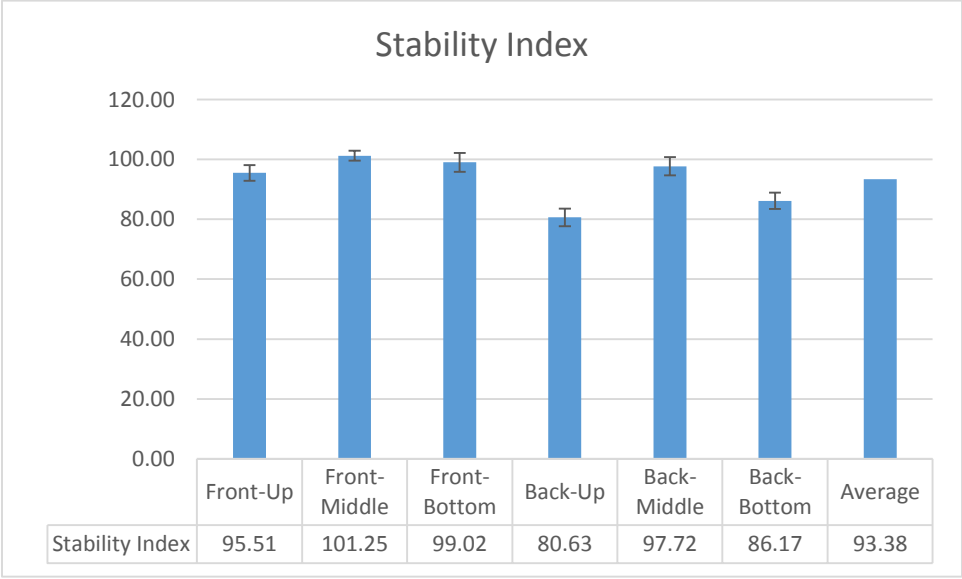

Figure 4-21: Stability Index for all the test locations for S5-9-10-R80. Relative Standard Deviation is used for error bars

4.1.6) Sample S6-11-12-W

Figure 4-22 depicts the Load vs. Displacement graph for this sample. The displacement rate for this test was 1 mm/min.

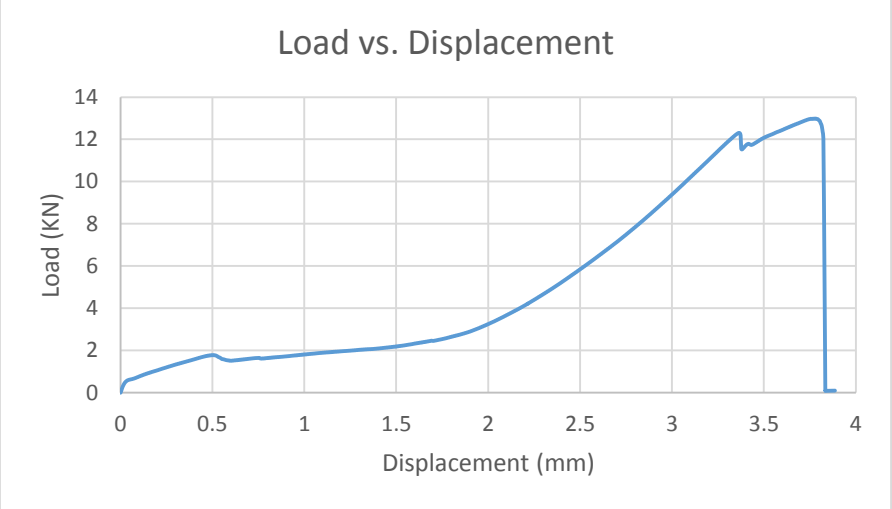

Figure 4-22: S6-11-12-W-Load vs. Displacement

Figure 4-23 depicts the fracture surface for this sample. Per Figure 1-2 classification, this failure mode can be classified as a fracture mixed-mode that indicates well bonded joint.

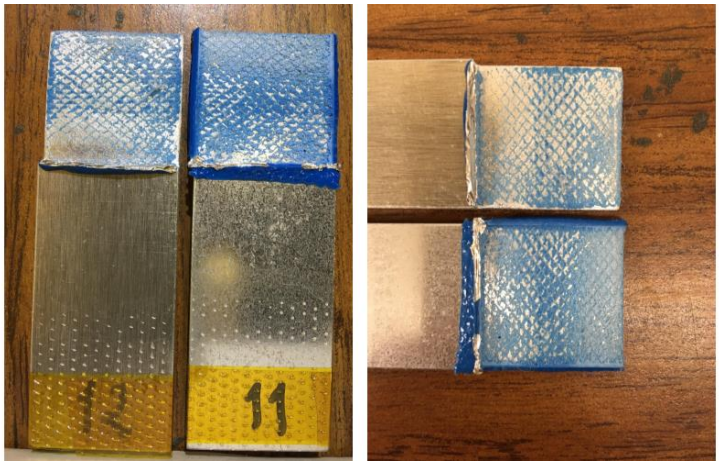

Figure 4-23: S6-11-12-W- Fracture Surface

Figure 4-24 depicts the QPD result for the middle of the bond. The result match what is expected from a well bond. Figure 4-25 summarizes the stability index, which is proportional to the maximum energy return for all the test locations. By Comparing the results for the two samples with a well bond (S4-7-8-W & S6-11-12-W), it is determined that the stability index higher than 111 is a reasonable limit that is representative of a well bond.

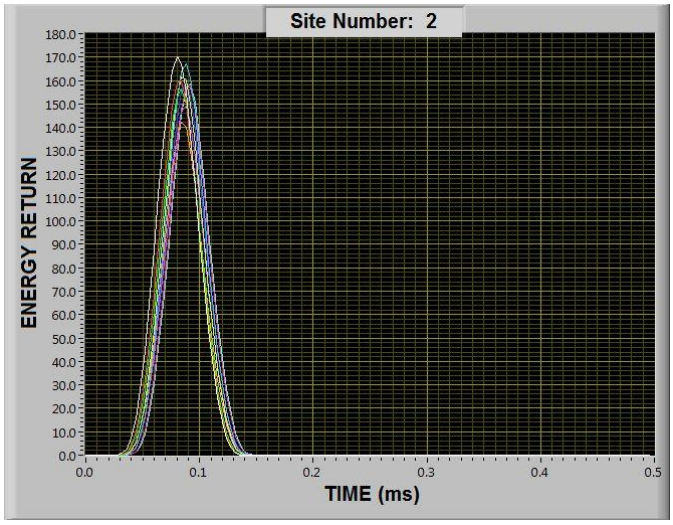

Figure 4-24: S6-11-12-W-QPD for the middle of the bond on the front side.

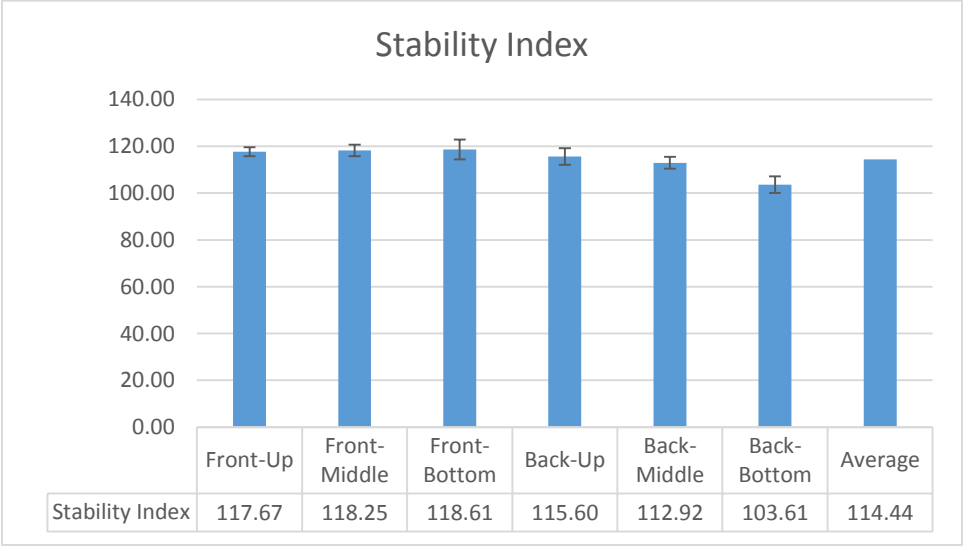

	Front-Up	Front-Middle	Front-Bottom	Back-Up	Back-Middle	Back-Bottom	Average
Stability Index	117.67	118.25	118.61	115.60	112.92	103.61	114.44

Figure 4-25: Stability Index for all the test locations for S6-11-12-W. Relative Standard Deviation is used for error bars

4.1.7) Sample S7-13-15-R30

Figure 4-26 depicts the fracture surface for this sample. As mentioned in Figure 1-2, the smooth fracture surface and appearance of adhesive on only one substrate indicate an interfacial-mode of fracture, which represents a kiss bond.

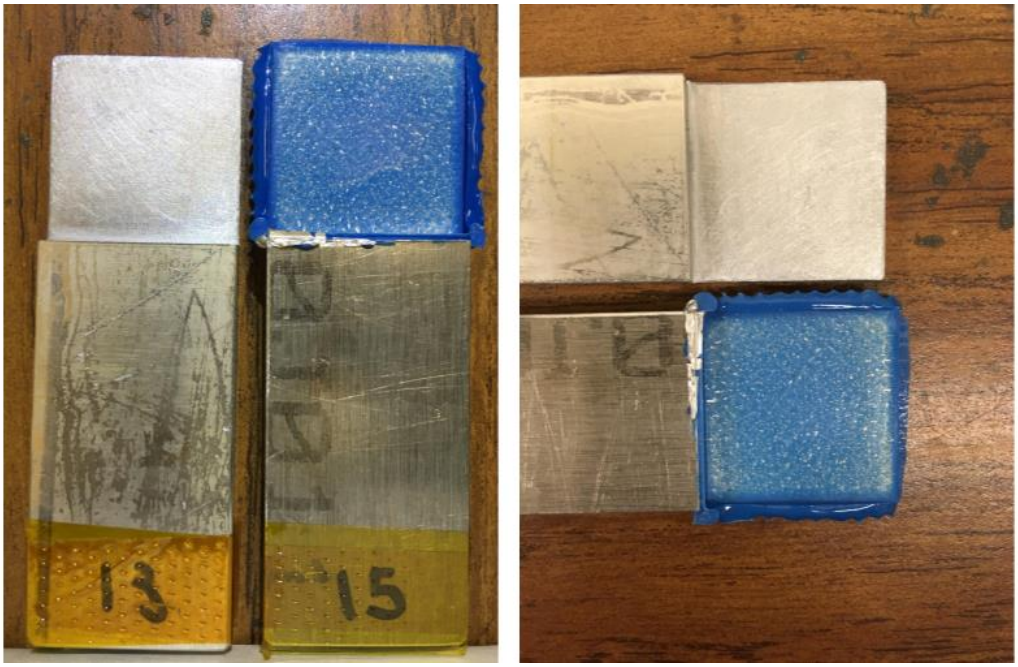

Figure 4-26: S7-13-15-R30-Fracture Surface

Figure 4-27 depicts the QPD result for the middle of the bond. The maximum energy return is about 140 which is lower than the value for a well bond (around 180). This difference could be a factor to distinguish between a well bond and a kiss bond.

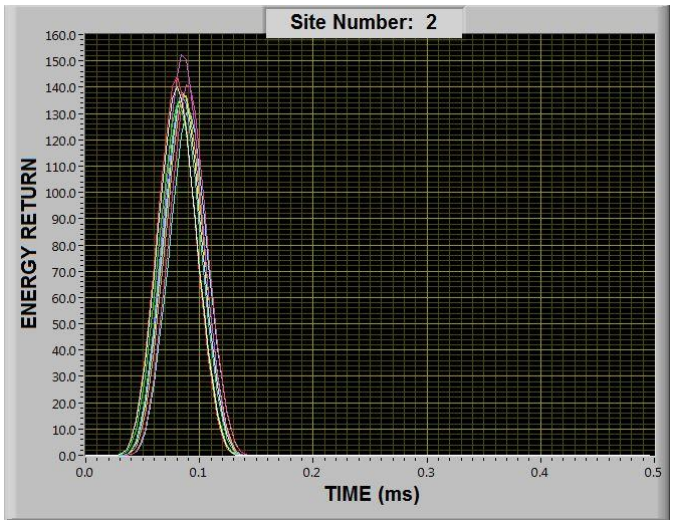

Figure 4-27: S7-13-15-R30-QPD for the middle of the bond on the front side

Figure 4-28 summarizes the stability index, which is proportional to the maximum energy return for all the test locations.

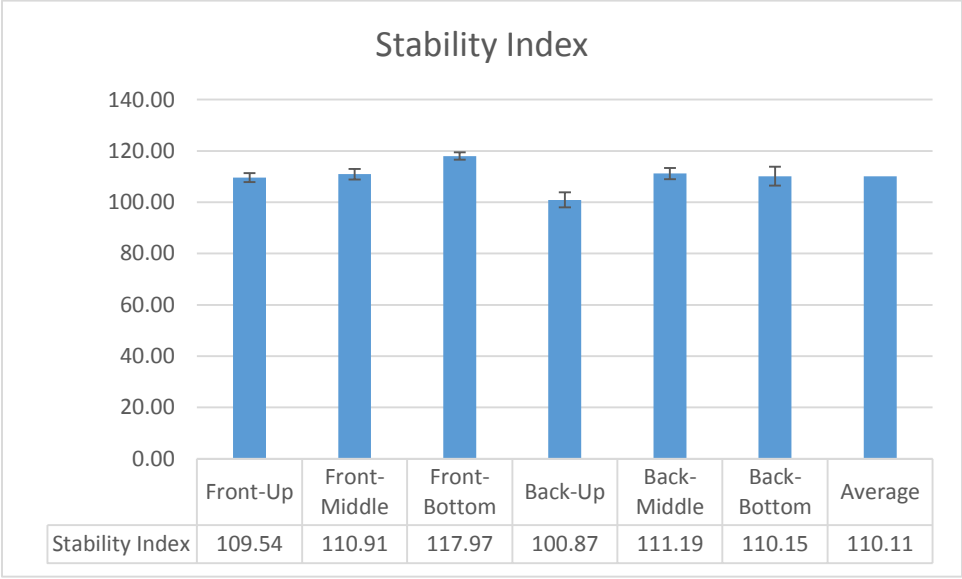

	Front-Up	Front-Middle	Front-Bottom	Back-Up	Back-Middle	Back-Bottom	Average
Stability Index	109.54	110.91	117.97	100.87	111.19	110.15	110.11

Figure 4-28: Stability Index for all the test locations for S7-13-15-R30. Relative Standard Deviation is used for error bars

4.1.8) Sample S8-14-16-R30

Figure 4-29 depicts the fracture surface for this sample. As mentioned in Figure 1-2, the smooth fracture surface and appearance of adhesive on only one substrate indicate an interfacial-mode of fracture, which represents a kiss bond.

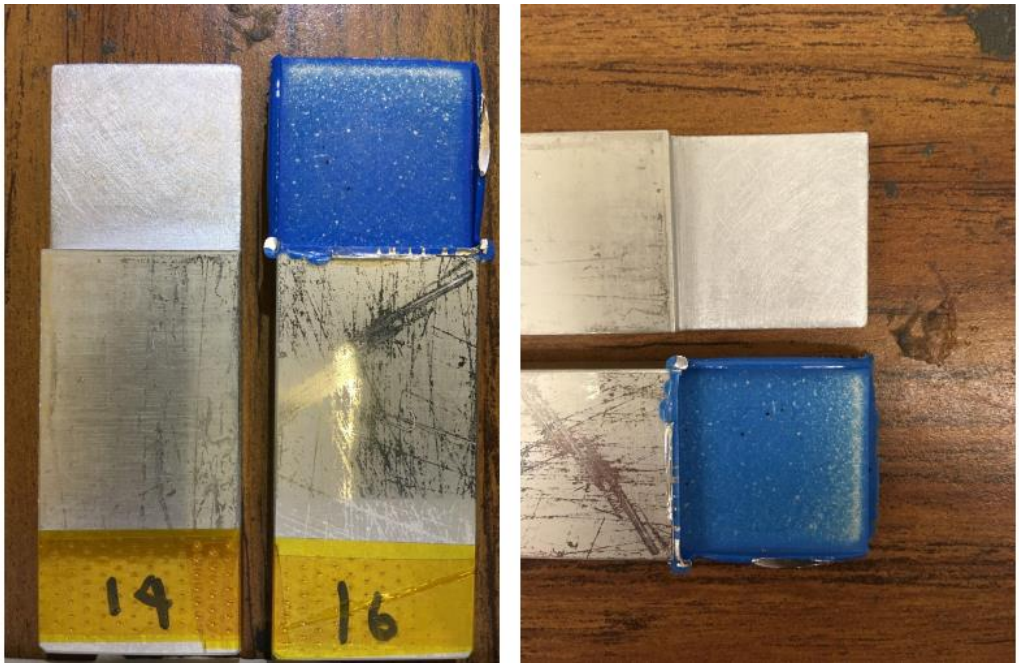

Figure 4-29: S8-14-16-R30-Fracture Surface

Figure 4-30 depicts the QPD result for the middle of the bond. The maximum energy return is about 130 which is lower than the value for a well bond (around 180). This difference could be a factor to distinguish between a well bond and a kiss bond.

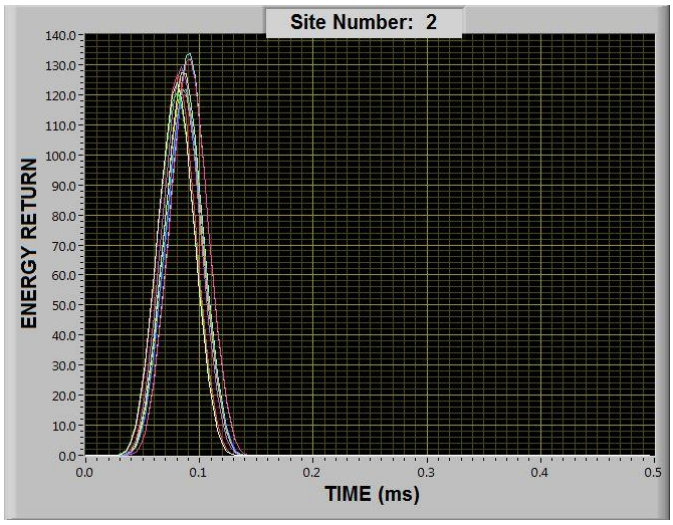

Figure 4-30: S8-14-16-R30-QPD for the middle of the bond on the front side

Figure 4-31 summarizes the stability index, which is proportional to the maximum energy return for all the test locations.

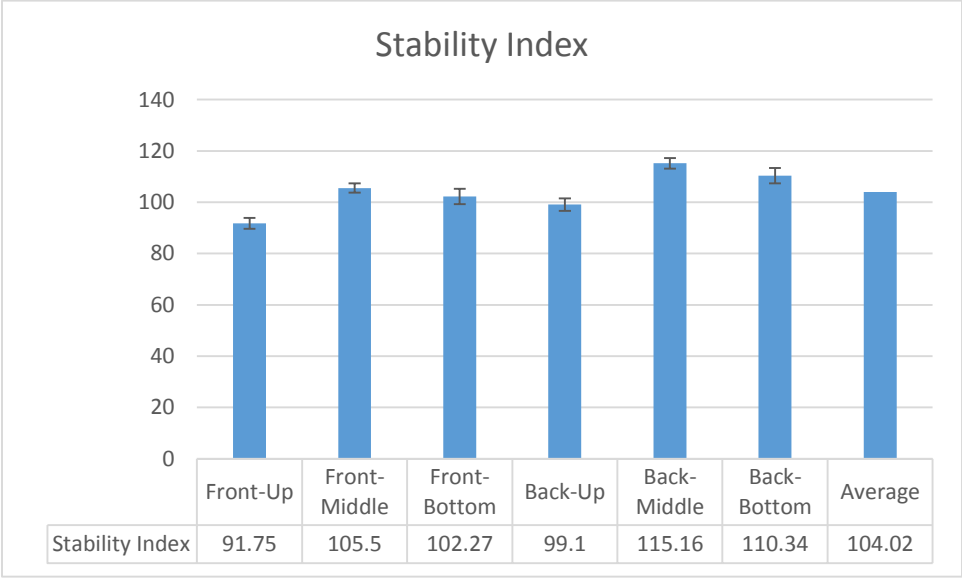

Figure 4-31: Stability Index for all the test locations for S8-14-16-R30. Relative Standard Deviation is used for error bars

4.1.9) Sample S9-17-18-W

Figure 4-32 depicts the Load vs. Displacement graph for this sample. The displacement rate for this test was 1 mm/min.

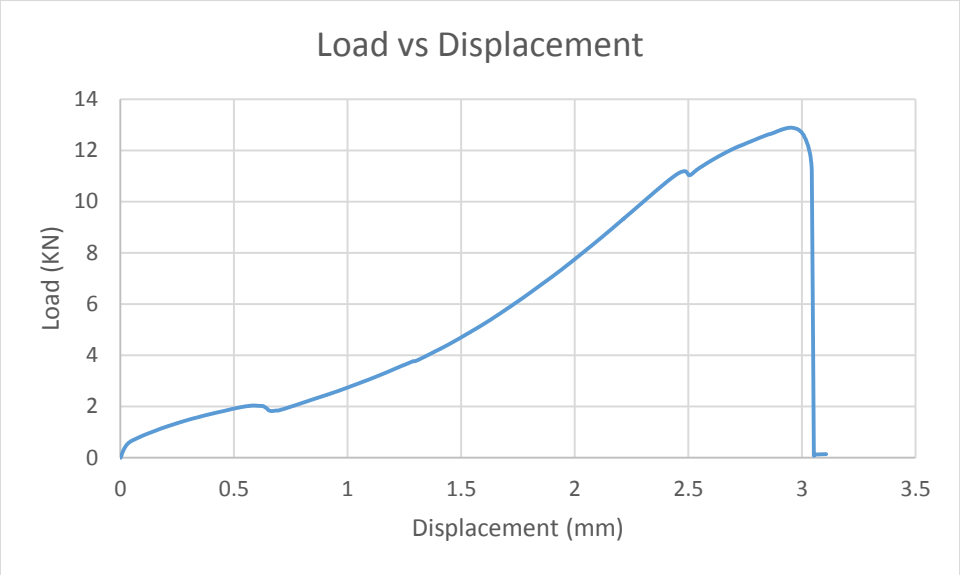

Figure 4-32: S9-17-18-W-Load vs. Displacement

Figure 4-33 illustrates the bending in this sample before failure.

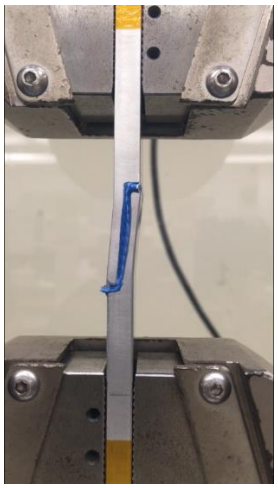

Figure 4-33: Bending in the S9-17-18-W stepped joint sample

Figure 4-34 depicts the fracture surface for this sample. As mentioned in Figure 1-2, the rough fracture surface and the appearance of both adhesive and the substrate at the same time, indicate a mixed-mode of fracture, which is representative of a well bond.

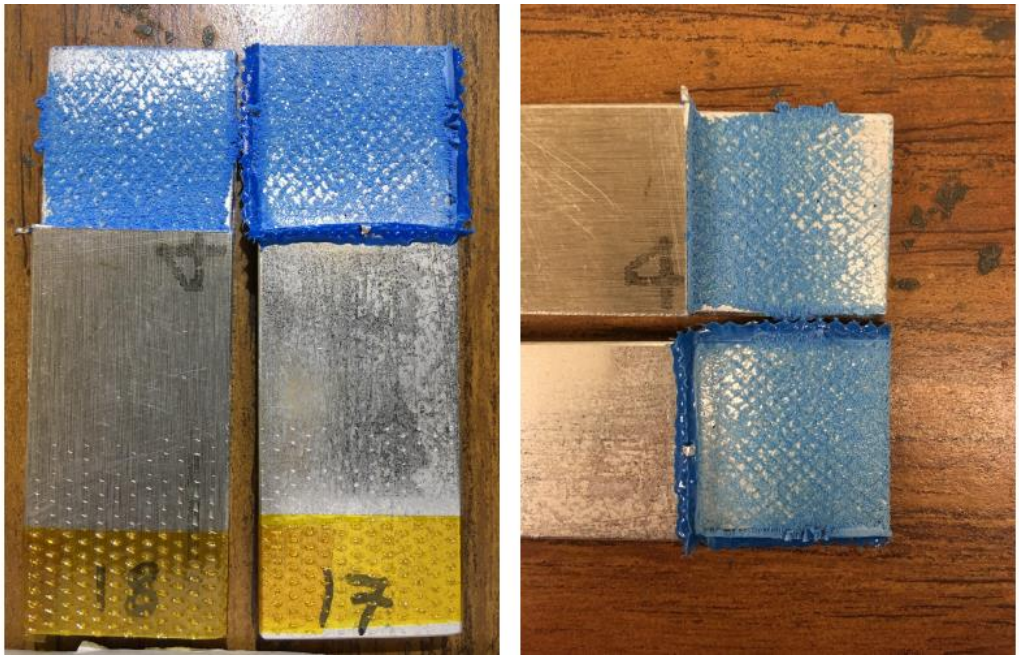

Figure 4-34: S9-17-18-W-Fracture Surface

4.2) Kiss bond samples using the introduction of aluminum tape

In this section, Aluminum tape is used to create a kiss bond. Four samples were fabricated. Two with 42% (17.78X15.24=270.97 mm^2) [0.7”X0.6”=0.42 in^2] released area and 2 with 24% (15.24X 10.16=154.84 mm^2) [0.6”X0.4”=0.24 in^2] released area. The released area is not applied symmetrically. Figure 4-35 depicts the shear and peel stress distribution for an SLJ with aluminum substrates. As it is apparent in Figure 4-35, the middle of the bond experience no significant load. So in order to magnify the effect of the released area, the released area’s geometry is chosen in

a way that it masks more in the direction of the bondline rather than the opposite direction.

Figure 4-36 depicts how Al tape is used to create the kiss bond.

Figure 4-35: Shear & Peel Stress Distributions in a SLJ based on the Goland and Reissner model for a joint with 25.2 mm bondline. The modulus of each substrate is 73.5 GPa. The thickness of each substrate is 3.09 mm. the modulus of the adhesive is 2 GPa. The bondline thickness is 74 µm. the width of the joint is 25 mm. the applied load in this case is 8697 N(Figure modified from the online program [13]).

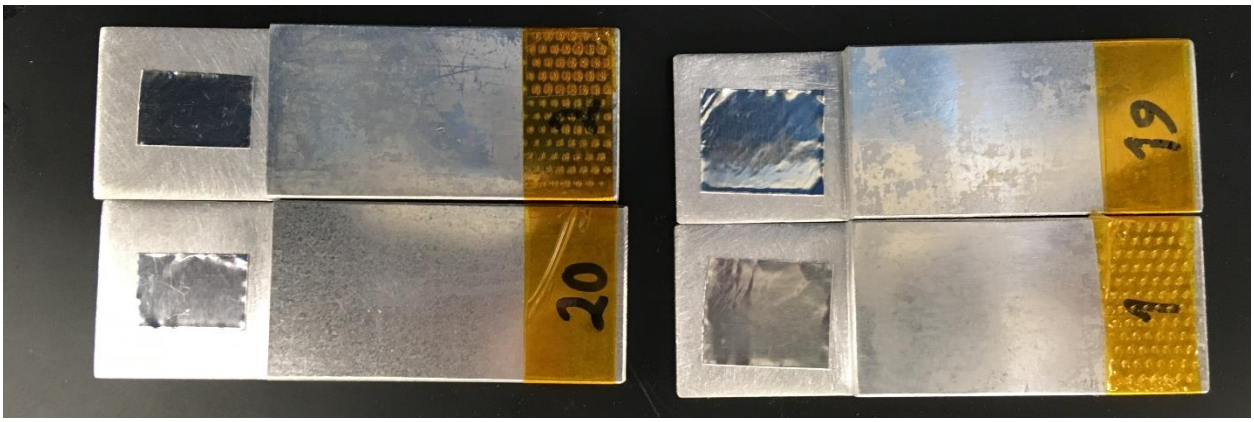

Figure 4-36: Al Tape used to create the kiss bond

Substrates 1, 2, 3, 9, 13, and 14 had been used before to create the previous set of samples with a kiss bond. All of these substrates were covered with the released agent. As it is apparent in Figure 4-6, Figure 4-9, Figure 4-12, Figure 4-19, Figure 4-26, and Figure 4-29, the failure in all of these cases was completely interfacial, and no adhesive remained on these substrates after failure. The remaining release agent was sanded off, and then the substrates were washed with soap and water. The thickness was measured in this step. The surface of these samples then wiped with acetone/ propanol/ acetone like previous samples to prepare them for bonding. The substrates 19 and 20 were machined from scratch and went through a surface preparation like previous substrates. The curing procedure was the same as the previous samples. Figure 4-37 illustrates the thickness of the substrates. Figure 4-38 illustrates the bondline thickness for these samples.

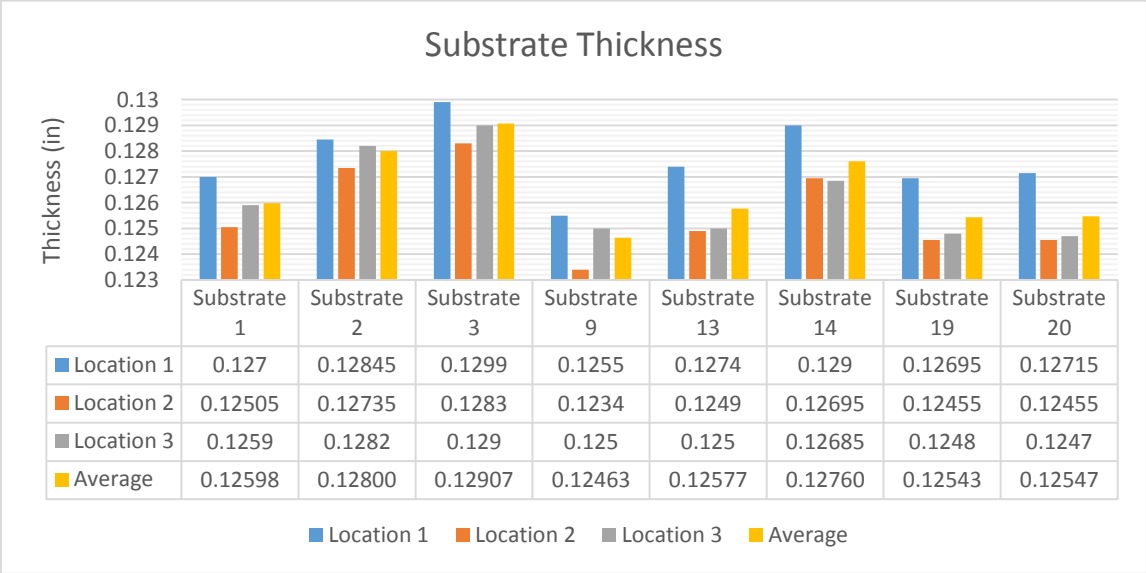

	Substrate 1	Substrate 2	Substrate 3	Substrate 9	Substrate 13	Substrate 14	Substrate 19	Substrate 20
Location 1	0.127	0.12845	0.1299	0.1255	0.1274	0.129	0.12695	0.12715
Location 2	0.12505	0.12735	0.1283	0.1234	0.1249	0.12695	0.12455	0.12455
Location 3	0.1259	0.1282	0.129	0.125	0.125	0.12685	0.1248	0.1247
Average	0.12598	0.12800	0.12907	0.12463	0.12577	0.12760	0.12543	0.12547

Figure 4-37: Thickness of the stepped joint coupons (1 in==25.4 mm)

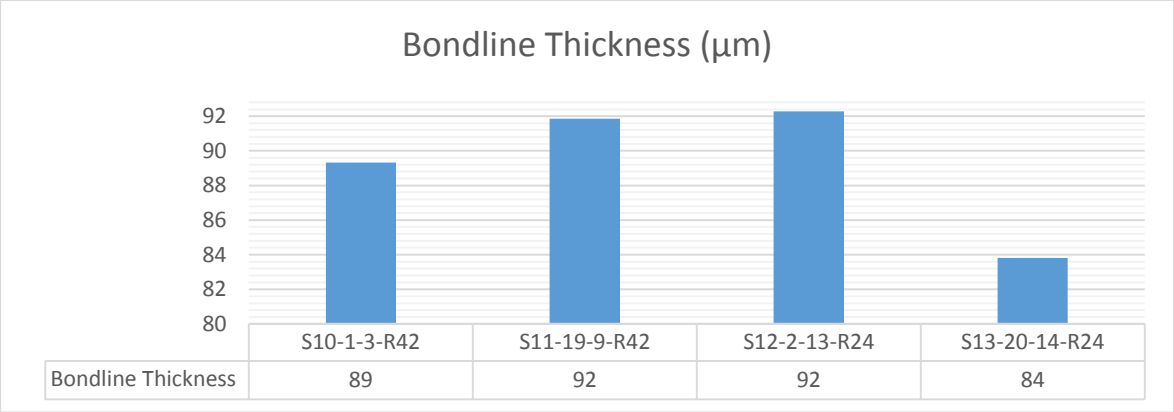

Figure 4-38: Bondline Thickness in micrometer (µm)

4.2.1) Sample S10-1-3-R42

Figure 4-39 depicts the Load vs. Displacement graph for this sample. The displacement rate for this test was 1 mm/min.

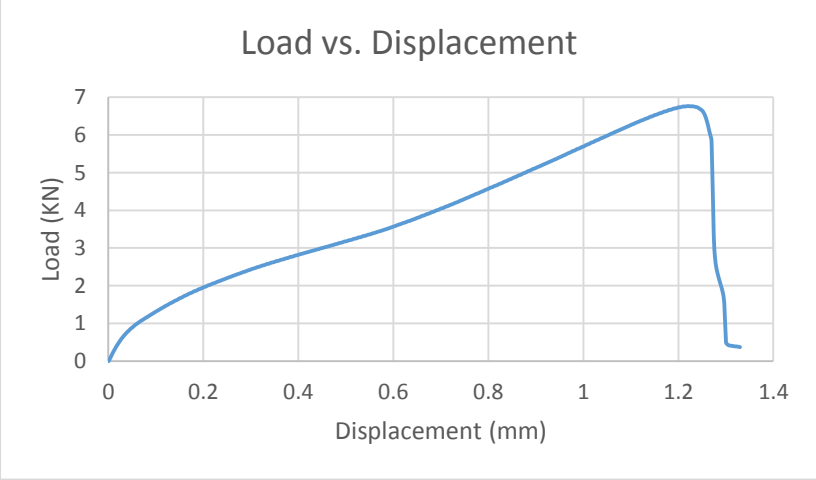

Figure 4-39: S10-1-3-R42- Load vs. Displacement

The failure was in the interface in the area that was covered with Al tape. Failure in the surrounding area was a mixed-mode that is representative of a well bond, like in previous samples with the well bond. Figure 4-40 depicts the fracture surface for this sample.

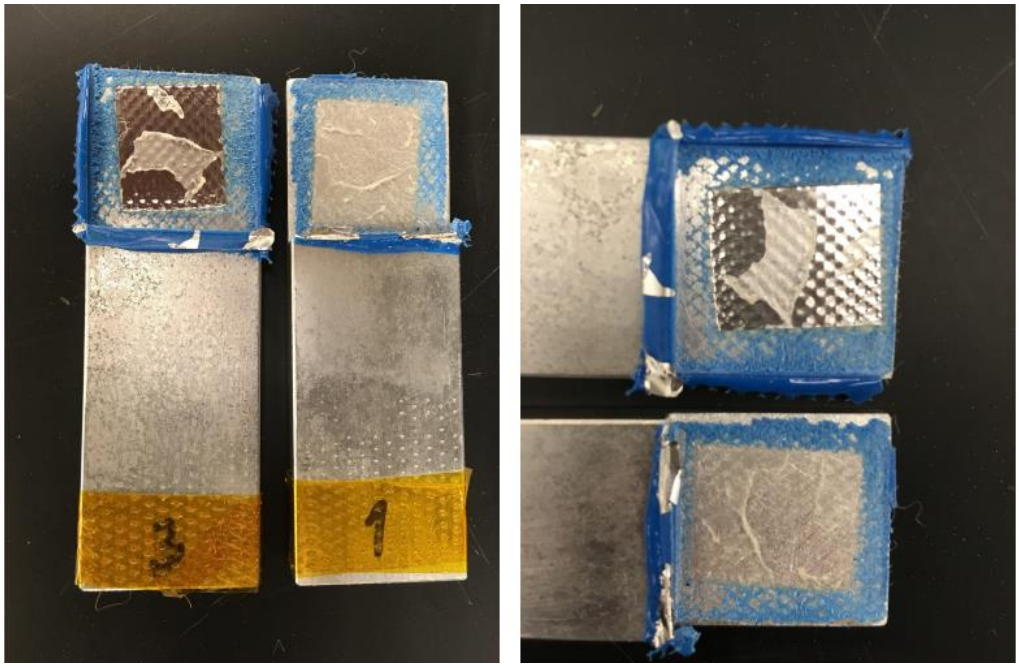

Figure 4-40: S10-1-3-R42- Fracture Surface

The QPD test was performed on this sample on 6 locations (3 locations from edge to edge and on both sides of the bond). The result for a test in the middle of the bond is as follows:

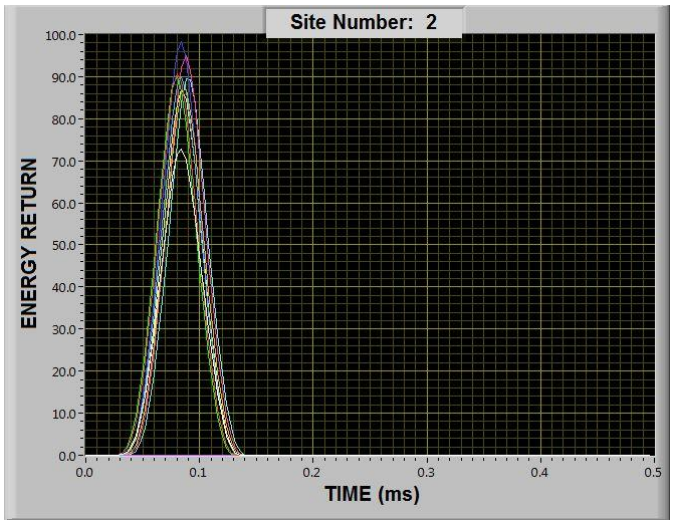

Figure 4-41: S10-1-3-R42-Front-middle

Figure 4-42 summarizes the stability index, which is proportional to the maximum energy return for all the test locations.

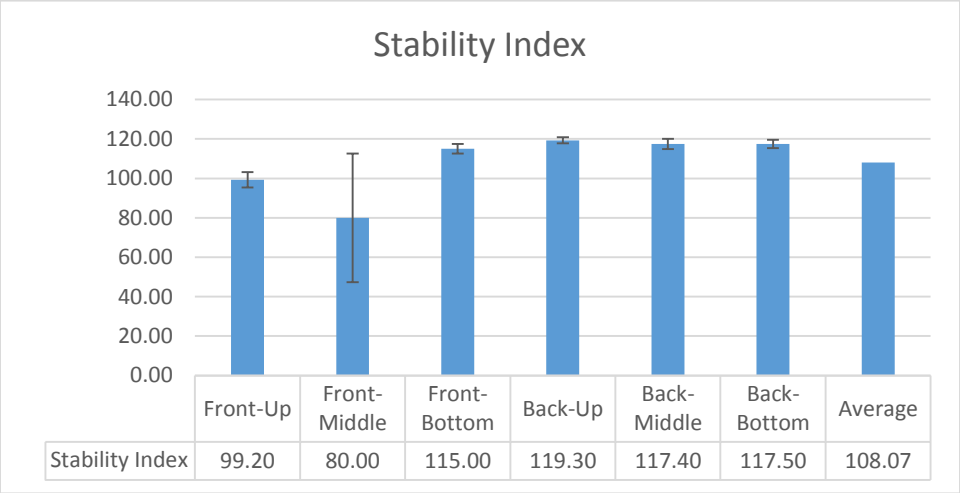

	Front-Up	Front-Middle	Front-Bottom	Back-Up	Back-Middle	Back-Bottom	Average
Stability Index	99.20	80.00	115.00	119.30	117.40	117.50	108.07

Figure 4-42: Stability Index for all the test locations for S10-1-3-R42. Relative Standard Deviation is used for error bars

It is possible to deduce several important points from this data. The stability index is lower when the test is performed on the front of the bond. Figure 4-43 schematically depicts the Al tape inclusion in the bond.

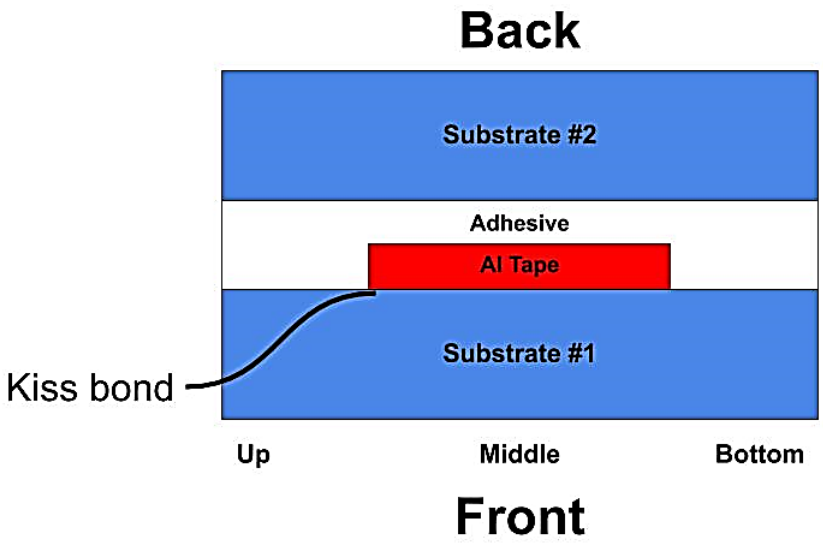

Figure 4-43: Schematic depiction of the Al tape inclusion

When the QPD test is performed in the front of the bond, the stress wave caused by the QPD test directly encounters the Al tape inclusion and the kiss bond caused by it. However, when the test is performed on the back of the bond, the stress wave has to progress through the adhesive layer in order to reach the kiss bond. By looking at the stability index results, it is apparent that the QPD is not able to detect the Al tape inclusion when the test is performed on the back of the bond. On the other hand, it is apparent that the test is sensitive to the Al tape inclusion when the test is performed on the front of the bond. More tests are required to investigate this phenomenon further. This could be a disadvantage for this technique because the access to both sides of the bond is not always possible, and also in practice, it is not known beforehand which substrate established a kiss bond with the adhesive layer. Some other NDTs suffer from such behavior as well. For example, Nagy reported that it was not possible to detect kissing bond by high angle ultrasonic test with 50 MHz from the other side [47].

The stability index data from the front of the bond shows that the result is also sensitive toward the relative position of the QPD probe in comparison to the kiss bond. The stability index is the lowest for the middle of the bond (80) when the probe is directly on the top of the kiss bond. The stability index for the location on the top of the bond (99.2) shows some sign of the Al inclusion. The stability index for the location on the bottom matches the result for a well bond (115). So in order to reliably detect a kiss bond, the probe should be directly on top of the defect. This means more data acquisition from closely located locations is necessary, which increases the duration to fully inspect a large part. Cawley & Adams investigated the presence of a defect with a coin-tap set up equipped with a force sensor. Their instrument is very similar to QPD. They observed

that the relative position of the probe in comparison to the defect affects the force vs. time behavior [33].

4.2.2) Sample S11-19-9-R42

Figure 4-44 depicts the Load vs. Displacement graph for this sample. The displacement rate for this test was 1 mm/min.

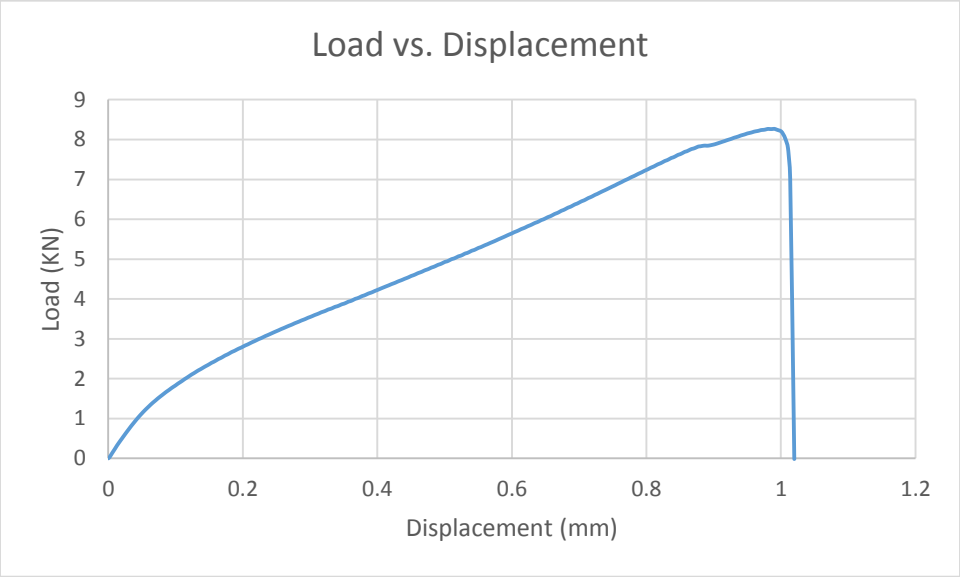

Figure 4-44: S11-19-9-R42-Load vs. Displacement

Here also failure is only interfacial in the area that was covered with Al tape. This means that the use of Al tape to create a kiss bond was successful and promising. The appearance of the meshing pattern of the nylon knit of the adhesive film on the Al film indicates that the bond experienced adequate pressure during the curing process. Figure 4-45 depicts the fracture surface for this sample.

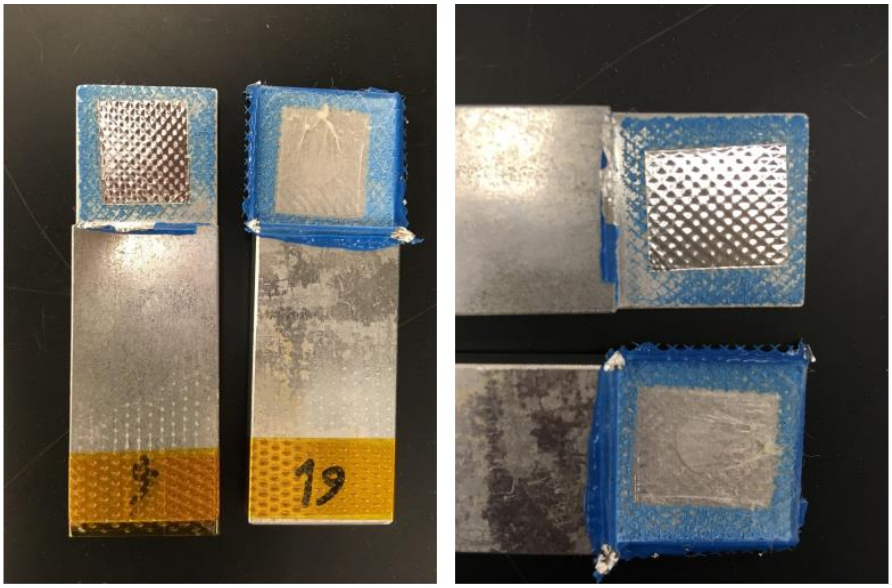

Figure 4-45: S11-19-9-R42-Fracture Surface

4.2.3) Sample S12-2-13-R24

Figure 4-46 depicts the Load vs. Displacement graph for this sample. The displacement rate for this test was 1 mm/min.

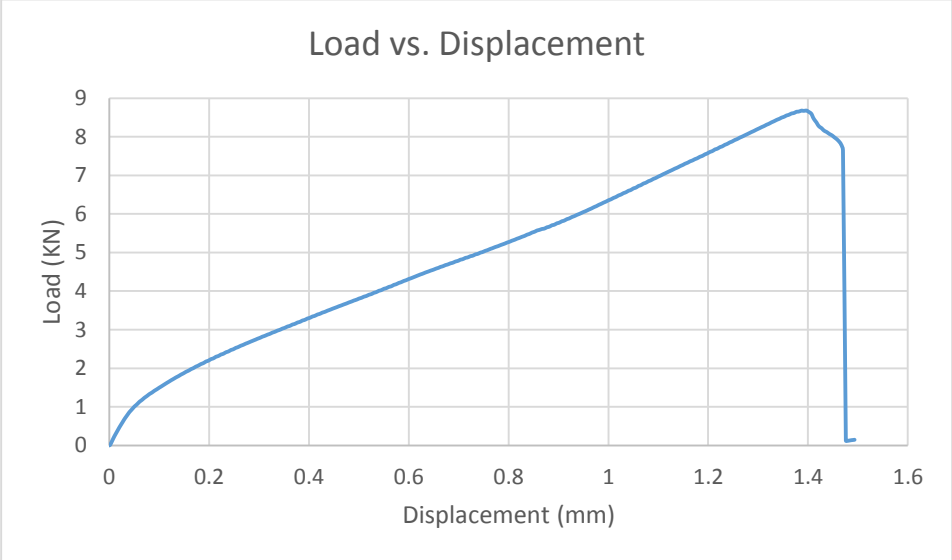

Figure 4-46: S12-2-13-R24-Load vs. Displacement

Here also failure is only interfacial in the area that was covered with Al tape. This means that the use of Al tape to create a kiss bond was successful and promising. Figure 4-47 depicts the fracture surface for this sample.

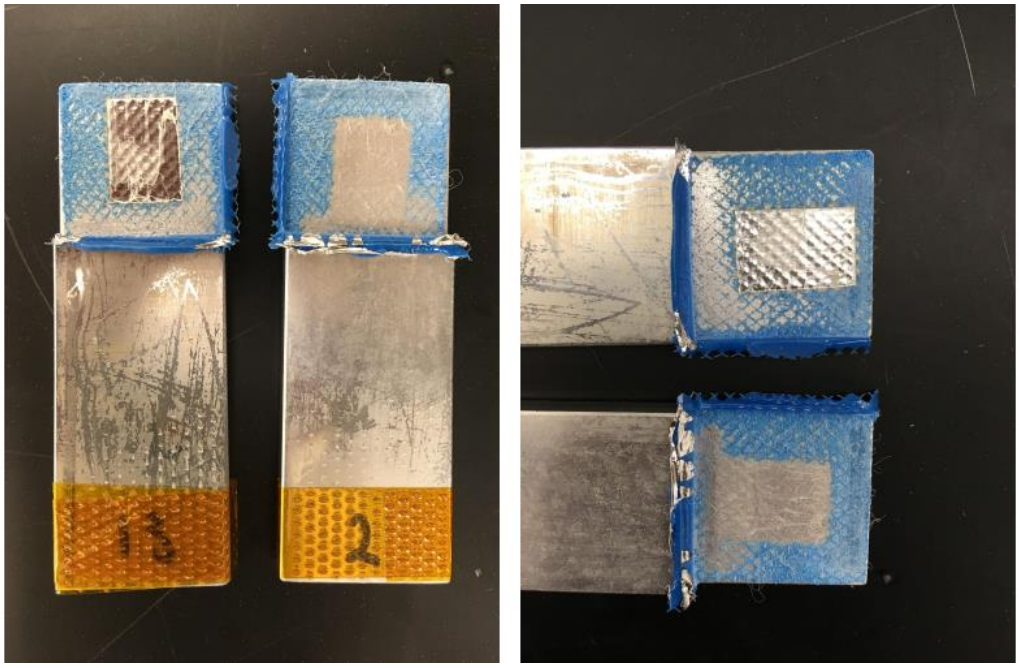

Figure 4-47: S12-2-13-R24-Fracture Surface

4.2.4) Sample S13-20-14-R24

Figure 4-48 depicts the Load vs. Displacement graph for this sample. The displacement rate for this test was 1 mm/min.

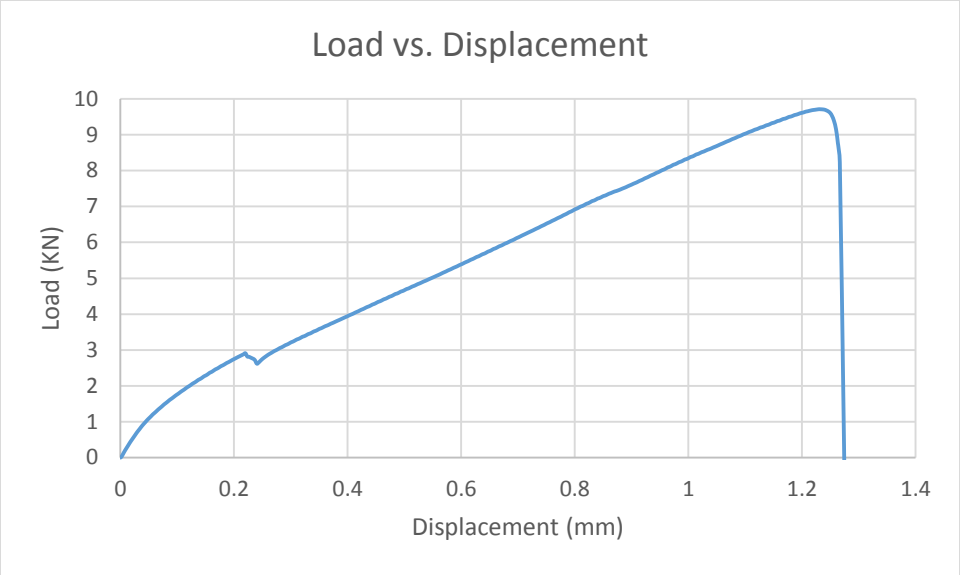

Figure 4-48: S13-20-14-R24- Load vs. Displacement

Here also failure is only interfacial in the area that was covered with Al tape. This means that the use of Al tape to create a kiss bond was successful and promising. Figure 4-49 depicts the fracture surface for this sample.

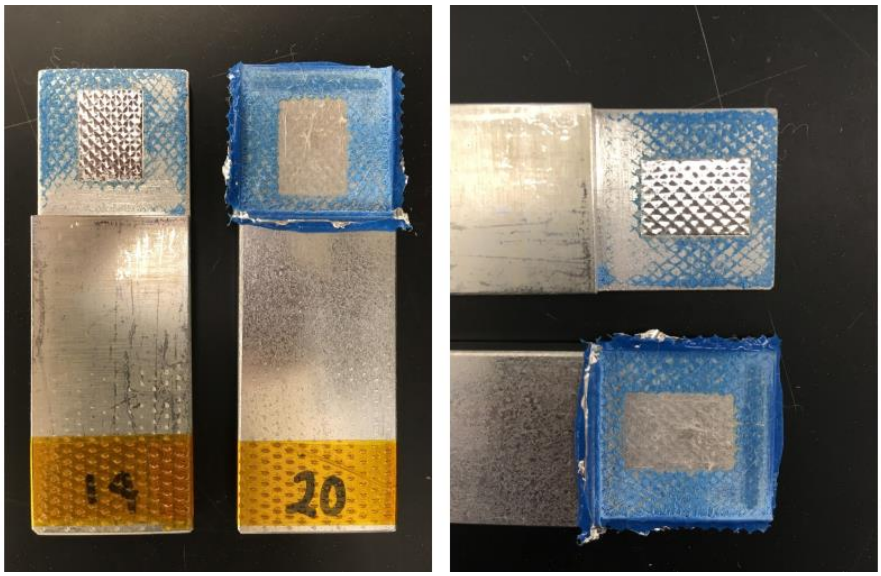

Figure 4-49: S13-20-14-R24-Fracture Surface

Due to my mistake, the data for QPD results for S11, S12, S13 was not saved on the computer. Additional samples should be fabricated to further investigate the QPD response of these sorts of samples.

4.3) Comparison of the mechanical performance of the stepped joint samples

Figure 4-50 illustrates the max load for all the samples with well bond or with partial flaw created by Al tape. The average max load for the well bonded samples is around 13 KN. The samples with 42% released area, have 100-42=58% well bonded area. By using this ratio, the max load for these samples should be 7.66 KN. The results for two samples with 42% released area (6.76, 8.27 KN) match that pretty well. The same is true for the 24% released samples. By using this ratio, the max load for these samples should be 9.9 KN. The results for two samples with 24% released area (8.7, 9.7 KN) match that pretty well.

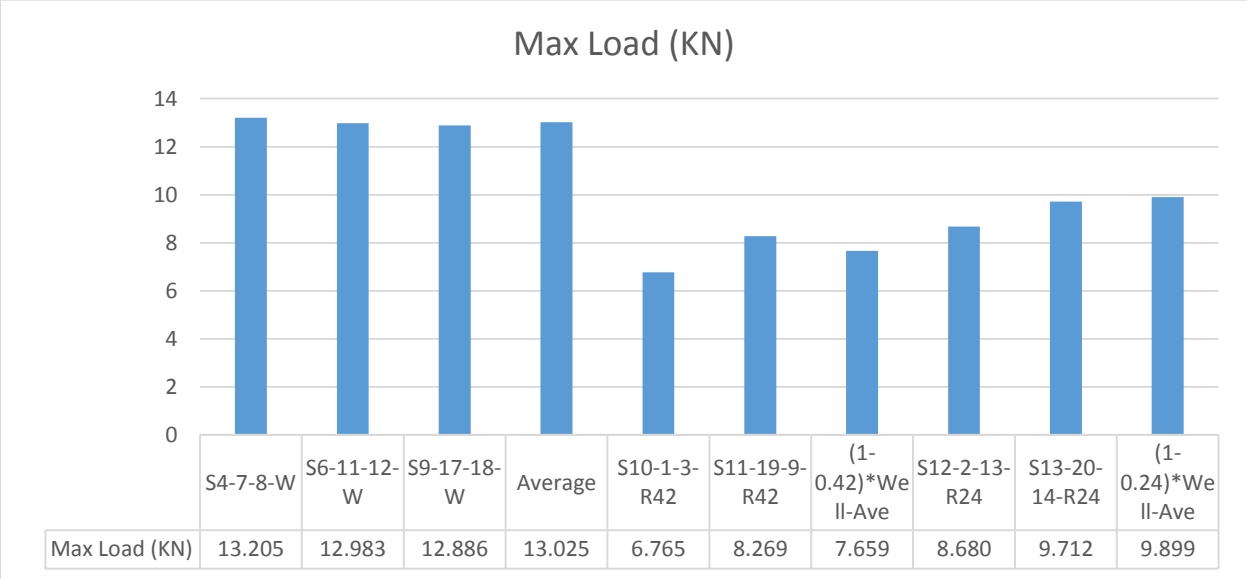

	S4-7-8-W	S6-11-12-W	S9-17-18-W	Average	S10-1-3-R42	S11-19-9-R42	(1-0.42)*Well-Ave	S12-2-13-R24	S13-20-14-R24	(1-0.24)*Well-Ave
Max Load (KN)	13.205	12.983	12.886	13.025	6.765	8.269	7.659	8.680	9.712	9.899

Figure 4-50: Maximum load for all the samples with well bond and with partial flaw created by Al tape inclusion

It is worth talking about the strange behavior of the stepped joint samples with a well bond (S4, S6, and S9). Figure 4-51 presents the load vs. displacement curve for these samples alongside each other. The behavior for all three samples follows the same abnormal pattern. The expected behavior from an SLJ with a brittle adhesive is a straight line with almost a constant slope up to the point of failure. However, here there is a plateau region (first red oval in the figure below). It is hard to explain this behavior. The adhesive is brittle, and the assumption that this plateau is due to the adhesive yield does not make sense. Plus, the load is much lower than the threshold to cause yield in the aluminum substrates. Then the stress increases sharply (second red oval in the figure below). If we ignore the first step, the second step matches the typical behavior of an SLJ with a brittle adhesive. Subsequently, a dent happens in the curve (the red circle in the figure below). This point represents the moment that the aluminum substrates yield, and the work hardening begins. The occurrence of the yielding in the aluminum substrates triggers excessive bending in the joint and subsequently develop high peel stress in the bond. The bond cannot survive under this circumstance and fail right after aluminum substrates yield.

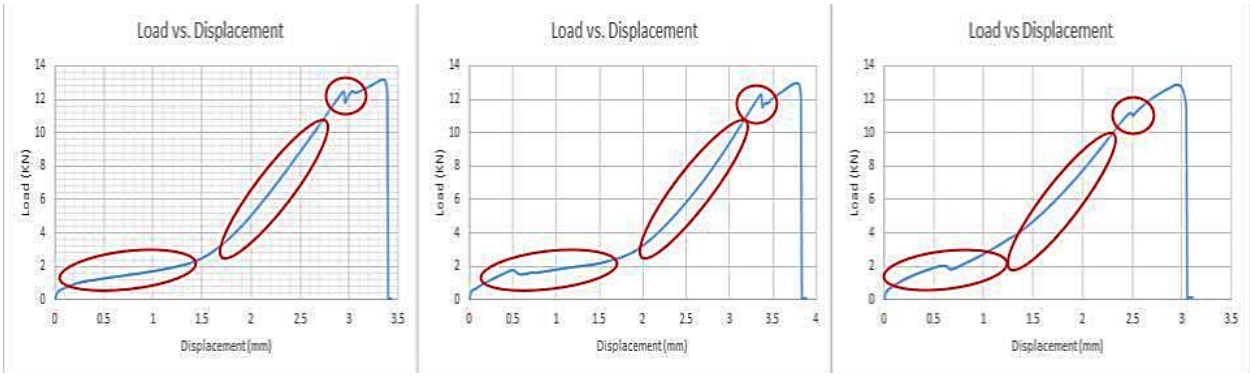

Figure 4-51: The load vs. displacement curve for samples with a well bond. Left) Sample S4, Middle) Sample S6, Right) Sample S9

On the contrary, for the samples with a partial kiss bond (S10 through S13), the load vs. displacement almost follows a straight line with a constant slope up to the point of failure. The failure load for these samples is lower than the threshold to cause yield in aluminum substrates. That leads to no excessive bending in the joint, and substrates do not sustain any residual bending after the mechanical test. Substrates from well-bonded samples experience residual bending after the mechanical test, and the detail of this matter is studied in section 4.6.

Table 4-1 summarizes the mechanical performance of all the stepped joint samples with a well bond or a partial flaw created by Al tape. The bond area is roughly 645.16 mm^2 (1 in^2). An interesting observation from the data in Table 4-1 is that the existence of a partial kiss bond does not alter the initial response of the adhesively-bonded joint and only alter the failure load. Figure 4-52 illustrates the comparison between the initial tangents among all the samples. Contrary to intuition, by looking at the trend for initial tangent and Max. load/Max. Displacement data, it seems that samples with a partial kiss bond experience higher brittleness characteristics. It is hard to explain this phenomenon at this point. More tests are required to examine this idea more thoroughly.

Table 4-1: Summary of mechanical properties for stepped joint samples

	S4-7-8-W	S6-11-12-W	S9-17-18-W	S10-1-3-R42	S11-19-9-R42	S12-2-13-R24	S13-20-14-R24
Max Load (kN)	13.205	12.983	12.886	6.765	8.269	8.680	9.712
Max Load/ Bond area (Mpa)	20.468	20.124	19.973	10.486	12.817	13.454	15.054
Max Displacement (mm)	3.350	3.774	2.954	1.220	0.990	1.397	1.230
Bondline Thickness (µm)	38	68	152	89	92	92	84
Max Displacement/ bonline thickness	87.895	55.367	19.487	13.662	10.780	15.139	14.674
Max Load/ Max Displacement (KN/mm)	3.942	3.441	4.363	5.544	8.350	6.213	7.896
Initial Tangent (KN/mm)	20.014	21.451	20.789	22.422	24.540	23.015	24.694

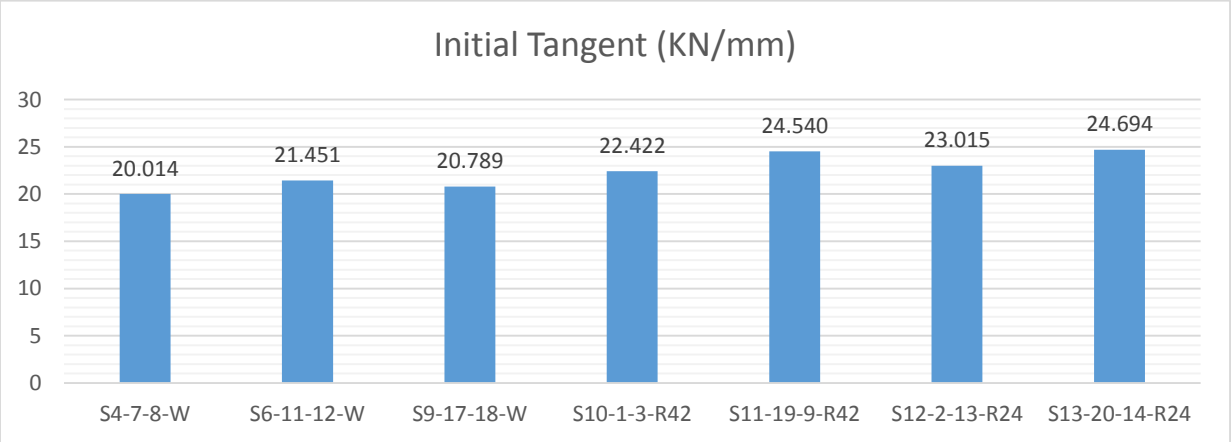

Figure 4-52: The Initial Tangent among all the samples. The Existence of a partial kiss bond does not alter the initial response of the adhesively bonded joint. The standard deviation is 1.79 for this set of data

4.4) Comparison of the QPD results of the stepped joint samples

A comparison of the QPD results of the samples determines that the stability index for a sample with a kiss bond is, on average lower than the stability index for a sample with a well bond. Figure 4-53 illustrates the average stability index for all the samples. The samples with a well bond are illustrated in red. Standard deviation is used to calculate the error bars. The data illustrates that even though the average value of the Stability Index is lower for a sample with a kiss bond, but there are instances that samples with a kiss bond also show high values for Stability Index which are close to the typical value of the Stability Index for a sample with a well bond. This makes it difficult to draw a definite conclusion based on the stability index data alone. More rigorous statistical comparison of the results are required.

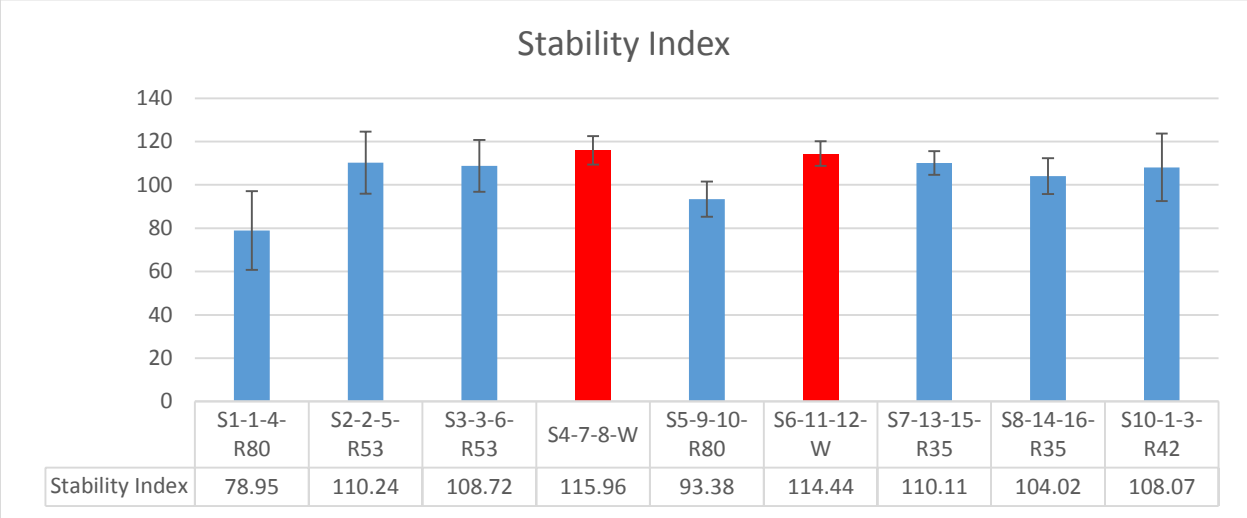

	S1-1-4-R80	S2-2-5-R53	S3-3-6-R53	S4-7-8-W	S5-9-10-R80	S6-11-12-W	S7-13-15-R35	S8-14-16-R35	S10-1-3-R42
Stability Index	78.95	110.24	108.72	115.96	93.38	114.44	110.11	104.02	108.07

Figure 4-53: Stability Index data for all the samples- standard deviation is used for calculating the error bars

The sample S4-7-8-W is taken as the reference sample with a well bond. By comparing the stability index data between two samples, it is possible to calculate the p-value. The paired t-test

was conducted between two sets of data and the one-tail p-value was calculated. If the value is less than 0.05, it means that there is a significant difference between two sets of data (0.02 would be a more sensitive limit).The p-value when the stability index data for the two samples with a well bond (S4-7-8-W & S6-11-12-W) is compared, is 0.362>>0.05. It means that there is no significant difference between the two sets of data. So the stability index data for the samples with a well bond is consistent.

The sample S4-7-8-W is taken as the reference sample with a well bond, and the stability index data for all the other samples with a kiss bond is compared to it in order to calculate the p-value. Figure 4-54 illustrates the p-value for all the samples. The p-value for most of the samples with a kiss bond other than S2 & S10 is less than 0.05, which indicates a significant difference between their QPD results and a reference sample with a well bond.

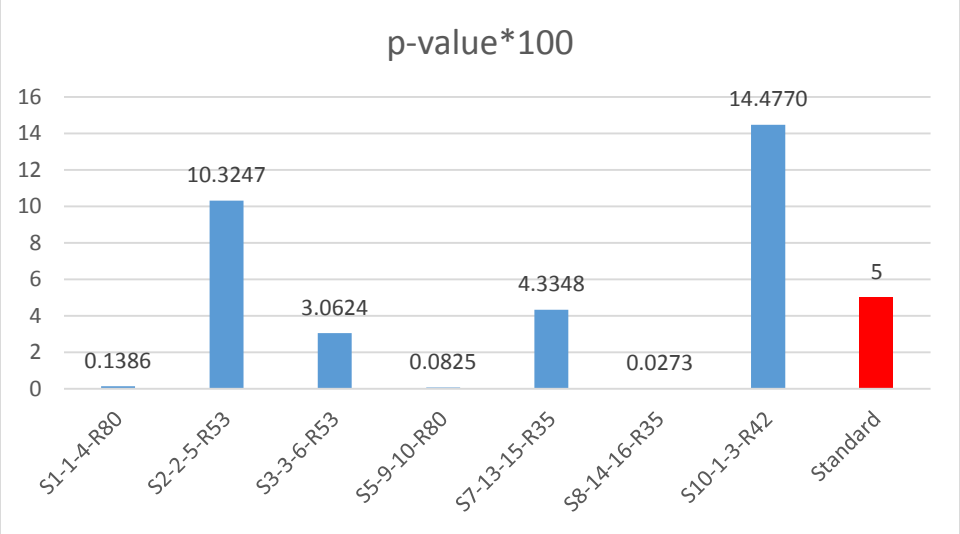

Figure 4-54: the p-value for all the samples compared to S4-7-8-W

Based on the two arguments mentioned above, it is possible to conclude that performing a high number of tests and then comparing the data with a reference sample with a well bond by calculating the p-value is a more reliable and more definite procedure to detect a kiss bond rather than comparing the average Stability Index values. More samples should be prepared, and more tests should be performed to enhance the statistical confidence.

4.5) Inspecting the fracture surface of samples with KEYENCE™ optical microscope

The topography of a well-bonded sample and a sample with a kiss bond is investigated with a KEYENCE™ Optical Microscope. This instrument can generate the topography of a surface by adjusting the depth of focus.

Figure 4-55 illustrate the topography for a well-bonded sample. Due to the fact that the mode of failure is a mixed-mode in a well bond, the topography is very erratic with a lots of hills and valleys. Figure 4-56 illustrates the topography for a sample with a kiss bond. The failure here is interfacial, and the fracture surface is very smooth, which is apparent in the topography. Mr. Zack McKee from KEYENCE™ captured all of these images as a part of a demonstration that I organized.

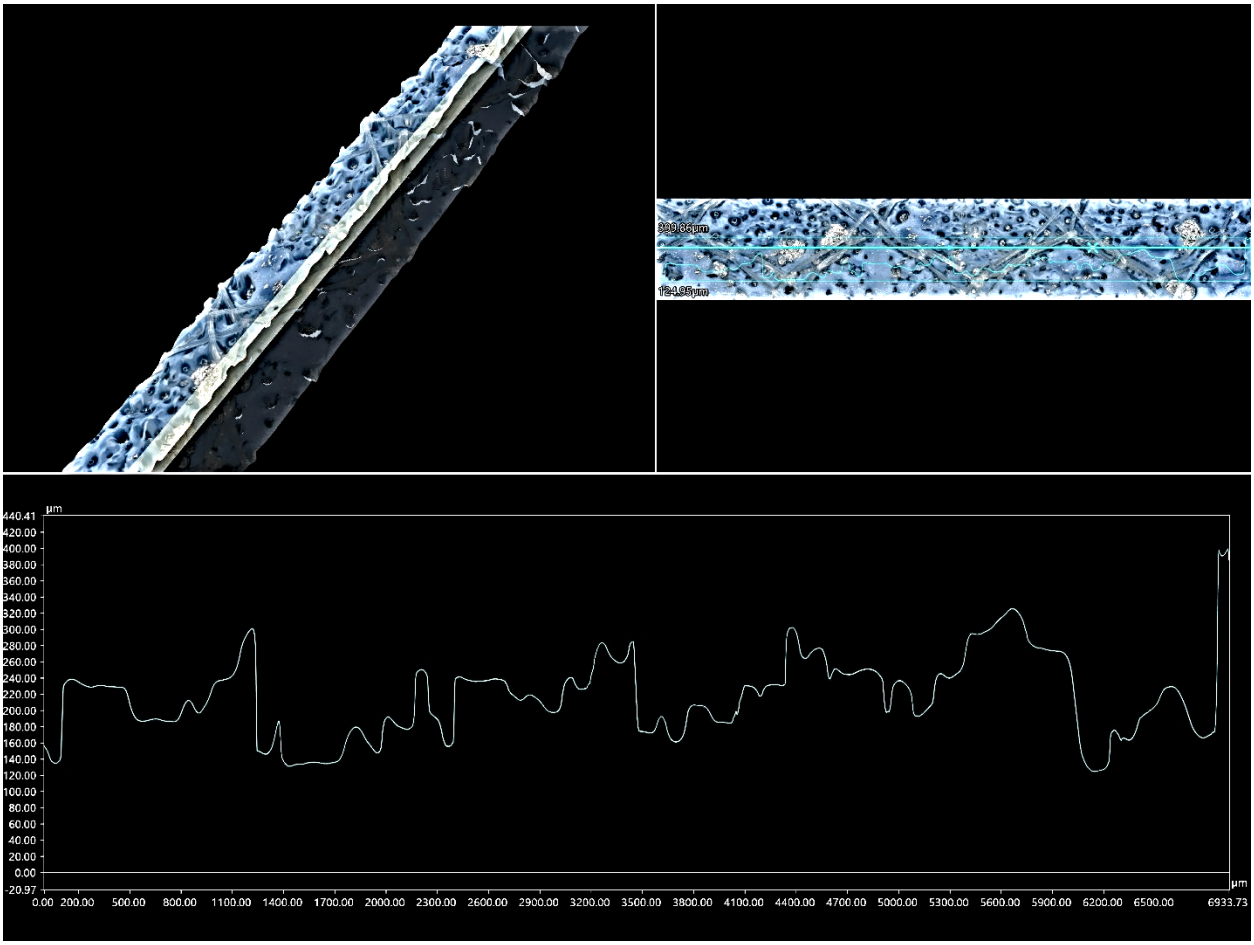

Figure 4-55: Topography of a well-bonded sample derived with KEYENCE™ optical microscope

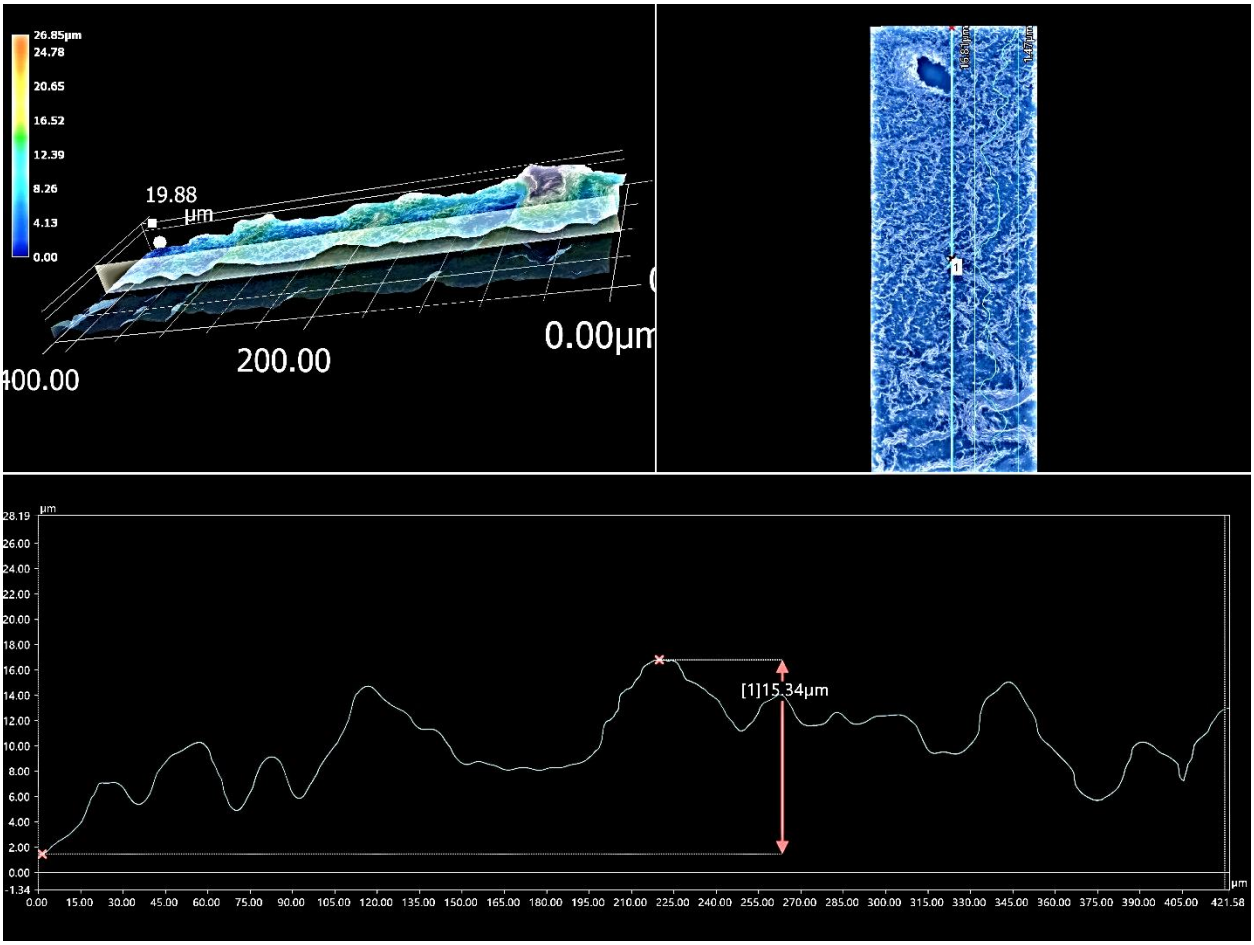

Figure 4-56: Topography of a sample with a kiss bond derived with KEYENCE™ optical microscope

4.6) Bending contour of a well-bonded sample

Figure 4-57 illustrates the bending contour of a substrate #7 of a well-bonded sample.

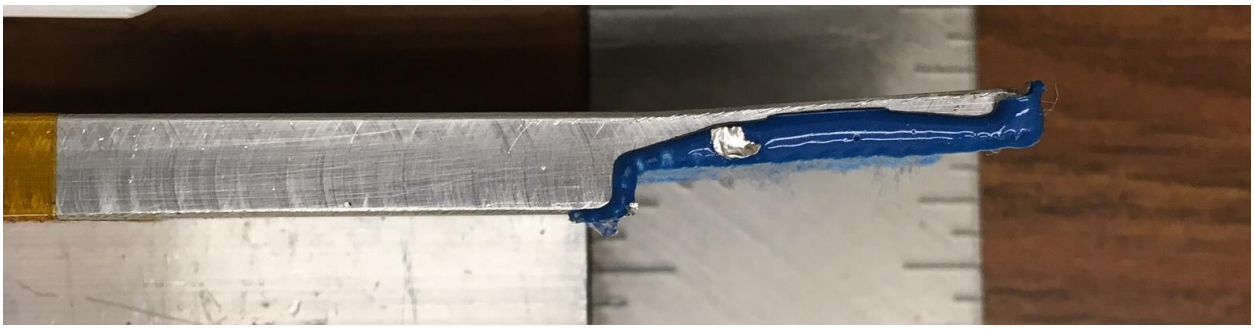

Figure 4-57: Bending contour of substrate #7

The ImageJ software is used to determine the bending contour. A linear and a polynomial trend line is fitted on the result. Figure 4-58 illustrate the result. The polynomial trend line is as follow:

$y = -0.0514x^6 + 0.2668x^5 - 0.4676x^4 + 0.3046x^3 - 0.0193x^2 + 0.0301x$

$R^2 = 0.9992$

The linear trend line is: $y = 0.0623x$

$R^2 = 0.9856$

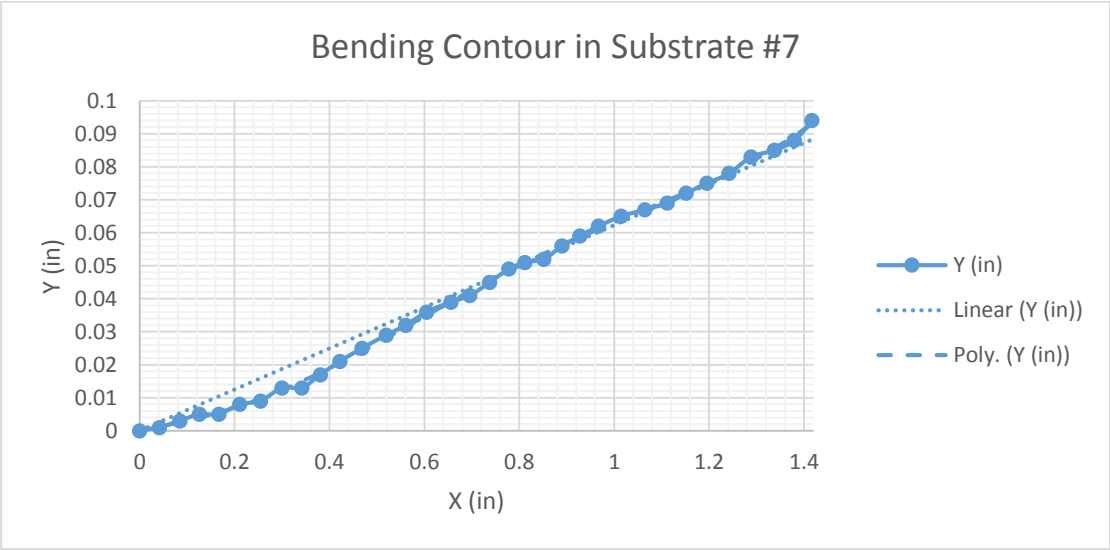

Figure 4-58: Bending Contour of substrate #7

Same process was used for other substrates of well bonded samples.

Substrate #8:

Figure 4-59 illustrates the bending contour for this substrate

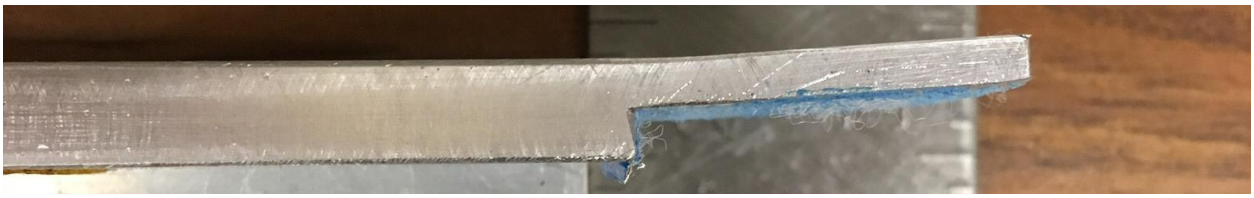

Figure 4-59: Bending contour of substrate #8

A linear and a polynomial trend line is fitted on the result. Figure 4-60 illustrates the result. The polynomial trend line is as follow:

$y=0.0384x^6-0.1769x^5+0.3345x^4-0.3409x^3+0.1996x^2+0.0097x$

$R^2 = 0.9994$

The linear trend line is: y = 0.064x

$R^2 = 0.9897$

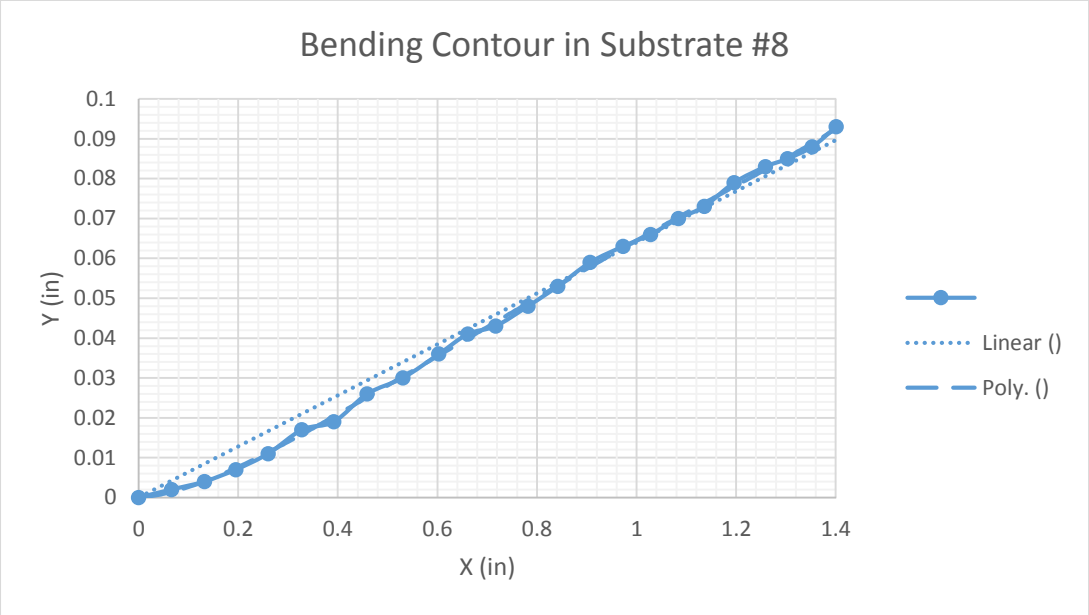

Figure 4-60: Bending Contour of substrate #8

Substrate #11

Figure 4-61 illustrates the bending contour of this substrate.

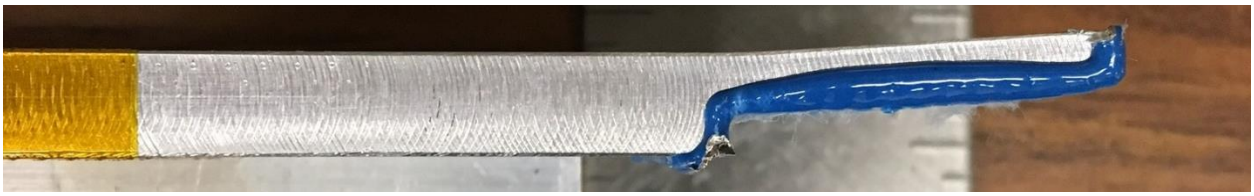

Figure 4-61: Bending contour of substrate #11

A linear and a polynomial trend line is fitted on the result. Figure 4-62 illustrates the result. The polynomial trend line is as follow:

$y=0.0542x^6-0.2612x^5+0.5031x^4-0.5002x^3+0.2762x^2-0.0192x$

$R^2 = 0.9992$

The linear trend line is: y = 0.0518x

$R^2 = 0.9696$

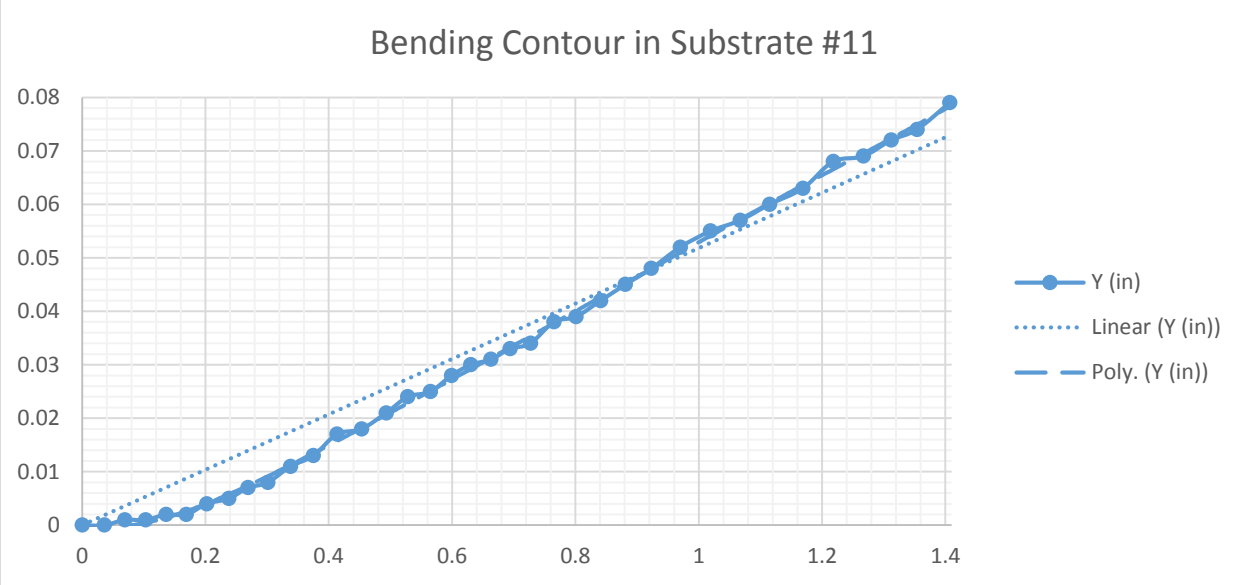

Figure 4-62: Bending contour of substrate #11

Substrate #12

Figure 4-63 illustrates the bending contour of this substrate.

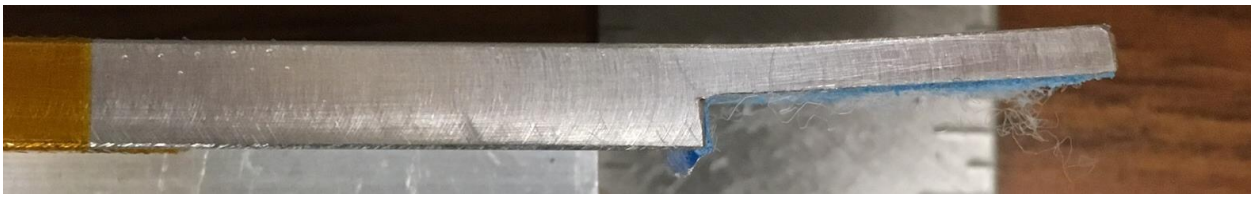

Figure 4-63: Bending contour of substrate #12

A linear and a polynomial trend line is fitted on the result. Figure 4-64 illustrates the result. The polynomial trend line is as follow:

$y=-0.0671x^6+0.3044x^5-0.4975x^4+0.3256x^3-0.0248x^2+0.0039x$

$R^2 = 0.9991$

The linear trend line is: $y = 0.044x$

$R^2 = 0.9312$

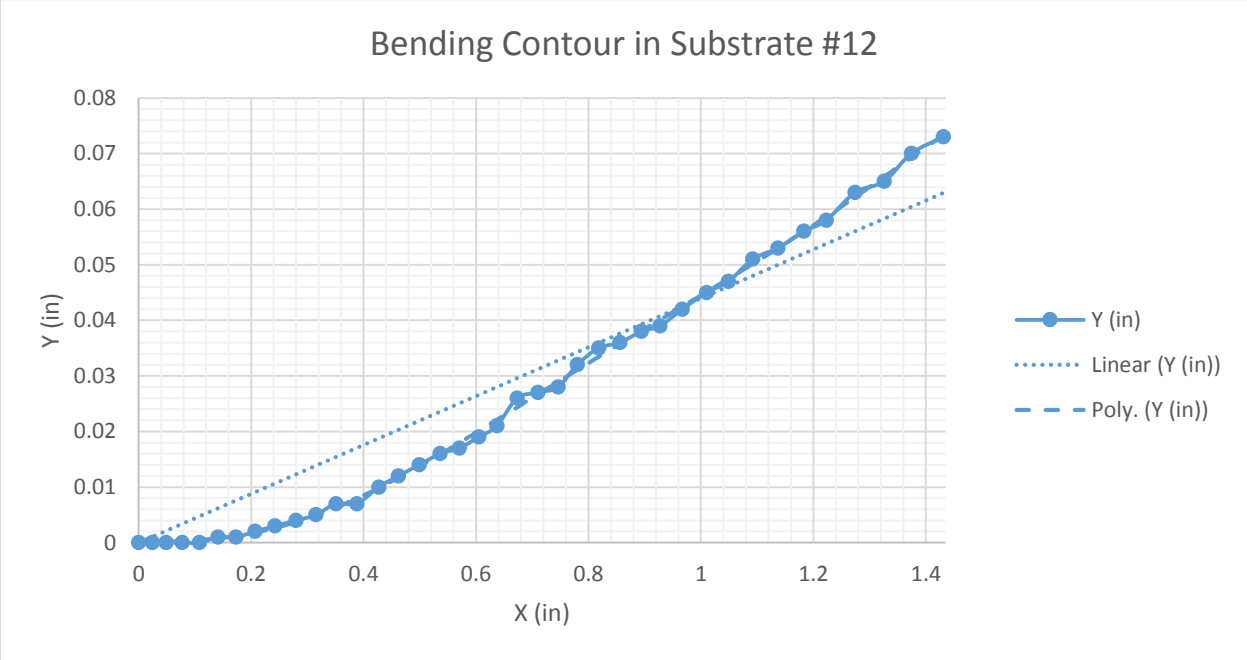

Figure 4-64: Bending contour of substrate #12

Substrate #17

Figure 4-65 illustrates the bending contour of this substrate.

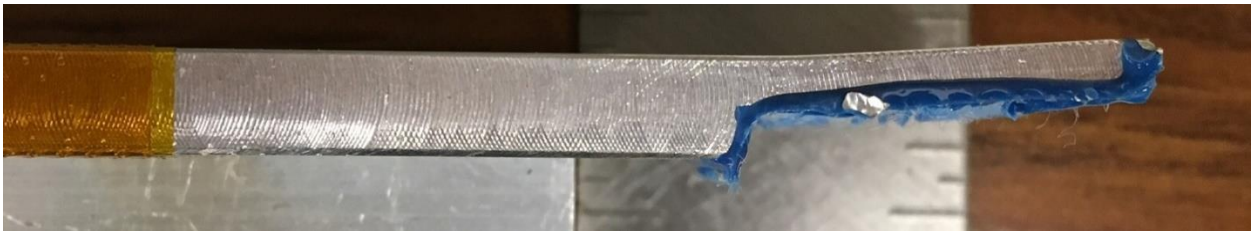

Figure 4-65: Bending contour of substrate #17

A linear and a polynomial trend line is fitted on the result. Figure 4-66 illustrates the result. The polynomial trend line is as follow

$y=-0.0125x^6-0.0058x^5+0.147x^4-0.2776x^3+0.2174x^2-0.0266x$

$R^2 = 0.9984$

The linear trend line is: $y = 0.0424x$

$R^2 = 0.9444$

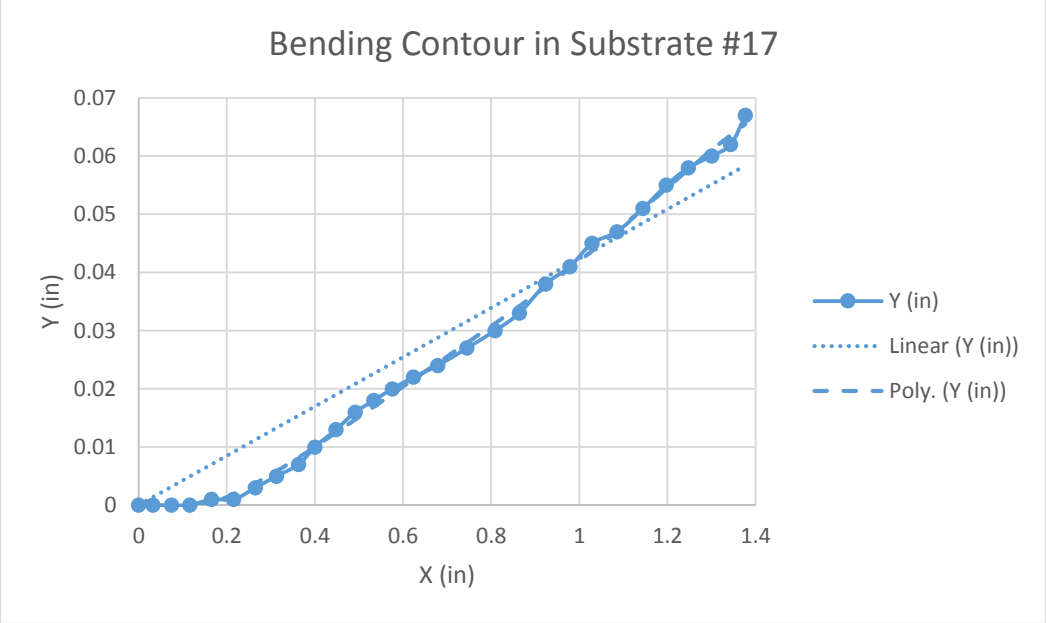

Figure 4-66: Bending contour of substrate #17

Substrate #18

Figure 4-67 illustrates the bending contour of this substrate.

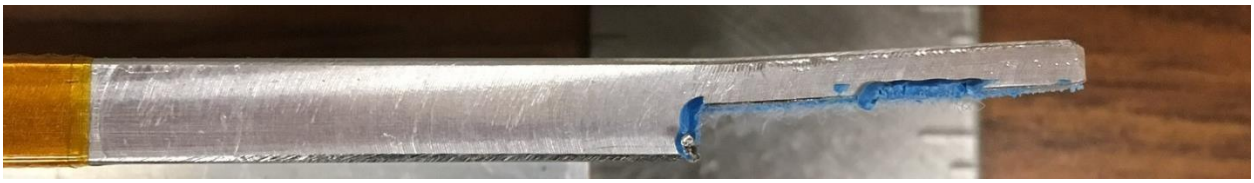

Figure 4-67: Bending contour of substrate #18

A linear and a polynomial trend line is fitted on the result. Figure 4-68 illustrates the result. The polynomial trend line is as follow:

$y=0.0081x^6-0.0546x^5+0.1038x^4-0.0921x^3+0.0625x^2+0.0241x$

$R^2 = 0.9995$

The linear trend line is: y = 0.0503x

$R^2 = 0.9856$

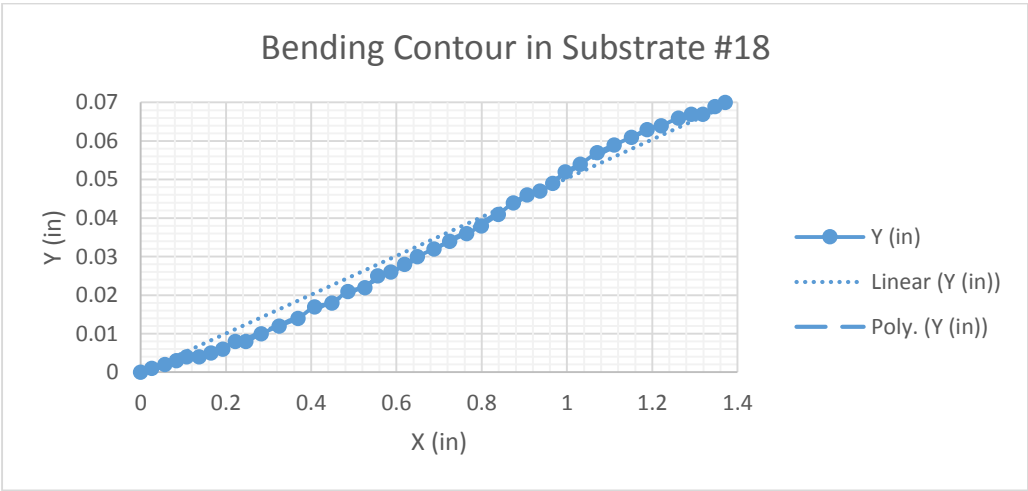

Figure 4-68: Bending Contour of substrate #18

Figure 4-69 illustrates the comparison between the maximum displacements of all the substrates.

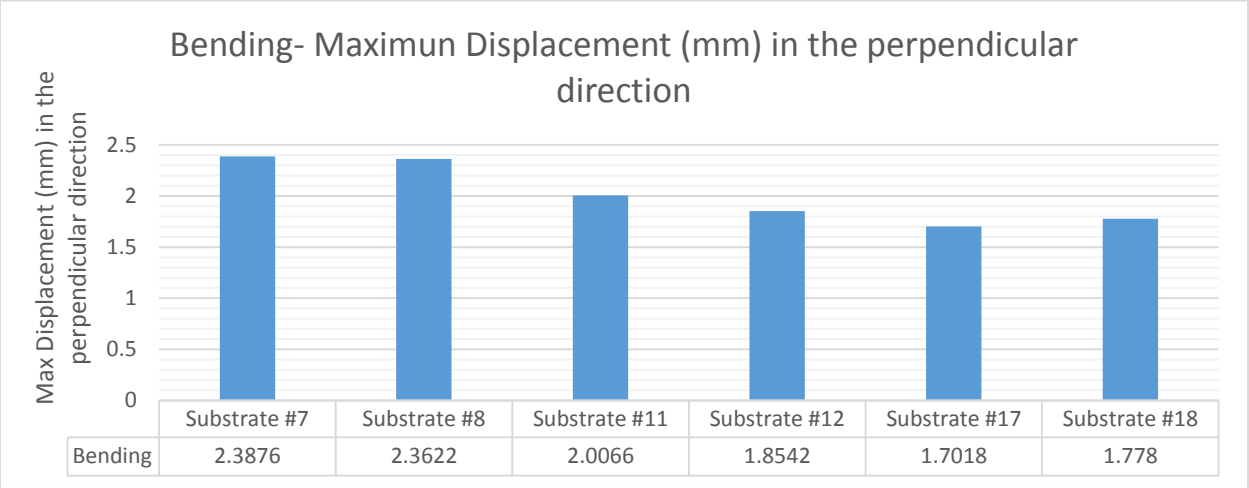

Figure 4-69: Bending Comparison between all the substrates- the standard deviation for this set of data is 0.296. The bending follows the same pattern for all the sample and there is no anomaly in the data set.

4.7) Samples with microscope slides as substrate

Five samples were fabricated using microscope slides as substrate under different conditions. One with adequate pressure during curing, one with no applied pressure, two with a partial area covered with a release agent, and one with the entire area covered with a release agent. There is no obvious difference in texture between these samples. However, in the case of one of the samples that is covered with a release agent, there is some sign of moisture ingress. Further investigation with higher resolution microscopes could lead to more understanding. Figure 4-70 depicts these samples.

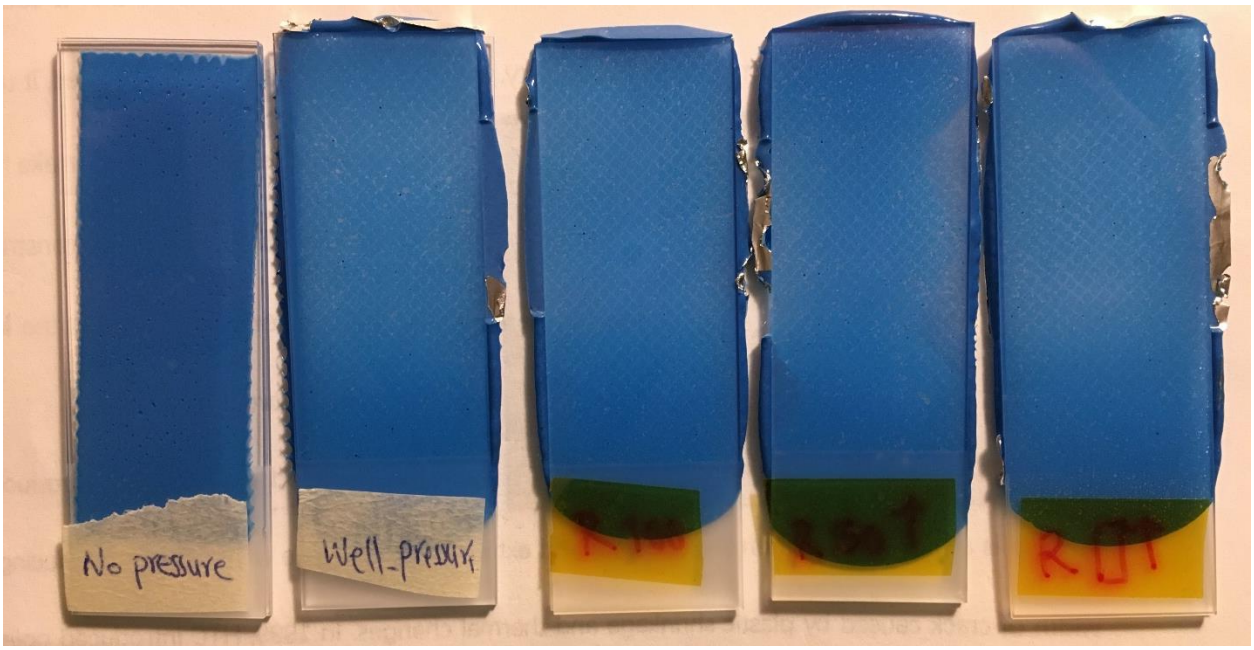

Figure 4-70: Samples which microscope slides were used as substrates. From Left: no pressure, Well pressured, 100% release, 50% released, masked

4.8) Second set of samples with aluminum tape inclusion to create a kiss bond

Eight new substrates were machined to fabricate four new samples. Figure 4-71 illustrates the thickness of these substrates. The surface preparation was the same as the previous samples. The Al tape was used again as an inclusion to create a kiss bond. Figure 4-72 illustrates the substrates with Al tape as inclusion.

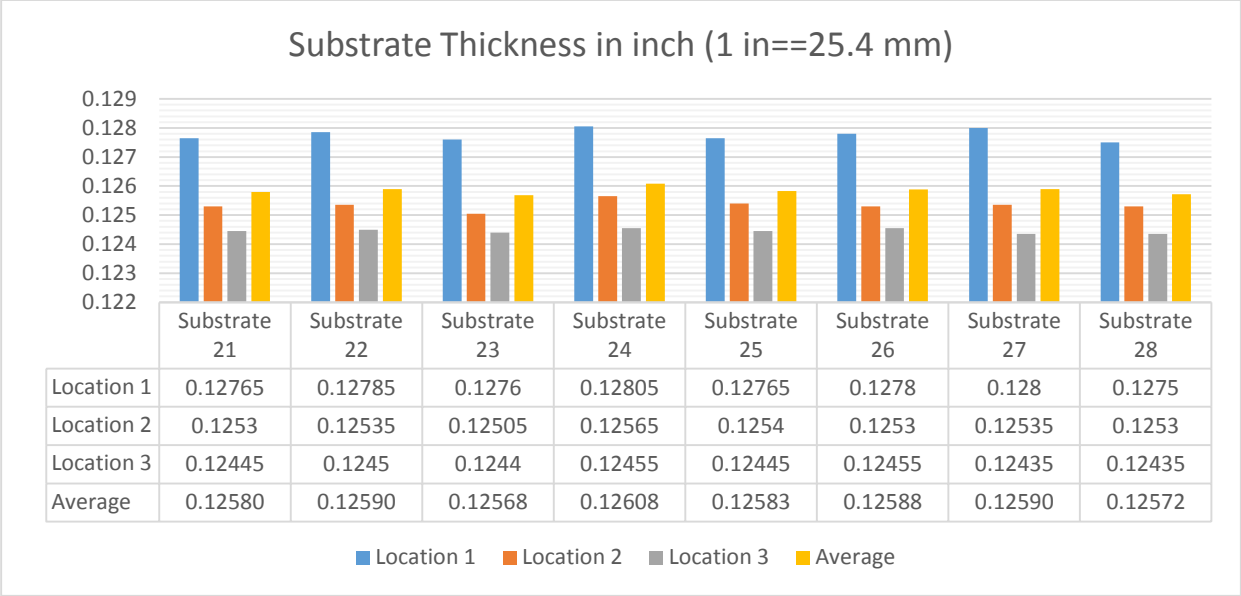

	Substrate 21	Substrate 22	Substrate 23	Substrate 24	Substrate 25	Substrate 26	Substrate 27	Substrate 28
Location 1	0.12765	0.12785	0.1276	0.12805	0.12765	0.1278	0.128	0.1275
Location 2	0.1253	0.12535	0.12505	0.12565	0.1254	0.1253	0.12535	0.1253
Location 3	0.12445	0.1245	0.1244	0.12455	0.12445	0.12455	0.12435	0.12435
Average	0.12580	0.12590	0.12568	0.12608	0.12583	0.12588	0.12590	0.12572

Figure 4-71: Thickness of the stepped joint coupons for the 2nd set of samples with Al tape inclusion

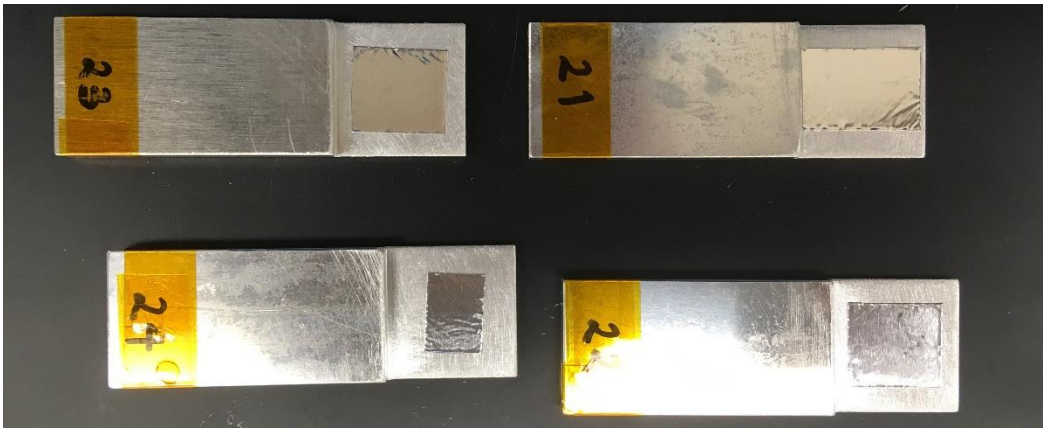

Figure 4-72: Substrates with Al tape inclusion. Top right: substrate 21 (%54 released area), Bottom right: 22 (%42 released area), Top left: 23 (%42 released area), Bottom left: 24 (%24 released area)

As mentioned before, the middle of the bond experience a lower load compared to the edges. The dimension of the Al tape in the direction of the bondline was chosen as a variable to investigate its effect alongside the gross effect of the released area percentage. The Al tape

dimension for all the substrates is shown in Table 4-2. Figure 4-73 depicts the fabrication setup for these samples.

Table 4-2: Al Tape dimensions

	In the direction of the bondline-mm [in]	Other direction-mm [in]	Released Area Fraction
Substrate 21	22.86 [0.9]	15.24 [0.6]	0.9X0.6=0.54
Substrate 22	17.78 [0.7]	15.24 [0.6]	0.6X0.4=0.42
Substrate 23	17.78 [0.7]	15.24 [0.6]	0.6X0.4=0.42
Substrate 24	10.16 [0.4]	15.24 [0.6]	0.4X0.6=0.24

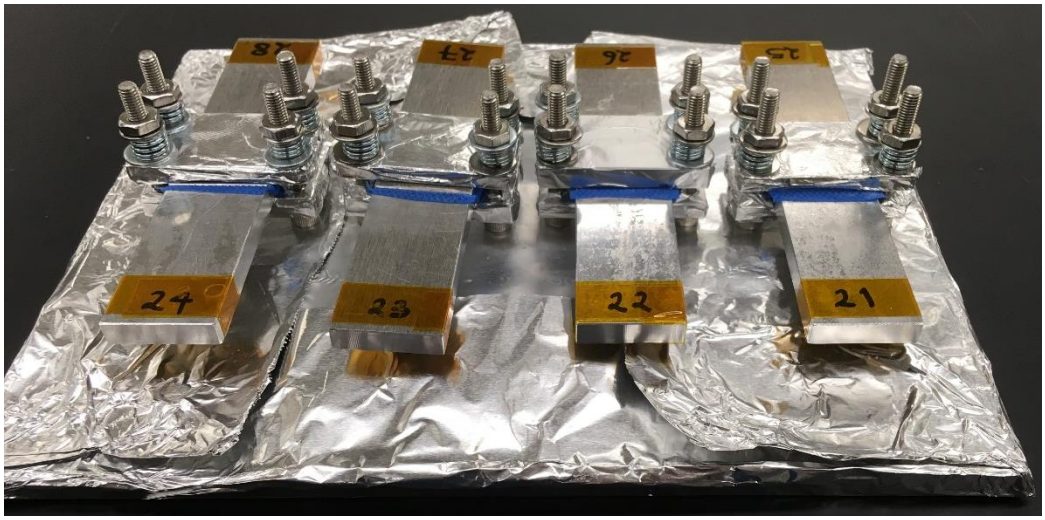

Figure 4-73: Fabrication setup

For these samples, the furnace was programed, which contained three steps:

1. Temperature ramp with 10 °C/min until temperature reaches 178 °C
2. A soaking step for 75 min

3. The furnace was turned off, and the lid was removed, and the sample was left to cool down

There is no significant difference between the curing cycle of the previous sample and these new samples, and this should not alter the properties.

The testing results for these samples would be reported later due to the occurrence of the COVID-19 pandemic.

5) Finite Element Modelling (FEM)

FEM is used to study the stress distribution and bending moment for different joint configurations and conditions.

5.1) Comparison between different joint configurations

In this section, the stress distribution and the extent of bending in different joint configurations are studied using FEM. In all cases, one side of the joint was fixed, and the other side could only have a displacement in the longitudinal direction. In all cases a load equal to 3 KN is applied to the side that can only have longitudinal displacement. The part is initially meshed with the default setting. Subsequently, a contact mesh with 1mm element size is applied and an edge meshing with 2 divisions is applied to the adhesive body to increase the sensitivity of the mesh around the bond. Table 5-1 mentions the mechanical properties and the dimensions of the substrates.

Table 5-1: Dimensions for FEM of different joint configurations comparison

	Modulus, GPa [ksi]	Length, mm [in]	Width, mm [in]	Thickness, mm [in]
Substrate- Al 6061 T4	70.113 [101690]	76.2 [3]	25.4 [1]	3.175 [0.125]
Adhesive	2.273 [330]	Overlap- 25.4 [1]	25.4 [1]	0.4mm [0.015748]

5.1.1) Double-Strap Joint

Figure 5-1 depicts the true-scale deformation and the Von-Mises stress distribution. Figure 5-2 depicts peel stress distribution at bond-line. Figure 5-3 depicts the shear stress distribution at bond-line.

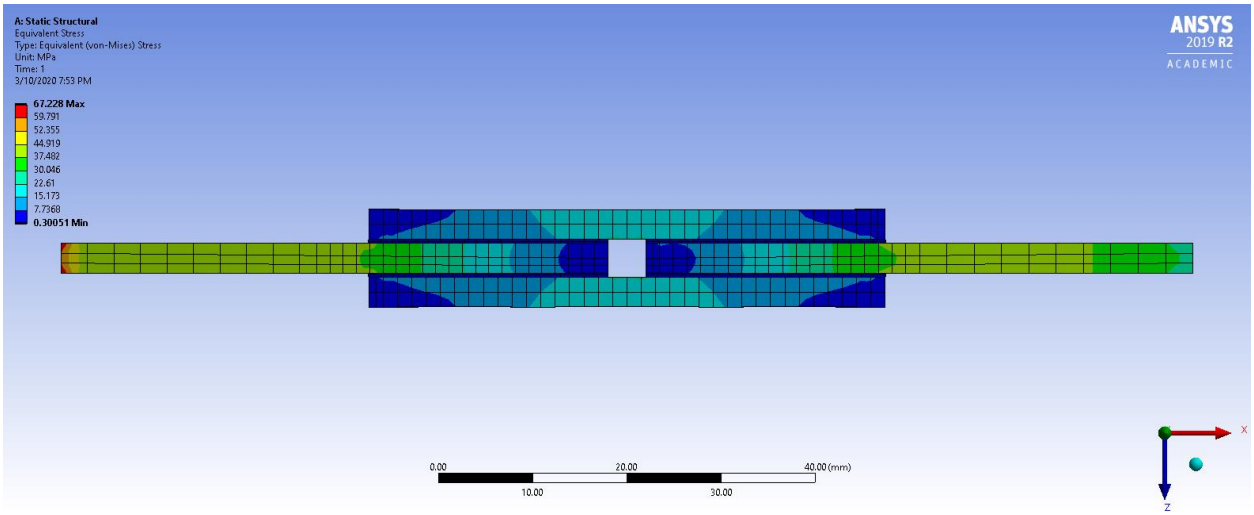

Figure 5-1: Double-Lap Joint-true-scale Von-Mises stress distribution

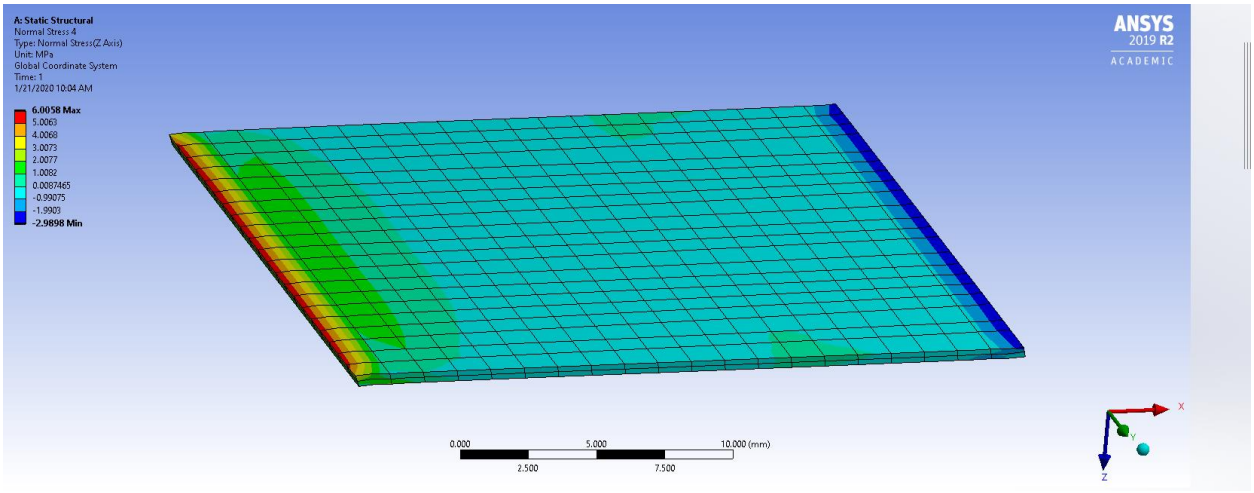

Figure 5-2: Double-Lap Joint-Peel stress distribution at bondline

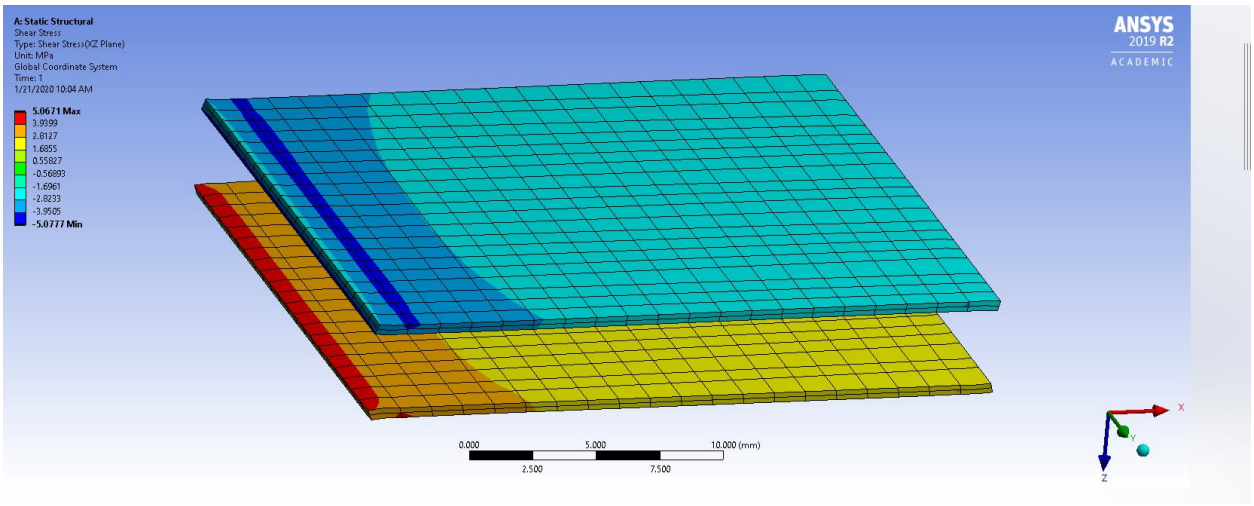

Figure 5-3: Double-Lap Joint-Shear stress distribution at the bondline

5.1.2) Single Strap Joint

The thickness of each substrate is 3.175 mm [0.125 in]. Substrates are 76.2 mm [3 in] long.

True-scale Von-Mises Stresses:

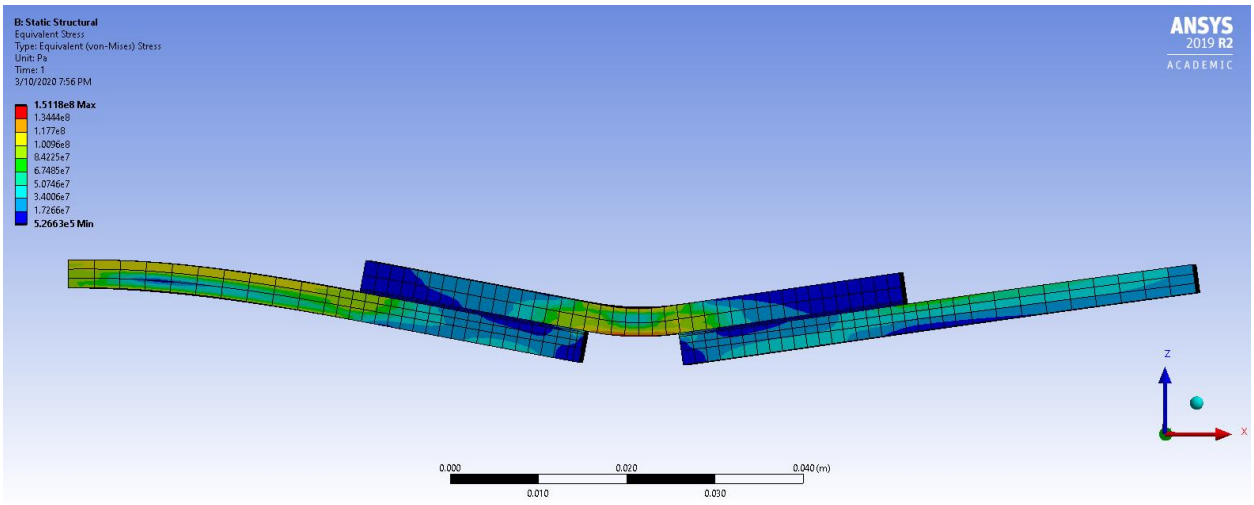

Figure 5-4: Single Strap Joint- True-scale Von-Mises Stress Distribution

Peel Stresses:

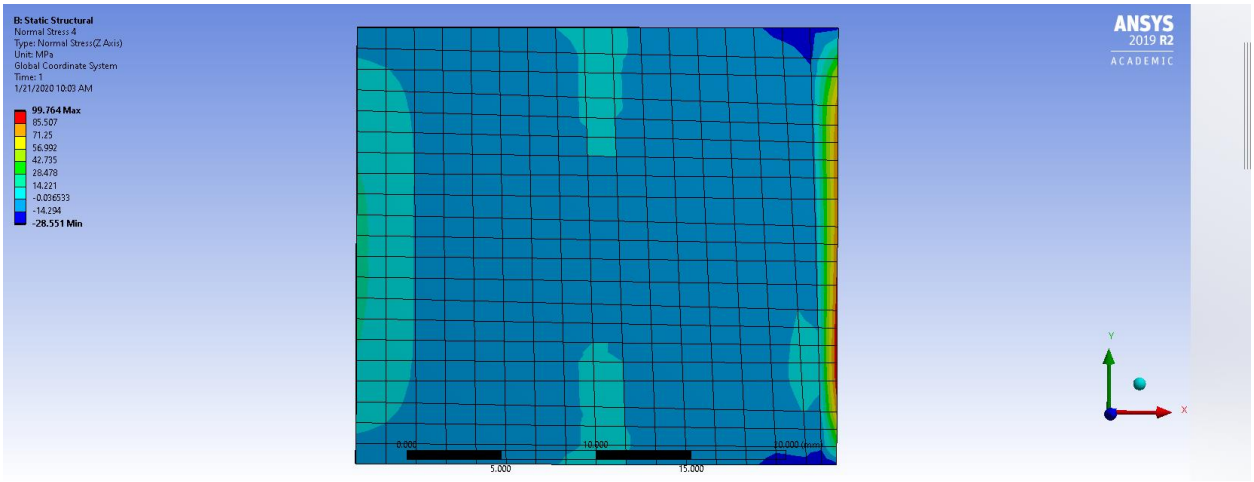

Figure 5-5: Single Strap Joint-Peel stress distribution

Shear Stresses:

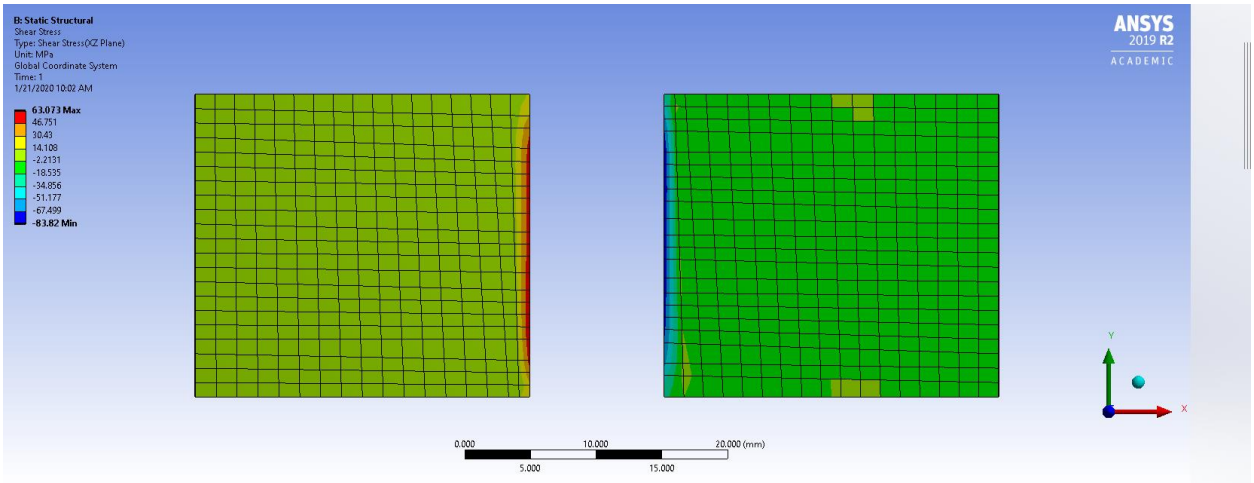

Figure 5-6: Single Strap Joint-Shear stress distribution

5.1.3) Stepped Joint

The dimension is the same as the stepped coupons for the stepped joint samples.

True-scale Von-Mises Stresses

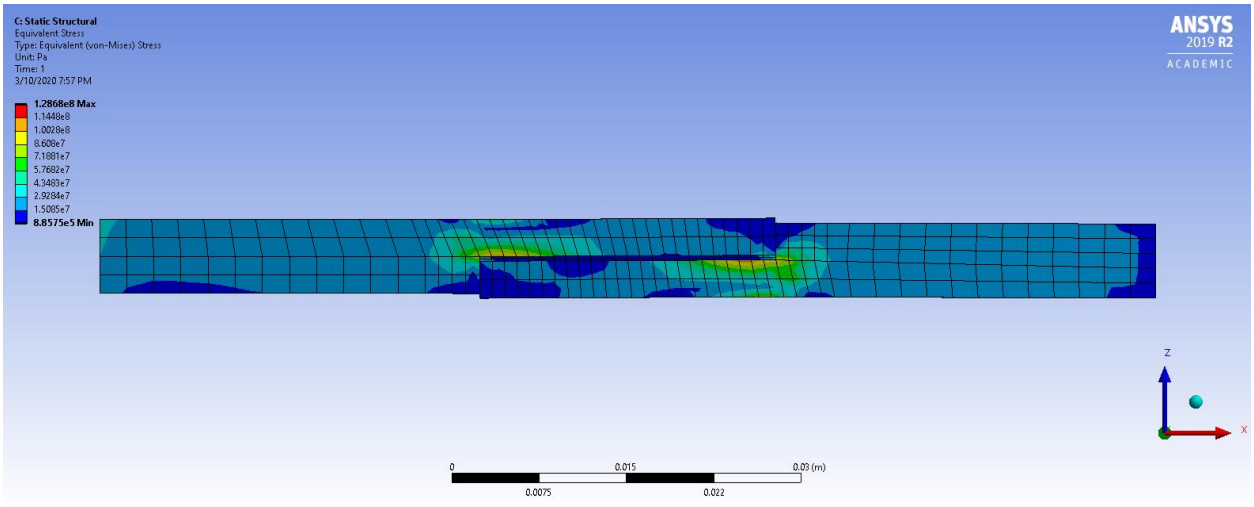

Figure 5-7: Stepped Joint-True-Scale Von-Mises stress contours

Peel Stresses:

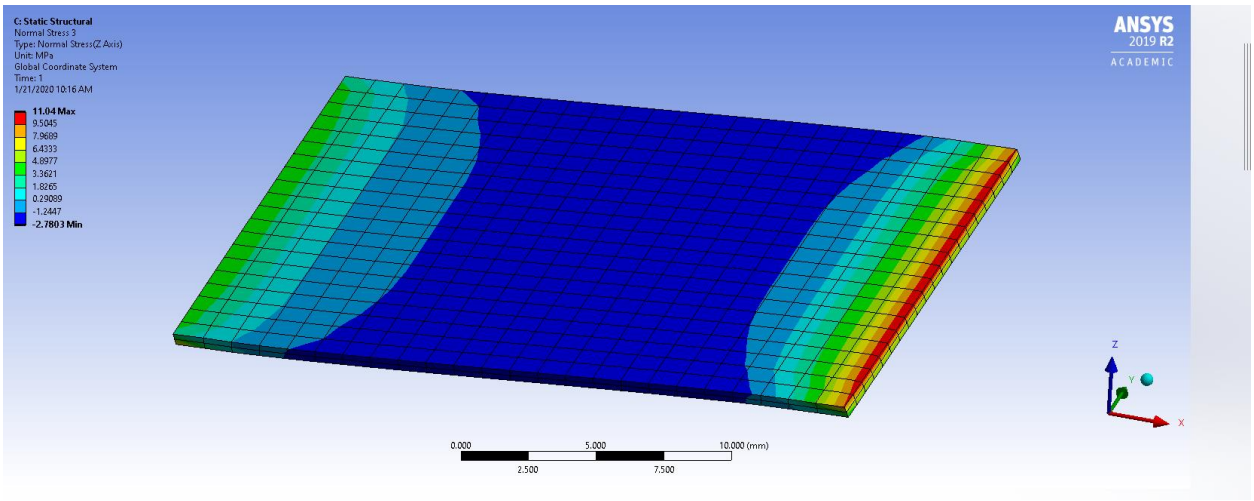

Figure 5-8: Stepped Joint-Peel stress contours

Shear Stresses:

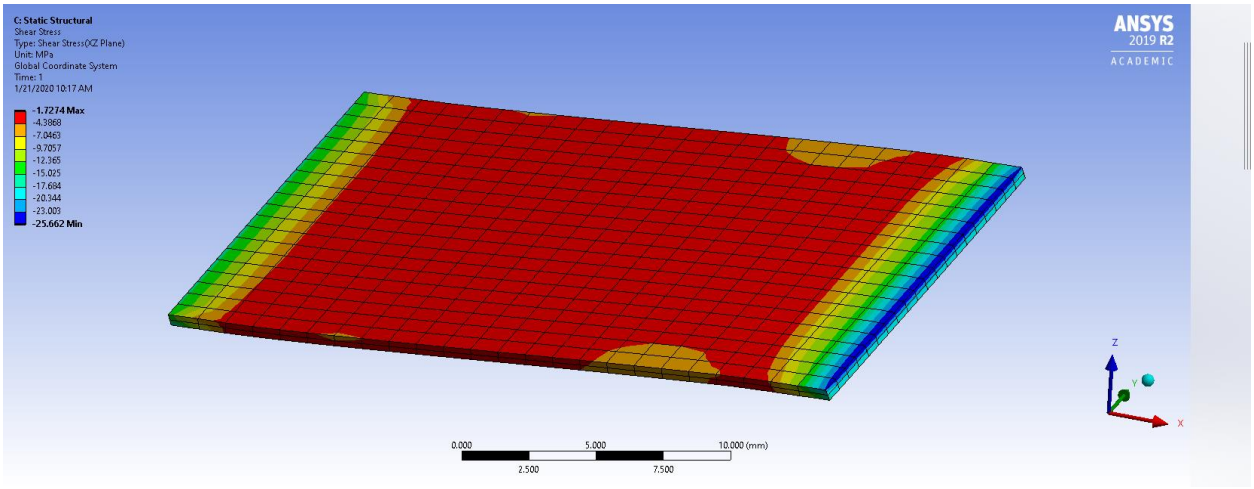

Figure 5-9: Stepped Joint-Shear stress contours

5.1.4) Single Lap Joint (SLJ)

The thickness of each substrate is 3.175 mm [0.125 in]. Each substrate is 76.2 mm [3 in] long.

True-scale Von-Mises Stresses:

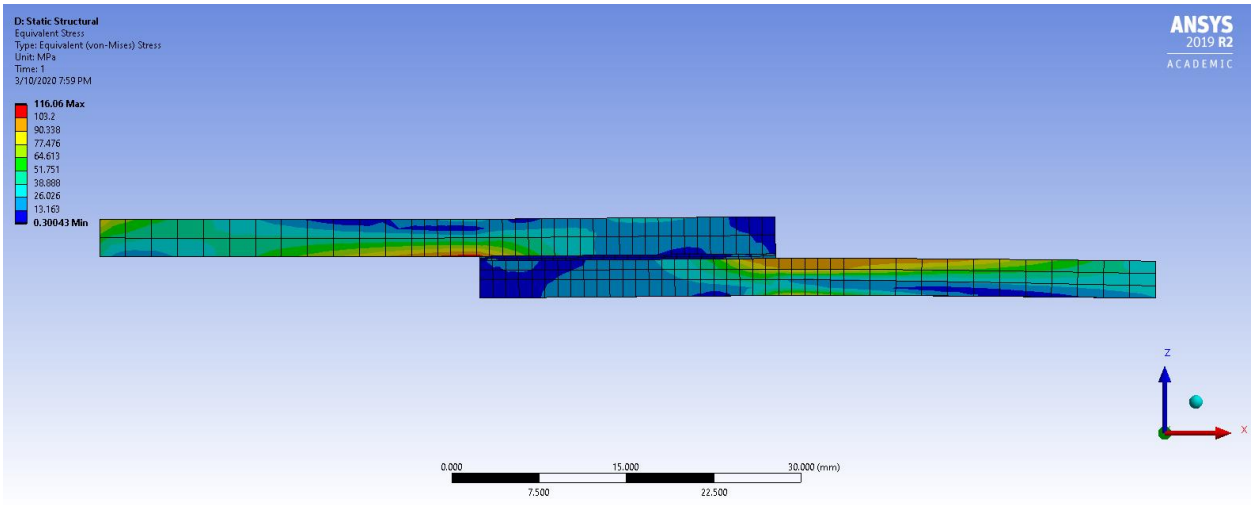

Figure 5-10: Single Lap Joint (SLJ)-True-Scale Von-Mises Stress Distribution

Peel Stresses:

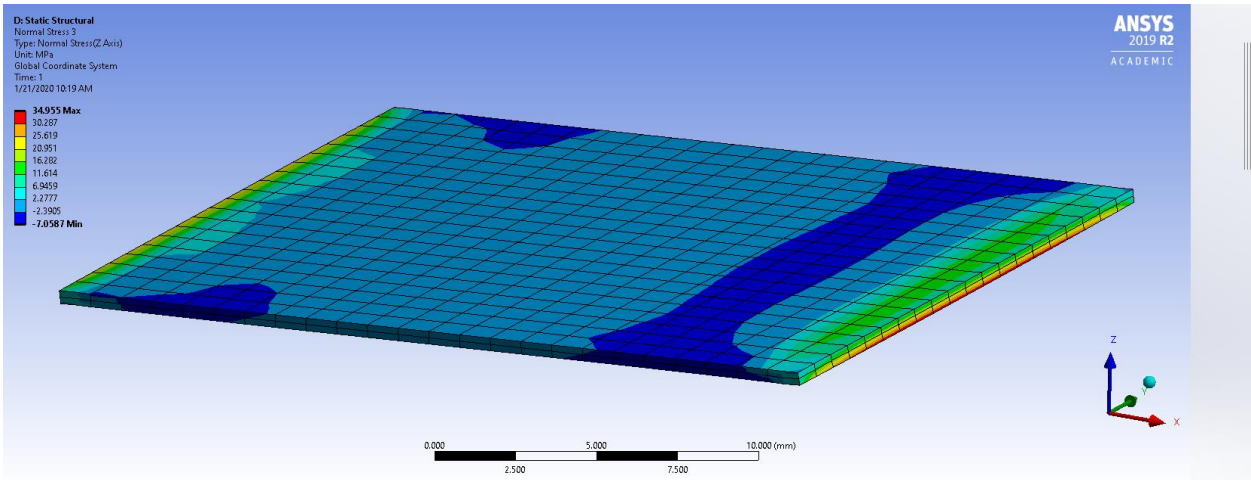

Figure 5-11: Peel stress distribution in Single Lap Joint (SLJ)

Shear Stresses:

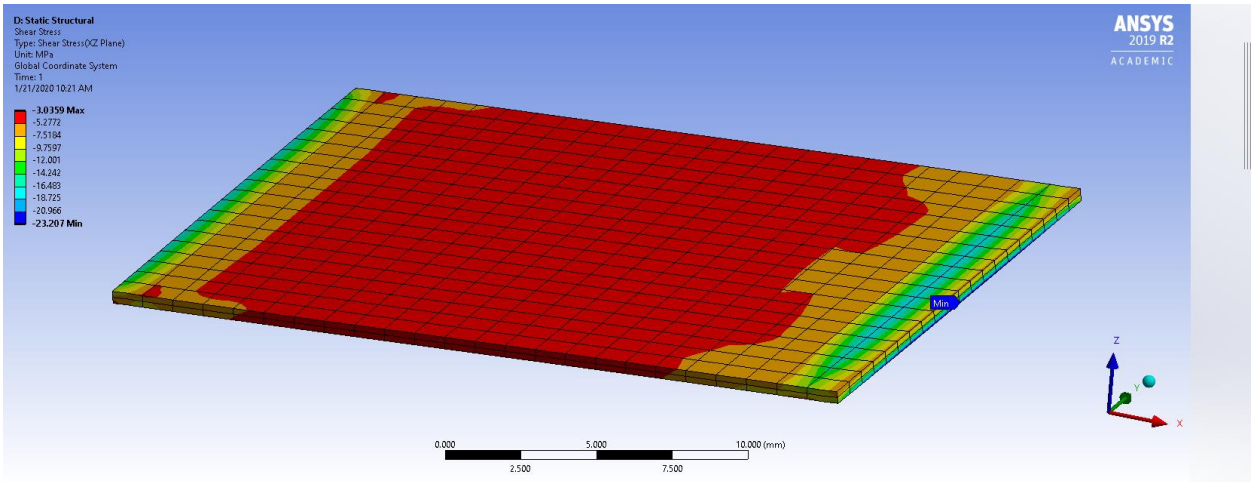

Figure 5-12: shear stress distribution in Single Lap Joint (SLJ)

Figure 5-13 illustrates the values for maximum peel stress and maximum shear stress among different joint configurations. As expected, the double strap joint, which has the least amount of eccentricity, shows the best performance.

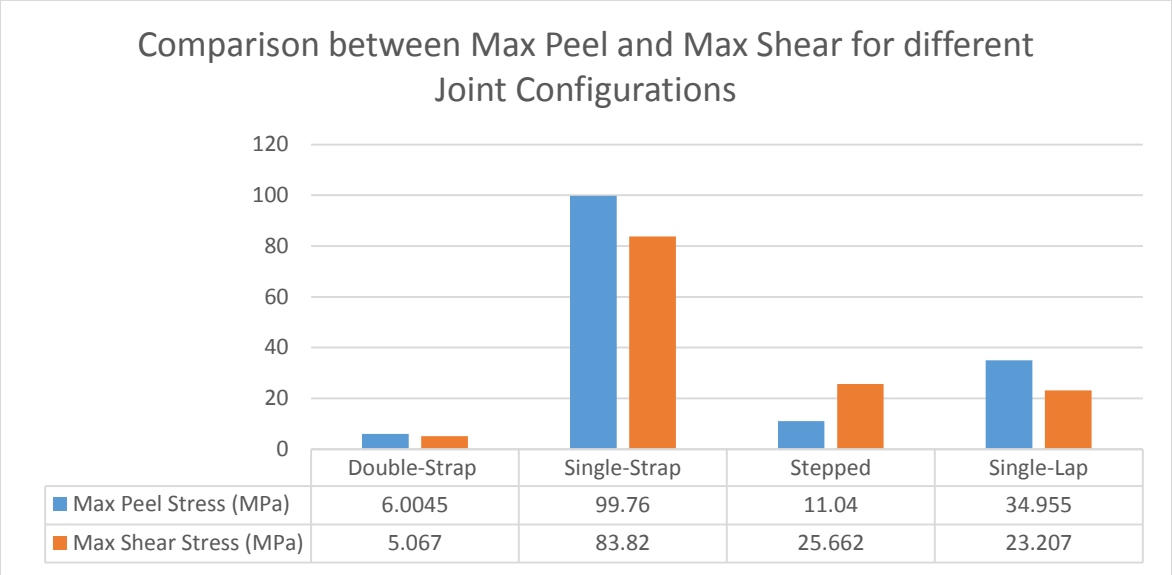

Figure 5-13: Comparison between Maximum Peel and Maximum Shear Stresses among different Joint Configurations. As expected, the double strap joint, which has the least amount of eccentricity, shows the best performance

5.2) Aluminum vs. Stainless Steel substrate

In this section, the effect of the substrate's modulus on the bending, peel, and shear stress is investigated. The grip is fixed on one side and can only have a longitudinal movement on the other side. The applied load on the side that can move is 5kN in this case. The part is initially meshed with the default setting. Subsequently, a contact mesh with 1mm element size is applied and an edge meshing with two divisions is applied to the adhesive body to increase the sensitivity of the mesh around the bond. The dimensions and mechanical characteristics of the substrate and the adhesive is mentioned in Table 5-2.

Table 5-2: Dimensions and material properties for FEM comparison between Al & SS

	Modulus, GPa [ksi]	Length, mm [in]	Width, mm [in]	Thickness, mm [in]
Substrate- Al 6061 T4	70.113 [10169]	58.42 [2.3]	16 [0.63]	3.175 [0.125]
Stainless Steel	200 [29007.5]	58.42 [2.3]	16 [0.63]	3.175 [0.125]
Adhesive	2.273 [330]	Overlap-12.7 [0.5]	16 [0.63]	0.4 [0.015748]

Al-true-scale Von-Mises stresses:

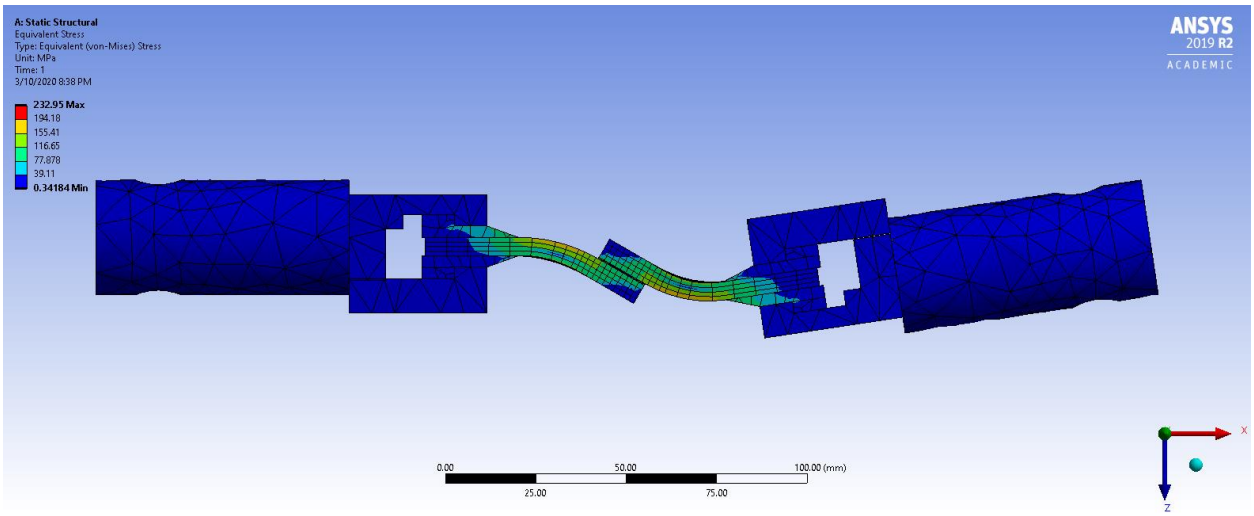

Figure 5-14: Aluminum True-Scale Von-Mises Stress Distribution

Peel Stresses:

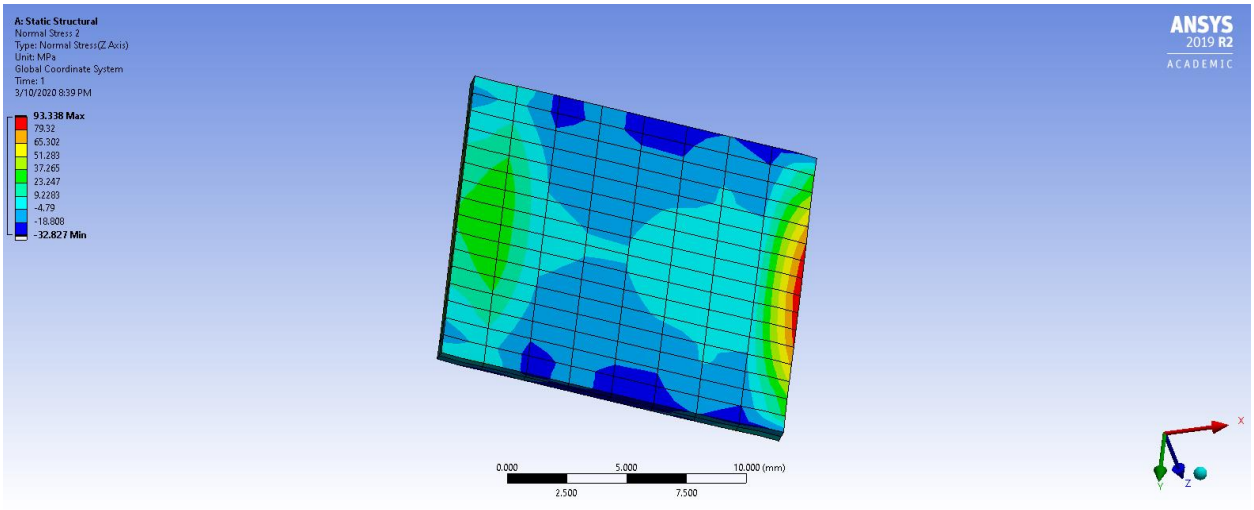

Figure 5-15: Aluminum Peel Stress Distribution

Shear Stresses:

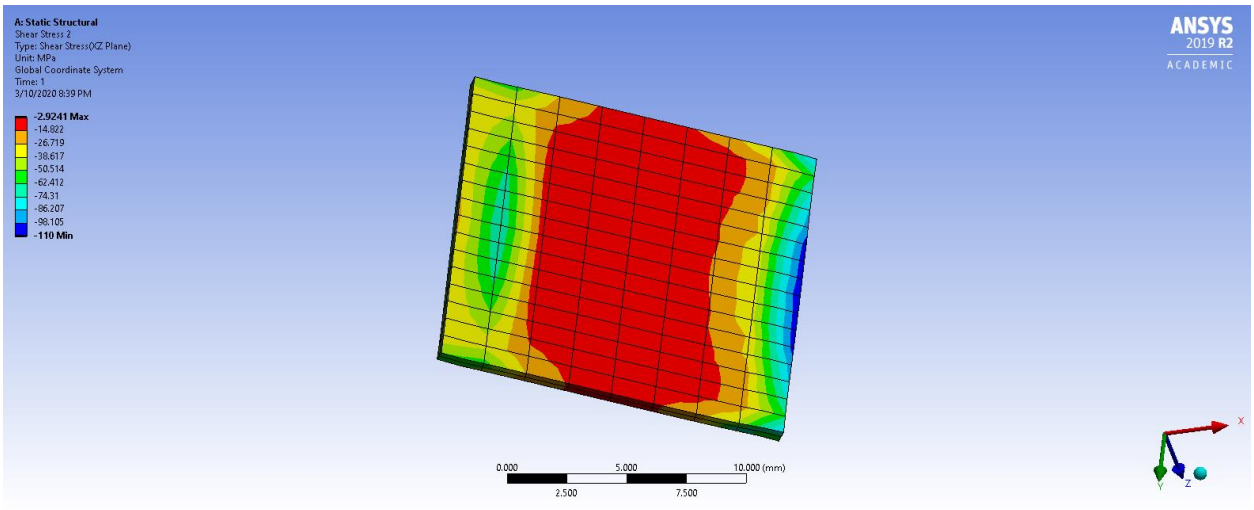

Figure 5-16: Aluminum Shear Stress Distribution

SS-true-scale Von-Mises Stresses:

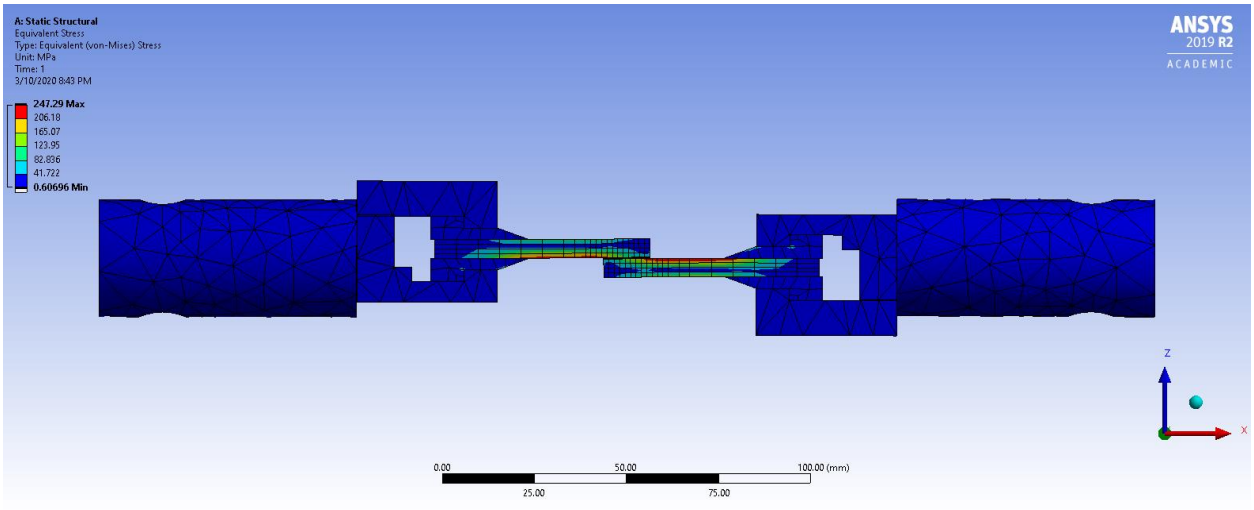

Figure 5-17: SS-True-Scale-Von-Mises Stress Distribution

Peel Stresses:

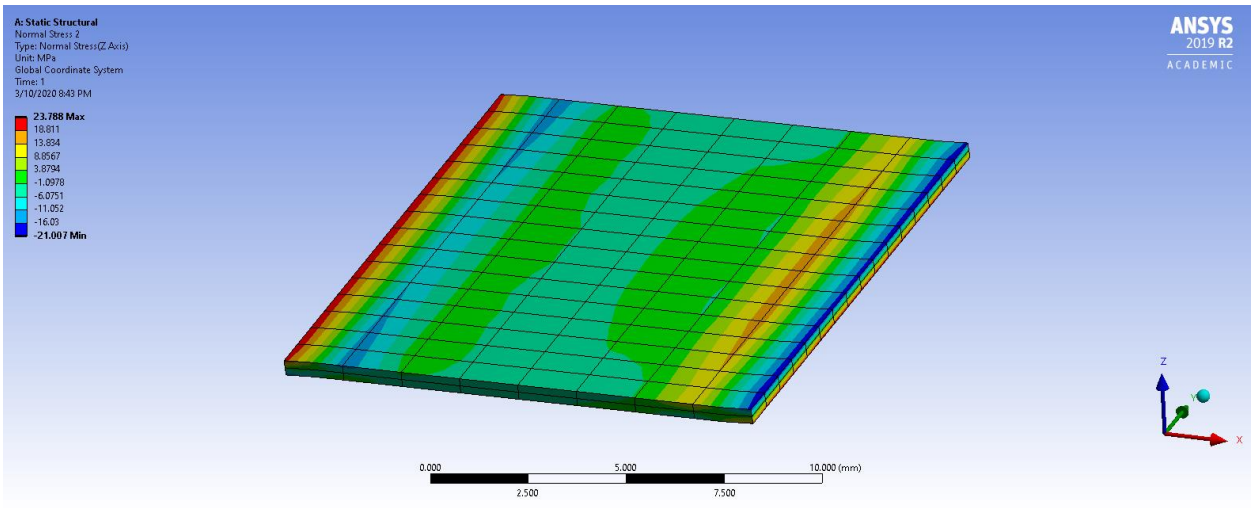

Figure 5-18: SS-Peel Stress Contours

Shear Stresses:

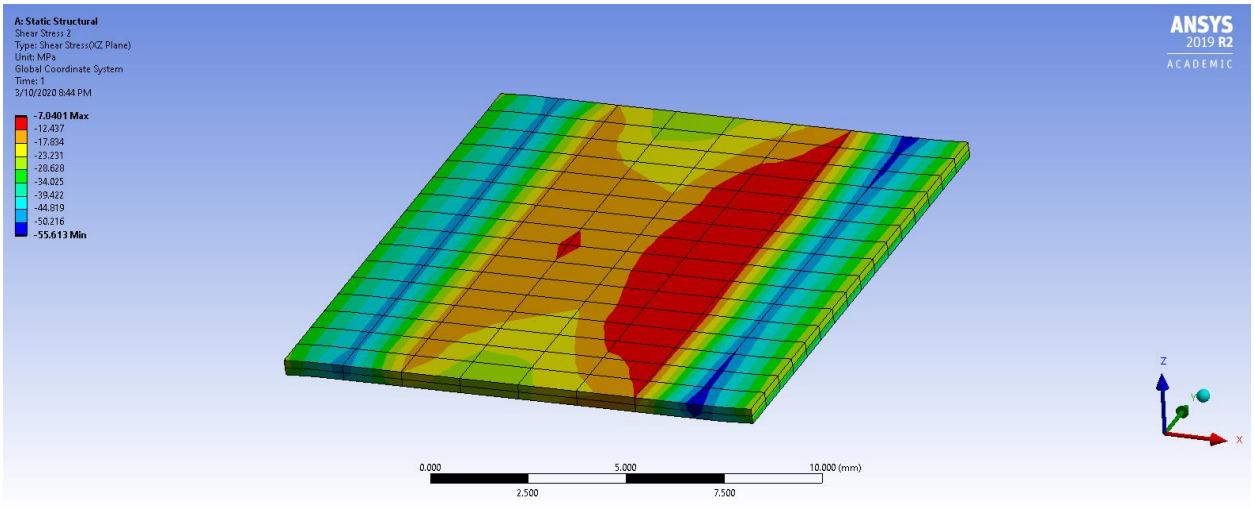

Figure 5-19: SS-Shear Stress Contours

Figure 5-20 depicts that both the shear and peel stresses are much lower in the case of Stainless Steel substrates. The higher modulus of SS leads to lower bending, and that leads to lower peel stress.

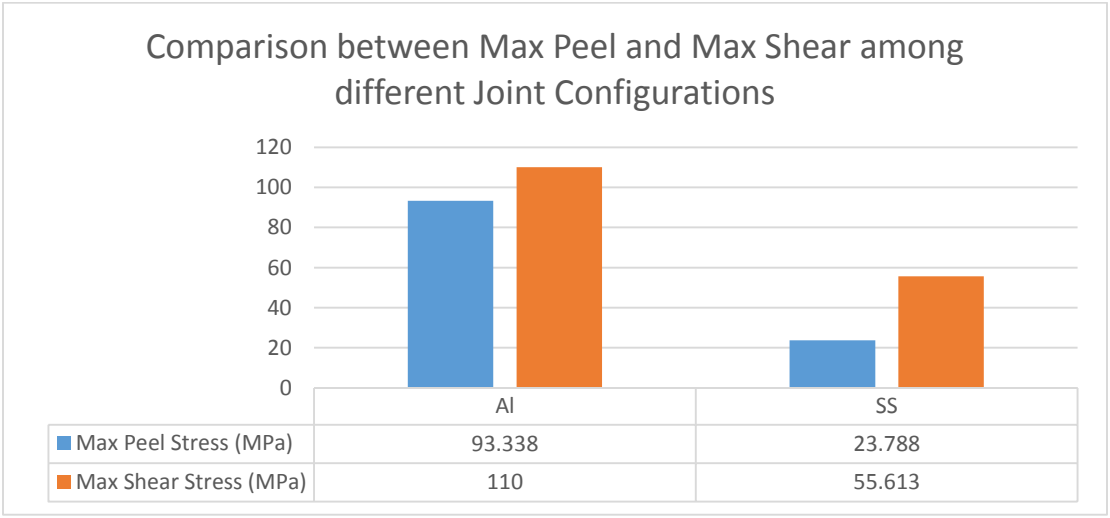

Figure 5-20: Comparison between Maximum Peel and Maximum Shear for Al vs. SS. The higher modulus of SS leads to lower bending, and that leads to lower peel stress.

5.3) Effect of overlap length on the peel and shear stresses

In this section, peel and shear stress in the bond were calculated through FEM, Goland & Reissner model, and Volkersen model. The width of the bondline is 25.4 mm [1 in]. The thickness of the bondline is 0.4 mm [0.015748 in]. Substrate is Al 6061 T4 with modulus 70 GPa, and the adhesive is epoxy with modulus 2.27 Gpa. Figure 5-21 illustrates the Goland & Reissner peel and shear stress distribution for 70 mm [2.756 in] bondline [12]. Figure 5-22 illustrates the Volkersen shear stress distribution for 70 mm [2.756 in] bondline [12]. Figure 5-23 illustrates that peel stress decreases as the overlap length increases. Figure 5-24 illustrates that shear stress also goes down as the overlap length increases.

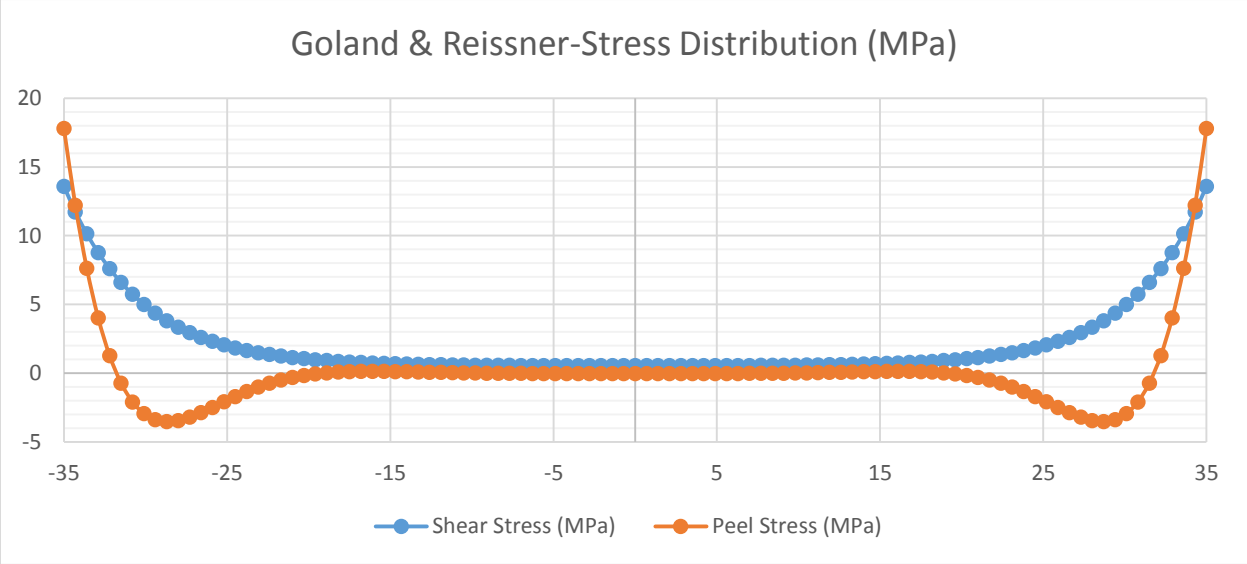

Figure 5-21: G&R peel and shear stress distribution at 70mm bondline (Derived with JointDesigner online program [12])

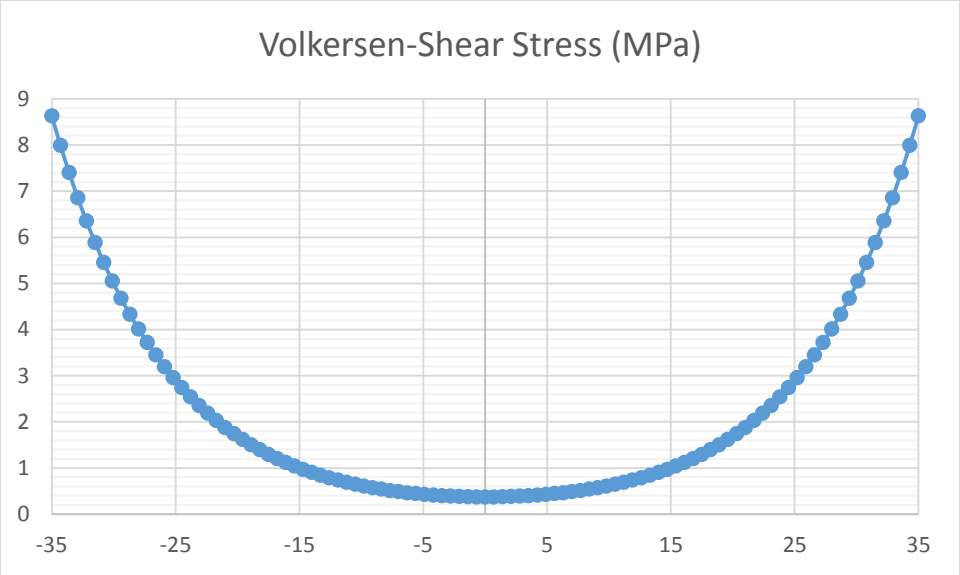

Figure 5-22: Volkersen shear stress distribution at 70mm bondline (Derived with JointDesigner online program [12])

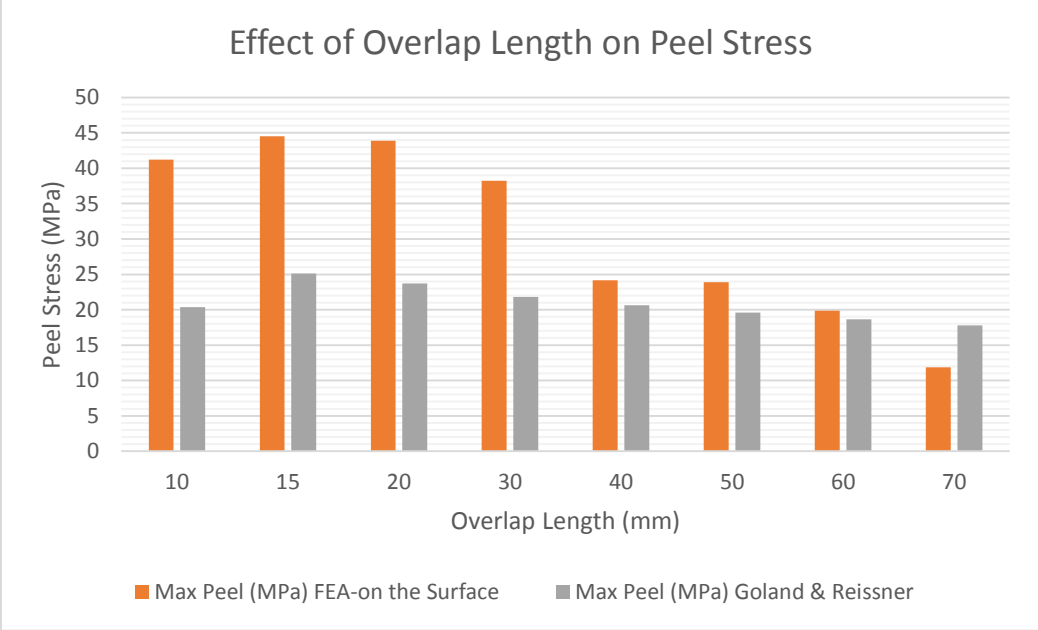

Figure 5-23: Effect of Overlap Length of Peel Stress. As the bondline overlap length increases, the peel stress decreases.

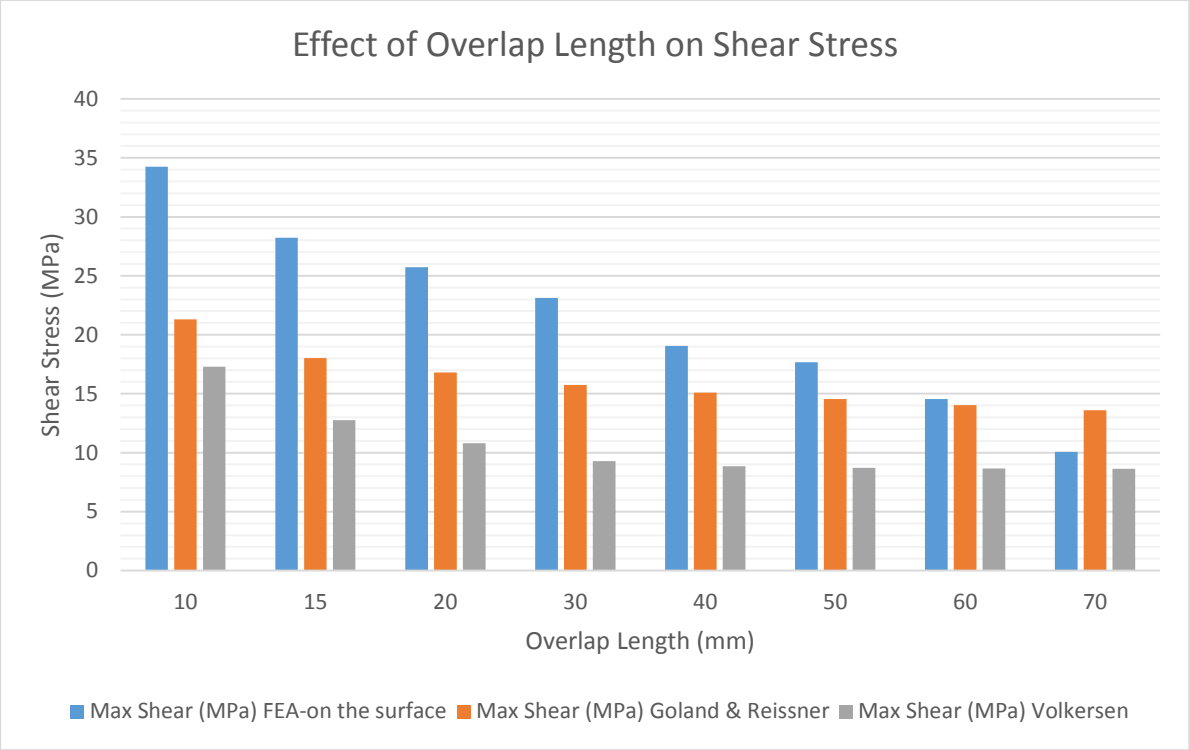

Figure 5-24: Effect of Overlap Length on Shear Stress. As the bondline overlap length increases, the shear stress decreases.

6) CFRP (Carbon Fiber Reinforced Polymer) Composites Lamination

6.1) Introduction

In recent decades, Fiber Reinforced Polymers (FRPs) composites gained serious attention due to their exceptional mechanical performance, lightweight, and chemical and environmental resistance. In FRPs, a high strength fiber such as carbon, glass, Kevlar, boron, etc. is embedded into a low strength polymeric matrix. Fibers are in charge of carrying the load and matrix glues fibers together, shaping the finals product, and providing chemical and environmental durability. Fibers are generally either unidirectional or woven. The polymeric matrix is divided into two main subcategories: Thermoset and Thermoplastic. In the thermoset matrix, polymer chains are chemically cross-linked, and a 3D network is created. This process is irreversible, and there is no cost-effective and efficient method to recycle the final product. Thermoset polymeric matrix consists of two main parts: the resin and the curing agent. The curing agent act as a bridge and chemically react with two resin chains and create a 3D network. Some of the most prominent thermoset resins include epoxy, polyester, vinyl ester, BMI, etc. Thermoplastic resins flow upon applying heat and then solidify upon cooling. There is no chemical reaction involved in this case, and the process is reversible, so reiteration and recycling is possible. Some of the prominent thermoplastic resins include PEEK, PEKK, PA, PP, etc. Polymers have high toughness, and good fatigue performance and that translates to the FRP as well. The majority of FRP composites in the market right now have a thermoset matrix due to lower cost and ease of fabrication.

Carbon fiber is mainly used for high-end applications such as aerospace, military, race cars, etc. due to its superior strength and higher cost compared to other mainstream fibers.

CFRPs have exceptional specific strength[5] and stiffness[6], which enables the designing engineer to achieve high strength and low weight at the same time. Table 6-1 summarizes the mechanical properties for steel, aluminum alloy, and CFRP. As it is apparent, the CFRP outperforms both steel and aluminum alloy.

Table 6-1: Comparison between Mechanical Properties of Steel, Al, and CFRP (Adapted from [48])

Material	Density- ρ- (X10^3 kg/m^3)	Tensile Modulus-E (GPa)	Tensile Strength-σ (MPa)	Specific Modulus- E/ρ- (10^6*Nm/kg)	Specific Strength- σ/ρ (10^6*Nm/kg)
Steel, AISI 1045	7.7-8.03	205	585	26.3	0.073
Al 6061-T6	2.7	69	270	25.5	0.10
Carbon Epoxy (61%)- Unidirectional	1.6	142	1730	89.3	1.08

Figure 6-1 illustrates the strength of engineering material vs. density. Composites provide the same strength as metallic alloys with much lower density.

[5] Specific Strength is the strength of a material divided by its mass.
[6] Specific Stiffness is the Young modulus of a material divided by its mass.

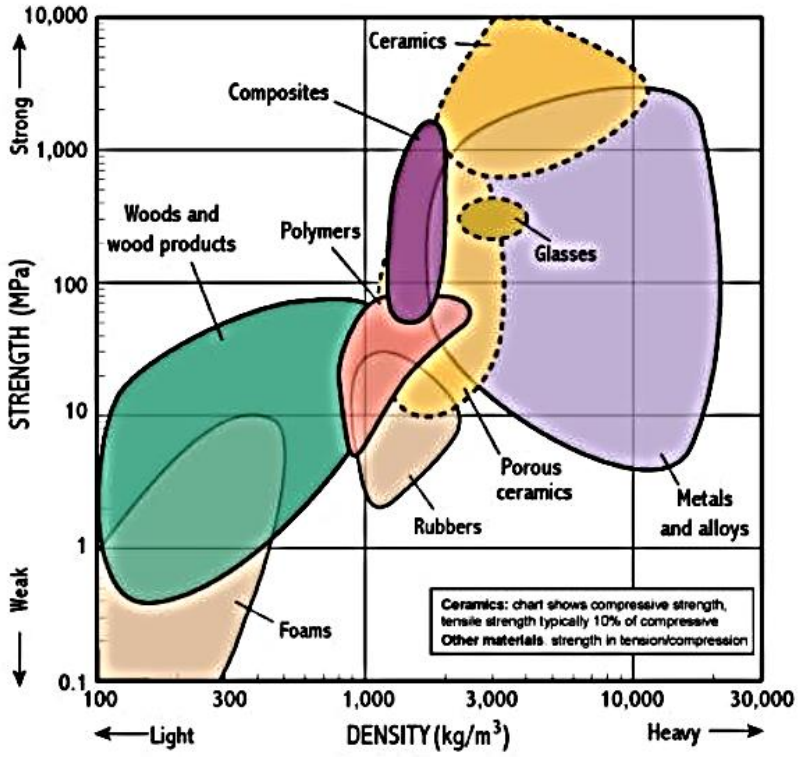

Figure 6-1: Strength vs. Density for engineering materials [49]

Mechanical fasteners such as rivets, bolts, etc. include drilling a hole to attach two materials. This will lead to a stress concentration around the hole. The stress concentration would be devastating for CFRPs, due to the fact that they are inhomogeneous and anisotropic in nature and have low transverse and local bearing strength [3, p. 1050]. Stress concentration could cause crack initiation and propagation in the polymeric matrix, which can lead to devastating failure. The exceptional mechanical properties of the CFRPs are related to continuous fiber reinforcement. Drilling a hole in a CFRP material breaks the fibers and destroys the continuity of fibers, and therefore damages the mechanical performance of the CFRPs extensively [9].

Machining CFRPs is more challenging than machining metallic alloys. Carbon fiber is very abrasive, and therefore special tools with carbide or preferably diamond coating are necessary to cut or drill CFRPs efficiently. These tools are costly and are not readily available in all machine shops. Plus, machining CFRPs produce dust instead of chips, and specialized equipment is necessary to contain the dust during the machining. Particular attention should be paid to choosing the proper tool, feed rate, and cutting speed to prevent the tool wear, delamination of the CFRP laminate as the result of excessive stresses cause by the machining, and overheating the CFRP laminate during the machining [50]. The excessive heat can degrade and burn the polymeric matrix and release toxic fumes in some cases. The production of dust and the release of toxic fumes during machining dictate that machining CFRPs should take place in an isolated area with adequate air circulation. The air should go through a HEPA[7] filter to filter out small carbon particulates. All of these factors make the machining of CFRPs more challenging and more expensive.

Adhesive bonding has a smooth stress transfer and avoids drastic stress concentration, plus it will eliminate the drilling step. All of this makes adhesive bonding the most suitable case for joining CFRP substrates. As mentioned before, most adhesives are polymers, which leads to good chemical matching between the adhesive and polymeric matrix of the CFRPs in most cases.

[7] high-efficiency particulate absorbing

CFRPs laminates were fabricated in order to investigate the behavior of adhesively bonded joints between CFRP substrates.

6.2) Fabricating the CFRP laminate with Hand Wet Lay-Up Process

Three sets of CFRP laminates (2plies, 3plies, and 4 plies) were fabricated by hand lay-up using the unidirectional carbon fiber and epoxy resin system provided by DYMAT. The lamination was performed at 22°C [72°F] and %50 RH. The dimensions of each laminate is mentioned Table 6-2.

Table 6-2: Dimensions of the CFRP laminates

Number of Plies	Length-mm [in]-in the direction of fibers	Width-mm [in]-perpendicular direction
2 plies	685.8 [27]	241.3 [9.5]
3 plies	457.2 [18]	292.1 [11.5]
4 plies	330.2 [13]	292.1 [11.5]

In order to calculate the mixing ratio of any resin system, two parameters are necessary [4]:

- Amine Hydrogen Equivalent Weight (AHEW)

$$AHEW = \frac{Molecular\ Weight\ of\ Amine}{\#\ of\ Amine\ Hydrogens} \qquad (6\text{-}1)$$

- Epoxide Equivalent Weight (EEW) of epoxy resin: weight of epoxy resin in gr that contains 1 mole of epoxide functional group

These parameters are usually provided by the manufacturer of the resin and the curing agent. The weight of curing agent per 100 part epoxy resin (phr) would follow Equation (6-2):

$$phr = \frac{AHEW\ of\ Curing\ Agent}{EEW\ of\ Epoxy\ Resin} X100 \qquad (6\text{-}2)$$

Table 6-3 mentions all the required properties for the resin, curing agent, and carbon fiber.

Table 6-3: Properties of resin, curing agent, and carbon fiber

Carbon Fiber	
Reinforcement Areal Weight (RAW) (Kg/m2)	644.21*10^-3
Density of Fiber (Kg/m^3)	1.74*10^3
Resin	
Density of Resin (Kg/ m^3)	1.162*10^3
Curing Agent	
Density of Curing Agent (Kg/ m^3)	0.945*10^3

In order to calculate the amount of resin and curing agent for each case, the volume percentage of fiber should be known. This parameter varies with the fabrication process, and for hand lay-up, the fiber volume percentage around 30% is achievable. By knowing the phr for the resin system, area of the laminate and number of plies, in order to calculate the amount of resin and curing agent, Equation (6-3) & Equation (6-4) should be solved simultaneously:

$$\frac{mre + mcu}{\frac{mcu}{\rho cu} + \frac{mre}{\rho re}} \times (1 - vf) \times \frac{RAW \times A \times n}{\rho f \times vf} = mcu + mre \qquad (6\text{-}3)$$

$$mcu = \frac{phr \times mre}{100} \times 1.1 \qquad (6\text{-}4)$$

mre= resin mass, mcu=curing agent mass, ρcu=density of curing agent, ρre=density of resin, v_f=volume fraction of fiber, RAW= Reinforcement Areal Weight of the fiber, A= area of the laminate, n=number of plies, ρ_f=density of fiber

In this study, three MATLAB codes were developed. Code I calculates the resin & curing agent mixing ratio for a laminate with a known thickness (# of plies is the variable). Code II calculates the resin & curing agent mixing ratio for a laminate with a known number of plies and fiber volume percentage. Code III calculates the resin & curing agent mass and volume based on the phr and number of plies. The phr for this epoxy resin system is 28.5715, which means 28.5715 gr curing agent is required for 100 gr epoxy resin. Therefore, code III is relevant in this case. Usually, a 10% more curing agent is used to ensure complete crosslinking (that is the reason behind multiplying the mass of curing agent by 1.1 in Equation (6-4). The codes are mentioned in Appendix B.

A small batch of resin and curing agent was mixed in order to measure the pot life of the resin system. The pot life of the resin system exceeds 2 hours.

Table 6-4 summarizes the amount of resin and curing agent that was used for each laminate. The amount of resin and curing agent used per each ply per square inch is roughly 0.435 and 0.136 gr. The area of each laminate is mentioned in the parentheses in each case.

Table 6-4: Resin and Curing Agent Weight Fractions

	Resin (gr)	Curing Agent (gr)
2 plies (0.166 m^2 [257 in^2])	224	69.8
3 plies (0.133 m^2 [207 in^2])	280.6	87.2
4 plies (0.096 m^2 [149.5 in^2])	249.6	78.4

The Silicone-based Frekote 770 was applied to the base substrate in order to facilitate the demolding. Uni-Directional carbon fiber was placed on the top of the base substrate, and its perimeter was taped to the base substrate in order to fix the carbon fiber orientation and prevent any movement or wrinkling. The resin system was added gradually. Brush and spatula were used in order to impregnate the carbon fiber fabrics. This procedure was repeated until the fibers were fully saturated. The same process was repeated for consequent plies. At the end, a release film was placed on the top, and then a top substrate was used to produce two flat surfaces for the laminate. Adequate weight was placed on the top of the top substrate to ensure sustained pressure during the curing process. Samples were left at room temperature in order to cure for 72 hours. The laminates were demolded without any trouble. Figure 6-2 illustrates the laminating process.

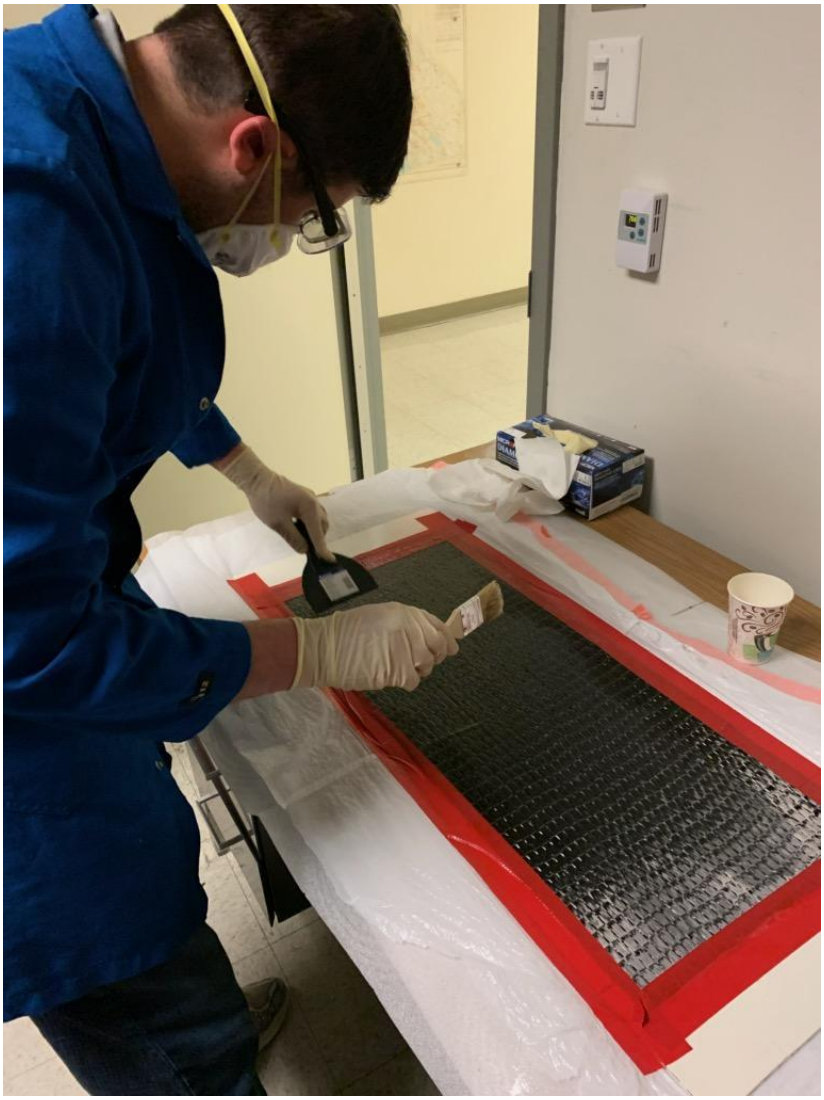

Figure 6-2: CFRP laminate fabrication by hand wet lay-up

A rotary saw with a Tungsten-Carbide blade is used to cut the laminate into coupons for future testing. Figure 6-3 illustrates the cutting process.

Figure 6-3: Cutting of the cured CFRP laminate

Due to the lack of time, the testing of the CFRP coupons' mechanical properties and the adhesively bonded joints between CFRP laminates did not take place.

7) Conclusions and Future Work

7.1) Conclusions

Climate crisis is pushing engineers to switch to lighter materials to decrease the CO_2 emission. The transportation section heavily contributes to global CO_2 emission. Lowering the weight of any car or airplane not only decreases the CO_2 emission but also increases the operational range and therefore reduces the operational cost. Environmental and economic considerations are in favor of using lighter materials for structural components. The first step in this journey was switching from steel to aluminum alloys. In recent decades, Fiber Reinforced Polymer (FRP) composites gained serious attention due to their exceptional mechanical performance, lightweight, and chemical and environmental durability. FRPs consist of a high strength fiber embedded in a polymeric matrix with low mechanical strength. Fibers are in charge of carrying the load, and matrix glues fibers together, shapes the finals product, and provides chemical and environmental durability. The matrix consists of a 3D network of polymer chains. Polymers have high toughness and good fatigue performance, and that translates to the FRPs as well. FRPs are inherently inhomogeneous and anisotropic. There is a stark difference between the mechanical properties of fibers and matrix. This could lead to local residual stresses. All of these characteristics make FRPs more prone to stress concentration. Traditional mechanical fasteners like rivets, bolts, etc. require drilling a hole into the substrate. There would be enormous stress concentration in the vicinity of the hole. The stress concentration can cause cracks to initiate and propagate in the matrix, leading to devastating premature failure. Besides, drilling a hole into FRP laminates require special tooling and stringent environmental caution. Adhesive bonding creates a smooth stress transfer and eliminates the need to drill a hole into FRP laminates. Adhesive

bonding has other advantages over mechanical fasteners, including reducing the final weight of the assembly, protecting the assembly against galvanic corrosion, absorbing shock and vibration, and introducing the ability to repair damaged assemblies.

Surface characteristics of the substrates play the most critical role in establishing a strong bond between the adhesive and the substrates. Most substrates should undergo some sort of surface treatment before bonding to ensure a strong bond will be formed between the adhesive and the substrates. Contamination interferes with adhesion and prevents a strong bond between the adhesive and the substrates. It is crucial to remove any contaminant from the surface of the substrates prior to bonding. Solvent wiping, chemical etching, mechanical abrasion, etc. are some of the typical methods of removing the contaminants. The surface texture also plays an essential role in the adhesion process. Rougher surfaces have a higher surface area and provide sites for mechanical interlocking. Roughness could be enhanced on a surface through hand abrasion, grit blasting, etc. There are surface treatments that increase the surface energy of the substrate by introducing reactive chemical groups into the surface, such as flame treatment, corona treatment, plasma treatment, etc.

Initially, it seems that the stress state in adhesively bonded joints other than the butt joint consists of a uniform shear stress distribution over the bond area. However, in adhesively bonded joints other than the butt joint, loads are not in line, and that results in the development of bending. The bending develops peel stress in the bondline. So the bond experience both peel and shear stresses. In fact, in most cases, peel stress is the primary reason that contributes to the failure of a joint. The shear and peel stresses are not distributed uniformly throughout the bondline. The value of the shear and peel stresses is maximum at both edges of the bond and is

minimum in the middle. Higher symmetry in a joint configuration results in less peel stress in the bond. That is why double strap joint performs better than any other joint configuration. The single-lap joint (SLJ) has the lowest symmetry level, but it is the most represented joint in research due to its ease of fabrication. Both shear and peel stresses are maximum at the edges of the bondline. So failure would most likely initiate at the edges of the bond and propagates toward the center. Increasing the bondline overlap decreases the stress concentration at the bond edges. Bondline thickness also contributes to the joint's performance, and in most cases, a thin adhesive layer between 0.1-0.2 mm is desirable.

There are multiple Non-Destructive Tests (NDTs) to investigate the integrity of the bond. The most challenging defect to be investigated when it comes to adhesively bonded joints is a “kiss bond.” Kiss bond refers to the state that adhesive and substrate are in contact with each other, but there is a very weak bond or no bond at all between them. None of the mainstream NDTs right now have the required resolution and sensitivity to reliably detect a kiss bond.

In the Quantitative Percussion Diagnostics (QPD) test, a probe equipped with a force sensor is accelerated using an electromagnetic coil. The probe impacts the surface, and the returned force vs. time is recorded and send to a computer. The shape and amplitude of the force vs. time curve can give us valuable information about the test sample. Comparing the QPD response between a sample and a reference flawless sample can help us detect the presence of defects.

The force vs. time curve for a flawless sample resembles a perfect symmetrical bell-shaped curve. The presence of any discontinuity such as cracks, void, porosity, debond, delamination, etc. distorts the shape of the curve, and a curve with more than one peak is achieved. The amplitude

of the force vs. time curve indicates how much kinetic energy from the probe is elastically restored in the sample and returned to the probe. High amplitude means that sample has low energy dissipation and, therefore, low damping characteristics. The presence of any flaw increases the damping characteristics of the sample by increasing the internal friction and other mechanisms.

QPD found to be effective in detecting any discontinuity such as crack, debond, void, delamination, etc. however, when it comes to detecting a kiss bond, things are more challenging. In a kiss bond, there is no clear discontinuity and stress wave produced by the collision between the probe and the sample can still propagate in the sample. The presence of a kiss bond increases the damping of a sample and therefore affects the amplitude of the force vs. time response. Stability Index parameter, which is proportional to the amplitude of the force vs. time curve, could be used in order to distinguish between a kiss bond and a sample with a well-prepared bond.

In the first iteration, stepped joint samples were prepared. A Silicon-based release agent (Frekote 770) was sprayed on the bond area to create a kiss bond. Masks were used to cover only a specific portion of the bond surface with the release agent. Stepped joint samples with a well bond were also prepared as the reference. The fracture surface of the samples with the release agent indicates interfacial failure throughout the bond area. The bond in these samples showed no mechanical strength what so ever and failed during the demolding. All of these facts indicate that the procedure of masking and spraying the release agent to create a partial kiss bond was unsuccessful. In the second iteration, aluminum tape was used as an inclusion material to create a partial kiss bond. The fracture surface in these samples indicates that failure was interfacial in

the area with a kiss bond and mixed-mode (which represents a well bond) in the surrounding well-bonded area. The failure load for these samples was less than a well-bonded sample and was proportional to the bond area fraction with a kiss bond. All of these facts indicate that using aluminum tape as inclusion was effective in creating a partial kiss bond.

The average Stability Index is lower for a sample with a kiss bond, however, there are instances that samples with a kiss bond also show high values for Stability Index, which are close to the typical value of the Stability Index for a sample with a well bond. Calculating the p-value for data sets between a kiss bond and a reference well-bonded sample by conducting a t-test shows some promise. In most cases, the p-value is less than the standard 0.05, which determines a significant difference between the two sets of data.

The QPD result for the sample with aluminum tape as inclusion indicates important points. This is the only sample with a true partial kiss bond. The Stability index is low when the probe is directly on top of the kiss bond. However, the Stability Index matches a well-bonded sample when the test is performed on the back side of the joint. It indicates that the stress wave generated by the QPD cannot penetrate deep enough when the test is performed on the back of the bond and does not reach the kiss bond from the back side of the bond. This could introduce some challenges because, first of all, in practice, it is not known which substrate's surface is compromised. Second of all, in practice, access to both sides of the bond is not always possible. The relative position of the probe in comparison to the kiss bond also affects the QPD results. So QPD is only capable of detecting a kiss bond when the probe is directly on top of the kiss bond.

More research is required to come up with a repetitive procedure to fabricate a sample with a kiss bond representing what is encountered in practice. It is necessary to perform a combination of NDTs to find out the advantages and disadvantages of each technique. So far, it is not possible to reliably detect a kiss bond with any NDT. QPD shows some promise in order to detect a kiss bond. It is necessary to fabricate more samples and conduct more tests in order to achieve more statistical information.

7.2) Recommendations for future research

- The procedure of spraying the release agent and using mask proved to be ineffective. More trial and error is required to come up with a repetitive and reliable procedure to create a partial kiss bond. Usage of other substances such as hydraulic oil, sweat, etc. is mentioned in the literature and should be investigated. In the case of spraying the substrate's surface with a release agent, a sophisticated spray capable of depositing a particular amount of the released agent in each try is favorable to ensure the thickness of the applied release agent is constant for all the samples.
- The inclusion of aluminum tape to create a partial kiss bond proved to be effective. Other film inclusions such as Teflon could be investigated as well.
- Contact angle measurement could be used before and after surface preparation (solvent wiping) to evaluate the effectiveness of the preparation process.
- EDS or XPS could be used to evaluate the substrates' surface after applying any substance as a release agent. This can help determine the elemental composition of the release agent and the extent of coverage of the surface with the release agent. It can also give us some idea about the thickness of the applied release agent on the surface.

- EDS and XPS could be used to determine the elemental composition through the thickness of the bond. This can be helpful to see if there is any distinct difference between the elemental composition of the bulk of the adhesive and the interface between the adhesive and the substrates. This way, it is possible to keep track of the curing agent or other additives and investigate whether the migration from the bulk of the adhesive to the interface or vice versa happens. This could explain if the degree of cure differs between the bulk and the interface. It is also possible to determine whether the release agent migrates towards the bulk of the adhesive.
- Using polymeric composite laminates (e.g. CFRP, GFRP[8], AFRP[9], etc.) laminates as substrates and investigate the performance of adhesively bonded joints and the capability of QPD in detecting a kiss bond in that case.
- Detaching a small piece of adhesive from a fabricated sample and using DSC to determine the degree of cure.
- Finding a way to incorporate the DEA sensors into the fabrication process and monitor the curing.
- Studying the fracture surface with a high-resolution optical microscope that has the capability of determining the topography of the fracture surface.

[8] Glass Fiber Reinforced Polymer
[9] Aramid Fiber Reinforced Polymer

8) References

[1] K. Kendall, Molecular Adhesion amd Its Applications: The Sticky Universe, New York: Kluwer Academic/ Plenum Publishers, 2001.

[2] G. Dillingham, "BTG LABS," 2019. [Online]. Available: https://www.btglabs.com/. [Accessed 2020].

[3] L. F. da Silva, A. Ochsner and R. D. Adams, Eds., Handbook of Adhesion Technology, vol. 2, 2011.

[4] REICHHOLD, *Epoxy Resins & Curing Agents,* 2015.

[5] ASTM D2093-03: Standard Practice for Preparation of Surfaces of Plastics Prior to Adhesive Bonding, ASTM International, 2017.

[6] A. V. Pocius, Adhesion and Adhesives Technology: An Introduction, Cincinnati: HANSER publications, 2012.

[7] "Contact Angle," Rame-hart instrument co., [Online]. Available: http://www.ramehart.com/contactangle.htm.

[8] "biolinscientific," [Online]. Available: https://www.biolinscientific.com/measurements/dynamic-contact-angle. [Accessed 2019].

[9] A. A. Taib, R. Boukhili, S. Achiou, S. Gordon and H. Boukehili, "Bonded joints with composite adherends. Part I. Effect of specimen configuration, adhesive thickness, spew fillet and adherend stiffness on fracture," *International Journal of Adhesion & Adhesives,* vol. 26, pp. 226-236, 2006.

[10] A. S. Mosallam, "Design Guide for FRP Composite Connections," in *ASCE Manuals and Reports on Engineering Practice MOP#102*, Reston, Virginia: American Society of Civil Engineers (ASCE), 2011, p. 601.

[11] ASTM D4896-01: Standard Guide for Use of Adhesive-Bonded Single Lap-Joint Specimen Test results, ASTM International, 2016.

[12] "JointDesigner," [Online]. Available: http://www.jointdesigner.com/index.php. [Accessed 2020].

[13] S. Abbott, "Lap Joint Models: Kendall & Goland-Reissner," [Online]. Available: https://www.stevenabbott.co.uk/practical-adhesion/g-rlap.php.

[14] L. Liao, C. Huang and T. Sawa, "Effect of adhesive thickness, adhesive type and scarf angle on the mechanical properties of scarf adhesive joints," *Int JSolid Struct,* vol. 50, pp. 4333-40, 2013.

[15] L. F. da Silva, S. Budhe, M. Banea and S. de Barros, "An updated review of adhesively bonded joints in composite materials," *International Journal of Adhesion and Adhesives,* vol. 72, pp. 30-42, 2017.

[16] G. C. Mays and A. R. Hutchinson, Adhesives in Civil Engineering, 1992.

[17] B. M. Parker, "Some Effects of Moisture on Adhesive-Bonded CFRP-CFRP Joints," *Composite Structures,* vol. 6, pp. 123-139, 1986.

[18] M. K. Chawla, "How Clean Is Clean? Measuring Surface Cleanliness and Defining Acceptable Levels of Cleanliness," in *Handbook for Critical Cleaning: Applications, Processes, and Controls*, 2nd ed., CRC Press, 2017.

[19] M. K. Chawla, "Optically Stimulated Electron Emission: A Powerful Tool for Surface Cleanliness Monitoring," in *Developments in Surface Contamination and Cleaning: Contamination Sources, Measurement, Validation, and Regulatory Aspects*, Elsevier, 2015, pp. 69-107.

[20] K. Brune, L. Lima, M. Noeske, K. Thiel, C. Tornow, S. Dieckhoff, M. Hoffmann and D. Stübing, "Pre-bond Quality Assurance of CFRP Surfaces Using Optically Stimulated Electron Emission," 2013.

[21] B. M. Parker and R. M. Waghorne, "Testing Epoxy Composite Surfaces for Bondability," *SURFACE AND INTERFACE ANALYSIS,* vol. 17, pp. 471-476, 1991.

[22] S. M. P. Seah, "The quantitative analysis of surfaces by XPS: A review," *Surface and Interface Analysis,* vol. 2, no. 6, pp. 222-239, 1980.

[23] J. R. Fried, Polymer Science & Technology, 2nd ed., Prentice Hall, 2003.

[24] *Differential Scanning Calorimetry DSC 214 Polyma: Method, Technique, Applications,* NETZSCH.

[25] *DEA 288 Ionic – Dielectric Cure Monitoring: Method, Technique, Applications,* NETZSCH.

[26] P. N. Marty, N. Desaï and J. Andersson, "NDT of kissing bond in aeronautical structures," *Proceedings of the 16th world conference for NDT. Montreal, Canada,* 2004.

[27] C. Jeenjitkaew, Z. Luklinska and F. Guild, "Morphology and surface chemistry of kissing bonds in adhesive joints," *International Journal of Adhesion & Adhesives,* no. 30, pp. 643-653, 2010.

[28] S. L. Poveromo, Quantitative Percussion Diagnostics For Evaluating Bond Integrity Between Composite Laminates, 2015.

[29] R. Adams and E. Karachalios, "The effect of defects on the strength of adhesively-bonded joints and its significance for NDT," *conference Emerging Technologies,* 2007.

[30] "Introduction to Ultrasonic Testing," [Online]. Available: https://www.nde-ed.org/EducationResources/CommunityCollege/Ultrasonics/cc_ut_index.htm. [Accessed 2020].

[31] B. Drinkwater and P. Cawley, "An ultrasonic wheel probe alternative to liquid coupling," *Brit J NDT,* vol. 36, pp. 430-433, 1994.

[32] S. Yang, L. Gu and R. F. Gibson, "Nondestructive detection of weak joints in adhesively bonded composite structures," *COMPOSITE STRUCTURES,* pp. 63-71, 2001.

[33] P. Cawley and R. Adams, "THE MECHANICS OF THE COIN-TAP METHOD OF NON-DESTRUCTIVE TESTING," *Journal of Sound and Vibration,* vol. 122, no. 2, pp. 299-316, 1988.

[34] J. a. Schroeder, T. Ahmed, B. Chaudhry and S. Shepard, "Non-destructive testing of structural composites and adhesively bonded composite joints: pulsed thermography," *Compos. Part A Appl. Sci. Manuf,* vol. 33, p. 1511–1517, 2002.

[35] L. Hart-Smith and E. Thrall, "Adhesive bonding of aluminium alloys," New York, Marcel Dekker, 1985, p. 241–335.

[36] R. Bossi, D. Lahrman, D. Sokol and C. Walters, "Laser bond inspection for adhesive bond strength," *SAMPE proceedings, Long Beach, CA,* 2011.

[37] "Measurement Principles of Shearography," dantecdynamics, [Online]. Available: https://www.dantecdynamics.com/solutions-applications/solutions/laser-shearography-ndt/measurement-principles-of-shearography/. [Accessed 2020].

[38] Y. Hung, "Applications of digital shearography for testing of composite structures," *Compos. Part B Eng,* vol. 30, p. 765–773, 1999.

[39] "System and method for quantitative measurements of energy damping capacity.". United States of America Patent 6120466, 19 September 2000.

[40] D. A. Brenner and J. Earthman, "NOVEL INSTRUMENTATION FOR QUANTITATIVE DETERMINATION OF ENERGY DAMPING IN MATERIALS AND STRUCTURES," *Scripta Metallurgica et Materialia,* vol. 31, no. 4, pp. 464-471, 1994.

[41] J. D. Lincoln, L. E. Rieger and J. C. Earthman, "Instrumentation for Determining the Local Damping Capacity in Honeycomb Sandwich Composites," *Journal of Testing and Evaluation,* vol. 34, no. 3, 2006.

[42] S. Poveromo and J. Earthman, "Development of Percussion Diagnostics in Evaluating 'Kiss' Bonds Between Composite Laminates," in *Advanced Composites for Aerospace, Marine, and Land Applications*, T. Sano, T. Srivatsan and M. Peretti, Eds., Springer, Cham, 2014.

[43] B. Stanley, L. Bustemente and J. Earthman, "Novel Instrumentation for Rapid Assessment of Internal Damage in Composite Materials," *The Mineral, Metals,& Materials Society,* pp. 97-100, 1997.

[44] R. Jensen, D. DeSchepper, D. Flanagan, G. Chaney and C. Pergantis, "Adhesives: Test Method, Group Assignment, and Categorization Guide for High-Loading- Rate Applications – Preparation and Testing of Single Lap Joints," US Army Research Laboratory (ARL), 2016.

[45] ASTM D1002-10: Standard Test Method for Apparent Shear Strength of Single-Lap-Joint Adhesively Bonded Metal Specimens by Tension Loading (Metal-to- Metal), ASTM International.

[46] ASTM D3163-01: Standard Test Method for Determining Strength of Adhesively Bonded Rigid Plastic Lap-Shear Joints in Shear by Tension Loading, ASTM International, 2014.

[47] P. B. Nagy, "Ultrasonic detection of kissing bonds at adhesive interfaces," *Journal of Adhesion Science and Technology,* vol. 5, no. 8, pp. 619-630, 1991.

[48] "Engineering Materials," The Engineering ToolBox, [Online]. Available: https://www.engineeringtoolbox.com/engineering-materials-properties-d_1225.html. [Accessed 2020].

[49] "Strength vs. Density," Material Selection Charts, [Online]. Available: http://www-materials.eng.cam.ac.uk/mpsite/interactive_charts/strength-density/NS6Chart.html. [Accessed 2020].

[50] Harvey Performance Company, "Conquering Composites: Overcoming Milling and Holemaking Challenges," Harvey Performance Company, 21 May 2020. [Online]. Available: https://www.youtube.com/watch?v=gVPwK7ULSLk&list=LLOf334xNZXaUHfixjbiURDQ&index=2&t=0s. [Accessed 2020].

[51] "How to Perform an Adhesive Lap Joint Shear Strength Test – ASTM D1002," [Online]. Available: https://www.admet.com/how-to-perform-an-adhesive-lap-joint-shear-strength-test-astm-d1002/. [Accessed 2020].

9) Appendix A: Drawing for all the machined parts

Grip: 1st iteration:

Part1:

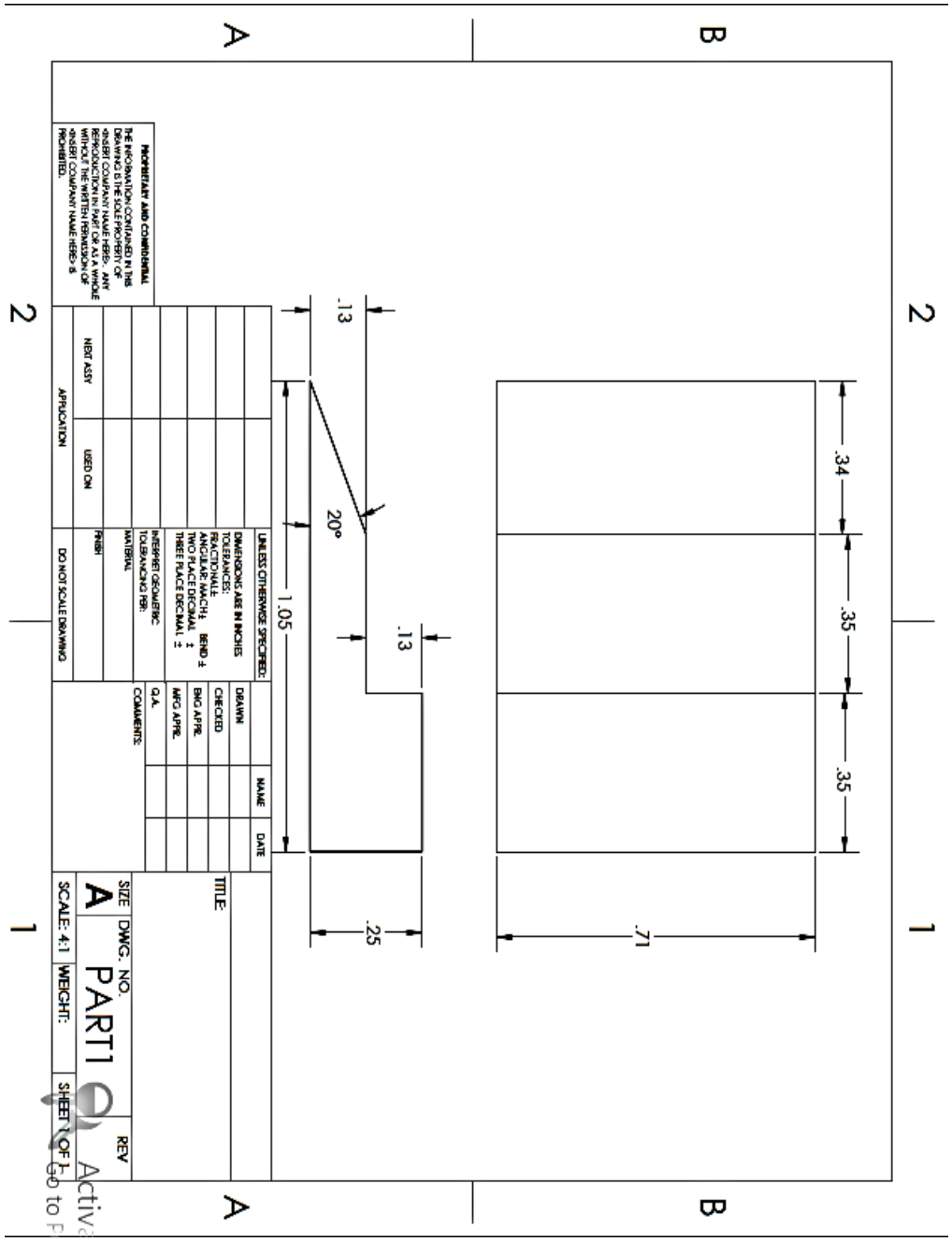

Figure A-1: Drawing of 1st Grip: Part1

Part2:

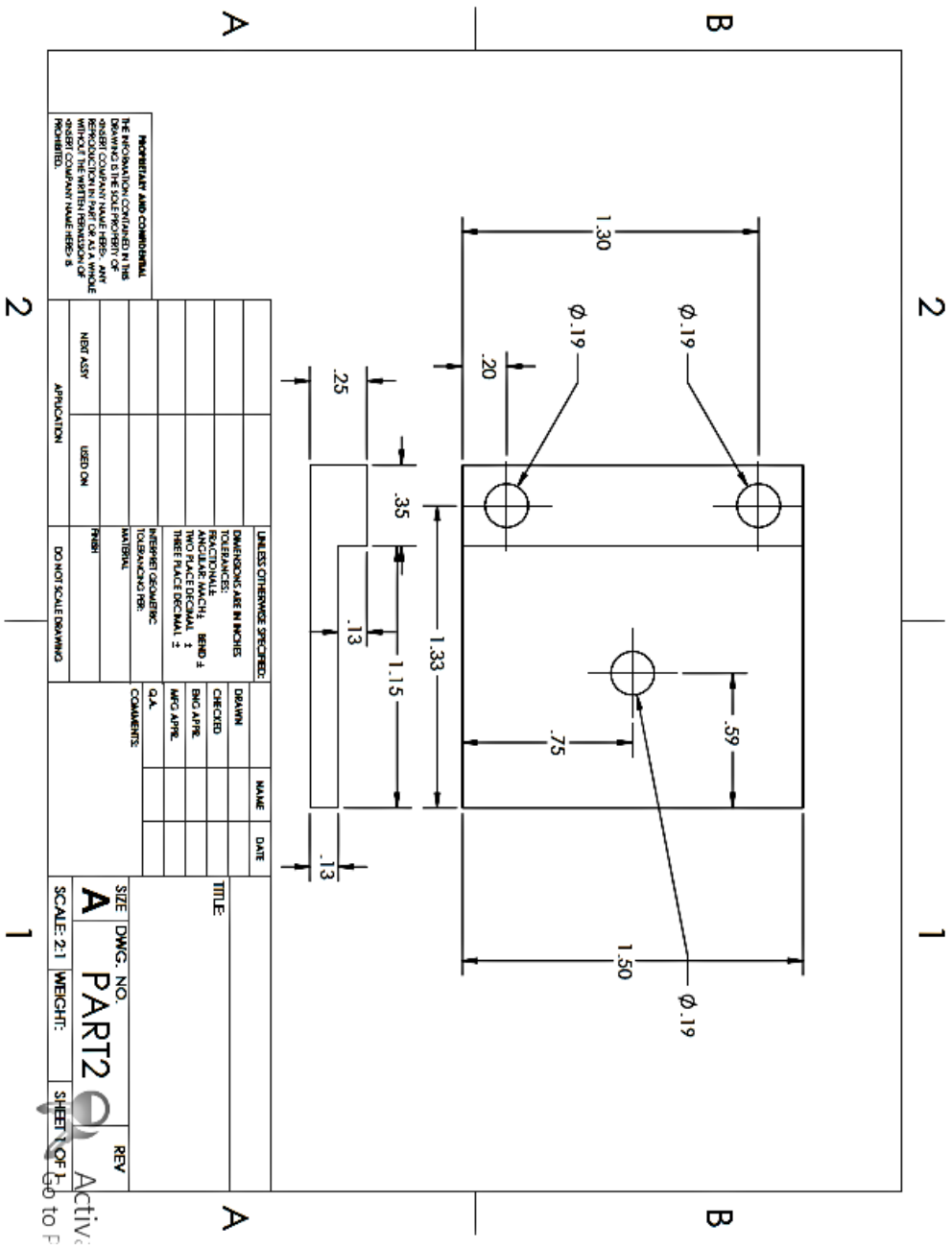

Figure A-2: Drawing of 1st Grip: Part2

Part3

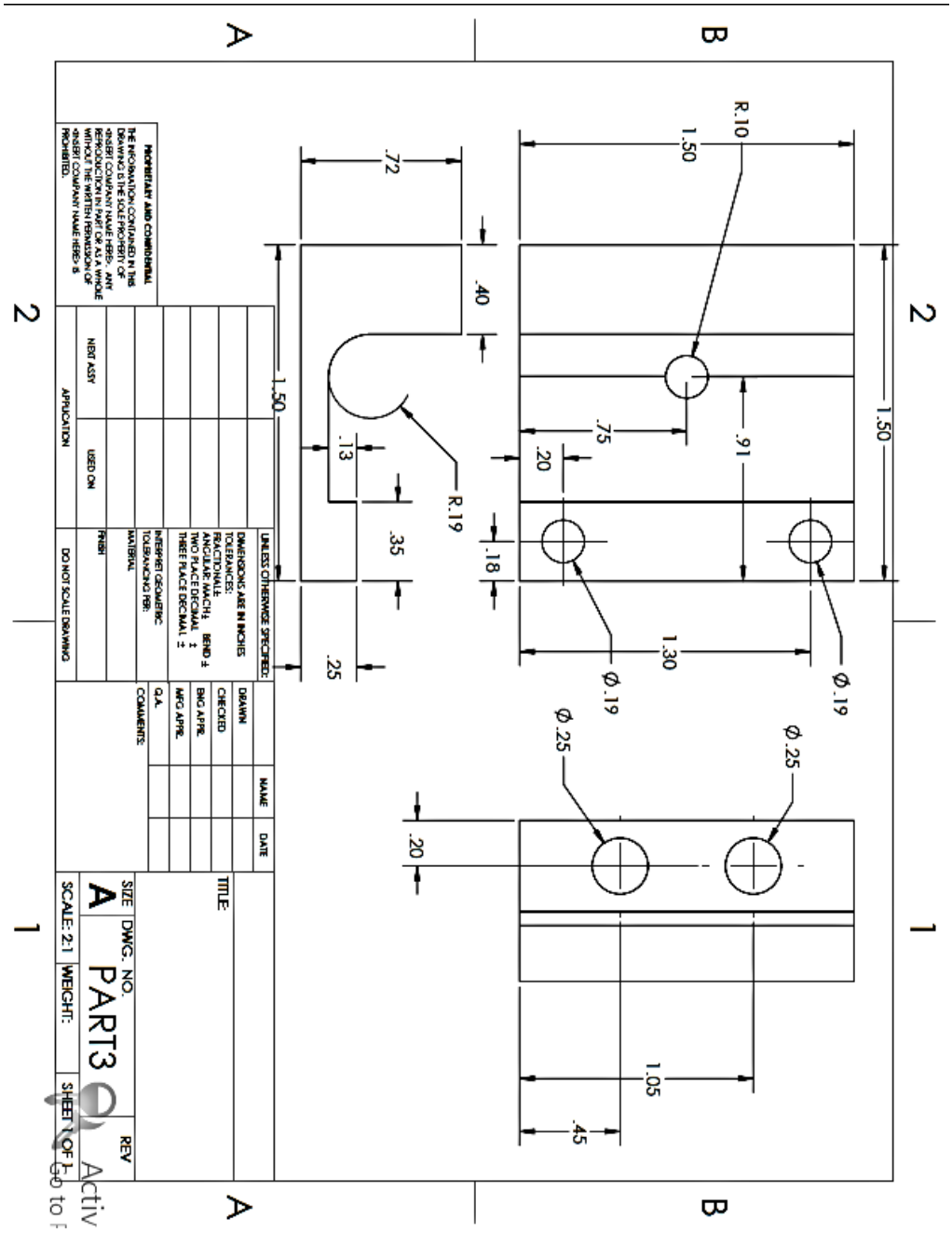

Figure A-3: Drawing of 1st Grip: Part3

Part4

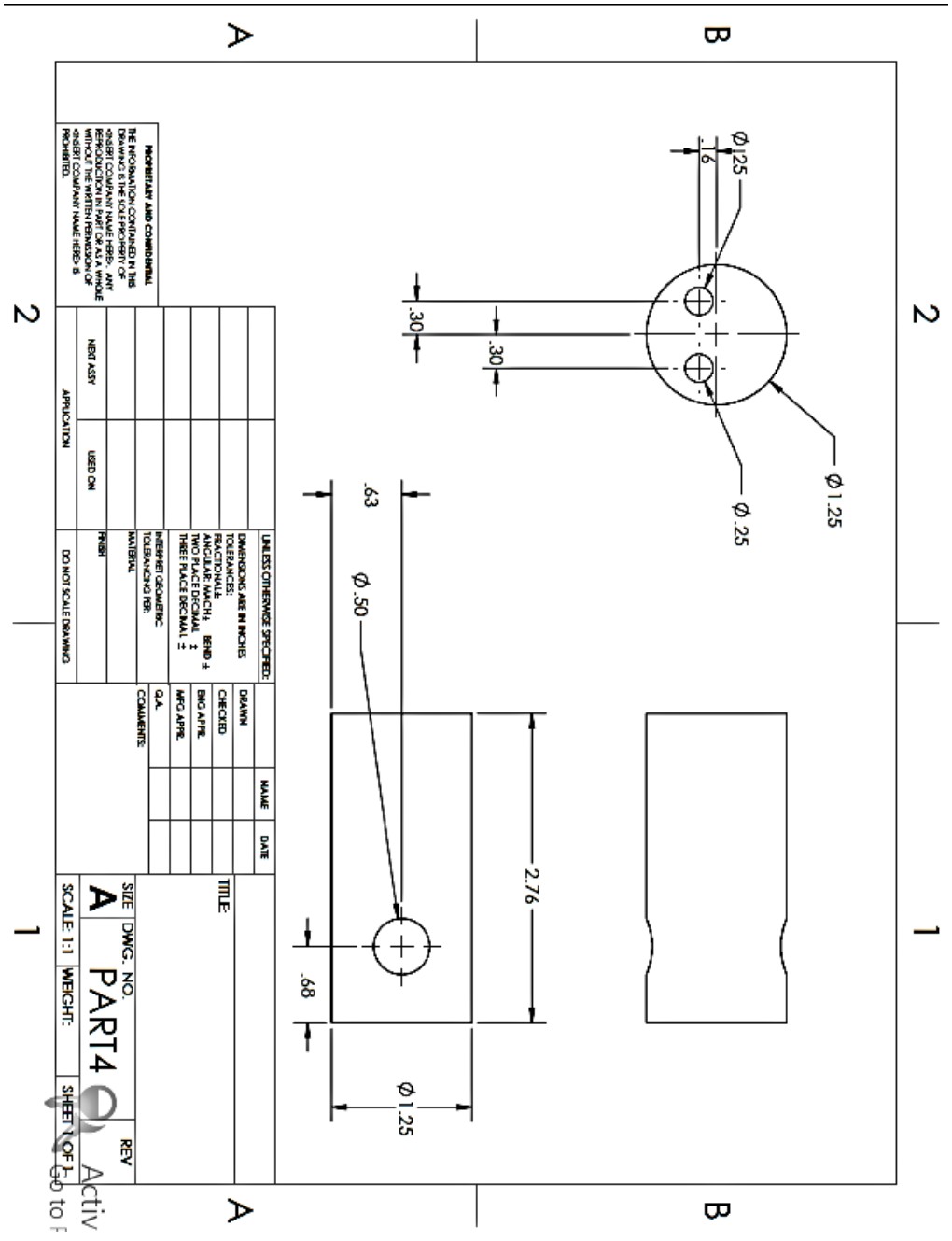

Figure A-4: Drawing of 1st Grip: Part4

Grip 2nd iteration

Part2

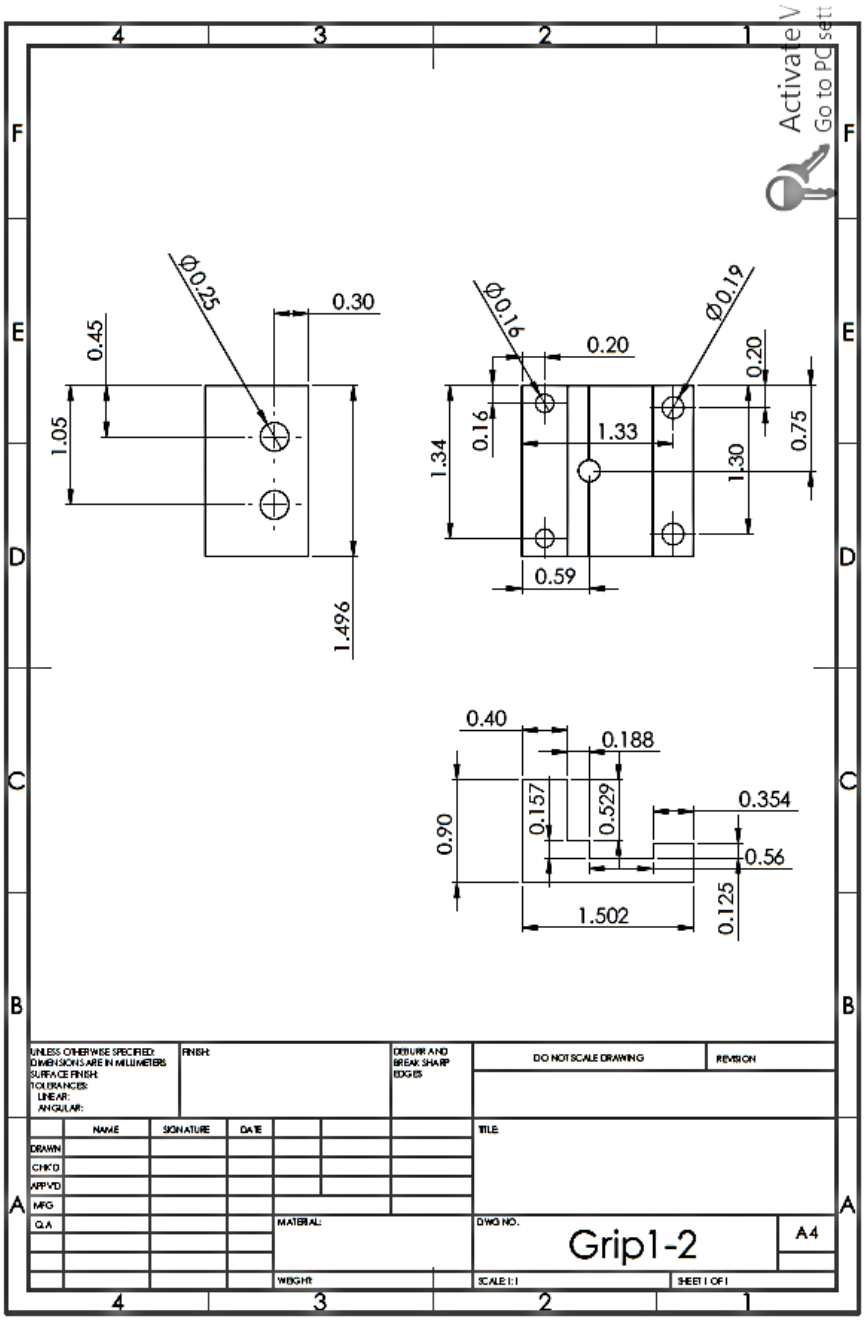

Figure A-5: Drawing of 2nd Grip: Part2

Part 3

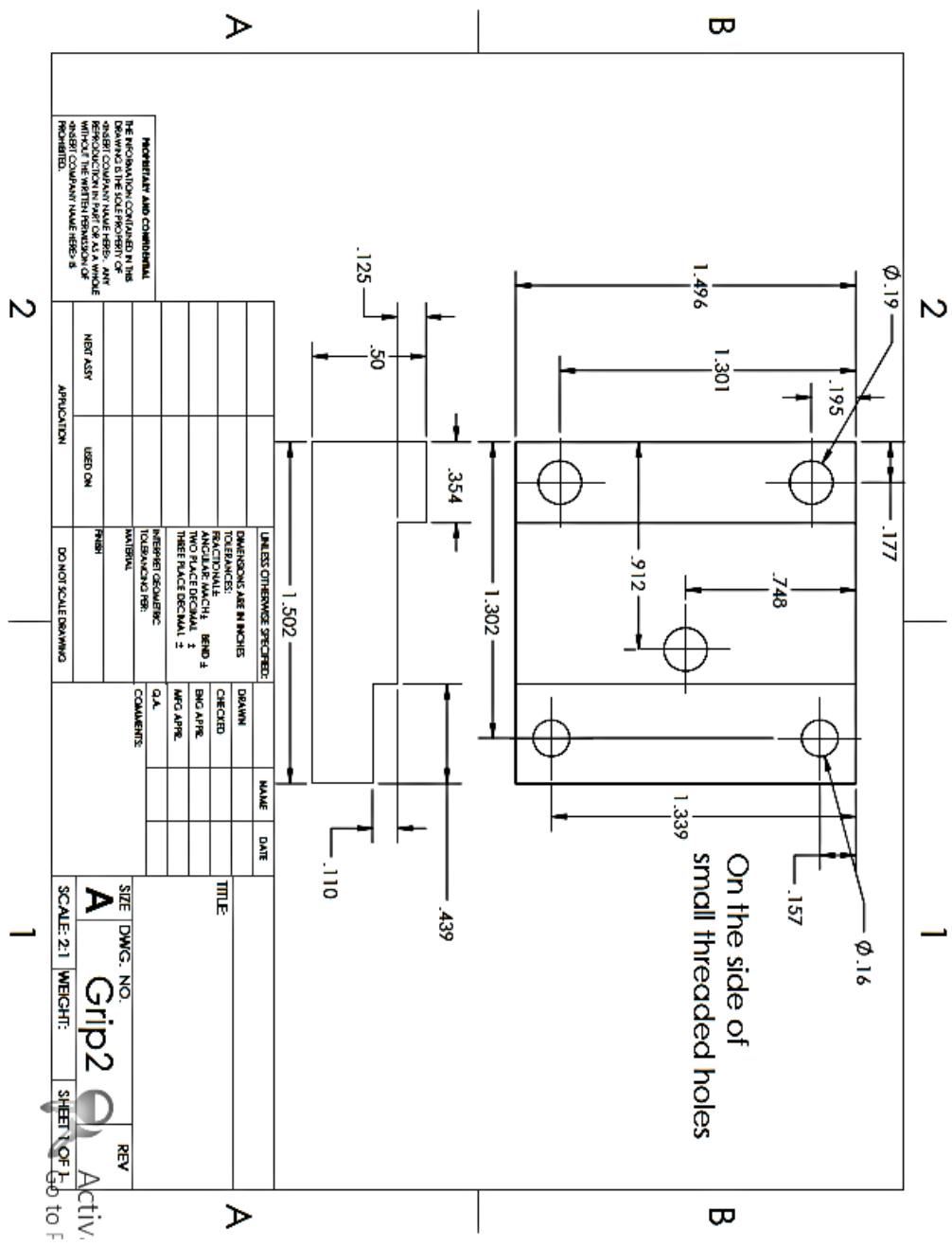

Figure A-6: Drawing of 2nd Grip: Part3

Holder

Main

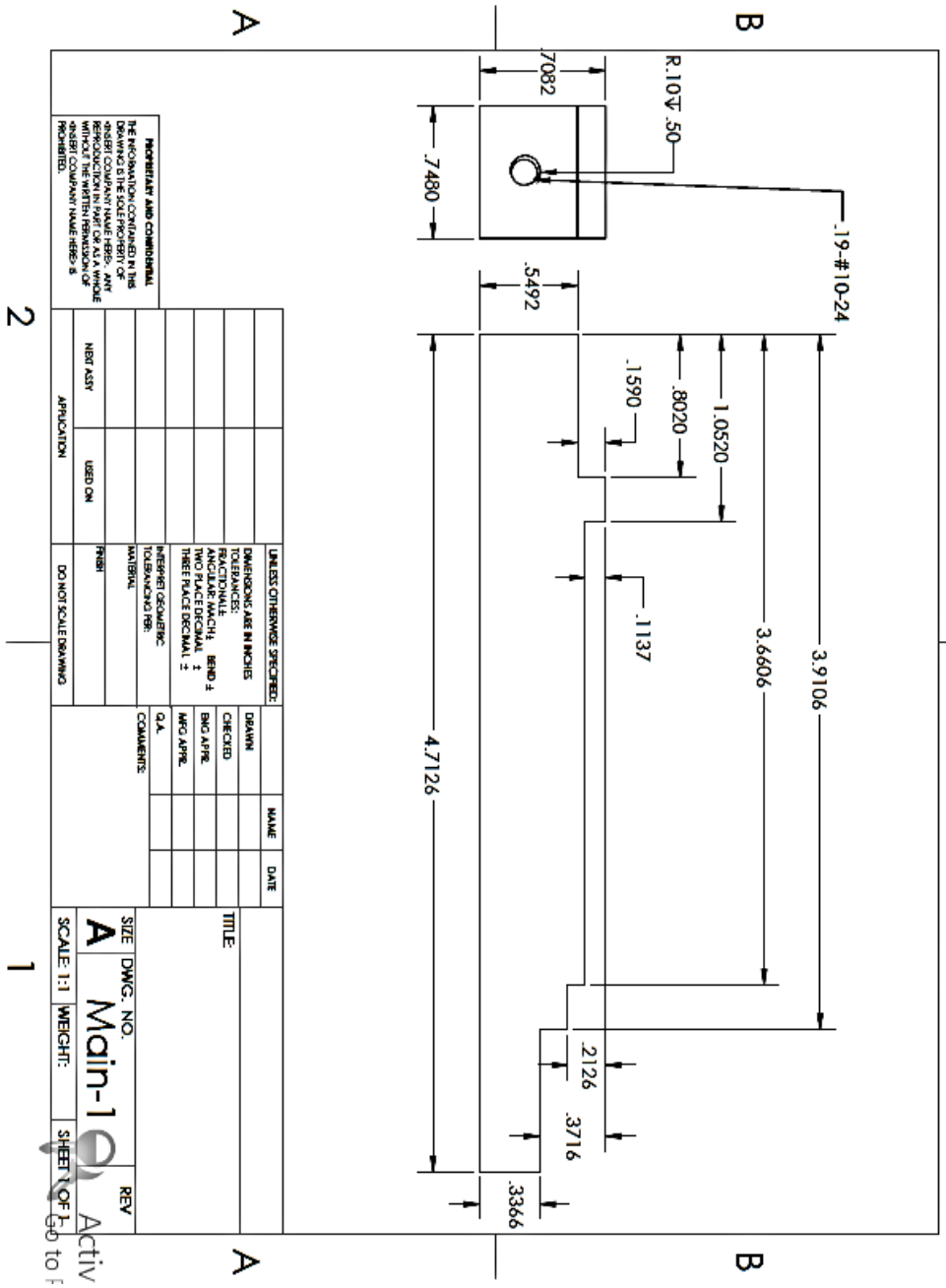

Figure A-7: Drawing of Holder Main

Main 2

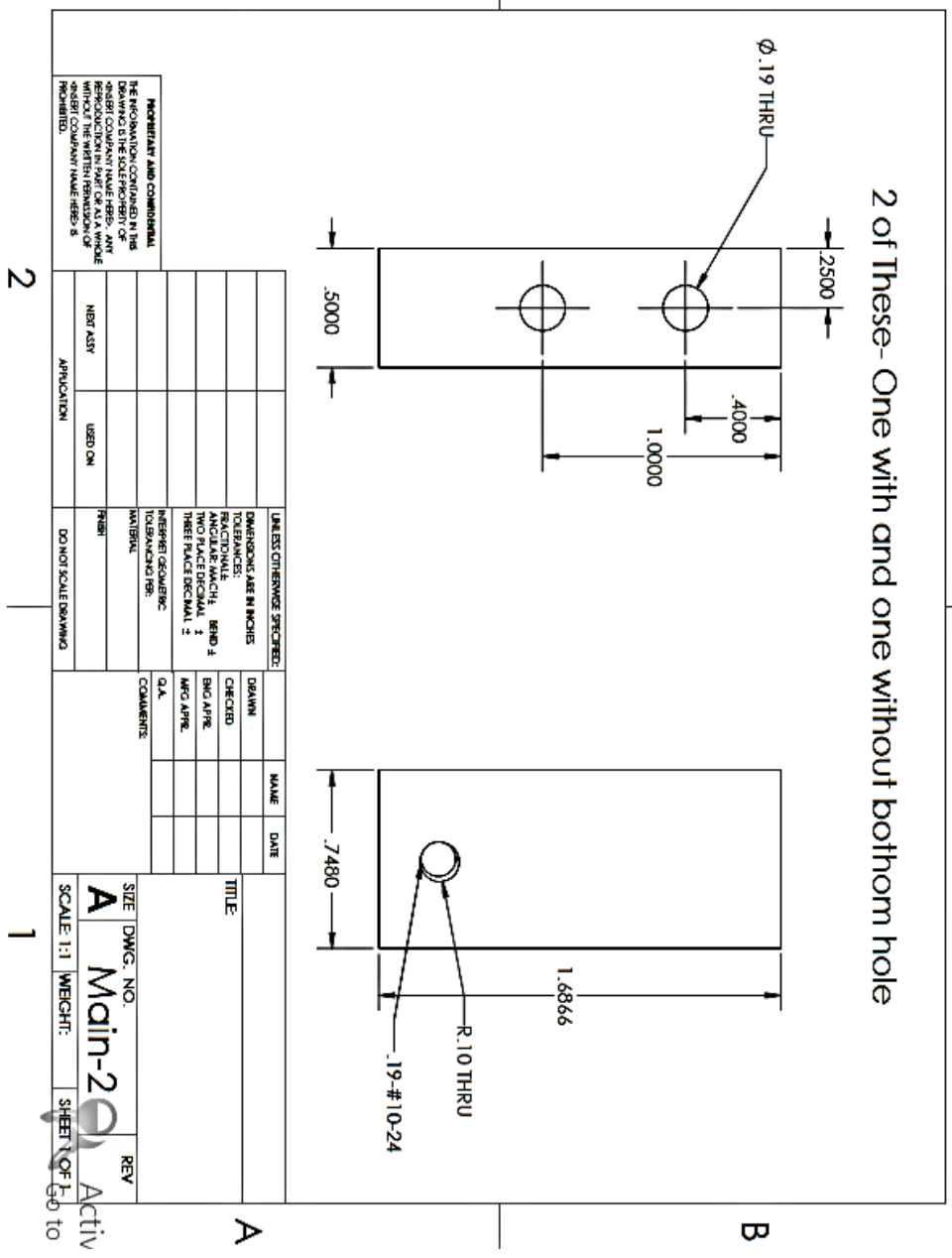

Figure A-8: Drawing of Holder Main2

Body 1

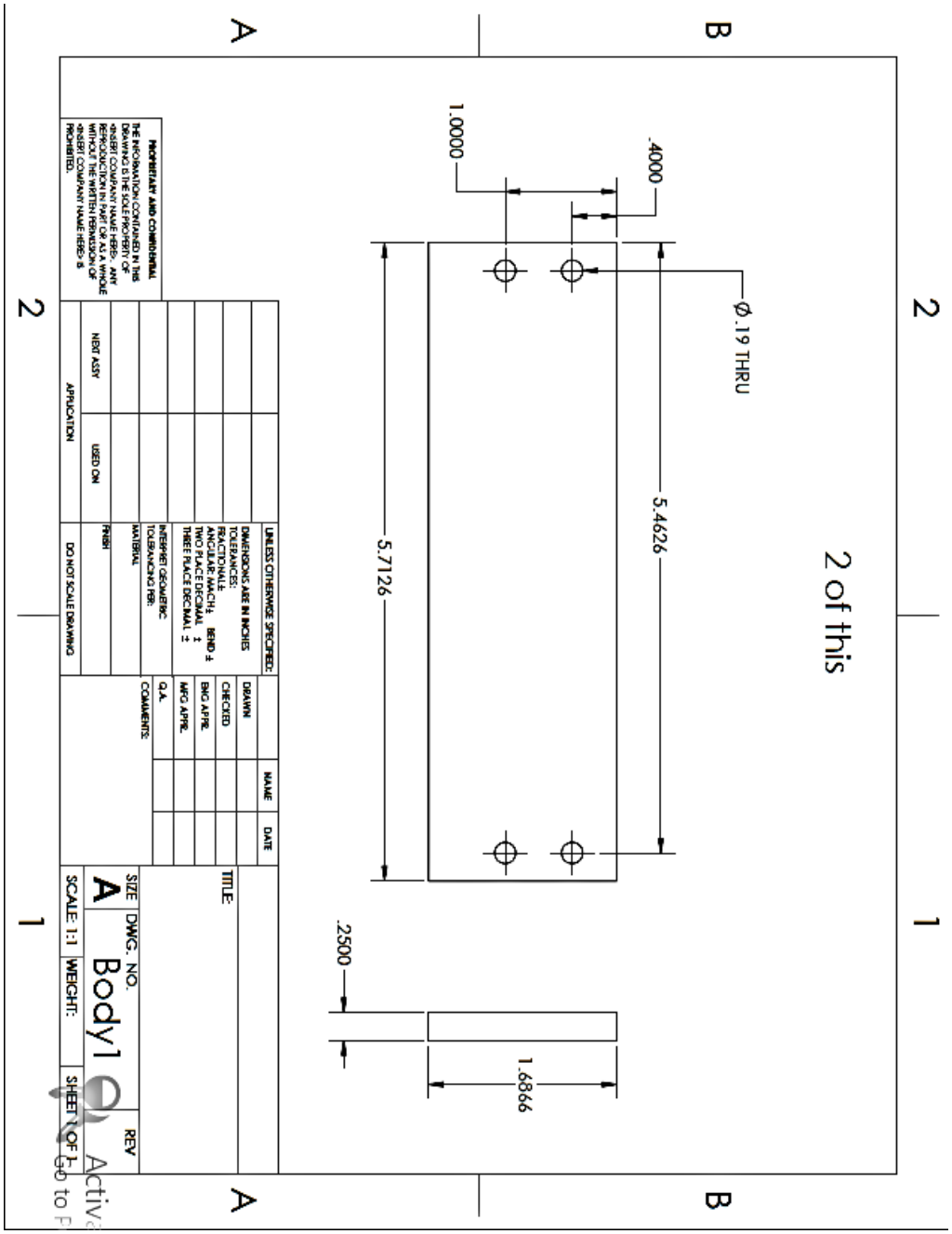

Figure A-9: Drawing of Holder Body

Multiple Sample at the same time

Bottom

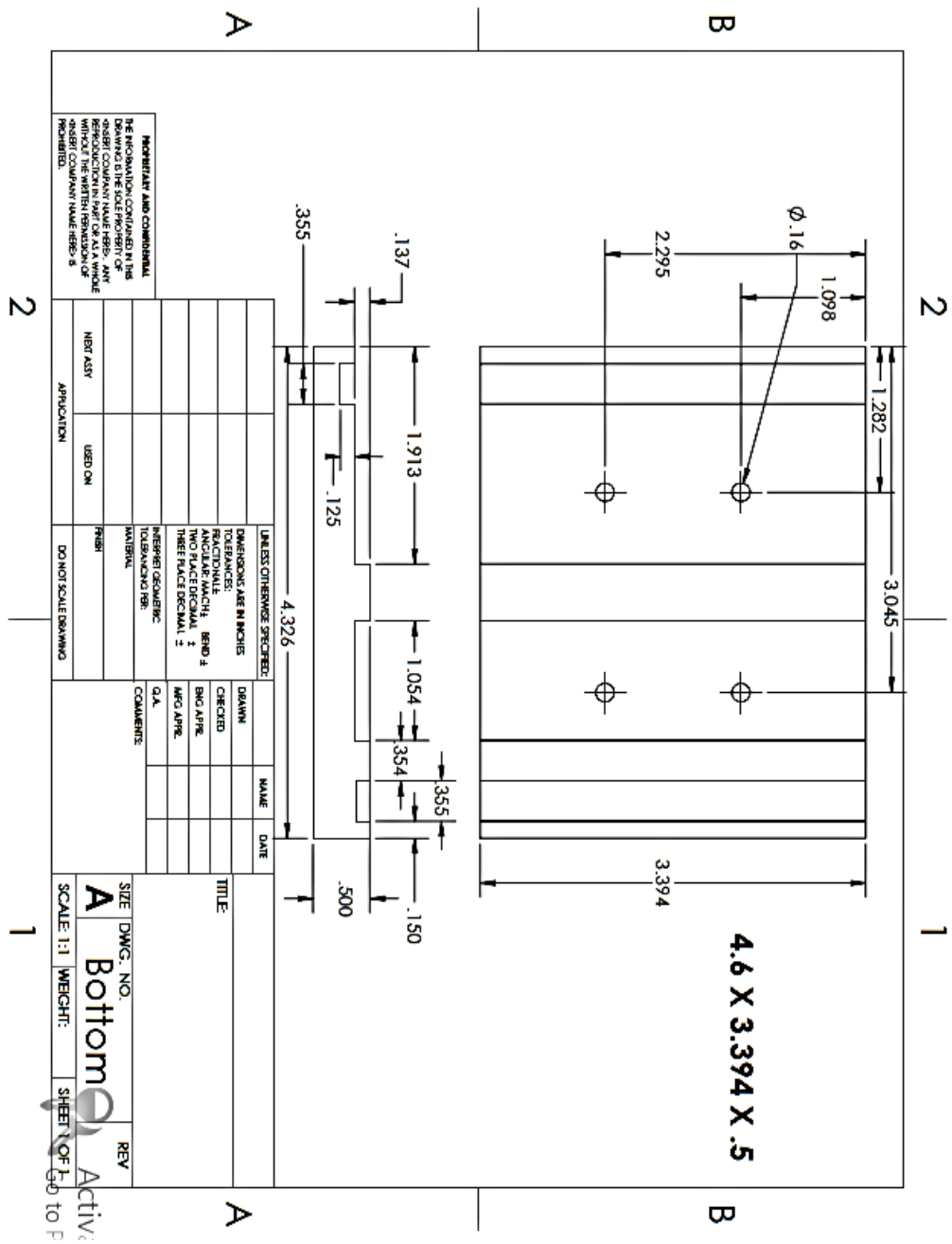

Figure A-10: Drawing of 2nd Holder Bottom

Underneath

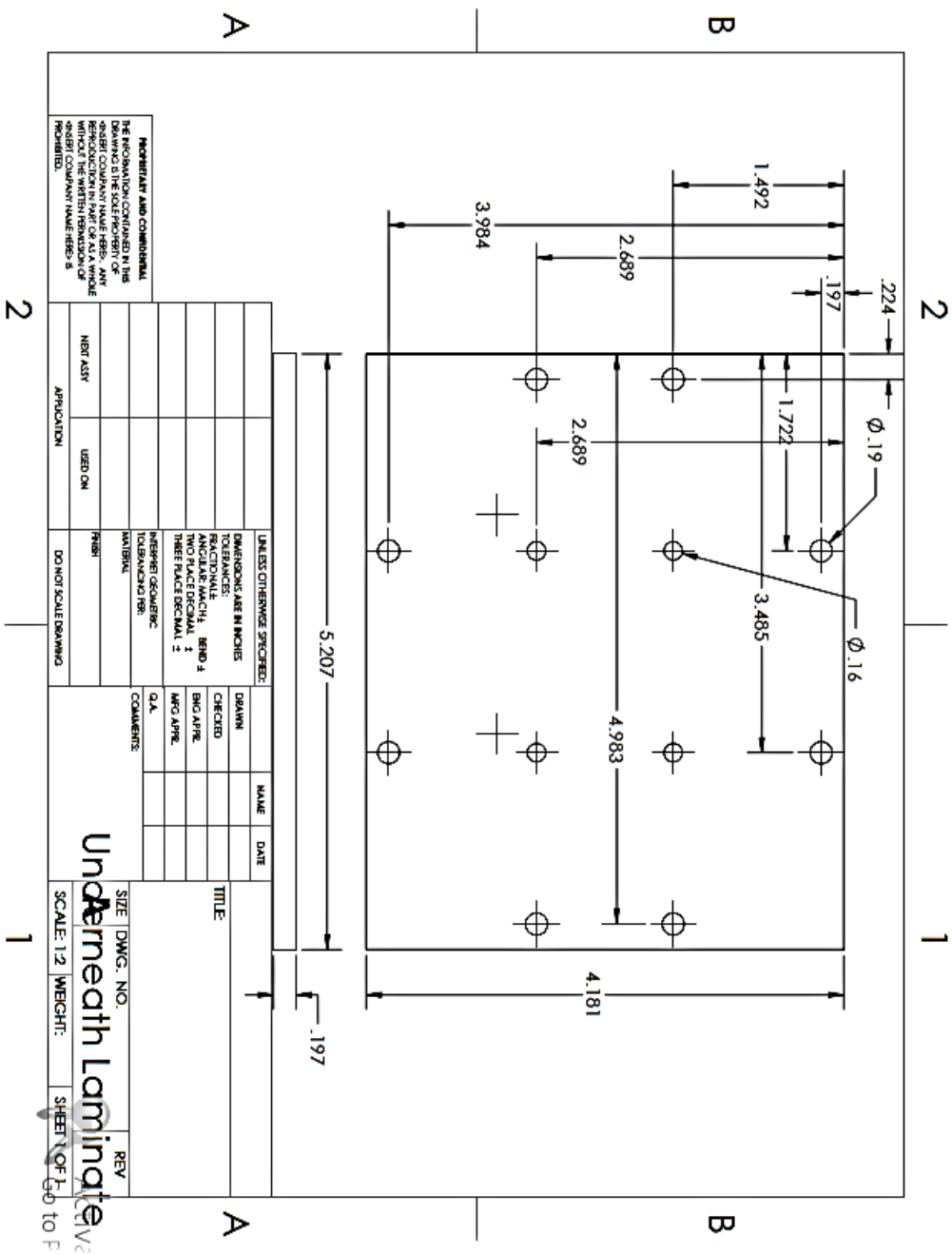

Figure A-11: Drawing of 2nd Holder Underneath

Stepped Joint Drawings

Coupon

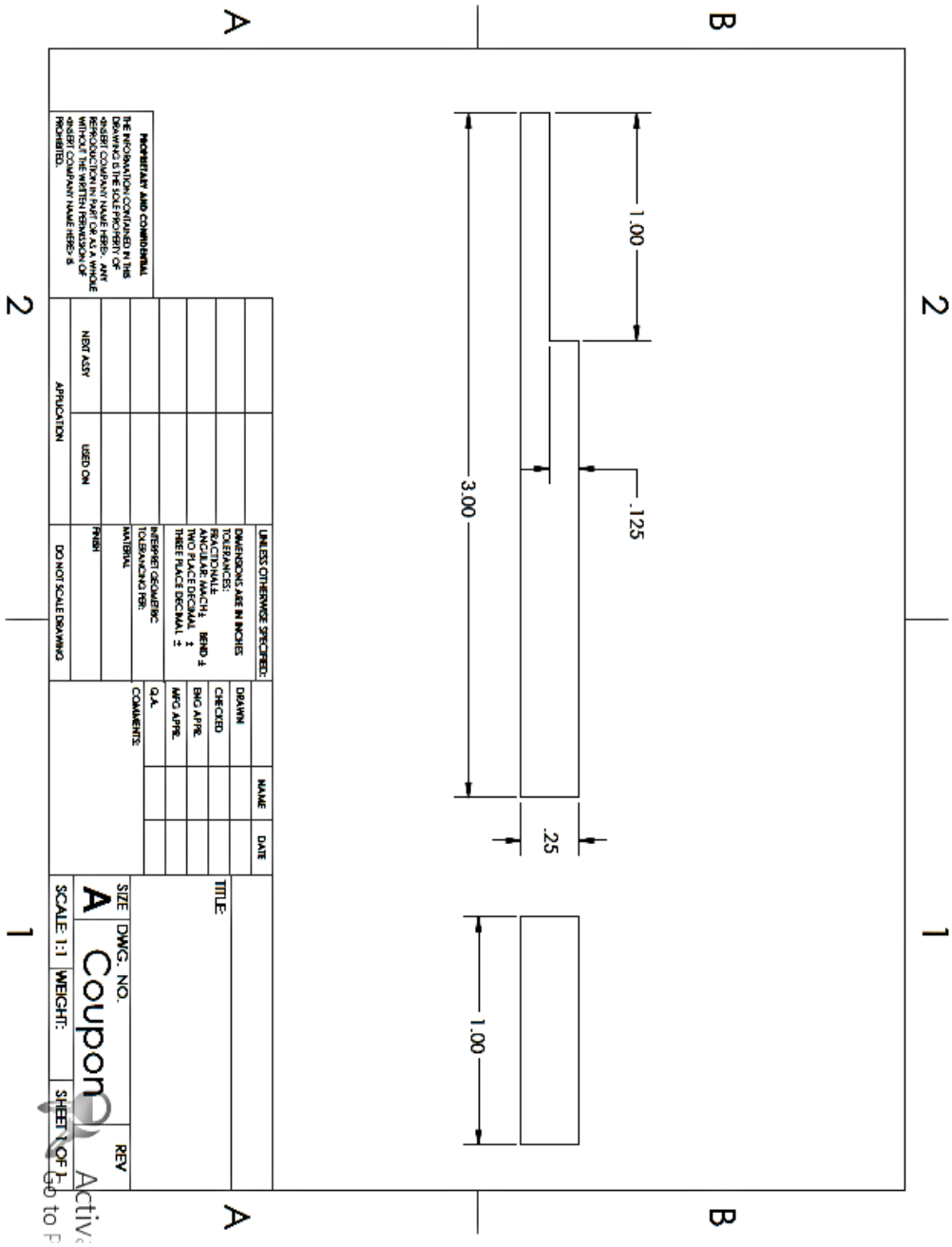

Figure A-12: Drawing for Stepped Joint Coupon

Holder

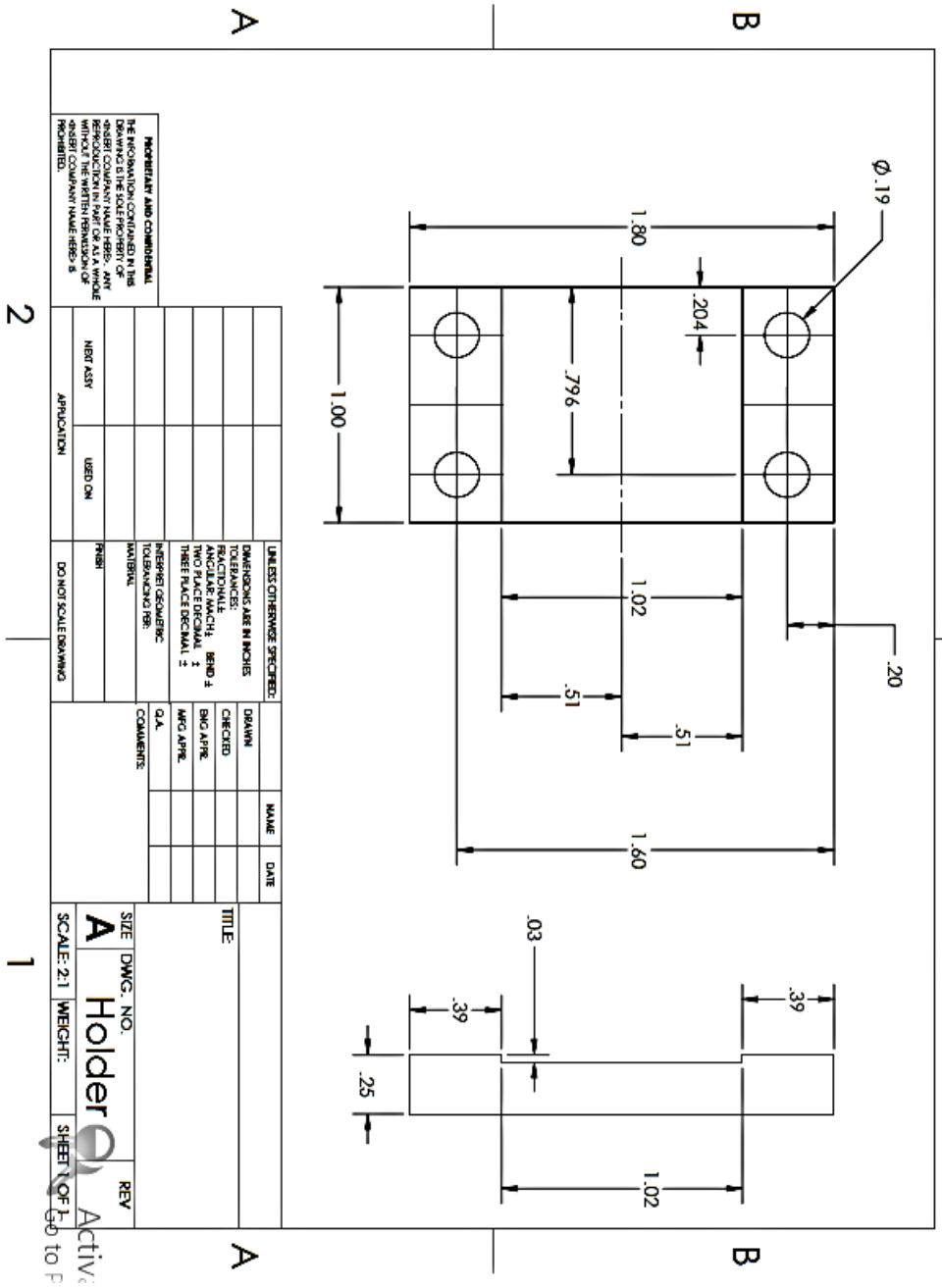

Figure A-13: Drawing for Stepped Joint Holder

Mask .8

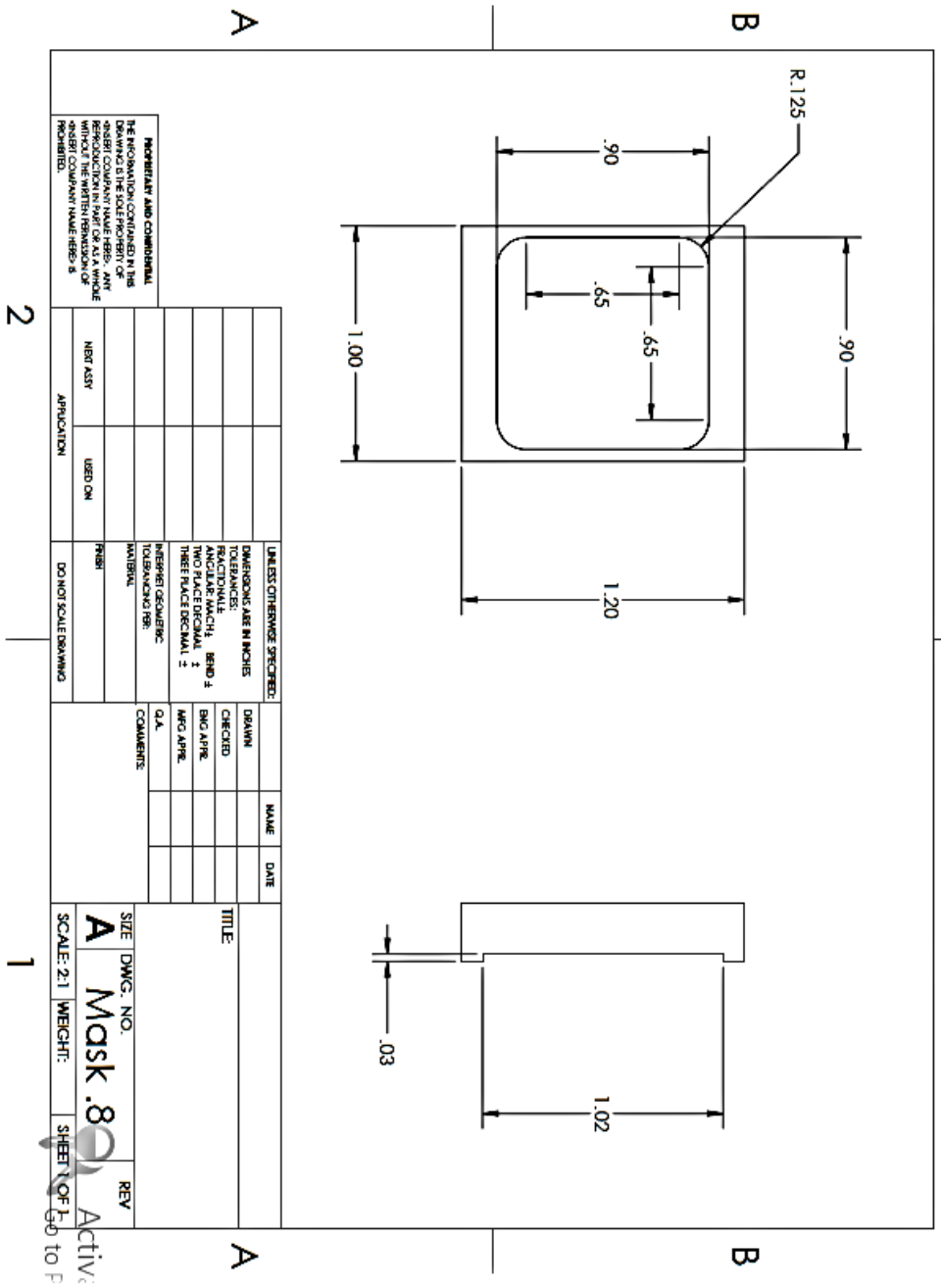

Figure A-14: Drawing for Stepped Joint Mask %80

Mask .53

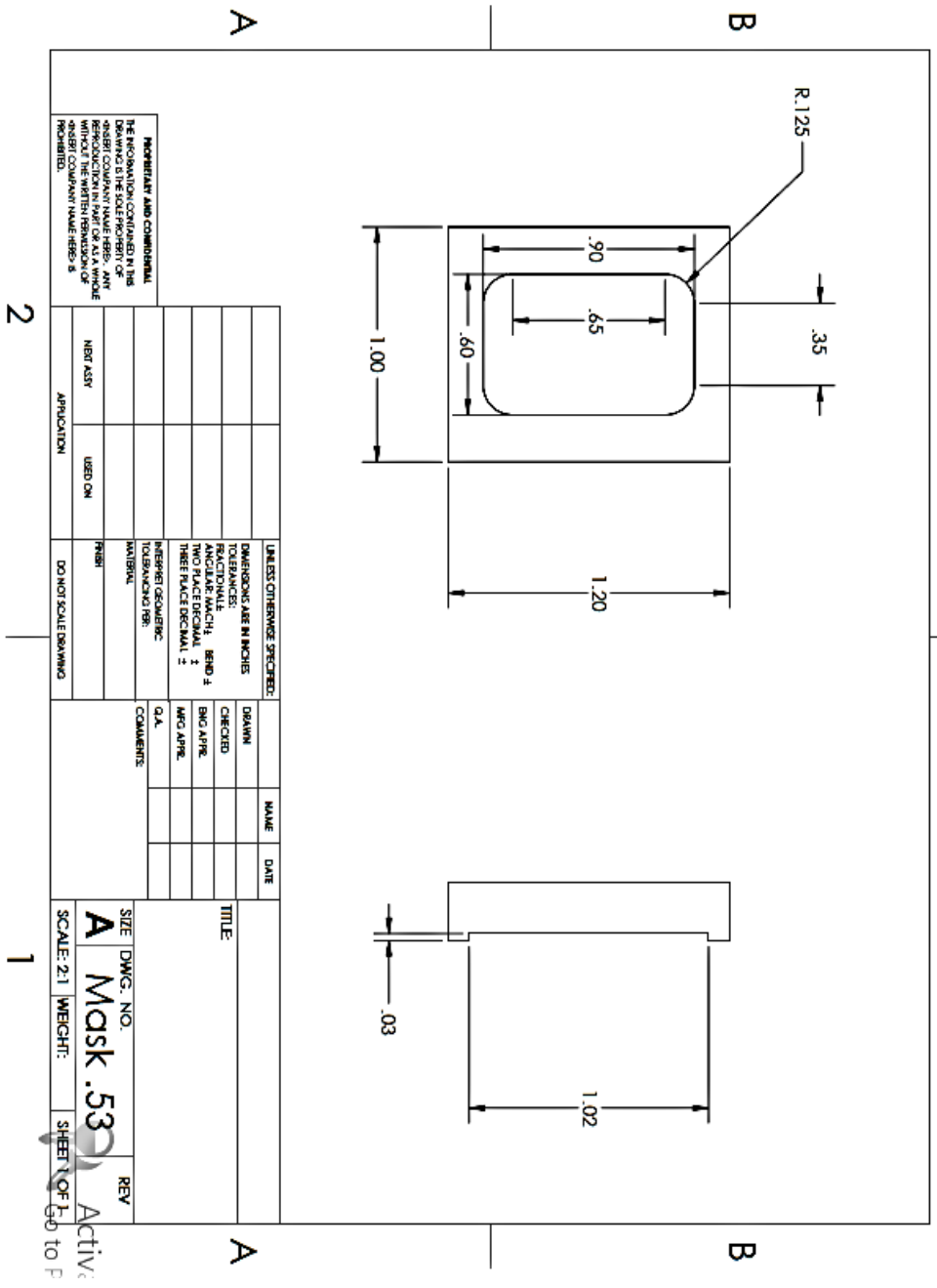

Figure A-15: Drawing for Stepped Joint Mask %53

Mask .35

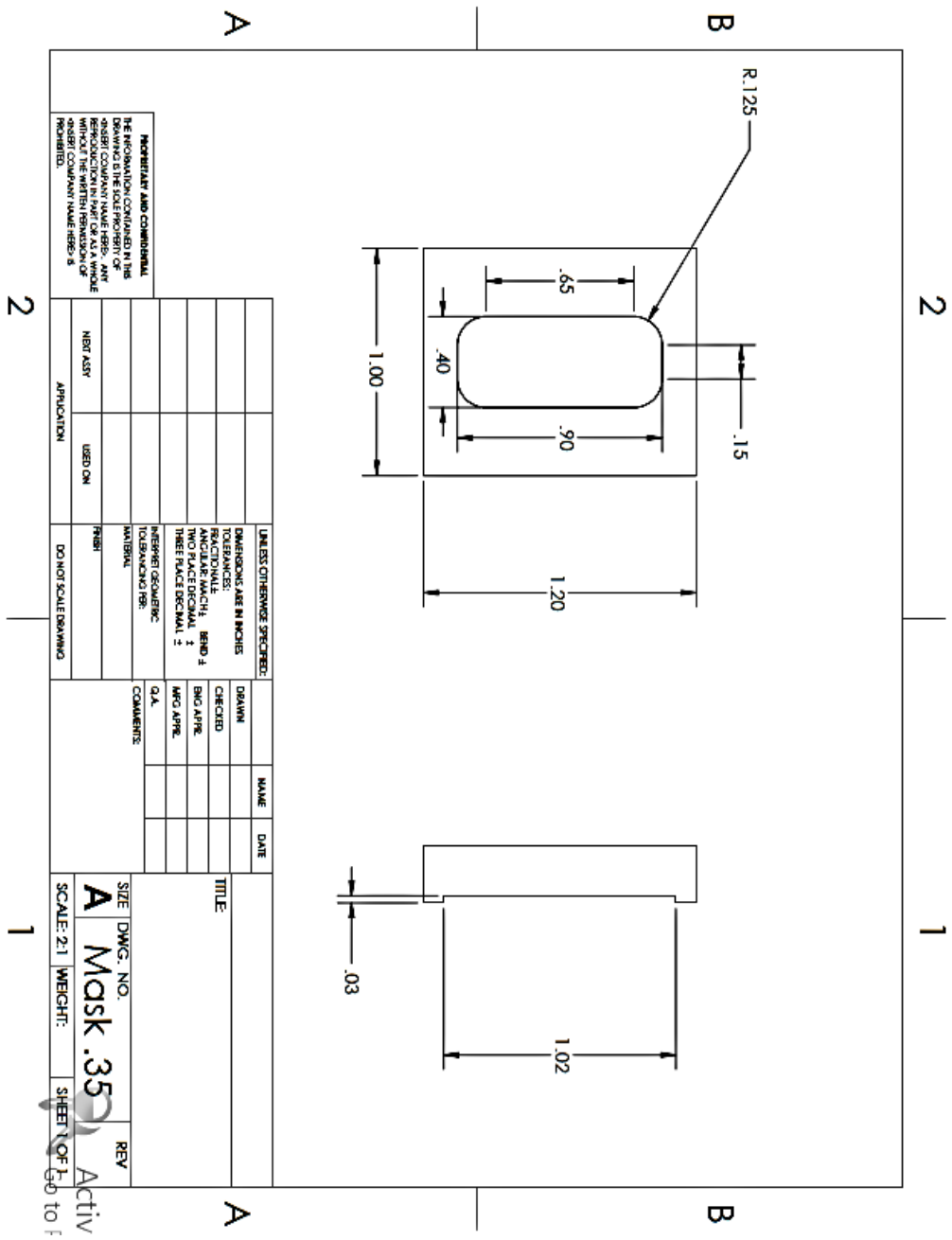

Figure A-16: Drawing for Stepped Joint Mask %35

10) Appendix B: Matlab Codes to calculate the amount of resin & curing agent

10.1) Code I: for a laminate with a known thickness

```
%Calculating Resin & Curing Agent Mixing Ratio for a laminate with known
%thickness (#of plys is the variable)
A=.5*.5              %Area of Laminate
t=2.5*10^-3          %Thickness of Laminate
RAW=500*10^-3        %Reinforcement Areal Weight (kg/m2)
n=4                  %Number of Plys
Ruf=1.78*10^3        %Density of Fiber
Rur=1.1*10^3         %Density of Resin
RuCu=.948*10^3       %Density of Curing Agent
EEW=188*10^-3        %Epoxide Equivalent Weight in kg
AHEW=115*10^-3       %Amine Hydrogen Equivalent Weight in kg
Vc=A*t               %Volume of Laminate
mf=RAW*A*n           %Fiber Mass
Vf=(mf)/Ruf          %Volume of Fiber
Vm=Vc-Vf             %Volume of Matrix
disp('Fiber Content=')
Nuf=Vf/Vc            %Volume Percentage of Fiber
if Nuf<.5
   disp('Fiber Volume % is less than %50')
end
syms mre mcu
eqns=[((mre+mcu)/((mcu/RuCu)+(mre/Rur)))*Vm==mcu+mre,mcu==((mre*AHEW)/EEW)*1.1];
[mre mcu]=vpasolve(eqns,[mre mcu]);
mre=mre*1000             %Resin Mass in gr
mcu=mcu*1000             %Curing Agent Mass in gr
Mm=(mre+mcu)             %Mass of Matrix in gr
Vre=(mre/Rur)*1000       %Resin Volume in ml
Vcu=(mcu/RuCu)*1000      %Curing Agent Volume in ml
Mc=(mre+mcu+mf*1000)     %Mass of Laminate in gr
RuC=(Mc/(Vc*10^6))       %Density of Laminate in gr/cm3
Rum=(Mm/Vm)*10^-6        %Density of Matrix (Resin + Curing Agent)
F=(mf./Mc)*1000          %Fiber Content Weight %
phr=100*mcu./mre         %phr of Curing Agent
ttop=.5*10^-3            %Thickness of the Top Coat (Gel Coat) in m
Vtop=A*ttop*10^6         %Volume of Top Coat in ml
Mtop=Vtop*Rum            %Mass of Top Coat in gr
Mretop=(Mtop*100)./(100+phr)%Mass of Resin for Top Coat in gr
Vretop=Mtop/Rur*10^3     %Volume of Resin for Top Coat in ml
Vcutop=Vtop-Vretop       %Volume of Curing Agent for Top Coat in ml
```

```
Mcutop=Mtop-Mretop          %Mass of Curing Agent for Top Coat in gr
T=(t+ttop)*1000             %Final Thickness of the Laminate including the Top Coat in mm
```

10.3) Code II: for a laminate with a known number of plies

```
%Calculating Resin & Curing Agent Mixing Ratio for a laminate with known
%ply number and fiber percentage
A=.3*.7              %Area of Laminate
RAW=644.21*10^-3         %Reinforcement Areal Weight (kg/m2)
n=4                  %Number of Plys
Ruf=1.74*10^3          %Density of Fiber
Rur=1.13*10^3          %Density of Resin
RuCu=.948*10^3         %Density of Curing Agent
EEW=188*10^-3          %Epoxide Equivalent Weight in kg
AHEW=115*10^-3         %Amine Hydrogen Equivalent Weight in kg
Nuf=.3               %Volume percentage of Fiber
Num=1-Nuf            %Volume percentage of Matrix
mf=RAW*A*n           %Fiber Mass
Vf=(mf)/Ruf          %Volume of Fiber
Vc=Vf/Nuf            %Volume of Laminate
Vm=Num*Vc            %Volume of Matrix
syms mre mcu
eqns=[((mre+mcu)/((mcu/RuCu)+(mre/Rur)))*Vm==mcu+mre,mcu==((mre*AHEW)/EEW)*1.1];
[mre mcu]=vpasolve(eqns,[mre mcu]);
mre=mre*1000             %Resin Mass in gr
mcu=mcu*1000             %Curing Agent Mass in gr
Mm=(mre+mcu)             %Mass of Matrix in gr
Vre=(mre/Rur)*1000       %Resin Volume in ml
Vcu=(mcu/RuCu)*1000      %Curing Agent Volume in ml
Rum=(mre+mcu)/(Vre+Vcu)    %Density of Matrix (Resin+Curing Agent)
Mc=(mre+mcu+mf*1000)       %Mass of Laminate in gr
RuC=(Mc/(Vc*10^6))         %Density of Laminate in gr/cm3
F=(mf./Mc)*1000            %Fiber Content Weight %
t=(Vc/A)*1000              %Thickness of the Laminate in mm
phr=100*mcu./mre           %phr of Curing Agent
ttop=.1*10^-3              %Thickness of the Top Coat (Gel Coat) in m
Vtop=A*ttop*10^6           %Volume of Top Coat in ml
Mtop=Vtop*Rum              %Mass of Top Coat in gr
Mretop=(Mtop*100)./(100+phr)%Mass of Resin for Top Coat in gr
Vretop=Mtop/Rur*10^3       %Volume of Resin for Top Coat in ml
Vcutop=Vtop-Vretop         %Volume of Curing Agent for Top Coat in ml
Mcutop=Mtop-Mretop         %Mass of Curing Agent for Top Coat in gr
T=t+(ttop*1000)            %Final Thickness of the Laminate including the Top Coat in mm
```

10.5) Code III: based on phr and number of plies

```
%Calculating Resin & Curing Agent mass and Volume based on phr and # of
%plies
A=.254*.4572              %Area of Laminate
RAW=644.21*10^-3       %Reinforcement Areal Weight (kg/m2)
n=3                 %Number of Plys
Ruf=1.74*10^3          %Density of Fiber
Rur=1.162*10^3          %Density of Resin
RuCu=.945*10^3         %Density of Curing Agent
phr=28.5715           %phr of the resin & Curing Agent mixing ratio
Nuf=.3               %Volume percentage of Fiber
Num=1-Nuf             %Volume percentage of Matrix
mf=RAW*A*n             %Fiber Mass
Vf=(mf)/Ruf           %Volume of Fiber
Vc=Vf/Nuf             %Volume of Laminate
Vm=Num*Vc             %Volume of Matrix
syms mre mcu
eqns=[((mre+mcu)/((mcu/RuCu)+(mre/Rur)))*Vm==mcu+mre,mcu==((phr*mre/100)*1.1)];
[mre mcu]=vpasolve(eqns,[mre mcu]);
mre=mre*1000              %Resin Mass in gr
mcu=mcu*1000              %Curing Agent Mass in gr
Mm=(mre+mcu)              %Mass of Matrix in gr
Vre=(mre/Rur)*1000         %Resin Volume in ml
Vcu=(mcu/RuCu)*1000        %Curing Agent Volume in ml
Rum=(mre+mcu)/(Vre+Vcu)     %Density of Matrix (Resin+Curing Agent)
Mc=(mre+mcu+mf*1000)       %Mass of Laminate in gr
RuC=(Mc/(Vc*10^6))         %Density of Laminate in gr/cm3
F=(mf./Mc)*1000           %Fiber Content Weight %
t=(Vc/A)*1000             %Thickness of the Laminate in mm
ttop=.1*10^-3             %Thickness of the Top Coat (Gel Coat) in m
Vtop=A*ttop*10^6          %Volume of Top Coat in ml
Mtop=Vtop*Rum             %Mass of Top Coat in gr
Mretop=(Mtop*100)./(100+phr)%Mass of Resin for Top Coat in gr
Vretop=Mtop/Rur*10^3       %Volume of Resin for Top Coat in ml
Vcutop=Vtop-Vretop         %Volume of Curing Agent for Top Coat in ml
Mcutop=Mtop-Mretop         %Mass of Curing Agent for Top Coat in gr
T=t+(ttop*1000)           %Final Thickness of the Laminate including the Top Coat in mm
```